Conducting Polymer-based Battery Electrode Matrices for Lithium-Ion Batteries

by

Van At Nguyen

A Thesis submitted to the Faculty of Graduate Studies of
The University of Manitoba
in partial fulfillment of the requirements of the degree of

MASTER OF SCIENCE

Department of Chemistry
University of Manitoba
Winnipeg

Approval from evaluation committee members

The thesis titled

"Conducting Polymer-Based Battery Electrode Matrices for Lithium-Ion Batteries"

by

Van At Nguyen

APPROVED BY:

Dr. Christian Kuss, Advisor

Department of Chemistry, University of Manitoba

Dr. David E. Herbert, Evaluation Committee Member

Department of Chemistry, University of Manitoba

Dr. Liang Xihui (Larry), Evaluation Committee Member

Department of Mechanical Engineering, University of Manitoba

Declaration of co-authorship and publication

I declare that the content of my thesis originates from my works at the University of Manitoba under the supervision of Dr. Christian Kuss.

I am aware of the academic integrity policy regarding the copyright, co-authorship of the thesis and hereby confirm that this thesis is my own work that has not been published elsewhere for a degree.

To the best of my knowledge, my thesis does not violate any copyright issues regarding ideas, techniques, and other intellectual belongings. Appropriate citations are placed in recognition of others based on the standard referencing protocol.

This thesis consists of several chapters that have published in or to be submitted to peer-reviewed journals as described below:

Chapter	Chapter Title	Publication Link	Publication Status
1	Introduction	N/A	N/A
2	Conducting Polymer-Based Binders for Lithium-Ion Batteries and Beyond	Nguyen, V. A. & Kuss, C. Review—Conducting Polymer-Based Binders for Lithium-Ion Batteries and Beyond. J. Electrochem. Soc. 167, 065501 (2020)	Published
3	Conducting polymer composites as water-dispersible electrode matrices for Li-Ion batteries: Synthesis and characterization	Nguyen, V. A., Wang, J. & Kuss, C. Conducting polymer composites as water-dispersible electrode matrices for Li-Ion batteries: Synthesis and characterization. J. Power Sources Adv. 6, 100033 (2020)	Published

4	Carbon-additive-free $LiNi_{1/3}Mn_{1/3}Co_{1/3}O_2$ cathode enabled by conducting polymer-based electrode matrix	N/A	To be submitted
5	Revisiting the degradation of Li-ion battery cathode containing conducting polymer-based electrode matrix	N/A	To be submitted
6	Conclusions and suggestions for future works	N/A	N/A

Author contribution for published works:

Chapter 2:

- Van At Nguyen: Conceptualization, Writing – Original draft, Writing – Editing.
- Christian Kuss: Conceptualization, Writing – Editing, Supervision, Funding acquisition.

Chapter 3:

- Van At Nguyen: Conceptualization, Methodology, Investigation, Writing – Original draft, Writing – Editing.
- Jian Wang: Investigation.
- Christian Kuss: Conceptualization, Methodology, Writing – Editing, Supervision, Funding acquisition.

Chapter 4 and 5:

- Van At Nguyen: Conceptualization, Methodology, Investigation, Writing – Original draft, Writing – Editing.
- Christian Kuss: Conceptualization, Writing – Editing, Supervision, Funding acquisition.

Abstract

This thesis describes efforts to develop a new class of battery electrode matrices based on conducting polymers. In the introduction section, a summary of Li-ion battery architecture is briefly provided. Following that, some technical challenges for commercializing high-energy-density Li-ion batteries are highlighted to emphasize the necessity of designing better battery electrode architectures, where electrode matrices play a key role. Electrode matrices are typically composed of adhesive binders and conductive additives. Despite being used at a small quantity in battery electrodes (less than 20 wt%), electrode matrices act as both mechanical and electrical connection frameworks for functional Li-ion batteries. The inherent issues associated with the conventional electrode matrix, polyvinylidene fluoride/carbon black (PVDF/C), are then briefly described to signify the necessity of developing alternative electrode matrices. Subsequently, research objectives and methodologies are stated to draw a roadmap towards the development of new conducting polymer-based electrode matrices. The second chapter is a comprehensive literature review, reviewing how conducting polymers are integrated into different types of rechargeable batteries in the forms of binders and electrode matrices. The review chapter also reveals several research gaps in designing and understanding electrode binders/matrices derived from conducting polymers. The third chapter demonstrates an initial effort in developing inexpensive, self-conductive, water-processable conducting polymer-based electrode matrices from pyrrole and carboxymethyl cellulose. By performing *in situ* chemical polymerization of pyrrole in an aqueous solution of sodium carboxymethyl cellulose, composites of polypyrrole and carboxymethyl cellulose (PPy:CMC) are synthesized and then characterized. The study has proven that PPy:CMC composites are functional electrode matrices in terms of electrical conductivity and adhesion/cohesion efficiency. Without adding additional binders and conductive additives, $LiCoO_2$/PPy:CMC cathodes perform as good as $LiCoO_2$/PVDF/C reference cathodes. Chapter 4 demonstrates the application of PPy:CMC composites as electrode matrices for $LiNi_{1/3}Mn_{1/3}Co_{1/3}O_2$, which is an industry-relevant cathode material. Chapter 5 is dedicated to investigating the degradation of $LiCoO_2$/PPy:CMC cathodes by means of electrochemical and post-mortem analyses. Several hypotheses on the degradation mechanism of $LiCoO_2$/PPy:CMC cathodes are drawn and investigated. The last Chapter summarizes research outcomes and suggests potential research directions to expand the understanding and application of conducting polymer-based electrode matrices in Li-ion batteries and beyond.

Acknowledgments

I would like to show my greatest gratitude towards my supervisor, Dr. Christian Kuss, for his guidance and support throughout all stages of this work. His sympathy and kindness encourage me to overcome challenging times. Given that my research project had been impacted by the Covid-19 pandemic, my work has not been done without his endless supports.

I wish to express my appreciation to my lab mates, especially Ms. Mariam Odetallah, during my time at the University of Manitoba. My trips to many places in Manitoba over the years with Ms. Mariam, Ms. Susan, and Mr. Kiran have recharged my internal battery. Without all of you, honestly, my journey would not that memorable.

Special thanks go to the Department of Chemistry for offering teaching/research assistantship and the University of Manitoba for awarding the University of Manitoba Graduate Fellowship. This work is financially supported by the Natural Sciences and Engineering Research Council of Canada (NSERC) through a Discovery Grant and the University of Manitoba.

I would like to thank Mr. Mihaela Dubuisson from Anton Paar for performing the scratch test, Mr. Dwayne D. Chrusch from the Nanosystem Fabrication Lab (University of Manitoba) for training in electrical conductivity measurement, Dr. Abdul Khan from Manitoba Institute for Materials (MIM) for helping with TEM and SEM measurements, Dr. Ravinder Shidu from MIM and Dr. Gabriele Schatte from Queen's University (Canada) for performing XPS measurement, Mr. Arun Krishnamurthy from the Kroeker group and Mr. Dmitry Vrublevskiy from the Bieringer group for helping with XRD measurement, and Dr. Jian Wang from Canadian Light Source (CLS) for STXM measurement. The STXM work at CLS is financially supported by the Canada Foundation for Innovation (CFI), the Natural Sciences and Engineering Research Council (NSERC), the National Research Council (NRC), the Canadian Institutes of Health Research (CIHR), the Government of Saskatchewan, and the University of Saskatchewan.

My thesis has been benefited from valuable comments from my advisory and evaluation review committee members including Dr. Sabine Kuss, Dr. Xihui Liang, and Dr. David E. Herbert.

I highly appreciate mental supports from my friends and lovely family members, who have always encouraged and supported me throughout the two years of my study program. Their love motivates me to get this research done.

To my lovely family!

Table of contents

List of Figures

Chapter 1:

Chapter 2:

Chapter 3:

Chapter 4:

Chapter 5:

Chapter 6:

Supporting Information for Chapter 3:

Supporting Information for Chapter 5:

List of Tables

List of Abbreviations

Abbreviation	Meaning
ASSLB	all-solid-state Li-ion batteries
C-Black	carbon Black
CMC	carboxymethyl cellulose
CP(s)	conducting polymer(s)
CP-based	conducting polymer-based
DMC:EC	dimethyl carbonate:ethylene carbonate:
EXAFS	extended X-ray absorption fine structure
GG	guar gum
LCO	$LiCoO_2$
LFP	$LiFePO_4$
Li-ion	lithium-ion
Li-S	lithium-sulfur
Na-CMC	sodium carboxymethyl cellulose
Na-ion	sodium-ion
NCA	$LiNi_xCo_yAl_{1-x-y}O_2$
NEXAFS	near-edge X-ray absorption fine structure
NMC	$LiNi_xMn_yCo_{1-x-y}O_2$
NMC111	$LiNi_{1/3}Mn_{1/3}Co_{1/3}O_2$
NMO	$LiNi_xMn_{1-x}O_2$
NMP	N-methyl-2-pyrrolidone
PAA	polyacrylic acid
PANI	polyaniline
PEDOT:PSS	poly(3,4-ethylenedioxythiophene):poly(styrene sulfonate)
PF-COONa	sodium poly(9,9-bis(3-propanoate)fluorine)
PPy	polypyrrole
ProDOT	poly(3,4-propylenedioxythiophene-2,5-dicarboxylic acid)
Pth	polythiophene

PVDF	polyvinylidene fluoride
PVDF/C	polyvinylidene fluoride/carbon black
SA	sodium alginate
SBR	styrene-butadiene rubber
SEM	scanning electron microscopy
STXM	scanning transmission X-ray microscopy
TEM	transmission electron microscopy
wt%	weight percent
XG	xanthan gum
XPS	X-ray photoelectron spectroscopy
XRD	X-ray Diffraction

Chapter 1. Introduction

I. Research Backgrounds

1) Fundamentals of Li-ion batteries

Since their initial commercialization in 1991, lithium-ion (Li-ion) batteries have been innovated to accommodate more energy per volume/weight unit, last longer, and charge faster. The production cost of Li-ion batteries has also been reduced significantly from the 90s along with their wider applications. In the next 10 years, the market of Li-ion batteries is expected to triple [1] (Figure 1. 1). The primary driving force for Li-ion battery technology advancement originates from the high demand for electric vehicles. To accelerate electric vehicle adoption, the U.S. Department of Energy (DOE) has placed ambitious targets for future Li-ion batteries that should be mass-produced at $80/kWh. The Li-ion battery packages should be able to power 300-mile range electric vehicles with a charging time of less than 15 minutes[2]. These goals have motivated multidisciplinary research focusing on battery material design, cell fabrication innovation, battery diagnosis & characterization tools, battery-package management system, and end-of-life recycling.

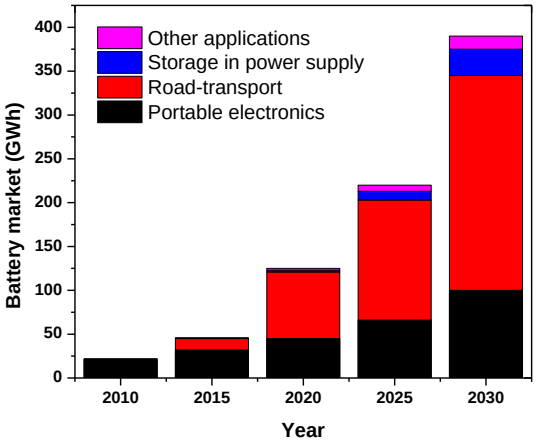

Figure 1.1. Li-ion battery market projection by 2030[1].

In general, Li-ion batteries belong to a broad class of energy storage devices that exploit the reversible movement of lithium ions between two electrodes to store and release electrical energy in the form of electrochemical energy. Even though Li-ion batteries can be constructed in

different geometries such as pouch cells, prismatic cells, cylindrical cells, and coin cells, their internal structure is identical with several main components including anode, cathode, electrolyte, separator, current collector, and casing (Figure 1.2).

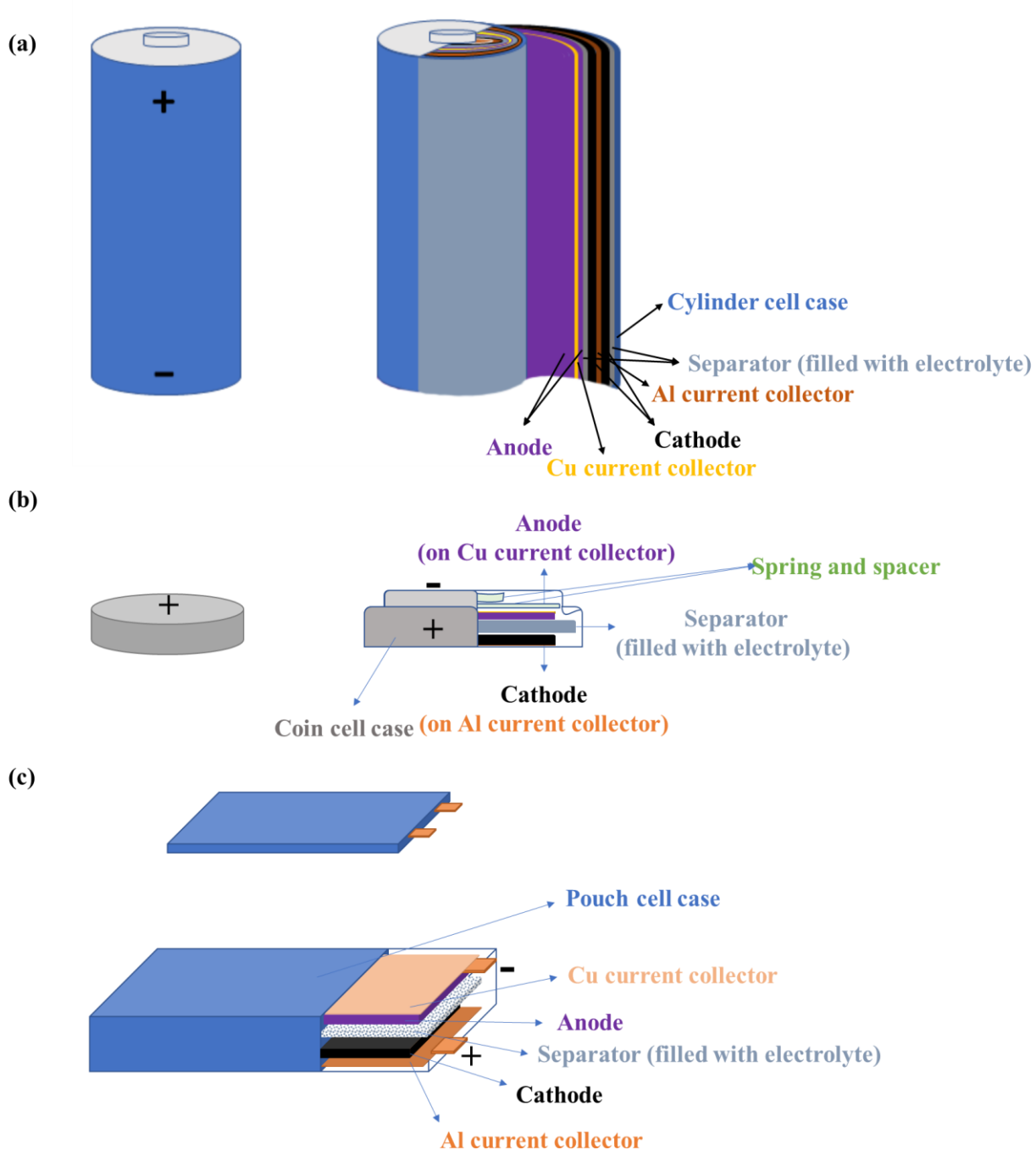

Figure 1.2. Schematic diagrams of (a) cylindrical cell, (b) coin cell, (c) pouch cell.

Each component plays a crucial role in the operation of Li-ion batteries. Cathode and anode are constructed from a mixture of electrode matrices and active materials. A conductive and adhesive electrode matrix not only creates good connections between active materials, ensuring electrode integrity during battery operation[3,4], but it also glues electrode materials to current collectors for facile battery fabrication. Cathode and anode active materials can be any materials that allow reversible Li-ion insertion and extraction without permanent structural destruction. During the charging process, a direct current (DC) is directed to flow from cathode to anode. To ensure charge balance, lithium ions are automatically extracted from cathode active materials to move towards the anode. Lithium ions are moving through a non-conductive and ion-permeable separator via lithium electrolytes. At the anode, lithium ions are inserted into the host anode active material structure. During the discharge process, the movement of electrons and lithium ions is in reverse order. Battery casings prevent internal components from air and moisture exposures, which might lead to thermal runaway and battery failure.

Among the aforementioned battery components, battery electrodes including anode and cathode are considered the most important parts, where Li-ion insertion/extraction takes place. Any improvements in electrode performance would significantly impact the overall performance of Li-ion batteries. Battery electrode development involves both active material and electrode matrix designs. Despite being inactive in Li-ion battery cells, a small quantity of electrode matrix is indispensable for ensuring mechanical integrity and electrical conductivity of battery electrodes. High-performance battery electrodes require good active materials to be embedded into a robust, highly efficient electrode matrix. In commercial Li-ion batteries, polyvinylidene fluoride/carbon (PVDF/C) mixture is considered the standard electrode matrix for Li-ion batteries due to their excellent film-forming ability. Their inherent drawbacks in terms of performance, cost, and toxicity motivate this study to design a better electrode matrix for Li-ion batteries.

A brief overview of each battery component is discussed in the following sections:

a) Cathode active materials

Lithium cobalt oxide ($LiCoO_2$) is considered the most well-known cathode active material in commercial Li-ion batteries. $LiCoO_2$ belongs to a class of layer transition metal oxides ($LiMO_2$, M=Co, Ni, Mn, Al, …). The most stable crystal structure of $LiCoO_2$ is O3-type[5,6], where lithium and cobalt ions occupy alternating layers at octahedral sites of the cubic closed-packed lattice of

oxygen stacked in ABCABC order (Figure 1.3). Their compact structure allows dense energy storage. Moreover, their layer structure enables fast lithium transport[7].

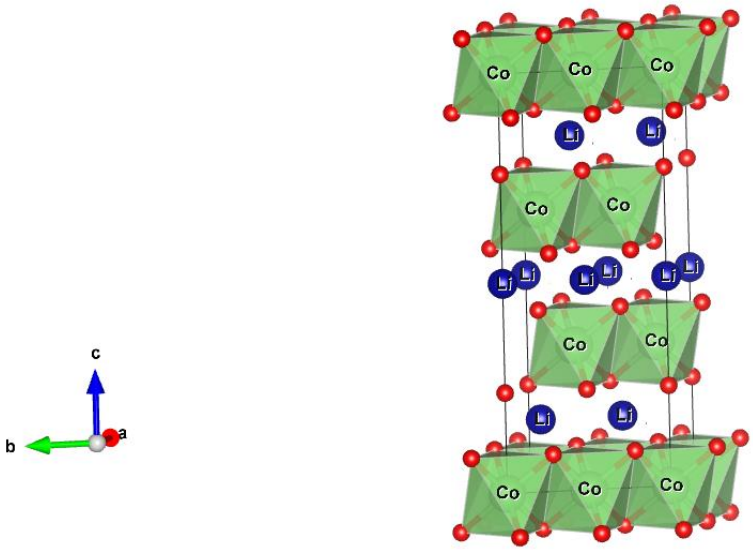

Figure 1.3. $LiCoO_2$ crystal structure.
Drawn by VESTA based on published lattice parameters[5].

Despite having a theoretical capacity of 274 $mAh.g^{-1}$ for a complete delithiation, $LiCoO_2$ is only able to de-lithiate to Li_xCoO_2 ($0.5 \leq x \leq 1$). Overcharging causes extreme anisotropic structure distortion[8]. As a result, the realistic theoretical capacity of $LiCoO_2$ is only around 160 $mAh.g^{-1}$. Unfortunately, the depletion of cobalt mines, as well as their uneven geographic distribution, has threatened the sustainability of $LiCoO_2$-based battery production[9]. As a result, using cobalt-less cathode materials has become a research trend. The two most promising types of cathode active materials are $LiNi_xMn_yCo_{1-x-y}O_2$ (NMC), and $LiNi_xCo_yAl_{1-x-y}O_2$ (NCA), which have been used by major battery manufacturers such as LG Chem (South Korea), Panasonic (Japan), BYD (China)[1]. These layered lithium transition metal oxides deliver high energy density, making them a great candidate for powering electric vehicles. Many works have been done to address their structural instabilities by surface coating[10–14], core-shell gradient structure formation[15–18], single-crystal synthesis[19–24], and electrolyte additive development[25–27].

Apart from layered lithium transition metal oxides, which are renowned for the possibility of delivering high energy density, lithium iron phosphate $LiFePO_4$ (LFP) is well-known for its highly stable olivine structure[28,29]. LFP cathode can cycle up to 10000 cycles with minimal

performance degradation[29]. The practical specific capacity of LFP is around ~170 $mAh.g^{-1}$, which is comparable to that of $LiCoO_2$. However, LFP exhibits low bulk density resulting in low volumetric capacity for portable devices[30]. Moreover, their narrow operating voltage window causes limited energy density, making them a better candidate for grid-scale energy storage applications where battery stability is the top priority. The main technical challenge for commercializing LFP cathode is their low ionic and electrical conductivity, which has been addressed by carbon coating[28,31–33].

In the current state of the art, boosting cathode performance is considered the most challenging task to enable high-energy-density Li-ion batteries[34,35]. The high cost and low energy density of cathode compared to that of anode have put cathode design at the forefront of battery research. Usually, the abovementioned cathode active materials are embedded in electrode matrices. Even though electrode matrices only account for a small weight/volume fraction in cathode composition and do not contribute to battery capacity, efficient electrode matrices are needed for high-performance cathodes, which is the main subject of this thesis.

b) Anode active materials

Graphite has long been used as an anode active material in commercial Li-ion batteries. Graphite contains multiple planar carbon layers arranged in either hexagonal or rhombohedral array. During the charging process, lithium ions intercalate into graphite layer structure, forming LiC_x ($0 \leq x \leq 6$)[36]. The maximum theoretical specific capacity of graphite negative electrode is 370 $mAh.g^{-1}$. In the last decade, several types of anode active materials have been developed that could deliver much higher theoretical specific capacity such as Si (~4200 $mAh.g^{-1}$)[37], SiO(~1000 $mAh.g^{-1}$)[38,39], and Sn (~850 mAh/g^{-1})[40,41]. As a result of lithium alloy formation, the volume of these host anode materials expands abruptly. For example, Si anode expands 300 times upon lithiation[42]. If the volume expansion is not well accommodated, particle cracking and pulverization will occur upon delithiation, thus, causing rapid capacity fade[43]. Numerous strategies have been deployed to alleviate this issue by utilizing nanomaterials[44,45], flexible electrode matrix[4,46,47], 3D electrode scaffold[48,49]. Among the above strategies, designing efficient electrode matrices seems to be a rational approach from the technical point of view. A good electrode matrix must accommodate volume changes effectively to ensure electrode integrity.

c) Electrolytes

Electrolytes are responsible for transferring lithium ions back and forth between battery electrodes. An ideal electrolyte for Li-ion batteries should possess some key features such as wide working potential window, high ionic conductivity, low viscosity, excellent chemical/thermal stability, low toxicity, low cost, and non-flammability[50–52]. However, no commercial electrolyte currently simultaneously meets all these targets. Most commercial Li-ion batteries use non-aqueous liquid electrolytes, which typically contain a lithium salt dissolved in alkyl carbonate organic solvents. For example, 1 M $LiFP_6$ in dimethyl carbonate:ethylene carbonate (DMC:EC) electrolyte has gained industrial acceptance due to its high ionic conductivity. Usually, some electrolyte additives are added to improve electrolyte stability, improve life cycle, scavenge oxygen and moisture formed in battery cells[53]. However, these non-aqueous liquid electrolytes are flammable due to the presence of organic carbonate solvents, posing a threat of explosion and fire[54]. Other types of liquid electrolytes being studied include ionic liquid electrolytes[55] and gel polymer electrolytes[56,57] however these have failed to gain a large market adoption for a number of reasons. Besides their high cost, ionic liquid electrolytes have high viscosity lowering their ionic mobility[58], which makes them unfit especially for making fast-charging Li-ion batteries. While polymer electrolytes suffer from their poor mechanical properties[58].

Non-flammable solid-state electrolytes have emerged as key materials for the next generation of all-solid-state Li-ion batteries (ASSLB)[59]. The absence of organic solvent and high thermal stability of solid electrolytes eliminates the risk of thermal runaway. Besides that, ASSLB might surpass conventional liquid-electrolyte Li-ion batteries in terms of gravimetric and volumetric capacities. For example, separator and electrolyte contribute approximately 15 wt% to conventional liquid-electrolyte Li-ion battery cells[60]. Using solid-state electrolytes would reduce the weight of battery cells, thus enhance battery energy density. More importantly, ASSLB enables bipolar stacked cell design that would make more compact battery cells than conventional stacked liquid electrolyte Li-ion batteries (Figure 1.4). The dead space between electrodes was reduced, thus giving more space for adding extra battery units. New classes of solid electrolytes such as Li_6PS_5X (X = Cl, Br, I) argyrodites[61–64] and lithium stuffed garnet-type electrolytes[65,66] (Ex: $Li_7La_3Zr_2O_{12}$) are reported to show excellent ionic conductivities that are comparable to that of the conventional liquid electrolytes. The commercial application of ASSLB,

however, is limited due to the high production cost, brittleness[66], and interfacial instabilities[67] of solid electrolytes.

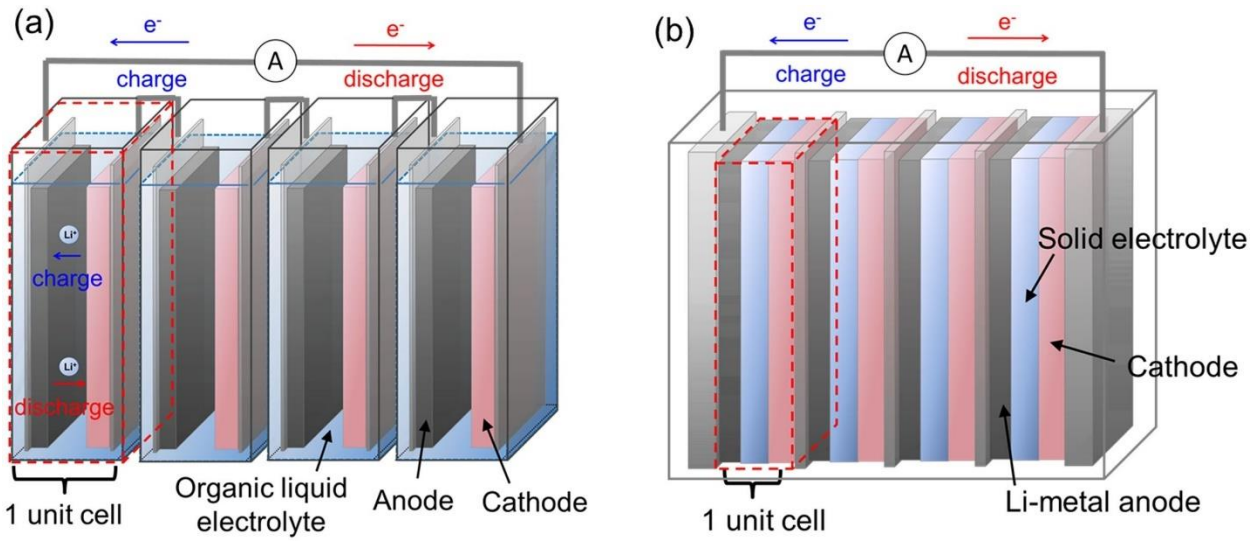

Figure 1.4. (a) Conventional stacked battery cell with liquid electrolytes, and (b) bipolar stacked battery cell with solid electrolytes. Reproduced with permission from reference[68].

d) Separators

For Li-ion battery cells that employ liquid electrolytes[52], a separator is a crucial component placed between anode and cathode as a physical barrier to avoid direct contact between electrodes. Besides, separators must be made of non-conductive materials to prevent an electric current from passing between anode and cathode, which ends up short-circuiting battery cells and induces thermal runaway. However, separators must be porous and possess micron-sized pores that allow lithium ions to move back and forth between the two electrodes.

Typical requirements for ideal battery separators include good mechanical strength, high electrochemical/chemical stability, excellent electrolyte wettability, good morphological stability, high porosity, and low cost[52]. Because the separator occupies space and adds dead-weight into Li-ion battery cells, the separator should be designed to be lightweight and thin without compromising performance. For safety reasons, separator pores should be closed in case of the thermal runway by melting separator materials. Three common types of separators are microporous polymer membranes, non-woven-fabric mats, and inorganic composite membranes, whose advantages are discussed in reference[52].

e) Current collectors

Current collectors are often employed as supporting substrates for battery electrode materials. By casting electrode materials on current collectors, the thickness and weight of electrode materials can be controlled easily. The material selection for electrode current collectors is based on corrosion protection and anti-alloying mechanisms. The normal operating potential window of anode and cathode is around 0-2.5 V vs Li/Li^+, and 2.5-4.5 V vs Li/Li^+, respectively. It is worth noting that the oxidation potential of Cu is around 3.3 V vs Li/Li^+, meaning that copper will be oxidized at cathode potentials[69]. Therefore, copper metal is electrochemically stable for usage as the anode current collector only. Aluminum, on the other hand, forms alloys with lithium at anode potentials, which makes them unsuitable as the anode current collector. However, a thin layer of aluminum oxide deposited on the aluminum surface prevents aluminum from being corroded at normal cathode working potentials[69]. Aluminum current collector suffers from pitting corrosion at high potentials due to the oxidation of carbonate electrolyte[70].

Electrode delamination is one of the reasons for battery failure[71]. Good electrode adhesion between active materials and current collectors is critical for successful battery fabrication and operation. Therefore, a highly adhesive electrode matrix should be developed, especially for high-energy-density batteries where the volume change of active materials disrupts electrode integrity and induces electrode delamination.

2) Fundamentals of Na-ion batteries

As the risk of lithium shortage continues to threaten the sustainability of Li-ion battery production, the abundance of sodium from seawater has motivated the research community to invest in Na-ion battery technology. The configuration and operation concept of Na-ion batteries are mostly similar to that of Li-ion batteries[72–75]. Instead of using lithium ions as charge carriers, Na-ion batteries use sodium ions (Na^+) to go back and forth between positive and negative electrodes during their operation. As shown in Table 1, It is worth noting that the standard electrochemical potential of sodium is less negative than that of lithium[73]. As a result, Na-ion batteries generally have smaller battery cell voltages than Li-ion battery counterparts. Because energy density is calculated by multiplying cell voltage with specific capacity density, Na-ion batteries usually have lower energy density than Li-ion batteries, making them more favorable for grid-scale application, where space and weight are not big concerns.

Table 1. Physical properties of lithium and sodium[73,76,77].

Physical properties	**Li**	**Na**
Atomic mass ($g.mol^{-3}$)	6.94	22.99
Cationic radius (Å)	0.76	1.02
Standard electrochemical potential (V vs SHE)	-3.04	2.71
Melting point (^oC)	180.5	97.7
Density ($g.cm^{-3}$)	0.971	0.534
Theoretical gravimetric capacity ($mAh.g^{-1}$)	3861	1165

Theoretically, the material selection and design concepts of Li-ion batteries could be applied to Na-ion batteries. Because the standard electrochemical potential of sodium metal is higher than that of lithium metal, therefore, anode material selection needs to be done more carefully to avoid lithium plating at the anode, which happens when the reduction potential of anode materials is smaller than that of sodium[73]. Similar to Li-ion batteries, Na-ion battery host active materials are classified into three main types of sodium ion insertion mechanisms including intercalation, alloying, and conversion[73,77]. Intercalation materials are the most commonly used electrode materials, whose structural integrity is retained upon (de)sodiation[74,75]. Alloying electrode materials refer to electrode materials reacting with sodium ions to form alloys[78]. While conversion electrode materials will change their crystal phases upon conversion reaction with sodium ions[79]. Even though alloying or conversion materials offer much higher specific capacity, they suffer from large volume expansion/contraction and structural instability.

Regarding anode materials, It is well-known that graphite is a common and successful anode material for Li-ion batteries[80]. However, sodium ions fail to integrate into graphite to a good extent. The common myth is that the large ionic size of sodium ions prevents them to insert into the layer structures of graphite. However, the main reason is a weak chemical binding between sodium and graphite substrate[81]. The development of Na-ion batteries has been resumed after the breakthrough in using hard carbon as Na-ion anode material[82]. Unlike graphite, hard-carbon constitutes graphene-like sheets in a matrix of amorphous carbon. Even though their specific capacity is approximately 300 $mAh.g^{-1}$, which is quite closed to that of graphite anode in Li-ion batteries (370 $mAh.g^{-1}$). There is a high risk of sodium plating due to the potential at which intercalation occurs is closed to the electrochemical standard potential of sodium, especially at

high charging rates. Other promising anode materials for Na-ion batteries include titanium-based materials (intercalation mechanism)[83], p-block element-based materials (Sn, P, Sb: alloying mechanism)[73], and metal oxides (conversion mechanism)[73,79]. It is worth noting that crystallite silicon, which is a promising material for Li-ion battery anode, is electrochemical inactive for Na-ion batteries due to their large diffusion barrier[84].

As for cathode materials, knowledge generated from years of research on Li-ion battery cathode materials could be readily transferred to design cathode materials for Na-ion batteries. Sodium transition metal oxides and polyanionic compounds are the two most promising families of cathode materials for Na-ion batteries[75]. Sodium transition metal oxides (Na_xMO_2 (M = Co, Mn, Fe, Ni, etc.) can be classified according to their structures (layer, tunnel), and the number of transition metals (single, multiple)[85]. Despite having low operating potential, they offer attractive capacity (~150-200 $mAh.g^{-1}$). The cycling life of Na_xMO_2 is limited due to irreversible structural changes, especially at high voltage. To solve these problems, cationic substitution is considered the most rational material design, where inactive metal ions such as Mg^{2+}, Ti^{4+}, Ca^{2+} replace transition metal ions in their crystal lattice[86–88]. Even though each single-metal transition metal oxide have their advantages such as $NaCoO_2$ (good ionic diffusivity), $NaFeO_2$ (high redox potential), and $NaMnO_2$ (high capacity), most of them suffer from low cycling stability. By designing sodium transition metal oxides with multiple transition metals (Mn, Co, Fe, Ni, etc), high electrode performance is expected due to the synergetic combination[75]. Polyanionic compounds are considered promising cathode materials for Na-ion batteries due to their structural diversity and stability[75]. Many types of polyanionic compounds are being studied such as phosphates ($NaFePO_4$, $Na_3V_2(PO_4)_3$), pyrophosphates ($Na_2MP_2O_7$ (M = Fe, Co, Mn, etc.)), fluorophosphate (Na_2MPO_4F (M = Fe, Co, Mn, etc.)), and sulfates ($Na_2Fe_2(SO_4)_3$). To lower electron transfer resistance and electrode polarization, carbon coating is often required. Nanosizing is also a good approach to reduce the diffusion length of sodium ions upon charging/discharging[75].

Similarly, Na-ion battery active electrode materials must be placed in an efficient electrode matrix to ensure good electrical and mechanical integrity upon repeated charge/discharge cycling. Several review papers have emphasized the importance of using alternative binders or electrode matrices for Na-ion battery electrodes[72,89,90]. Applying new electrode matrices on Na-ion

battery electrodes is out of the scope of this study. However, due to the similarity between Na-ion batteries and Li-ion batteries, it is expected that new electrode matrices designed in this study would work for Na-ion batteries as well.

3) Fundamental of Li-S batteries

Li-S batteries have been widely considered one of the most promising rechargeable energy storage technology in terms of energy density, material cost[91]. Their energy capacity is approximately 2-3 times higher than that of Li-ion battery cells. Instead of using transition metal oxides as cathode materials, Li-S batteries employ sulfur metal as an inexpensive cathode material. On the anode side, lithium metal is used.

Many studies have been carried out to study the operating mechanism of Li-S batteries, however, concrete and comprehensive understanding of chemical reactions happening in Li-S batteries is not available. Generally, during the discharging process, lithium metal anode is oxidized and dissolved into the electrolyte. As lithium ions migrate to the cathode, sulfur is reduced to form Li_2S_x ($2 \leq x \leq 8$) polysulfide species. As the discharging process going, the length of polysulfides becomes smaller. The discharging process ends when all lithium metal is stripped from the anode or sulfur is completely converted into Li_2S. Upon the charging process, the process direction reverses[91].

The commercialization of Li-S batteries is hindered for a number of reasons. First of all, the low electrical conductivity of sulfur and Li_2S discharged products requires a high amount of carbon additives to form a conductive Carbon-Sulfur (C-S) composite cathode[92]. Such a high volume and weight of carbon additives in cathode composition (~30 wt%) lower the volumetric and gravimetric capacity of Li-S batteries, which is against the objective of Li-S research. Using a highly conductive electrode matrix based on conducting polymers becomes a rational strategy to address the above issue[93–97]. Moreover, the poor interaction of PVDF/C electrode matrix with sulfur and Li_2S results in the shuttle effects, which is the migration of the intermediate redox products Li_2S_x ($6 < x \leq 8$) to lithium metal anode during the discharge process. The shuttle effect is responsible for the shortage of sulfur for operation, reducing battery coulombic efficiency[98,99]. This phenomenon can be addressed by using efficient electrode matrices as reported in the literature[93,100–104].

4) Conducting polymers (CPs)

The discovery of electrical conductivity in polyacetylene in 1977 has brought a Nobel Prize in Chemistry 2000 to three renowned scientists including Hideki Shirakawa, Alan MacDiarmid, and Alan Heeger[105]. Since then, tremendous studies have been carried out both on fundamental and application aspects. Conducting polymers (CPs) are conjugated polymers, whose chemical structure contains alternating single (σ) and double (π) bonds. Several common conducting polymers have been reported in the literature including polyaniline (PANI), polypyrrole (PPy), thiophene(Pth), and poly(3,4-ethylenedioxythiophene) (PEDOT).

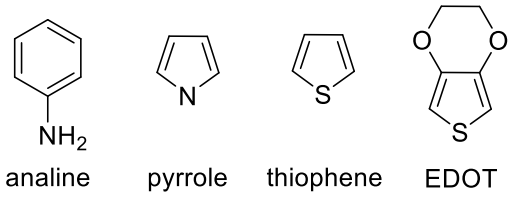

Figure 1.5. Chemical structure of conducting polymer monomers.

CPs are synthesized by polymerizing CPs monomers by chemical oxidative polymerization or electrochemical polymerization[106,107]. Figure 1.5 describes the chemical structure of common CP monomers. Neutral CPs are non-conductive, in which electrons are immobilized in the π-conjugated system. Doping is the process of withdrawing (p-type) or donating (n-type) electrons from the backbone of CPs by dopants, yielding charge carriers in the backbone of CPs in the forms of polarons (cations and anions) or bipolarons (dications, dianions)[105,108]. These charge carriers are usually delocalized over the polymer chain of CPs, allowing electrons to flow. Dopants can be small cations/anions (Cl^-, RSO_3^-, ClO_4^-, Na^+) or large polyanions/polycations (polystyrene sulfonate, carboxymethyl cellulose). It worth noting that n-type doping CPs are usually not as stable as p-type doping CPs. Most n-type doping CPs are easily oxidized upon exposure to air and converted to p-type doing CPs[109]. The electrical conductivity of conducting polymers depends on the doping level, in other words, the concentration of dopants.

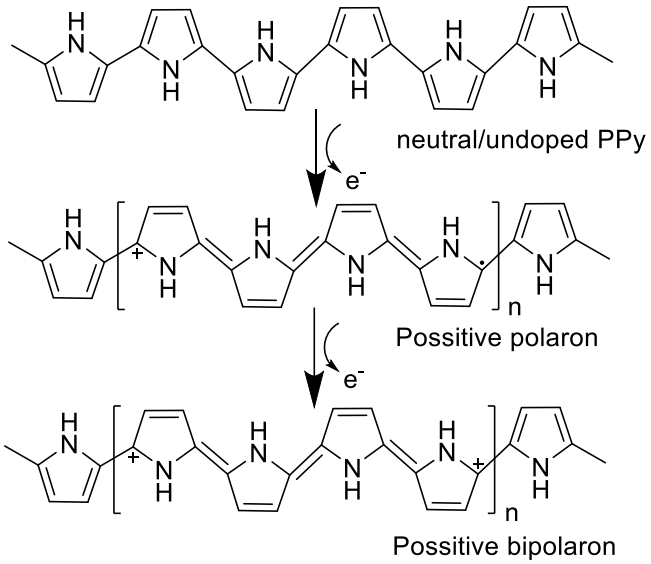

Figure 1.6. Evolution of the chemical structure of polypyrrole upon doping.

For example, undoped/neutral PPy is a non-conductive substance. As shown in Figure 1.6, conductive PPy exits in a form of p-type doping. During the oxidative polymerization of pyrrole, the polymer chain of PPy is oxidized and then doped by anionic dopants presented in the polymerization solution. Upon doping, a π-electron from the π-conjugated system of PPy is taken away from neutral PPy polymer chain, forming a positive polaron. The benzenoid structure is deformed to quinoid. As PPy continues to be oxidized, a second electron is extracted from the PPy chain, yielding a positive bipolaron.

Even though conducting polymers possess good electrical conductivity. Their usage in Li-ion batteries is very limited. Conductive carbon additives remain key conductive agents. By making carbon-additive-free battery electrodes, this study aims to prove that conducting polymers can offer sufficient electrical conductivity for battery electrodes.

II. Research Motivations

The emergence of high-energy-density active materials has sped up the development of high-performance Li-ion battery packages for electric vehicles. As new active materials allow much more lithium ions to accommodate in their structure, they are likely to suffer from large volume changes and subsequent structural instabilities upon Li-ion insertion and extraction. As a result, the battery performance deterioration has become a challenge for using high-energy-density electrode active materials.

Apart from many strategies for designing robust, stable active material themselves[7,110,111], the overall battery performance could be improved by designing a better electrode matrix, which provides stronger mechanical and electrical connections between individual active material particles. Without a sufficiently conductive electrode matrix, an electric current can not move within electrode architecture to induce Li-ion movement during operation. Weak mechanical supports from the electrode matrix are unable to accommodate volume changes of active materials happening during the Li-ion insertion/extraction, resulting in internal/external particle cracking and pulverization[4].

However, the importance of the electrode matrix in Li-ion batteries has been neglected since the introduction of polyvinylidene fluoride/carbon black (PVDF/C) electrode matrix. PVDF/C mixtures are well-known for providing good electrode electrical conductivity and electrode film formation[112]. Their limitations in terms of interaction with active materials have become problematic recently along with the successful development of high energy density active materials such as silicon anode and NMC-based cathode materials. Strong interaction/bonding with active materials is a prerequisite for accommodating volume changes and addressing structural instabilities in these high-energy-density active materials. Figure 1.7 shows several battery failure mechanisms related to the usage of high-energy-density electrode active materials with PVDF/C electrode matrix. For example, Si-based anode usually experiences particle cracking and pulverization as a result of large volume changes during operation (Figure 1.7 (a))[113]. NMC-based cathode materials often suffer from particle cracking, structural instability, loss of electrical contact with carbon additives, and so on (Figure 1.7 (b))[114]. These issues can be alleviated by using an effective electrode matrix that could form good physical and chemical interactions with active materials. In addition, carbon additives in the PVDF/C mixture tend to agglomerate, leaving some portions of battery electrode becomes electrically isolated or non-conductive (Figure 1.7 (c))[115]. To ensure that all electrode materials can continuously participate in charging/discharging processes, a strongly adhesive and conductive electrode matrix should be used.

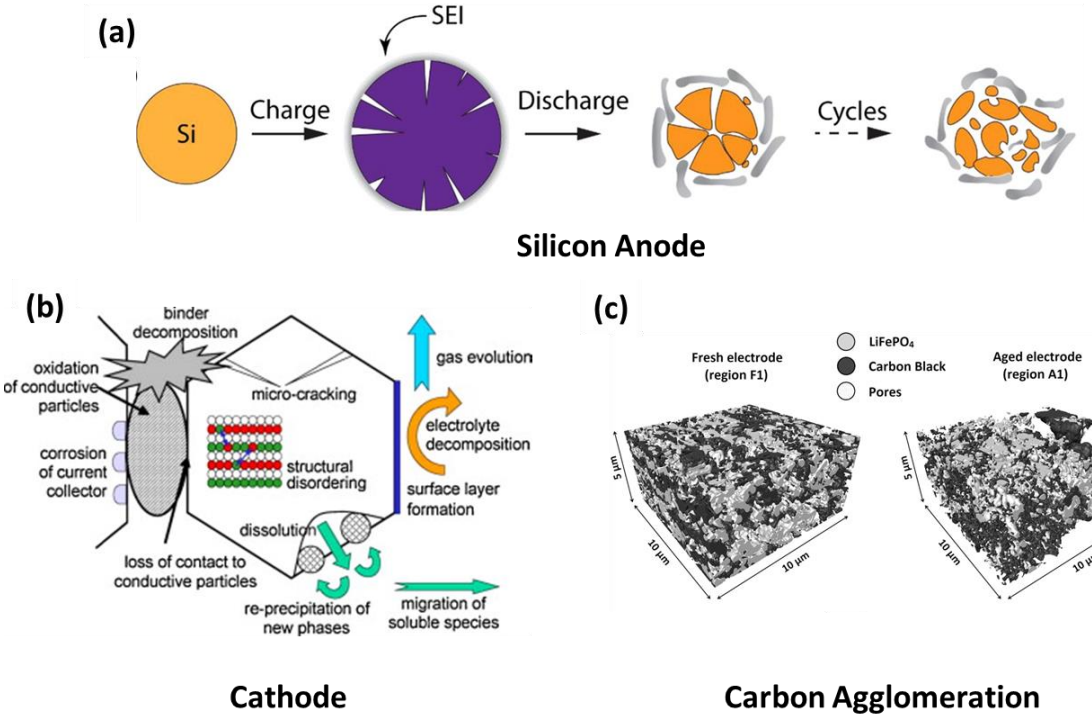

Figure 1.7. (a) Pulverization of Si-based anode materials[113], *(b) degradation mechanisms of cathode materials*[114], *(c) carbon agglomeration problem of PVDF/C electrode matrix*[115].

It is also worth noting that the most energy-intensive stages in the conventional electrode fabrication process are electrode drying and subsequent NMP solvent recovery, accounting for almost 47% of total energy consumed[116]. As the demand for Li-ion battery cells grows rapidly to power electric vehicles, the battery fabrication process must be operated in an environmentally friendly manner that minimizes energy consumption and pollution risks. The two most common solutions are using aqueous binders[117] and implementing solvent-free hot melt extrusion method[118]. The aqueous electrode processing seems to be more relevant to the current NMP-based electrode processing. No significant changes in the production line are demanded to shift NMP-based to water-based electrode processing.

Alternative electrode matrices are needed for the next generation of Li-ion batteries. The most common way to design electrode matrices is by combining water-processable binders such as carboxymethyl cellulose (CMC), alginate, polyacrylic acid (PAA), and styrene-butadiene rubber (SBR) with carbonaceous conductive additives such as carbon black, carbon nanotube, and graphene. As described in Chapter 2, there are pieces of evidence that adding conducting polymers

as conductive additives to battery electrodes could enhance electrode conductivity, thus improving electrode performance. However, most studies still consider carbon conductive additives are irreplaceable components in battery electrode composition.

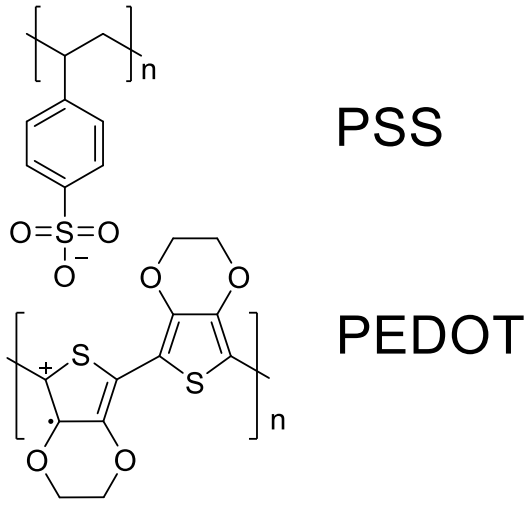

Figure 1.8. Chemical structure of PEDOT:PSS conducting polymer composites.

This work is inspired by the use of poly(3,4-ethylenedioxythiophene):polystyrene sulfonate (PEDOT:PSS) composites as mono-component electrode matrices for Li-ion batteries. No additional binders or carbon additives are used to fabricate Si/PEDOT:PSS anode [119], and $LiCoO_2$/PEDOT:PSS cathode[120]. These two great examples demonstrated the capability of conducting polymers to connect active materials electrically. The chemical structure of PEDOT:PSS suggests that conducting polymers need to be oxidized and doped by polyanions to form conductive composites (Figure 1.8). However, the production cost of PEDOT:PSS is relatively high for wide-scale applications in Li-ion batteries.

This study mimics the design concept of PEDOT:PSS composites by polymerizing cheaper conducting polymer monomers such as aniline, pyrrole, thiophene (Figure 1.9) in the presence of common battery aqueous binders that have negatively charged carboxyl groups on their chemical structures such as CMC, alginate, PAA (Figure 1.10). It is expected that molecular composites are formed when conducting polymer monomers are in-situ polymerized in carboxylate-containing polymer matrices. By this unique combination of two components, these conducting polymer-based (CP-based) composites are expected to be conductive, water-dispersible, and adhesive, which are essential features of battery electrode matrices.

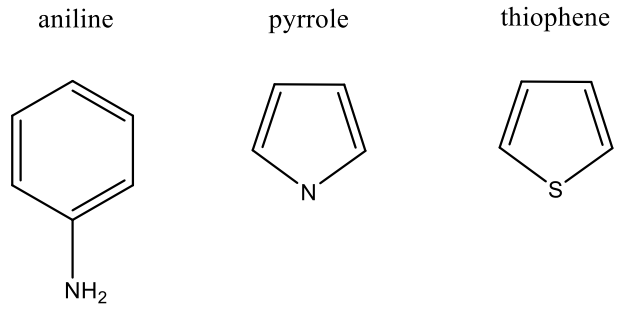

Figure 1.9. Chemical structures of conducting polymer monomers.

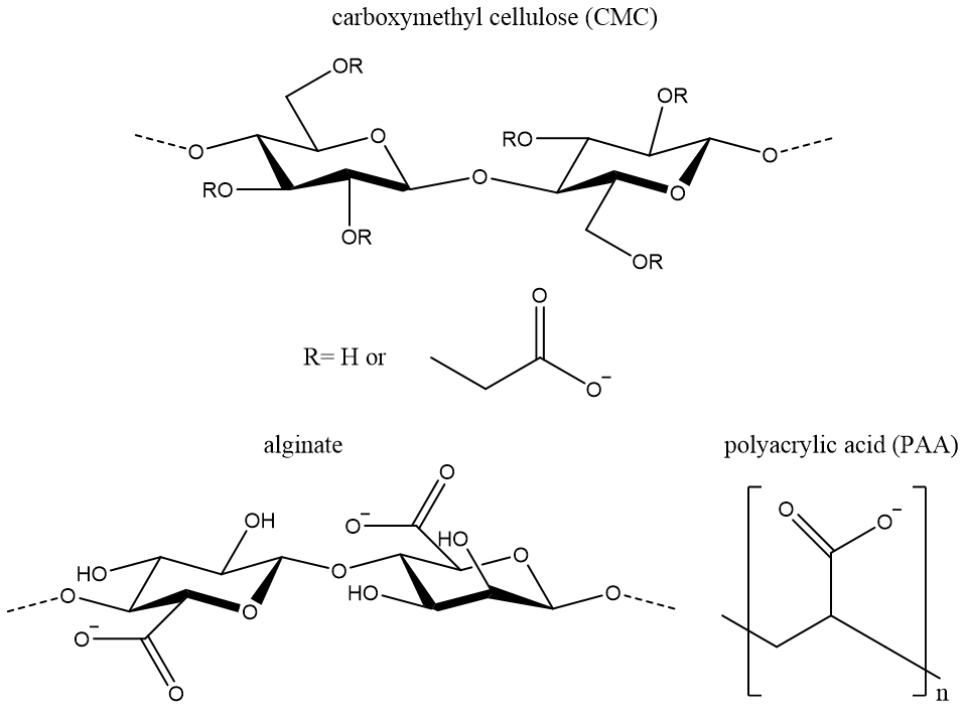

Figure 1.10. Chemical structures of carboxylate-containing polymers.

III. Methodologies

This work aims to develop a new class of alternative electrode matrices for Li-ion batteries. In particular, CP-based electrode matrices such as polypyrrole:carboxymethyl cellulose (PPy:CMC) composites were synthesized. Following that, the chemical, physical and electrochemical properties of CP-based electrode matrices were investigated by several microscopic, spectroscopic, and physical methods. Coin-cell prototypes were then used to study

the performance of CP-based electrode matrices in real Li-ion battery devices. The following sections describe the working principles and conditions for each method used in this work.

1) Material characterizations

a) Scanning Electron Microscopy (SEM)

SEM is a technique of examining the morphology and macrostructure of the sample of interest by scanning an electron beam across the sample's surface. When a focused electron beam is scanning across the sample, collisions between incident electrons and electrons at the outer shell of atoms result in the ejection of so-called secondary electrons (SE) with relatively low energies of 10-50 eV. The SE signals provide the topographic contrast of the sample surface, showing sample tomography and topography. Besides that, elastic interactions between incident electrons and atom nuclei yield backscattered electrons (BSE) with high energy. The contrast of BSE images represents the distribution of high and low atomic number (Z) atoms in the sample, in which atoms with high atomic numbers cause stronger scattering than atoms with low atomic numbers. The interaction between the incident electron beam and the sample also results in the ejection of characteristic X-rays. By using an energy dispersive spectrometer (EDS) or wavelength-dispersive spectrometer (WDS), characteristic X-rays can be measured and correlated to sample composition.

In this study, SEM measurement was used to observe the morphologies of CP composites and electrodes. Sample preparation varies depending on the type of material. As for PPy:CMC composites, their powders were pressed on pieces of double-side carbon tape attached to sample tubs. To avoid sample charging, a thin layer of Au-Pd was sputtered on the sample surface. While composite electrodes on Al foil were placed directly onto pieces of double-side carbon tape attached to sample tubs before bringing them to the analyzing chamber. No Au-Pd sputtering was applied for electrode imaging. All SEM measurement was performed on FEI Nova NanoSEM 450 at the Manitoba Institute for Materials (MIM).

b) Transmission Electron Microscopy (TEM)

The working principles of transmission electron microscopy (TEM) are similar to that of traditional transmission light microscopy. The shorter wavelength of electron beam used in TEM results in higher image resolution. Firstly, the electron beam generated from a field emission (FE) gun was accelerated by applying a high electrical voltage. Electromagnetic lenses were then used to focus the electron beam on the thin section of samples. After passing through the sample, the

transmitted electron beam is magnified by a series of electromagnetic lenses and then converted into images by detectors. The most common image mode is the mass-density contrast image, where the deflection of incident electrons represents the mass-density of the sample. The elemental mapping mode can be carried out by using an EDX detector to study the distribution of elements at a nano level.

In this study, FE-TEM measurement was used to study the microstructure of the CP composites, where the arrangement of composite components affects its characteristics. Samples were dispersed in isopropanol and sonicated to yield diluted homogeneous suspensions. Suspensions were then dropped on carbon-coated copper grids and dried naturally. TEM/EDX measurement was performed on FEI Talos F200X at the accelerating voltages of 80 keV.

c) X-ray Diffraction (XRD)

When a monochromatic X-ray beam is directed to a crystalline sample, the X-ray beam is diffracted by the parallel crystal planes with identical lattice spacings (d) of the crystalline sample. The intensity of the reflected X-rays is recorded during the rotation of the sample (θ angle) and detector (2θ angle). At certain diffraction angles (θ), interactions between X-rays and crystal planes result in constructive interferences of reflected X-rays and give intensity peaks. The condition for constructive interference is described by Bragg's law:

$$n\lambda = 2dSin\theta$$

in which n is integer numbers, and λ is an X-ray wavelength. XRD is generally used to identify the crystal structure of crystalline samples. By performing search-match analysis on the XRD diffractogram of samples with Crystallography Open Database (COD), their crystal structure will be identified given compositional elements are known.

In this study, the powder XRD technique is utilized to confirm the structure of lab-synthesized NMC111 cathode materials. All samples were ground in an agate mortar and pestle before transferring into polymer diffraction plates. XRD measurement was carried out by D4 Endeavor X-ray diffractometer with Cu Kα sources generated at 40 kV and 40 mA. The scanning 2θ-range and rate for different materials were mentioned in Chapter 4. Data analysis was done by QuaIX coupled with Crystallography Open Database (COD)[121].

d) Scanning Transmission X-ray Microscopy (STXM)

X-ray microscopy is a well-known type of imaging technique that utilizes X-rays to penetrate samples, yielding contrast images that represent the difference in X-ray absorption at different locations on the sample. Normally, synchrotron-based X-rays are used for X-ray microscopy imaging due to their tunable wavelength and intensity. Due to their high energy, X-rays can penetrate thick samples, which can not be achieved by electron beams in TEM.

Scanning transmission X-ray microscopy (STXM) is a special type of X-ray microscopy, where soft and focused X-ray beam scans through the sample. During the scanning, the energy of X-rays is also changed to cover a wide range of photon energies. Once the energy of the incident photon matches the excitation energy required for core electrons to jump to unoccupied levels, there is a large increase in X-ray absorption intensity, which is recorded as near-edge X-ray absorption fine structure (NEXAFS) spectra. It is worth noting that different elements have different absorption edges and the shape of NEXAFS spectra carries information of element of interest. By measuring the intensity of transmitted X-rays as a function of measuring locations and photon energies, the compositional mapping of the sample is obtained. This technique was employed to investigate the chemical and structural arrangement of PPy:CMC composites. The details on instrument, sample preparation, data collection, and analysis were provided in Chapter 3.

e) Near-edge X-ray Absorption Fine Structure (NEXAFS)

As the X-ray energy increases during STXM measurement, whenever the energy of incident X-rays matches the energy required for electron excitation from core orbitals to unoccupied orbitals, the electron will absorb X-rays and excite to unoccupied orbitals (Figure 1.11 (a)). The process results in a strong absorption considered as an absorption edge (Figure 1.11 (c)). There are many possible allowed transitions based on the selection rules (Figure 1.11 (b)), which leads to many absorption edges in the X-ray absorption spectra. If electrons are excited from the K-shell, transitions are considered K-edge absorption. The same naming principle applies for L-shell and M-shell electrons.

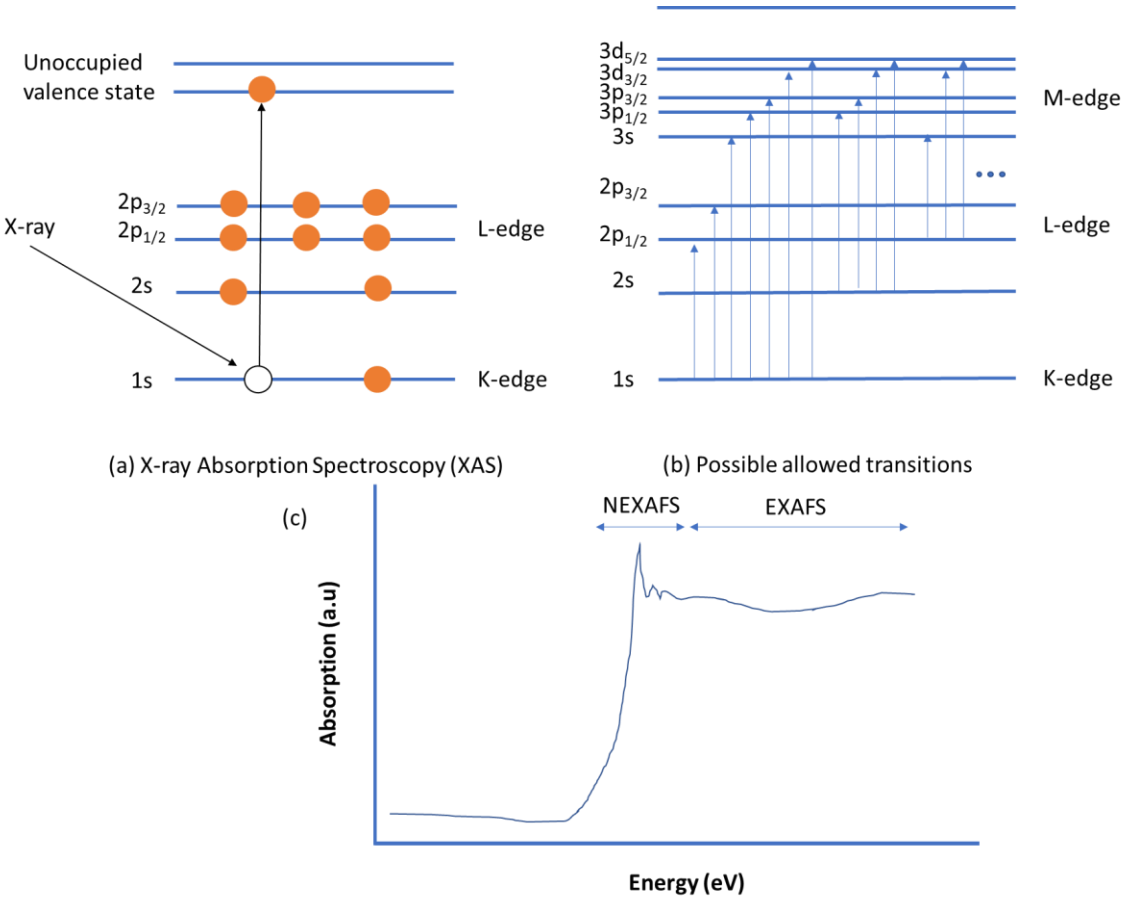

Figure 1.11. X-ray Absorption Spectroscopy (XAS) principles.

There are two regions in X-ray absorption spectra. Near-edge X-ray Absorption Fine Structure (NEXAFS) and Extended X-ray Absorption Fine Structure (EXAFS) regions. NEXAFS locates in the vicinity of the absorption edge. Besides the main transition peak, other sharp peaks are attributed to the scattering of photoelectrons and other transitions. NEXAFS provides information that can relate to the chemical structure of molecules.

f) X-ray Photoelectron Spectroscopy (XPS)

X-ray photoelectron spectroscopy (XPS) is a powerful surface-sensitive characterization technique, where only the top 10 nm of the sample is irradiated by a bright X-ray beam. Figure 1.12 shows the principle of XPS measurement. Instead of moving into unoccupied orbitals, the core electron that is bombarded by X-rays is emitted as element-specific photoelectrons[122–124]. By measuring the kinetic energy (KE) of emitted photoelectrons, their binding energy (BE) can be calculated by the following equation.

$$KE = hv - BE$$

In which, hυ is the incident photon energy. BE and KE are the binding energy and kinetic energy of photoelectrons, respectively.

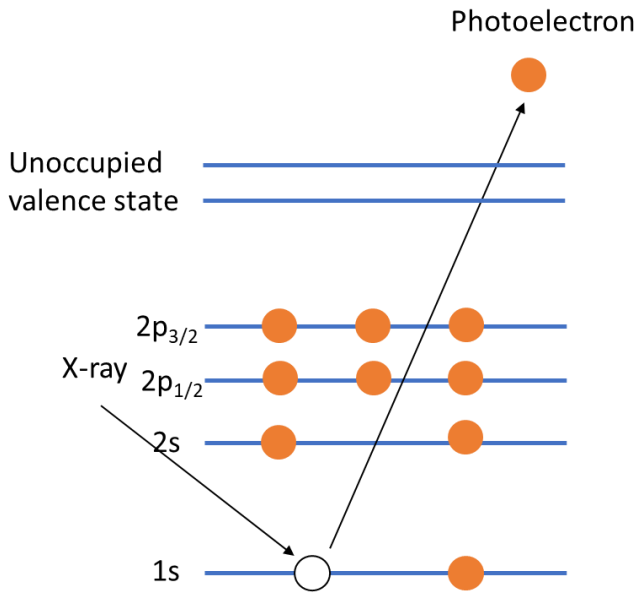

Figure 1.12. X-ray Photoelectron Spectroscopy (XPS).

Studying the binding energy of photoelectrons allows a better understanding of the electronic and chemical structure of elements and their surrounding environment. Given the complexity of PPy:CMC composites, XPS measurement enabled the identification of component arrangement and PPy doping agent. The details on sample preparation, data collection, and treatment were provided in Chapter 3.

g) Electrical conductivity measurement

The electrical conductivity of PPy:CMC samples were measured by means of the Four-point Probe Method on Miller Design FPP-5000 instrument. The tip spacing of the instrument is 1.59 mm. Typically, PPy:CMC composites were ground into powder by agate mortar and pestle. Approximately 100 mg of fine PPy:CMC powders were compressed at 200 MPa using a hydraulic press to form ½-inch pellets with an average thickness of 0.6 mm. By applying a direct current (DC) between the two outer probes, the potential difference between the two inner probes was measured (Figure 1.13). Because of its small thickness, the pellet is considered a thin sheet, whose electrical resistivity can be measured by the following equation:

$$\rho = \frac{\pi t}{ln2}\left(\frac{V}{I}\right) = \frac{\pi t}{ln2}R$$

in which t is the pellet thickness, R is the resistance recorded by the instrument[125]. Then, the electrical conductivity of PPy:CMC composites are calculated as $\sigma = \frac{1}{\rho}$ (S.cm^{-1}).

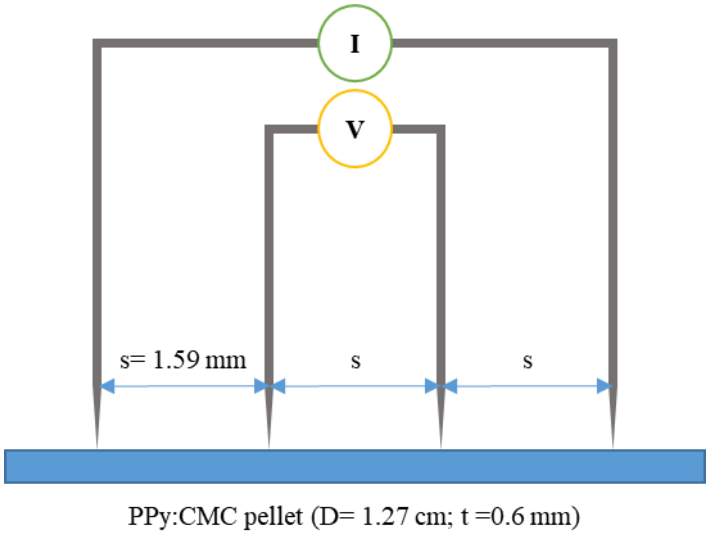

Figure 1.13. Schematic diagram of Four-point Probe measurement.

2) Coin cell fabrication

a) Working principles

The working principle of full-cell Li-ion batteries is well-documented in the literature[110,126]. In the full-cell battery configuration, the anode is often made of graphite and PVDF/C electrode matrix, while the cathode is made of intercalation materials such as $LiCoO_2$, NMC111, and PVDF/C electrode matrix. Testing full-cell Li-ion batteries require careful mass-balancing to avoid lithium plating[127]. The performance of full-cell Li-ion batteries is also affected by both anode and cathode preparation. Because this work focuses on testing the performance of cathodes constructed from mixtures of active materials and PPy:CMC composites, using half-cell battery configuration allows fast, reliable characterizations of electrode matrix performance. Figure 1.14 demonstrates the structure of a half-cell Li-ion battery. Lithium metal was used as an anode as well as a reference electrode. PVDF/C mixtures and PPy:CMC composites were used as electrode matrices and their performances were compared.

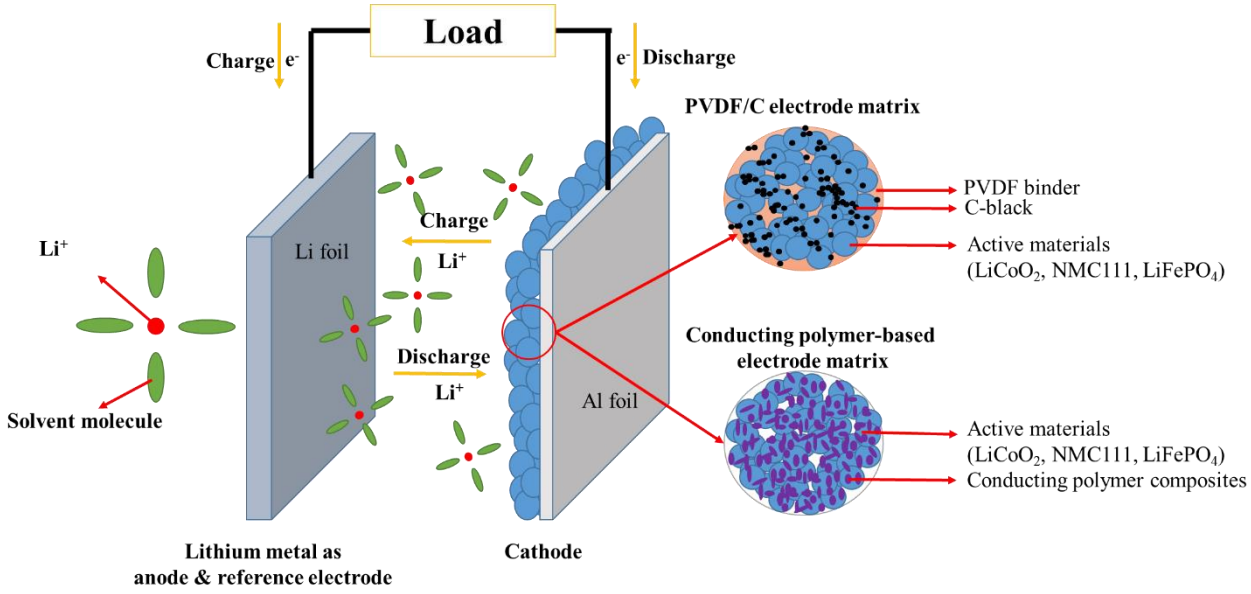

Figure 1.14. Schematic diagram of a half-cell Li-ion battery for testing cathode performance.

Upon charging, a current is applied between positive and negative electrodes so that electrons from d-orbital of transition metals are withdrawn from the hosting materials such as (LCO), $LiMn_{0.33}Ni_{0.33}Co_{0.33}O_2$ (NMC 111), and $LiFePO_4$ (LFP) to move towards the negative terminal via an external circuit. Simultaneously, lithium ions are removed from the layered structure of $LiCoO_2$, NMC111, LFP and dissolved into battery electrolyte and further deposited on lithium metal. At this stage, Li-ion batteries are storing energy. The transition metals of the positive electrode materials such as $LiCoO_2$, NMC111 are partially oxidized. During the discharging process, lithium metal is being oxidized, releasing lithium ions into the electrolyte. Subsequently, lithium ions are intercalated back into the structure of active cathode materials such as Li_xCoO_2. Likewise, electrons are moving from the negative to positive electrodes but through the external circuit.

b) Coin cell fabrication procedure

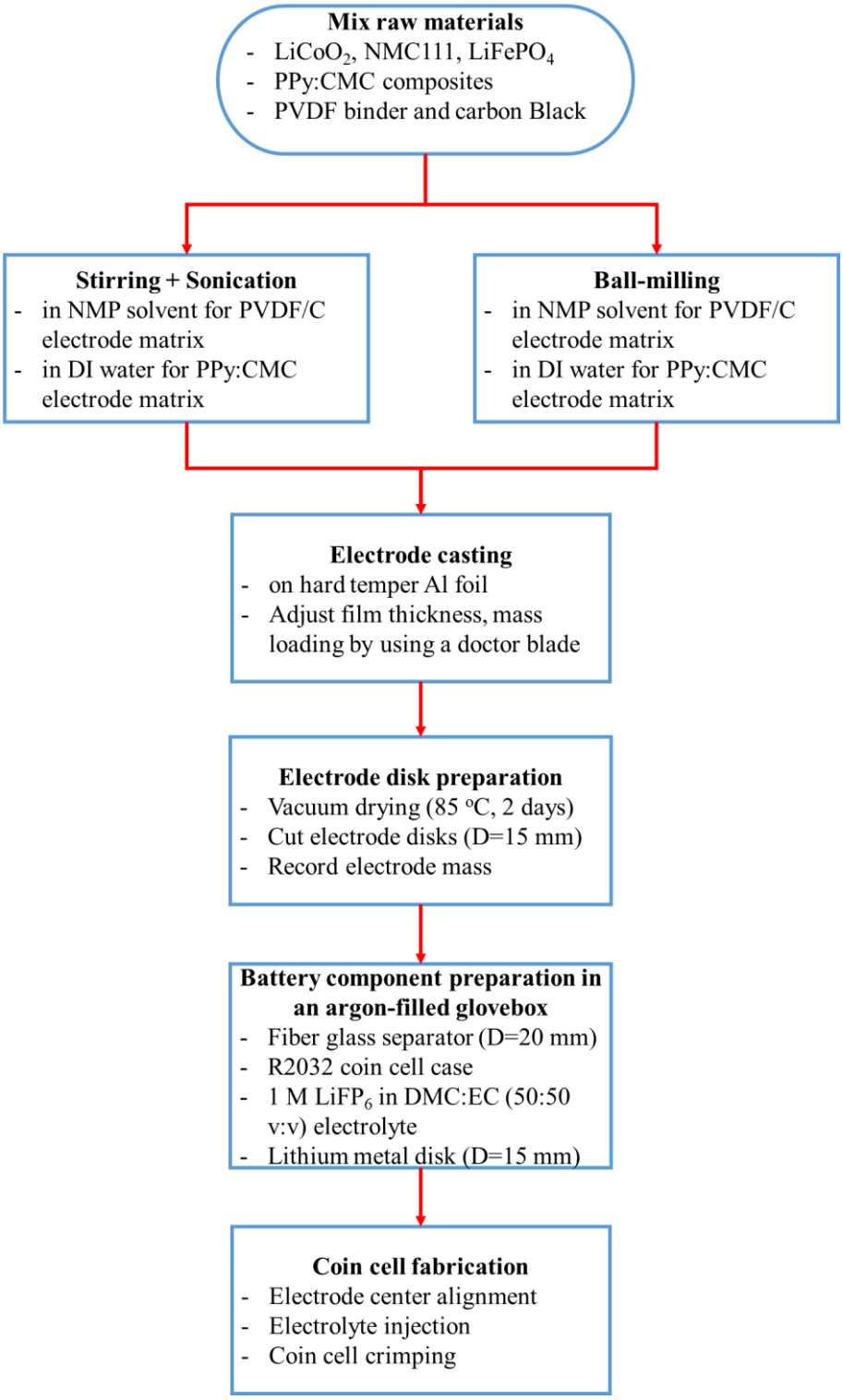

Figure 1.15. The procedure of making coin cell Li-ion batteries.

Coin cells are the most reliable types of battery cells that allow rapid battery electrode evaluation in the initial research stage. The most common types of coin cells are CR2032-type coin cells, which means that these coin cells have a diameter of 20 mm and a thickness of 3.2 mm. A typical procedure for fabricating CR2030-type coin cells is described in Figure 1.15. Firstly, raw materials must be mixed by ball-milling or mechanical stirring in water for PPy:CMC electrode matrix or NMP solvent for PVDF/C electrode matrix. The solid content in electrode slurries must be controlled to ensure suitable electrode viscosity. The electrode slurries were then cast on temper hard aluminum foil by using a doctor blade to control electrode thickness and mass loading. The wet electrode films were dried in a vacuum oven for 2 days at 85 ^{o}C. The dried electrode film was cut into 15 mm in diameter electrode disks. Coin cell fabrication was performed in an argon-filled MBRAUN UNIlab glove box with oxygen and moisture levels below 0.1 ppm. Figure 1.16 shows the structure of a CR2032 coin cell that was used to test battery performance. After aligning electrodes in the center of the coin cell, the electrolyte was injected. Finally, coin cells were crimped to prevent electrolyte leakage.

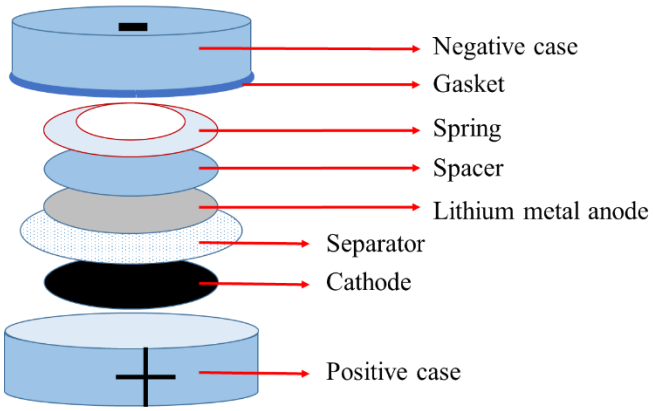

Figure 1.16. Schematic diagram of a CR2032 coin cell.

3) Battery testing

The electrochemical performance of coin cells was quantitatively evaluated employing galvanostatic cycling, differential capacity analysis, and electrochemical impedance spectroscopy (EIS).

a) Galvanostatic charge/discharge cycling

During galvanostatic cycling, a constant current is applied between positive and negative terminals, causing the movement of lithium ions between two electrodes. As a result, a potential difference between two electrodes, commonly referred to as cell voltage, is changing with time. To simplify the naming, electrodes with $LiCoO_2$ or NMC111 active materials are referred to as cathodes.

The galvanostatic charge/discharge measurement was carried out by the Neware battery cycler, which controls the applied current density and measures cell voltage. The cell voltage must stay within a fixed potential window. Charging a battery cell beyond the potential window or discharging a battery cell below the potential window will cause permanent damages to battery materials such as irreversible phase transitions of active materials, and oxidation of electrolytes. The operating potential window of Li-ion batteries depends on the types of active materials and supporting electrolytes. For example, $LiCoO_2$-based cathode can be cycled between 2.8 V and 4.2 V vs Li/Li^+ with the commercial electrolyte of 1 M $LiFP_6$ in EC:DMC (1:1 v:v).

The applied current density (*I)*) is determined by dividing the theoretical specific capacity of battery materials (Q) to the testing time for one charging or discharging step (t).

$$I = \frac{Q}{t} = \frac{(mAh.g^{-1})}{h} = mA.g^{-1}$$

To standardize testing parameters, most battery manufacturers have used the term "C-rate" to describe how fast battery cells are being charged or discharged. C-rate is inversely proportional to the length of time that a battery cell is charged or discharged. For example, a battery cell charged at a fixed C-rate of 0.1 C means that the battery cell will finish charging or discharging in approximately 10 hours.

$$C\text{—}rate = \frac{1}{t}$$

$$I = Q \times C\text{—}rate$$

The data from the galvanostatic charge/discharge cycling can be plotted as voltage versus capacity plot or voltage profile in this work. Another way to describe the cycling performance is by plotting charge/discharge capacity and coulombic efficiency versus cycle numbers. The

coulombic efficiency is the ratio between discharge and charge capacity, which is usually less than 100%.

$$CE = \frac{Discharge\ Capacity}{Charge\ Capacity} \times 100\%$$

b) Differential Capacity Analysis (dQ/dV)

Differential capacity plot (dQ/dV versus V) shows the amount of charge being stored per change in cell voltage as a function of cell voltages. By analyzing the differential capacity plot, the redox reaction of electrode materials will be easier to study. For example, when electrode active material such as $LiCoO_2$ undergoes reversible redox reaction during the phase transitions upon charge/discharge process (Ex: $LiCoO_2 \leftrightarrow Li_xCoO_2$), there is a sharp increase in charge storage at redox potentials in the dQ/dV vs. V plot. Simultaneously, there is a plateau in the voltage profile of that electrode. In Chapter 5, differential capacity analysis is used to check whether conducting polymers participate in redox processes at battery electrodes during cycling or not.

c) Electrochemical Impedance Spectroscopy (EIS)

Impedance is the opposition of electrical circuits upon the application of alternating current. By applying an alternating current (AC) potential (E(t)) into a measurement cell, the response current (I(t)) is recorded to calculate cell impedance (Z) as the following equation:

$$Z = \frac{E_t}{I_t} = \frac{E_o \times sin(\omega t)}{I_o \times sin(\omega t + \phi)} = Z_o \times \frac{sin(\omega t)}{sin(\omega t + \phi)}$$

In which ω and ϕ are radical frequency and phase shift, respectively. Cell impedance (Z) can also be presented as a complex number:

$$Z = Z_o e^{j\theta} = Z_o\big(\cos(\theta) + j\sin(\theta)\big)$$

The EIS results can be visualized by bode plot (Phase vs Frequency) and Nyquist plot (Z_{img} vs Z_{real}). EIS analysis allows measuring electrode impedance that can relate to the chemistry of battery cells. Normally, cell impedance increases over charge/discharge cycles as a result of growing passivation layers, electrical contact loss, and so on. Therefore, EIS can be used as a non-destructive technique to monitor and predict changes in battery performance[128].

It is a common practice to build an EIS equivalent circuit containing several circuit elements, connected in series or parallel, to represent electrochemical processes in Li-ion battery cells. Electrolyte resistance is recorded at a high frequency. A Randles circuit is usually used to depict electrochemical phenomena at battery electrodes. The Randles circuit consists of charge transfer resistance in series with the Walburg element, which was then connected in parallel with the constant phase element (CPE). The charge-transfer resistance is the resistance during the charge transfer process at the electrode interface. The Walburg element represented the diffusion of ions in battery cells. Meanwhile, the constant phase element mimicked the behavior of the double-layer capacitor as a result of charge buildup at the electrode surface. In Chapter 5, EIS measurement is employed to acquire information about the cell performance of $LiCoO_2$-based cathodes.

IV. Research objectives

Developing alternative electrode matrices seems to be a rational approach that opens the bottleneck in battery technology development[4]. This study focuses on designing an alternative class of electrode matrices derived from the unique combination of conducting polymers (CPs) and aqueous carboxyl-containing polymers. Because cathode is the determining component in terms of battery cost and performance[34,129], within the scope of this study, the performance of new electrode matrices will be tested solely at the cathode.

The study is divided into several main tasks:

1. ***Developing the synthetic concept for CP composites as electrode matrices.***

For practical wide-scale applications, the synthetic process was designed to be facile and compatible with the current method of producing bulk CPs. Conceptually, CP monomers (aniline, pyrrole) were *in situ* polymerized in the presence of carboxyl-contained polymers (CMC, SA, PAA) to yield CP composites. Among several composites synthesized, polypyrrole:carboxymethyl cellulose (PPy:CMC) composite shows the most promising preliminary results. As a result, this study focused mainly on exploring PPy:CMC composite as a representative for the class of conducting polymer-based electrode matrices.

2. ***Studying the structure and properties of PPy:CMC composites.***

The formation of PPy:CMC composite structure was investigated by the means of Transmission Electron Microscopy coupled with Energy Dispersive X-ray detector (TEM/EDX),

Scanning Electron Microscopy (SEM), X-ray Photoelectron Spectroscopy (XPS), and X-ray Scanning Transmission Microscopy (STXM). The physical properties of PPy:CMC composites such as electrical conductivity, water-processability, film-adhesion ability were also investigated.

3. ***Fabricating and testing carbon-additive-free cathodes with PPy:CMC composites as electrode matrices***

Carbon-additive-free cathodes contained PPy:CMC composites and cathode intercalation materials such as commercial $LiCoO_2$ (LCO), lab-synthesized $LiMn_{0.33}Ni_{0.33}Co_{0.33}O_2$ (NMC 111). The galvanostatic charge/discharge process was performed at different C-rate to evaluate the cycling performance and rate-capability of carbon-additive-free electrodes, which allowed the performance assessment of CP composites in comparison to that of the PVDF/C electrode matrix.

4. ***Studying the compatibility of PPy:CMC composites in Li-ion battery cells.***

Post-mortem analyses were carried out to investigate the chemical and electrochemical stability of PPy:CMC composites during the operation of Li-ion batteries. The degradation mechanism of carbon-additive-free $LiCoO_2$/PPy:CMC cathode was investigated. Such investigation would address knowledge gaps and proliferate further applications of CP composites in Li-ion batteries.

The thesis contains 6 chapters:

- Chapter 1 provides an overview of Li-ion battery architecture and highlights the need for developing new battery electrode matrices. Brief reviews of Li-S batteries and Na-ion batteries are also added to emphasize that designing alternative electrode matrices is crucial for the next generation of rechargeable batteries. Besides that, a short introduction of CPs is added to provide general concepts of CPs and their conduction mechanism.
- Chapter 2 reviews the use of CPs and their composites as electrode binders/matrices. This chapter also mentioned some knowledge gaps that needed to address for future utilization of CPs in Li-ion batteries.
- Chapter 3 describes the design concept of CP-based electrode matrices. PPy:CMC composites were chosen as representatives for CP-based electrode matrices as a proof of concept. The structure and properties of PPy:CMC composites were studied to access their ability to be used as electrode matrices. The fabrication of carbon-additive-free $LiCoO_2$/PPy:CMC cathodes was described in this chapter, followed by battery testing to evaluate the performance of PPy:CMC electrode matrices.

- Chapter 4 presents the fabrication of carbon-additive-free NMC111/PPy:CMC cathodes, which indicated the versatility of PPy:CMC electrode matrices.
- Chapter 5 focuses on studying the causes of capacity fading of $LiCoO_2$/PPy:CMC cathodes. Furthermore, an activation protocol for CP-based electrode matrices is proposed with some supporting evidence from the voltage profiles of $LiCoO_2$/PPy:CMC, NMC111/PPy:CMC $LiCoO_2$/PANI:CMC cathodes.
- Chapter 6 summarizes the research findings and provides future research suggestions.

Chapter 2. Conducting Polymer-Based Binders for Lithium-Ion Batteries and Beyond

Abstract

This review chapter focuses on reviewing the current progress in using CPs and their derivatives as battery binders or electrode matrices for Li-ion batteries. Main research strategies on how to incorporate CPs into Li-ion batteries were discussed and evaluated. Besides that, the application of CPs and their composites in other types of rechargeable batteries were also mentioned to signify their versatile and promising applications. The review suggested that combining CPs with carboxylate-containing aqueous binders could yield promising battery electrode matrices. But this approach has not been carried out, which motivates this research project. Knowledge gaps in understanding the compatibility of CPs in Li-ion batteries were also mentioned.

I. Introduction

In the era of smart electronic devices and electric vehicles, rechargeable Li-ion batteries have become an indispensable technology. The award of the 2019 Nobel Prize in Chemistry to John B. Goodenough, M. Stanley Whittingham, and Akira Yoshino includes implicitly a recognition of the first application of conducting polymers in Lithium-ion batteries. Yoshino's pioneering work on Li-ion batteries dates back to the 1980s when he used polyacetylene (PA), a conducting polymer, as an anode material and combined it with a $LiCoO_2$ cathode, which was invented by Goodenough[130], to form a $LiCoO_2$/PA full cell Li-ion battery[126]. The working principle of Li-ion batteries relies on the lithium intercalation electrochemistry of electrode materials, which was developed by Whittingham in the 1970s[131]. Even though polyacetylene functions well in Li-ion batteries, it has some drawbacks, such as low density and chemical instability. To overcome these issues, Yoshino replaced PA by carbonaceous materials as the anode, which resulted in the invention of the widely used $LiCoO_2$/C Li-ion batteries. Since its first commercialization in 1991, lithium-ion batteries have quickly proceeded to dominate the rechargeable battery market due to their versatile design, low weight, and high power density[110,132].

In recent years, to keep track of the fast development of electronic devices, tremendous research effort has been devoted to the pursuit of new generation Li-ion batteries, in which batteries

can store more energy and run for a longer time without degradation or safety issues. A cursory view of the relevant literature shows that most research focuses on developing cathode and anode active materials. At the anode, graphite is being replaced by silicon, tin, and titanium-based nanostructures, which possess higher theoretical energy capacity compared to graphite[40,133–138]. However, as these materials store more lithium, they also exhibit larger volume expansion and contraction during cycling. For example, the volume of silicon (Si) particles upon full lithiation is three-times larger than that of the fully delithiated Si[139]. Such repeated variations in particle size induce cracking and pulverization of the anode, which subsequently results in mechanical and electrical contact loss, side reactions, and capacity fading[37,139,140]. At the cathode, traditional $LiCoO_2$ (LCO) is being substituted by materials with lower Co content to reduce cost and sourcing restrictions, such as $LiFePO_4$ (LFP)[34,141], $Li[Ni,Co,Mn]O_2$ (NMC)[39,142,143], and $Li[Ni,Co,Al]O_2$ (NCA)[144]. Among them, $LiFePO_4$ exhibits thermal stability[145], inexpensive synthesis[29,146,147], considerable specific capacity (170 $mAh.g^{-1}$)[148], and high cycling stability[33], but shows a low voltage plateau (~3.5 V)[148],[31]. NMC and NCA have gained a widespread application as intercalation materials, with high specific capacity at approximately 200 $mAh.g^{-1}$ and 234 $mAh.g^{-1}$ for NCA and NMC, respectively, but lower cycle life because of ion-dissolution[149], phase changes[150,151], and electrode cracking[152]. These effects obstruct the replacement of $LiCoO_2$ cathode materials[112,149,153].

A closer look at the electrode structure of alternative electrode materials suggests that many of their performance problems originate in weak electrode interconnection, in which battery binders play a central role. Good binders should maintain electrode integrity even in the case of large volume changes and suppress ion-dissolution and side-reactions through a strong binding affinity towards active materials. Even though Polyvinylidene fluoride (PVDF) is the most successful and widely used binder for conventional lithium batteries, it exhibits several limitations. First of all, the non-polar structure of PVDF is only able to form weak intermolecular interactions with active materials and current collectors[154,155]. Therefore, over repeated charge/discharge cycles, the homogeneous composite structure of the pristine electrode is disrupted due to substantial volume changes, leading to mechanical failure and capacity decay. Secondly, the electrically insulating nature of PVDF requires the addition of carbon additives to boost the electrical conductivity of electrodes. In traditional Li-ion batteries, carbon additives are essential for providing electron-conducting networks within battery electrodes. However, carbon additives

tend to agglomerate, which increases internal resistance[115,156]. Furthermore, since the PVDF/C mixture exhibits little capacity on its own, adding carbon additives reduces the overall battery energy density. Lastly, the environmental concern of using volatile and toxic N-Methyl-2-pyrrolidone (NMP) solvent during the casting process of PVDF/C/active-material electrodes also needs to be considered.

Several studies have pointed out that cyclability problems of some of the most promising advanced anode and cathode materials could be alleviated by using more efficient battery binders[90,140,154,157,158]. The ideal electrode matrix should be able to 1) form strong interactions with active materials to maintain adhesion over cycling; 2) offer strong adhesion towards current collectors to prevent electrode delamination; 3) provide a continuous conductive network within the electrode; 4) exhibit sufficiently high failure strain to accommodate volume changes during charge/discharge cycling without breaking; 5) be electrochemically and chemically stable in the harsh battery environment; 6) be applicable with the slurry casting method to be compatible with current electrode fabrication facilities; 7) be accessible at low cost to commercialize at wide-scale.

Several research groups have been searching for alternative binders that can be applied for high energy density batteries such as sodium carboxymethyl cellulose (CMC)[90,159–162], sodium carboxymethyl chitosan (CCTS)[49,99,163–165], sodium alginate (SA)[149,166–169], styrene-butadiene rubber (SBR)[159,170], or polytetrafluoroethylene (PTFE)[171–173]. Many of these binders exhibit strong polar interactions, even hydrogen bonds, with the surfaces of cathode intercalation and anode conversion materials, due to the presence of hydroxyl and carbonyl groups. This same chemistry makes them also more easily dispersed in polar solvents, allowing for aqueous processing. Just as other standard binders, these polymers are insulating, necessitating the addition of carbon powders. This can be overcome by the use of CPs as binders. CPs exhibit a backbone with an extended π-electron network. Undoped CPs are semiconductors. However, upon doping, the electrical conductivity of CP changes significantly to metallic-like electron conduction[105]. Dopants partially oxidize or reduce the polymer chain backbone which creates charge carriers within the extended π-electron network. Even though CPs have been widely used in many industrial applications[105,174–176], the use of CPs as binders for lithium-ion batteries has been restricted because of difficulties in their processing. These polymers exhibit low thermal

stability, making melt processing difficult, and few CPs can be directly dispersed in solvents for solution processing.

Acknowledging contributions of conducting polymers to energy storage, several reviews have summarized the design concept and application of CP-based structures for energy storage and conversion in general[46,47,177,178]. The present review emphasizes the most recent research advancements on developing CP-based battery binders. The first section summarizes and evaluates how CPs can be implemented into battery electrode structures of Lithium-ion batteries. Three routes addressing the processing of pristine CPs are evaluated. The second part describes the application of CP-based binders for next-generation rechargeable batteries, in particular, lithium-sulfur (Li-S), all-solid-state Li-ion, and sodium-ion (Na-ion) batteries. The third part discusses the knowledge gap in the understanding of CP-based binder properties.

II. Major research directions in conducting polymer-based binders

1) Conducting polymer composites

Even though CPs possess a tunable electronic conductivity, the processing of CPs is a challenging obstacle to overcome in their application as battery binders. One of the most straightforward strategies to obtain processable CP-based binders is forming composites of CPs and hydrophilic polymers. CPs can originate from monomers such as 3,4-ethylenedioxythiophene (EDOT), pyrrole, aniline, or thiophene. Water-dispersible polymers can be natural or artificial polymers containing hydrophilic groups such as carboxylate or sulfate groups. The most well-known representative of this group, poly(3,4-ethylenedioxythiophene):poly(styrene sulfonate) (PEDOT:PSS), is described in the next section. The following subsections discuss the synthesis of CP composites and their performance as binders in lithium-ion batteries.

1.1) PEDOT:PSS composites

PEDOT is a commercial conducting polymer that can also be purchased in an aqueous dispersion with PSS. The latter serves as a dispersive agent as well as an ionic dopant for PEDOT. The electrical conductivity of PEDOT:PSS composites could be enhanced significantly by adding additional dopants such as formic acid[119] or sulfuric acid[179] (secondary doping) or changing the proportions of PEDOT and PSS[120]. Mixtures of PEDOT:PSS and active materials are also compatible with aqueous slurry casting[32,104,119,120,180–184]. Moreover, some preliminary research has successfully used PEDOT:PSS as a binder component in anode and cathode

structures[161,185,186], suggesting that PEDOT:PSS has sufficient electrochemical stability over the operating potential window of Li-ion batteries. Due to these intriguing properties, PEDOT:PSS has been widely researched as a battery binder in both anode[119,181–184] and cathode[120,180] formulations of Li-ion batteries.

PEDOT:PSS composites could be either used directly or mixed with hydrophilic substances to modify its wettability and processability. With regard to the cathode, PEDOT:PSS was applied as a binder for the cathode of common intercalation materials such as LFP[32,104,180,187], and $LiNi_{1/3}Mn_{1/3}Co_{1/3}O_2$ (NCM 111)[180]. For example, Zhong *et al.* utilized a mixture of CCTS/SBR/PEDOT:PSS/C (1.6:2.4:3:3 wt%) as an alternative for PVDF/C in an LFP-based cathode[180] (Figure 2.1). By using self-conductive PEDOT:PSS composite, the proportion of carbon additives can be reduced by half to only 3 wt% of the electrode. They found that PEDOT:PSS binder formed continuous conductive bridges around LFP particles resulting in superior electrode performance even at a low loading of PEDOT:PSS. The electrode with PEDOT:PSS-containing binder could achieve a specific capacity of 155 $mAh.g^{-1}$ at C/2 and maintain ~100 % of its capacity after 1000 cycles. Moreover, the electrode could retain 98% capacity after 1000 cycles at 7 C, compared to 95% of PVDF/C/LFP electrode. Another study reported the use of a carbon-free LFP/PEDOT:PSS cathode, in which commercial PEDOT:PSS composite played a dual role as binder and conductive additive[32]. They reported that using solely PEDOT:PSS binder at only 8 wt% could lower the overpotential and subsequently improve capacity retention of the LFP/PEDOT:PSS cathode, which was 13% higher than LFP/PVDF/C (84:6:10 wt%) at charge and discharge rates of 5 C. This was observed in a system where the LFP/PEDOT:PSS cathode achieved a specific capacity of 110 $mAh.g^{-1}$ at 1 C without fading after 100 cycles compared to ~90 $mAh.g^{-1}$ of a LFP/PVDF/C (84:6:10 wt%) benchmark electrode[32].

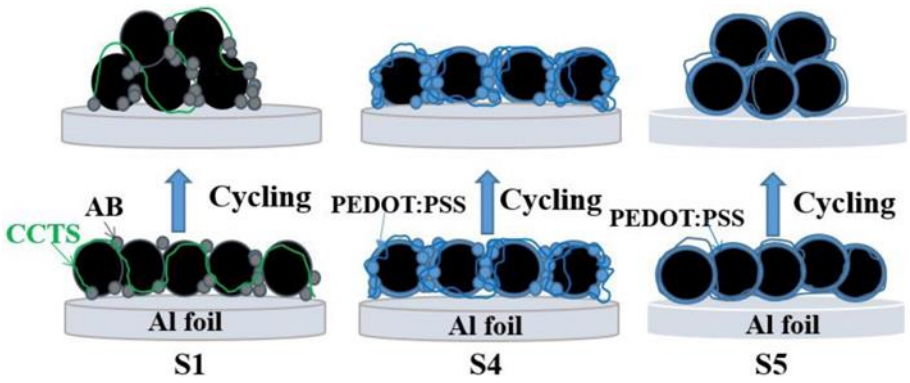

Figure 2.1. Application of PEDOT:PSS-based binder for LFP cathode. Schematic structures of cathode before and after cycling. From left to right: LFP/CCTS/SBR/C (S1); LFP/ CCTS/SBR/PEDOT:PSS/C (S4); LFP/ CCTS/SBR/PEDOT:PSS. Reprinted from reference [180]. *Copyright (2016), with permission from Elsevier.*

Apart from being used in cathodes, some studies exploited PEDOT:PSS composites as electrically conductive binders in advanced battery anodes, in which widely-used graphite (370 $mAh.g^{-1}$) is being replaced by materials that store more charge such as Si (3572 $mAh.g^{-1}$)[188] and Sn (990 $mAh.g^{-1}$)[189]. One of the main issues of increasing capacity in active materials to such high values is the intrinsically increased volume change during cycling. The PVDF/C matrix cannot withstand this mechanical stress, resulting in the breaking of electronic connections between active material and matrix, as well as within the matrix, leading eventually to significant capacity fade.

One study demonstrated the use of aqueous mixtures of PEDOT:PSS and CMC as battery binders for Si anodes, which resulted in superior initial capacity and capacity retention[181]. The PEDOT:PSS/CMC binders were easily prepared by homogeneously dispersing commercial PEDOT:PSS solution into aqueous CMC solution[181]. This combination exhibits the advantages of PEDOT:PSS, namely electronic conductivity and electrochemical stability, that can reduce the content of carbon additives in the electrode. Moreover, it benefits from the strong interaction between CMC and Si and Sn materials[137,162,165,183,190–192], which can buffer volume changes to ensure mechanical integrity of the electrode. For example, the interaction between Si and CMC, which involves physical adhesion, carboxyl-silanol covalent bonding as well as hydrogen bonding[193], might alleviate mechanical cracking of Si-based anodes.

Several Ti-based compounds are used as anode materials, among them $Li_4Ti_5O_{12}$ (LTO) has found significant commercial attention[194]. $Li_4Ti_5O_{12}$ exhibits virtually no strain upon cycling and has found particular attention in high-power applications. However, $Li_4Ti_5O_{12}$-based anodes with PVDF/C were reported to suffer from irreversible changes in surface composition, causing structural instability and capacity degradation[194,195]. To address the stability issue, Kondratiev *et al.* employed PEDOT:PSS/CMC binders[183] and found that this approach could reduce exposure of $Li_4Ti_5O_{12}$ to electrolyte, thus reducing interfacial side-reactions and irreversible structural changes without blocking Li-ion conduction pathway. The $Li_4Ti_5O_{12}$-based anode showed good cycling stability with ~1% capacity fading after cycling 100 cycles at 1 C.

Despite yielding promising results as binders for lithium-ion battery anode and cathode, in these studies, PEDOT:PSS composites needed to be mixed with non-conductive binders such as CMC, PVDF, or SBR along with carbon additives to fabricate electrodes[119,180], lowering the energy density of the electrode. Yet, PEDOT:PSS can theoretically serve as a single multi-functional binder, due to its tunable conductivity and elasticity. Recently, some studies have made the full replacement of PVDF/CMC/C by one single PEDOT:PSS binder possible. Nicolosi *et al.* found that utilizing commercially available PEDOT:PSS as a sole binder component in a Si-anode could yield an outstanding battery performance with high initial capacity and cycle life[119] (Figure 2.2). This study used formic acid (FA) as a secondary doping agent to increase PEDOT:PSS electrical conductivity by two orders of magnitude compared to pristine commercial PEDOT:PSS, which were 4.2 S/cm and 36 mS/cm for FA-PEDOT:PSS and PEDOT:PSS, respectively. Due to the high dielectric constant, FA could partially replace negatively charged PSS ions that were bonded to positively charged PEDOT chains, effectively removing excess insulating PSS from the PEDOT:PSS structure[119,196]. The high electrical conductivity of FA-PEDOT:PSS enabled it to be used as a single conductive battery binder. A carbon-free (FA-PEDOT:PSS)/Si-NPs 20:80 wt% anode with a mass loading of ~1 g/cm^2 showed excellent initial lithiation capacity up to 3685 $mAh.g^{-1}$ at 0.14 C, but only 78% coulombic efficiency was achieved in the 1st cycle. The following galvanostatic cycling at 0.28 C yielded 1950 $mAh.g^{-1}$ after 100 repeated cycles. However, longer cycling data were not reported, leaving a question about electrochemical stability and capacity retention.

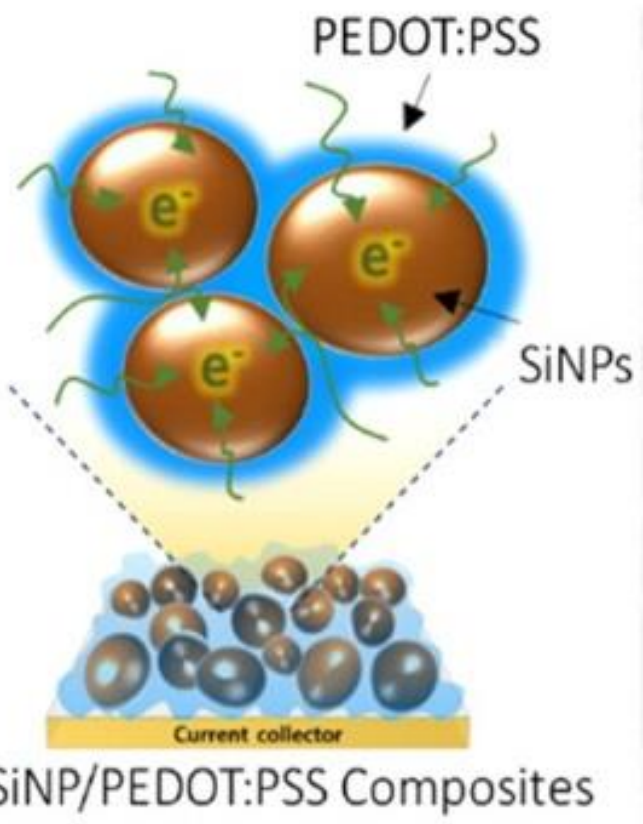

Figure 2.2. Application of PEDOT:PSS composite as a multifunctional binder for Si anode. Schematic structure of PEDOT:PSS/Si-NPs anode. Reprinted with permission from reference [119]. *Copyright 2016 American Chemical Society.*

Another study reported the facile coating of commercial PEDOT:PSS composite on LCO to yield a cathode made solely of PEDOT:PSS-skinned LCO particles (Figure 2.3). A 25-nm ultrathin layer of PEDOT:PSS acted as a multifunctional binder for LCO[120], providing both physical connections and mixed electronic-ionic pathways between LCO particles. The electrical conductivity of the PEDOT:PSS layer, which was vital for utilizing PEDOT:PSS as a single binder, was controlled by varying the PSS content and modifying polymer conformation. Thanks to the low binder loading of only ~ 0.4 wt%, a good energy density cathode could be obtained with reasonable electrode thickness and mass loading of 55 μm and 27 $mg.cm^{-2}$, respectively. The PEDOT:PSS-skinned $LiCoO_2$ electrode achieved a good initial specific capacity of ~ 100 $mAh.g^{-1}$, which remained at 81% after 150 cycles at 1 C.

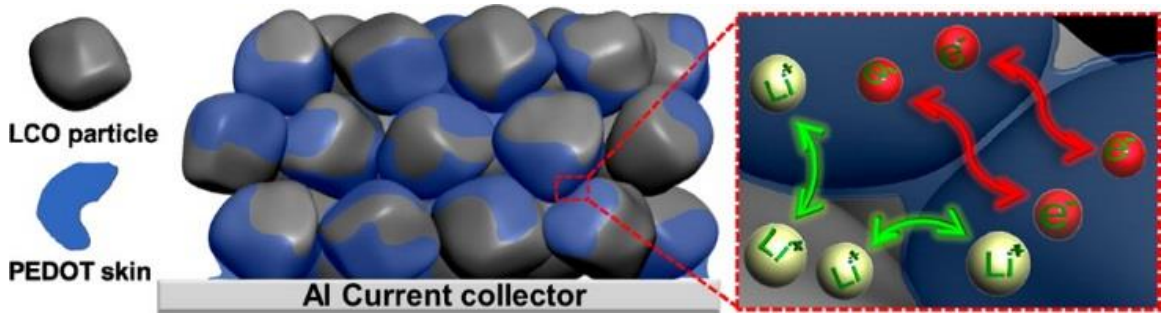

Figure 2.3. Application of PEDOT:PSS composite as a single, multifunctional binder for LCO cathode. Morphological structure of ultra-skinned PEDOT:PSS on LCO surface and ionic/electronic transport within LCO/PEDOT:PSS cathode. Reprinted with permission from reference [120]. *Copyright 2014 American Chemical Society.*

Applying commercially available PEDOT:PSS composites as battery binders seems to be a straightforward and efficient approach for achieving high energy density batteries. PEDOT:PSS binder provides robust conductive frameworks, replacing conventional PVDF/C while maintaining a competitive battery performance. Based on a summary of normalized capacities of electrodes with PEDOT:PSS-based binders (Table 2 and 3) PEDOT:PSS-based binders appear to be able to yield higher reversible energy storage capacities. Even though PEDOT:PSS binder shows promising results, the cost of PEDOT:PSS is significantly higher than the PVDF/C matrix. Further innovation in synthesizing and purifying PEDOT:PSS in an economical manner could allow the wide-spread use of this particularly successful CP-based binder in commercial batteries.

Table 2. Conducting polymer binders and cathode materials: capacities normalized by electrode weight.

Electrodes	**C-rate (C)**	**Normalized discharge capacity ($mAh.g^{-1}_{electrode}$)**	**References**
LFP/PEDOT:PSS/SBR-CTS/C (90:3:4:3 wt%)	0.2	140	[180]
LFP/PEDOT:PSS (92:8 wt%)	0.2	110	[32]
	1	97	
LFP/PVDF/C (84:6:10 wt%)	0.2	94	
	1	76	
LFP/SA-PProDOT (80:20 wt%)	0.1	136 (400 cycles)	[197]
	1	96 (400 cycles)	
Hydrogel-derived Cu-PPy/C-LFP (~ 15:85 wt%)	1	128	[178]
		~128 (1000 cycles)	
LCO/PEDOT:PSS-Skinned (99.6:0.4 wt%)	0.2	140	[120]
LCO/PVDF/C (95:3:2 wt%)	0.2	133	
(*In situ polymerized* PANI/LiV_3O_8)/PVDF/C (85:10:5 wt%)	0.1	204	[198]
		195 (30 cycles)	
	1	157	
		160 (55 cycles)	

Table 3. Conducting polymer binders and anode materials: capacities normalized by electrode weight.

Electrodes	**C-rate (C)**	**Normalized discharge capacity ($mAh.g^{-1}_{electrode}$)**	**References**
Si/PEDOT:PSS/CMC/C (70:10:10:10 wt%)	~ 0.06 (0.2 $A.g^{-1}$)	2700	[181]
	~ 2.8 (10 $A.g^{-1}$)	609	
LTO/PEDOT:PSS/CMC/C (90:2:2:6 wt%)	0.2	141	[183]
	1	138	
Si/FA-PEDOT:PSS (80:20 wt%)	0.28	1542	[119]
Si/PANI:PAA (75:2.5:22.5 wt%)	0.1	1484	[199]
Si/PANI:(dopamine-grafted PAA) (75:2.5:22.5 wt%)	0.1	1964	[200]
Hydrogel-derived Si/PANI:PAA (80:14:6 wt%)	0.2	1,680	[201]
Sn/PFCOONa (80:20 wt%)	0.2	760	[136]
		416 (500 cycles)	
Si/PF-COONa (66.6:33.4 wt%)	0.1	2180	[202]
		1852 (100 cycles)	
SiO/PFM (95:5 wt%)	0.1	1140	[39]
		902 (500 cycles)	
SiO-SnCoC/PFM/C (80:5:15 wt%)	1	645	[203]
		556 (40 cycles)	

SiO-SnCoC/PFM/graphite/C (60:5:20:15 wt%)	1	408	
		368 (40 cycles)	
(*In situ polymerized* PEDOT:PSS/Si)/CMC/AB (60:8:30 wt%)	~ 0.024 (100 $mA.g^{-1}$)	516	[204]
		398 (20 cycles)	
		154 (50 cycles)	
Hydrogel-derived P-PANI/Si (~ 25:75 wt%)	~ 0.071 (300 $mAh.g^{-1}$)	1875	[205]
	~ 0.71 (3000 $mAh.g^{-1}$)	825	
	~ 0.24 (1000 m $mAh.g^{-1}$)	900 (1000 cycles)	
Hydrogel-derived Cu-PPy/C-Fe_3O_4) (~ 15:85 wt%)	0.1	1071	[206]
	1	851	
	~ 0.18 (100 $mA.g^{-1}$)	935 (55 cycles)	
Hydrogel-derived Sn@PANI-SA (~ 65:35 wt%)	0.2	534	[207]
		400	
Hydrogel-derived Si/P-PPy/CNT (~ 70 wt%Si; ~ 0.2 wt% CNT)	0.78	1120 (1000 cycles)	[48]

1.2) Conducting polymer/carboxyl-containing polymer composites

Alternative polymeric binders that mimic the PEDOT:PSS structure to allow aqueous slurry-based electrode casting and improved binding efficiency, but rely on a lower-cost binder production is another research direction for effective new binder and conductor systems. Recent publications have pointed out a promising class of binders that combines simpler CPs (polyaniline (PANI), polypyrrole (PPy), polythiophene (Pth)) with carboxylate-containing polymers (PAA, CMC, CCTS, SA). In such composite structure, CPs offer a continuous conductive matrix that facilitates ionic and electronic transport, while carboxylate-containing polymers serve as dopants for CPs, dispersing agents, and strengthen binder-active material bonding. There are two main ways to synthesize conducting polymer/carboxyl-containing polymer composites that involve mechanical blending and *in situ* polymerization.

Mechanical mixing is considered the easiest way to combine the advantages of different components. Each component is synthesized beforehand and then mixed to form composites. Kukjoo *et al.* reported a new composite binder of PANI:PAA for Si anodes. PAA was blended with PANI, in which a proton exchange between the PAA carboxyl group and the PANI amine group leads to a strong and lasting ionic interaction between the two polymers[199], yielding a self-conductive composite binder that allows the fabrication of a carbon-free (PANI:PAA)/Si-NPs anode. Moreover, carboxyl groups on the PAA structure formed strong hydrogen bonds with hydroxyl groups at the Si-NPs surface[208]. Such interactions resulted in a robust electrode structure, improving capacity retention and cycle life of Si electrodes[199]. By using a PAA:PANI composite with an optimum ratio of 90:10 wt%, the (PANI:PAA)/Si-NPs anode (75 wt% Si-NPs) could achieve a high initial discharge specific capacity of 1979 $mAh.g^{-1}$ at 0.1 C. However, there are no mass-loading and thickness of the (PANI:PAA)/Si-NPs anode reported as well as limited capacity retention of 56.6% at 0.5 C after 300 cycles, leaving a question of its practical application for high energy density batteries. In order to improve the cycling performance, the same group carried out an additional grafting of dopamine onto the PAA structure, which allowed the formation of strong adhesion between catechol groups of dopamine and the hydroxyl–decorated Si particle surface[200]. As a result, the bonding strength of (dopamine-grafted PAA):PANI composite binder towards Si particles was significantly enhanced, buffering the large volume

change and preventing capacity fading. The initial capacity and capacity retention were 2619 $mAh.g^{-1}$ at 0.1 C and 66% after 300 cycles at 0.5 C, which were more than 10% better than that of conventional PAA:PANI/Si-NPs anode[200].

Instead of fabricating CP-based composite binders by physical mixing, they can be derived from *in situ* polymerization, in which CP monomers are polymerized in the presence of carboxyl-containing polymers. The *in situ* polymerization allows the formation of homogeneous nanocomposites. More importantly, this method also favors the instant doping process of negatively charged carboxyl groups into positively charged CP chains, thus anticipating to yield high electrical conductivity composites. For example, Wang *et al.* synthesized a novel three-dimensional PANI:PAA binder for Si anode via *in situ* polymerization[201]. By adding phytic acid, which contains six phosphate groups in each molecule, PANI was doped and cross-linked to form a highly conductive, porous PANI:PAA framework that not only allowed a complete replacement of carbon additives[201], but also acted as a buffer for Si-NP volume changes[201,209,210]. The abundance of carboxyl groups from the PAA polymer chain established hydrogen bonds with SiO_2 on the Si surface, which offered a self-healing function[201,208,211]. The flexible hydrogen bonding system can be broken and reformed instantly during volume expansion and contraction, which improves electrode connection. Consequently, these interactions between the three-dimensional PANI:PAA framework and Si NPs resulted in excellent mechanical integrity and suppressed capacity fading during the (de)lithiation process. The PANI:PAA/Si-NPs anode was able to retain 71% and 67.7% of its initial discharge specific capacity at 1 C after 800 and 1000 cycles, respectively. However, the initial specific discharge capacity was only 890 $mAh.g^{-1}$ at 1 C at a mass-loading of 1 $mg.cm^{-2}$.

In general, the obvious benefit of using conducting polymer/carboxyl-containing polymer composites as battery binders is their ease of production along with outstanding binder performances. The composites can be easily prepared either by milling and stirring commercially available polymers or by carrying out *in situ* polymerization of monomers, which is compatible with the production process of CPs. The high normalized capacities reported in Table 2 and 3 suggest that such binders can enable carbon-additives-free electrodes with reasonable active material loading (75-80 wt%). Despite those advantages, the number of studies on these types of composites as binders is still limited. Recent work introduces new conducting polymer/carboxyl-

containing polymer composites, which were synthesized by *in situ* polymerization, such as PPy/CMC nanospheres[212,213], PPy/NFC fibers[212], PANI/SA mat-like nanofibers[214], PANI/CMC rods[215]. However, no application in Li-ion batteries was found for these composites[212–214,216], suggesting promising space for future development.

2) Functional group-modified conducting polymers as battery binders

Apart from integrating hydrophilic polymers with CPs to form composite binder via physical, ionic[12,119,217], and acid-base interactions[199], CPs could also be turned into useful battery binders by chemical modification. Through the addition of hydrophilic groups to the CP structure, the processing of CPs can be significantly improved, yielding conductive and water-dispersible battery binders.

As discussed above, increasing the polarity of the binders has a dual purpose in improving dispersion in polar solvents, including water, while simultaneously increasing intermolecular forces with anode materials[49,193,208,218] (Si, Sn, Ti-based materials) or cathode intercalation materials (NMO[163], NMC[39], LFP[165,192]) to improve battery performance. For these reasons, modifying the side chain of CPs with carboxyl or hydroxyl groups stands out to be a rational approach to synthesize multifunctional, efficient battery binders. For example, sodium alginate grafted poly(3,4-propylenedioxythiophene) (SA-PProDOT) was synthesized as a novel multifunctional, conductive binder[197] (Figure 2.4). The starting precursors included sodium alginate (SA) and poly(3,4-propylenedioxythiophene-2,5-dicarboxylic acid) (ProDOT). By using an emulsion system of cyclohexane, water, and dodecyl benzenesulfonic acid (DBSA), SA and ProDOT could be dispersed in aqueous and oil phases, respectively. The esterification reaction between -COOH group of ProDOT and -OH group of SA occurred simultaneously with the polymerization reaction of ProDOT and SA-grafted ProDOT, in which $FeCl_3$ acted as an oxidative polymerization agent. The SA-PProDOT/LFP electrode showed higher electrode adhesion strength (peel test) and hardness (nanoindentation, scratch test) compared to electrodes made of PVDF, CMC, or SA binders. However, the mechanism for the improvement of the mechanical properties of the SA-PProDOT/LFP electrode has not been elucidated. Interestingly, by using SA-PProDOT as a single component for the LFP electrode matrix, the carbon-free SA-PProDOT/LFP cathode was able to reach 170 $mAh.g^{-1}$ at 0.1 C without significant capacity reduction after 400 cycles, but only achieved ~120 $mAh.g^{-1}$ at 1 C. The authors reported that SA-PProDOT/LFP

showed lower impedance than LFP/SA/C. However, the electrical conductivity value of the SA-PProDOT binder was not reported, leaving a question about how the SA-PProDOT binder interacts with LFP particles and contributes to electrode conductivity.

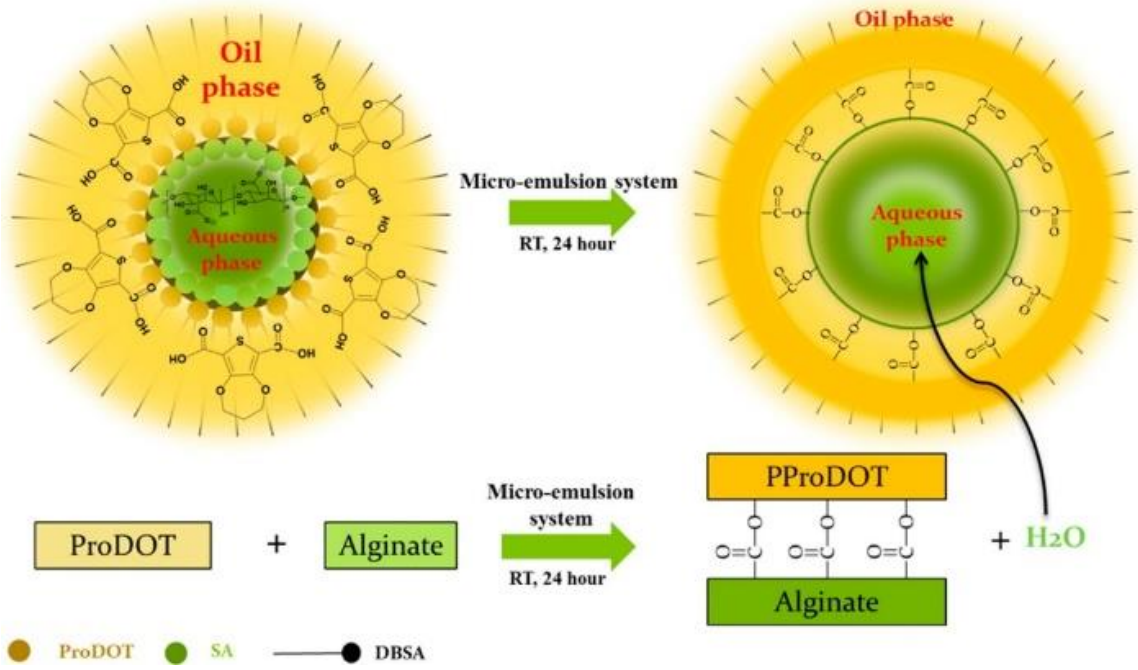

Figure 2.4. Microemulsion synthetic procedure for SA functionalized PProDOT as a binder for Si anode. Reprinted with permission from reference [197]. *Copyright 2015 American Chemical Society.*

Zhao *et al.* designed a novel sodium poly(9,9-bis(3-propanoate)fluorine) (PF-COONa) binder and applied it to Si[202] and Sn[136] anodes of Li-ion batteries (Figure 2.5). By adding carboxyl groups to the side chain of the PF structure, the PF-COONa binder was made conductive and water-dispersible. The authors concluded that PF-COONa provided a robust conductive network within the electrode resulting in a carbon additive-free anode. Furthermore, the abundance of carboxyl groups on PF-COONa binder facilitated the formation of strong intermolecular interactions with Si and Sn particles, which suppressed particle disconnection and maintained electrode mechanical integrity after many charge/discharge cycles. For example, a Sn/PF-COONa anode (m_{sn}= 1 mg.cm^{-2}, 80 wt% Sn) delivered initial and 500th discharge specific capacities of 950 mAh.g^{-1} and 520 mAh.g^{-1}, respectively, at a current density of 0.2 A.g^{-1} (about 0.2 C). In contrast, while yielding high initial discharge specific capacities at ~1400 mAh.g^{-1}, the traditional

Sn/PVDF/C anode showed fast capacity degradation, dropping to ~100 mAh.g^{-1} after 10 cycles at 0.2 C[136]. In combination with silicon, the PF-COONa binder yielded a high-performance Si/PF-COONa anode (m_{si}= 0.61 mg.cm^{-2}, 66.6 wt% Si) that could maintain a capacity of 2806 mAh.g^{-1} after cycling for 100 cycles at 0.42 A.g^{-1}, which corresponds to 85.2% of the initial discharge specific capacity[202]. In comparison, the Si/AB/CMC anode showed a high initial discharge capacity of ~2700 mAh.g^{-1} but quickly decayed to only 1500 mAh.g^{-1} after 100 cycles at 0.42 A.g^{-1}. These results suggest that the conductive PFCOO-Na binder could prevent electrical contact loss during the cycling process better than PVDF and CMC binders.

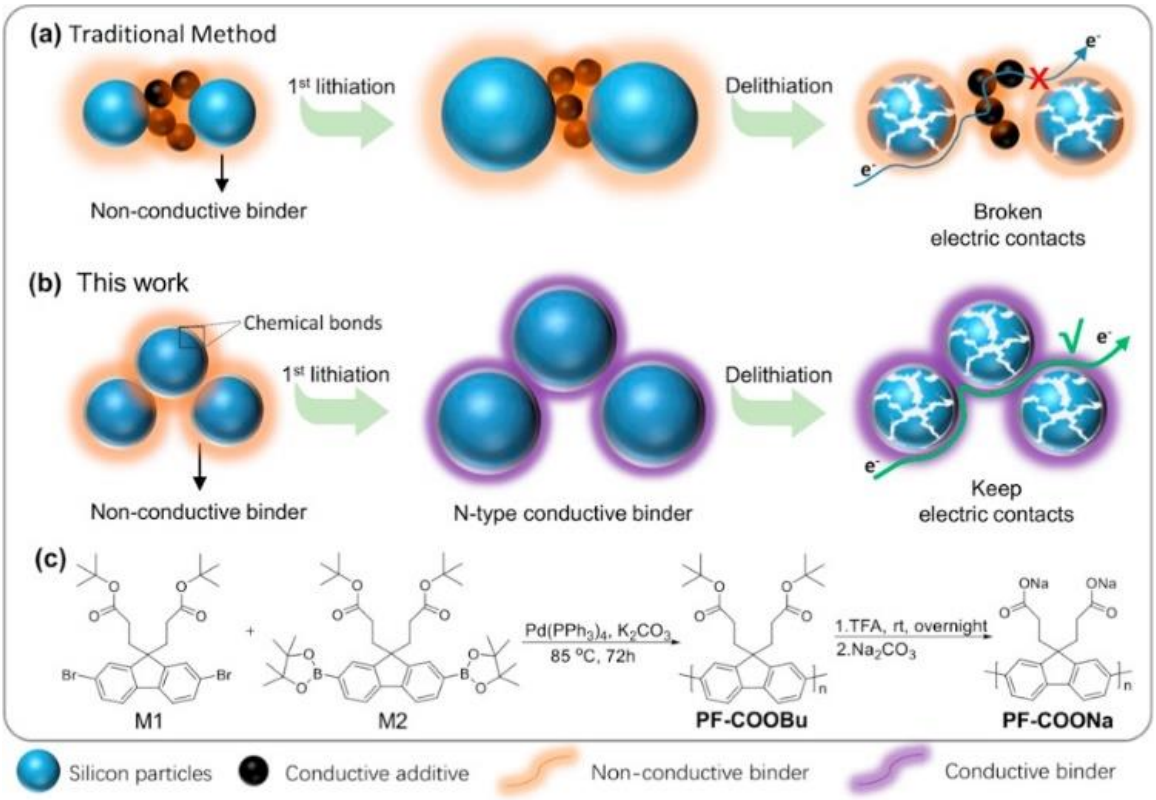

Figure 2.5. Application of PF-COONa binder for Si anodes. (a,b) Schematic illustration of how conventional binder and novel PF-COONa binder perform in anodes of Li-ion batteries. (c) The synthetic procedure of PF-COONa. Reprinted from reference [202]. *Copyright (2017), with permission from Elsevier.*

Liu's research group developed poly(9,9-dioctylfluorene-co-fluorenone-co-methyl benzoic ester) (PFM) containing different functional groups with different polarities (Figure 2.6) for SiO[39] and SiO-SnCoC[203]. This work found that the methylbenzoic ester functional group

of the PFM binder underwent a trans-esterification reaction with hydroxyl groups on the surface of SiO particles to form a chemical bond (Figure 2.6 (c)), providing strong interactions between PFM binder and SiO active materials[39]. This chemical bonding ensured the integrity of the electrode and offered an interconnected electronic connection between SiO particles. These effects prevented the loss of electrical contact between Si-based anode materials during cycling, which is an issue with carbon conductive additives[39,203]. Without using additional carbon additives, a PFM/SiO (98:2 wt%) anode could be fabricated with high initial discharge capacity of ~1000 $mAh.g^{-1}$ and 90% capacity retention after cycling for 500 cycles at 0.1 C. However, the areal capacity was low at ~1 $mAh.cm^{-2}$, which is much lower than the benchmark for Si-based anodes (>3 $mAh.cm^{-2}$)[219]. To achieve an areal capacity of ~2 $mAh.cm^{-2}$, 5 wt% PFM was needed. The SiO/PFM (95:5 wt%) anode showed high coulombic efficiency of >99%, high initial capacity of ~1200 $mAh.g^{-1}$, and good capacity retention of ~950 $mAh.g^{-1}$ after 500 cycles at 0.1 C. However, no cycling data was reported at higher C-rate. Another study from the same group combined PFM binder with carbon additives to make an electrode matrix for a SiO-SnCoC anode that could cycle at higher C-rate than the SiO/PFM anode[203]. The SiO-SnCoC/PFM/C (80:5:15 wt%) anode achieved 806.6 $mAh.g^{-1}$ and 695.3 $mAh.g^{-1}$ in the first and 40^{th} cycles at 1 C, which were higher than the capacity of the SiO-SnCoC/PVDF/C (80:5:15 wt%) anode after cycling at 0.1 C for 40 cycles (~300 $mAh.g^{-1}$). The authors reported the successful fabrication of SiO-SnCoC/PFM/graphite/C (60:5:20:15 wt%) at a high areal capacity of 3.5 $mAh.cm^{-2}$, which met the benchmark for the areal capacity of Si-based anodes[219]. However, the initial specific capacity was only 510 $mAh.g^{-1}$, which reduced to 460 $mAh.g^{-1}$ after 40 cycles at 1 C.

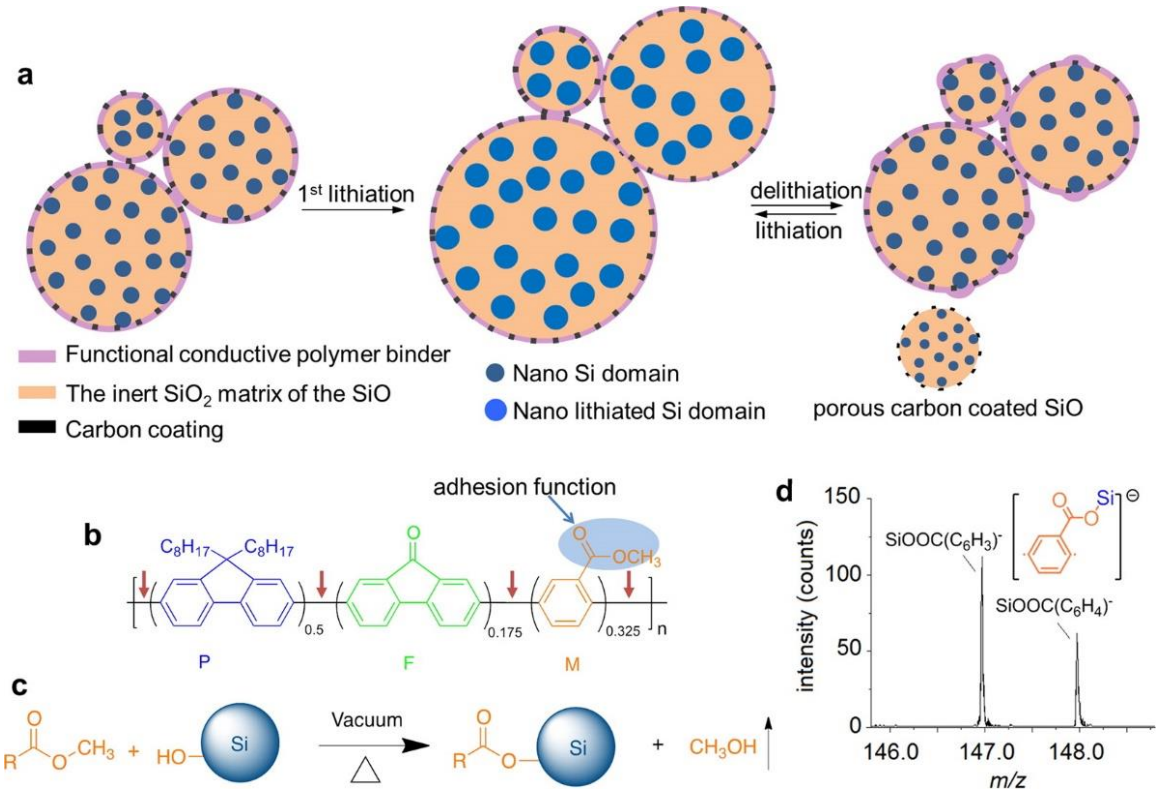

Figure 2.6. Application of PFM-based conducting polymer binders with different functional groups. (a) Schematic illustration of PFM/SiO electrode (b) Chemical structure of the PFM binder; blue ellipse emphasizes the ester group in the PFM structure that will form a chemical bond with Si-OH on the SiO anode. (c) The trans-esterification mechanism between the ester group and Si-OH. (d) TOF-SIMS result of the PFM/SiO electrode indicates a chemical bond between PFM binder and SiO active materials. Reprinted with permission from reference [39]. *Copyright 2014 American Chemical Society.*

In general, although the side chain-modified conductive polymers have shown very intriguing properties as battery binders, such as high electrical conductivity, sufficient water-dispersible ability, and enhanced binding affinity towards active materials[39,197,202,203], it is currently unclear whether these materials could be produced at sufficiently low cost to allow wide-spread use in Li-ion batteries. Nonetheless, these functional binders demonstrated high normalized capacities and good cycling performances (Table 2 and 3). Therefore, their use in high-reliability, high-energy-density applications, such as in personal medical devices and implants, might present a technology within which these binders can be assessed for more routine applications.

3) Capitalizing on conducting polymer microstructure for hierarchically porous electrodes

The current battery electrode manufacturing process involves the preparation of active materials, battery binders, and conductive additives separately. These components are then vigorously mixed to yield electrode slurries, which are subsequently cast onto current collectors to form electrode sheets, producing electrodes with homogenous particle distribution and few agglomerates. This processing method is economical and scalable. However, the control of porous microstructures in such electrodes is limited. Electrode microstructure has been shown to have an important impact on performance[220–222]. The synthesis of CPs can be exploited to give stronger control over microstructure and develop hierarchically porous structures that serve as ideal electrode frameworks for intercalation materials.

To this end, recent studies have developed methods of making three-dimensional electrode frameworks, in which a network of CPs is *in situ* polymerized in the presence of active materials. CPs could be derived from pyrrole[178,206], aniline[198,205,207], thiophene[223], or EDOT[204,224] by polymerizing CP monomers with chemical oxidants, such as ammonium persulfate[178,204,224] or iron (III) chloride[206]. Meanwhile, active materials can either be anode[204–207,224–226] or cathode[178,198] materials as long as they are chemically stable during polymerization. The CP network serves as a multifunctional, conductive binder matrix that tightly links active materials together. After mixing with a small amount of binder and conductive additives, the electrode slurry is ready for processing. In some cases, the slurry of a three-dimensional electrode framework can be cast directly on a current collector without further modification[178,187,205,227,228].

Within the three-dimensional electrode structure, the CP matrix not only works as a soft skeleton for active materials[178,224], but it also enhances electronic transport within the electrode[204,229]. Yue *et al.* carried out *in situ* polymerizations of EDOT monomer in the presence of Si-NPs and an aqueous PSS solution[204]. As a result, Si-NPs were homogeneously embedded in a porous PEDOT:PSS structure. The authors confirmed that PEDOT:PSS acted as a conductive and elastic binder matrix for Si-NPs, enhancing initial coulombic efficiency and capacity retention compared to bare Si-NPs. The PEDOT:PSS/Si electrode slurry was mixed with Acetylene black (AB) and CMC with up to 30 wt% and 8 wt% of electrode composition, respectively, to fabricate an electrode sheet. PANI has also been used to design three-dimensional

CP frameworks for intercalation electrodes from LiV_3O_8[198] and V_2O_5[230]. A three-dimensional electrode structure of PANI/LiV_3O_8 was synthesized by allowing the polymerization of aniline in the suspension of LiV_3O_8 NPs with the assistance of a surfactant[198]. PANI formed a continuous conductive matrix surrounding LiV_3O_8 NPs that allowed full lithiation/delithiation of active materials. As a result, the PANI/LiV_3O_8 based electrode exhibited better initial capacity and capacity retention in comparison with an electrode made of pristine LiV_3O_8 [198]. However, here too, a PVDF/C binder system was still necessary for processing the PANI/LiV_3O_8/PVDF/C composite electrode, decreasing overall active material mass loading and leaving challenges with respect to electrode processing cost and environmental impact unresolved.

To take full advantage of three-dimensional CP networks in optimizing energy density and cycling performance, researchers have been aiming to replace PVDF binder and carbonaceous additives completely. Several studies reported carbon additive-free electrodes by forming ready-to-use electrode hydrogels composed of CPs and active materials that could be directly cast on aluminum and copper foils[178,205–207]. Polyvalent anions as cross-linkers and dopants for the CP are crucial in these electrode hydrogels[178,205–207]. This approach mitigates the drawbacks of using carbon additives and enhances the specific capacity of the battery. For example, phytic acid-doped PANI/Si (P-PANI/Si) hydrogel was synthesized by mixing aniline, Si NPs, and phytic acid (acting as dopant and cross-linker), followed by adding ammonium persulfate to polymerize aniline[205]. The viscous gel was then cast on copper foil and dried to yield a hierarchically structured P-PANI/Si anode. Due to the continuous, porous, conductive hydrogel structure, Si-NPs had sufficient space for expansion and contraction during charge/discharge cycling. Even though Si-NPs still suffered from pulverization, the thick layer of P-PANI coating could hold these pulverized particles, maintaining good electron transport within the electrode even after long cycling. As a result, the P-PANI/Si electrode possessed a high specific discharge capacity of 2500 $mAh.g^{-1}$ and 1100 $mAh.g^{-1}$ at a current density of 0.3 and 3.0 $A.g^{-1}$, in the first cycle respectively. Moreover, the P-PANI/Si anode demonstrated good capacity retention of 91% after 5000 cycles at 6.0 $A.g^{-1}$. However, the P-PANI/Si electrode fabricated from P-PANI/Si hydrogel possessed a low mass loading of 0.3-0.4 $mg.cm^{-2}$ with ~75 wt% of Si, resulting in low areal energy density.

Yu *et al.* recently reported that copper(II) phthalocyanine tetrasulfonate salts (CuPcTs) could be used to cross-link PPy, in place of phytic acid, to form CuPcTs-doped PPy/carbon-coated

$LiFePO_4$ (Cu-PPy/C-LFP) hydrogels[178] (Figure 2.7). The four sulfonate groups serve as crosslinking agents by forming ionic bonds with the positively charged PPy backbone, forming a three-dimensional framework of PPy. After drying the Cu-PPy/C-LFP hydrogel, a hierarchically porous Cu-PPy/C-LFP composite electrode was formed[178]. The addition of CuPcTs also boosted electrode conductivity up to 7.8 $S.cm^{-1}$ despite the absence of carbon additives. The hybrid Cu-PPy/C-LFP electrode demonstrated a stable discharge capacity of approximately 80 $mAh.g^{-1}$ at 1 C within 1000 cycles, suggesting high robustness of the Cu-PPy/C-LFP electrode during the charge/discharge process. The electrode fabrication relies on the casting of the mixture of hydrogel precursor (LFP, Py, CuPcTs, APS), leaving it overnight to complete polymerization and doping and consequent immersion in water to remove excess reagents. In addition, no mass loading or thickness information was reported. A similar synthetic approach was applied for synthesizing PPy-Fe_3O_4 hydrogel[206], in which a robust, porous PPy-Fe_3O_4 hydrogel was formed by polymerizing pyrrole in a Fe_3O_4 suspension with ammonium persulfate (APS) as oxidant and dopant, and Phytic acid or CuPcTs as cross-linkers. This three-dimensional electrode framework prevented the agglomeration of Fe_3O_4 particles even at high Fe_3O_4 content of 85 wt%, which is a significant problem with the PVDF/C binder matrix. CuPcTs doped PPy (Cu-PPy) was found to perform better than phytic acid doped PPy (P-PPy) in terms of electrical conductivity and binder performance. The authors found that the conductive Cu-PPy framework not only allowed faster ionic and electronic transport, confirmed by electrochemical impedance spectroscopy, but it also ensured mechanical integrity after many cycles[206], which was supported by excellent cycling data. The Cu-PPy/C-Fe_3O_4 cathode could yield a stable specific discharge capacity of ~1200 $mAh.g^{-1}$ during the first 50 cycles at 0.1 C, which was much better than Fe_3O_4/PVDF/C (75:15:5 wt%) electrode that only achieved 300 $mAh.g^{-1}$ after 50 cycles at 0.1 C. However, the mass loading of active material was typically only at 0.2-0.4 $mg.cm^{-2}$. Even though the initial specific discharge capacity of Cu-PPy/C-Fe_3O_4 was ~900 $mAh.g^{-1}$ at 1 C, no long-term cycling data at 1 C and higher C-rate were available. While the properties of Cu-PPy seem ideal as a binder, the exceptionally high porosity decreases energy density, and the price of Cu-containing salts may well be a hindrance to the widespread application of such technology.

Figure 2.7. Cross-linked CPs with active materials to form composite electrodes. Schematic demonstration for the formation of Cu-PPy/C-LFP hydrogel. After drying the hydrogel, the three-dimensional interconnected electrode structure will form. Reprinted with permission from reference [178]. *Copyright 2017 American Chemical Society.*

Apart from using cross-linking agents, some studies have attempted to synthesize hydrogel-based electrodes via an economical pathway by mimicking the production of CP hydrogels for medical application[177,207,224,231], in which CPs were polymerized in the presence of battery active materials and water-soluble polymers. For example, a novel Sn@PANI-SA nanofiber hydrogel was synthesized by *in situ* polymerization with SA[207]. After a rapid drop in specific discharge capacity from ~800 $mAh.g^{-1}$ to ~650 $mAh.g^{-1}$ within the first few cycles, the Sn@PANI-SA electrode showed a stable specific capacity of ~600 $mAh.g^{-1}$ and coulombic efficiency of 98% within 100 cycles at 0.2 C, which was much better than the Sn/PVDF/C electrode. The outstanding performance of the Sn@PANI-SA electrode was considered the outcome of a highly porous, conductive PANI/SA hydrogel network, which could reduce the internal impedance of the electrode and accommodate volume expansion[207]. Nonetheless, the mass loading and electrode thickness were not mentioned to justify its feasibility in high energy density batteries.

Yu *et al.* also suggested that addition of a small amount of carbonaceous additives to CP-active material hydrogels can form ternary nanostructured electrodes with promising performance. A Si/PPy/CNT electrode could maintain an excellent specific capacity of 1600 $mAh.g^{-1}$ after 1000 cycles at a current rate of 3.3 $A.g^{-1}$. (~ 0.8 C)[48]. Low active material loading (less than 70%),

low electrode mass loading (0.3-0.5 $mg.cm^{-1}$), as well as the high cost of cross-linking agents, remain a concern with hydrogel-derived electrodes. Further optimization of the ternary electrodes targeting cheaper synthesis precursors and higher electrode mass loading is required to exploit this promising electrode design concept.

By constructing a three-dimensional conducting polymer-active material network, active materials are strongly and uniformly embedded in conductive frameworks of CPs, which results in low electrode internal resistance and superior cycling performance. Using CPs eliminates partially or even completely carbon additives from the electrode and can increase the specific energy density of Li-ion batteries (Tables 2 & 3). CP hydrogels as active material matrix show good compatibility with the electrode slurry casting method, making this a realistic approach for wide-scale application. One of the often-cited advantages of these structures is their high porosity, resulting from the drying of the composite hydrogel. While this improves ionic conduction and accommodates larger volume changes, it also reduces significantly volumetric energy density of composite electrodes. The mass loading and proportion of active materials in these electrodes are usually not clearly reported[178,206] or significantly lower than commercially relevant electrodes[232–234] at 70-75 wt%[205,207] and 0.3-0.5 $mg.cm^{-2}$ [205], respectively. This raises questions about the applicability of this type of hydrogel-like electrode outside the scope of highly specialized high-power applications. A more systematic reporting of energy densities and mass loadings within reasonable ranges will be necessary to justify the relevance of CP hydrogel binders for widespread application in intercalation batteries.

III. Conducting polymer-based binders beyond lithium-ion battery technology

In addition to the development of CP battery binders for lithium-ion batteries, some recent studies focus on suitable binders for the next generation of rechargeable batteries such as Li-S[91,98], Na-ion[89,154,158], and all solid-state batteries[235,236]. The problems encountered in Li-S, Na-ion, and solid-state batteries with respect to binder design are similar to those of traditional Li-ion batteries, which is demonstrated by the large volume of studies on natural-based, water-dispersible binders[117,158] and multifunctional binders[94,104,154]. Therefore, CP-based compounds are also promising materials in these applications, exploiting CPs that are modified or combined with hydrophilic agents to enable processing into electrode films. The following sections

will discuss recent work on CP-based binders for Li-S, and Na-ion batteries as well as potential applications in all solid-state Li-ion batteries.

1) Lithium-sulfur batteries

In comparison to traditional Li-ion batteries, Li-S batteries exhibit outstanding energy storage capacity due to the high theoretical specific capacity of the elemental sulfur cathode at ~1673 $mAh.g^{-1}$ [237]. In a conventional Li-S battery electrode, the traditional mixture of PVDF/C is a common electrode matrix providing electrical and mechanical connections between sulfur particles. Despite the promising theoretical capacity, Li-S batteries remain at a low technology readiness level (TRL). This is due to inherent issues of low conductivity of sulfur, shuttle effect of polysulfides and the severe material deformation[91,94,98] that is typical to conversion-type active materials. Some studies suggest that these problems could be addressed by adding alternative binders that could form a strong interaction with sulfur derivatives to suppress shuttle effects as well as maintain continuous electric contact after a number of charge/discharge cycles[91,98].

In lithium-sulfur batteries, CP-based binders can fulfill multiple functions. They act as binding agents between electrode materials, sulfide capturing agents, and robust mechanical structures accommodating irreversible volume changes. Wang *et al.* investigated the use of sulfuric acid doped PANI (H_2SO_4-PANI) as a multifunctional binder for sulfur-wrapped activated carbon (C-S) as active materials[93] (Figure 2.8). In order to overcome the compact, rigid structure of H_2SO_4-PANI, which was not suitable for accommodating volume change of C-S, m-cresol was mixed with H_2SO_4-PANI to form an extended PANI polymer chain, denoted as meta-cresol(H_2SO_4-PANI). The meta-cresol(H_2SO_4-PANI) binder offered a cobweb that adhered to C-S (68 wt% S loading) active material via Van der Waals interaction. Moreover, it trapped negatively charged polysulfide species through electrostatic interaction with positively charged groups on the H_2SO_4-PANI polymer chain. These interactions could suppress sulfide shuttle effects, that are normally encountered with PVDF binders. The authors also claimed that C-S/C/m-cresol(H_2SO_4-PANI) (78:20:2 wt%) exhibited low internal resistance compared to C-S/C/PVDF (66.6:16.7:16.7 wt%), however, comparing two electrodes with different carbon contents. According to the cycling data at 0.36 C, the C-S/C/m-cresol(H_2SO_4-PANI) electrode showed a good initial specific discharge capacity of 725 $mAh.g^{-1}$ compared to only 410 $mAh.g^{-1}$ for C-

S/C/PVDF. The C-S/C/m-cresol(H_2SO_4-PANI) electrode demonstrated a capacity retention of ~52% after 100 cycles at 0.36 C and mass loading was not reported in this study.

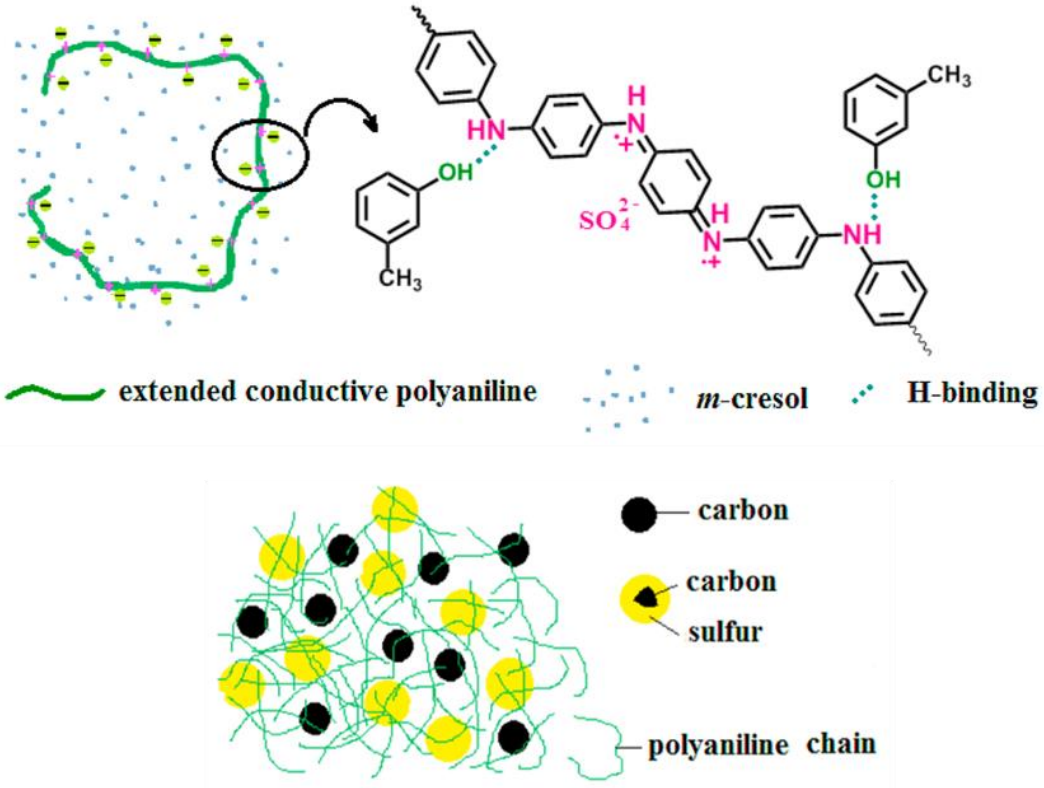

Figure 2.8. Application of CP-based binders in Li-S batteries. m-cresol(H_2SO_4-PANI) binder keeps carbon (C), sulfur-wrapped carbon (C-S) in place within the cathode of Li-S batteries. Reprinted from reference [93]. *Copyright (2017), with permission from Elsevier.*

Other works reported the promising application of PEDOT:PSS-based composites as alternative binders for Li-S batteries. Zhang *et al.* used PAA/PEDOT:PSS (40:60 wt%) composite as a multifunctional binder for Ketjenblack-sulfur (KJC-S) cathode materials[104], which were synthesized by a melt-diffusion process[238] with a sulfur proportion of 70 wt%. Ketjenblack, which is a highly conductive and porous type of carbon black, accounted for 30 wt% of the KJC-S electrode to ensure good electrical conductivity of electrode. PAA/PEDOT:PSS composite was easily prepared by physical blending of PAA and PEDOT:PSS, which are commercially available, to combine the advantages of the two polymers. Even though PEDOT:PSS can provide good electrical connections and suppress lithium polysulfides dissolution[96,97,104], confirmed by cyclic voltammetry[104], PEDOT:PSS suffers from poor electrolyte affinity[104]. PAA, on the

other hand, experiences a high degree of electrolyte swelling, allowing good electrolyte exposure for S, which is considered a weak ionic conductor. Therefore, combining PAA and PEDOT:PSS could take advantage of both components. As a result, the electrode with PAA/PEDOT:PSS binder performed better than electrodes with solely PAA or PEDOT:PSS binders. A C-S/C/(PAA/PEDOT:PSS) (70:20:10 wt%) cathode could achieve a high initial specific capacity of 1121 mAh.g^{-1} at 0.5 C. However, the electrode mass loading was only 0.8 mg.cm^{-2}. After cycling for 80 cycles at 0.5 C, it retained 74% of its initial capacity. Another study addressed the stability of lithium-sulfur batteries by using ionically cross-linked PEDOT:PSS-Mg^{2+} binder[239]. The divalent Mg^{2+} ions act as ionic cross-linkers to PSS by binding to two sulfonate groups. The robust conductive network of PEDOT:PSS-Mg^{2+} withstood structural degradation and suppressed the shuttle effects by introducing strong ionic interactions between immobilized positive charges on the binder and negatively charged sulfides. As a result, the specific capacity reached 1097 mAh.g^{-1} in the 1st cycle and remained at 74% capacity after 200 cycles at 0.5 C rate, which was superior compared to PVDF/C binder-based Li-S batteries[239].

One study mimicked the structure of PEDOT:PSS by introducing PPy:PSS as a mixed ionic-electronic conductor [92], in which PSS worked as a PPy dopant. However, instead of mechanically mixing S particles with the PPy:PSS composite, they heated a mixture of PPy:PSS and S at 155 ^{o}C for 6 hours to irreversibly bind S to the PPy:PSS surface. The heat-treated PPy:PSS-S (10:90 wt%) powder was mixed with PVDF/C to form a PPS:PPy-S/PVDF/C (85:10:5 wt%) electrode with high S-content, high mass loading of 6.0 mg.cm^{-2}, and high initial areal capacity of 6.6 mAh.cm^{-2}, which met the benchmark for Li-S electrodes[240]. Besides reducing charge-transfer resistance within the electrode, which was confirmed by EIS measurement, PPy:PSS also played a key role in suppressing severe polysulfide dissolution through the interaction between sulfide species and PPy. These positive influences resulted in a good initial capacity of 1108 mAh.g^{-1} and moderate capacity retention of 64% after 200 cycles at a 0.1 C discharge rate.

Several publications have demonstrated the interactions between heteroatoms in CP-based binders and polysulfide species (Li_2S, Li_2S_2), which suppresses the sulfide shuttle effect and increases cycling performance. Besides the representative studies mentioned above, other approaches such as coating sulfur surface with CPs or trapping sulfur in multi-dimensional CP

frameworks represent promising strategies for improving Li-S battery performance. A more detailed discussion on using CPs in Li-S batteries can be found in the literature[91,98,102,241].

2) Sodium-ion batteries.

Na-ion battery electrodes experience similar issues to those of Li-ion batteries, such as electrode cracking[218,242], and ion-dissolution[77,149,243], which eventually results in capacity decay. Previous work addressed the stability problem by introducing alternative binders that contain an abundance of hydroxyl and carboxyl groups such as SA[149] and CMC[117]. These studies underline the fact that hydroxyl and carboxyl groups in these aqueous binders can form hydrogen bonds with active materials, creating a strong interaction within electrodes that subsequently results in better lifespan and capacity retention[90]. Carbonaceous compounds such as carbon black remain the primary additive for offering electrically conductive pathways.

Dai *et al.* fabricated a composite electrode consisting of pure Sn NPs and conductive PFM binder[137] without adding carbon additives. Despite suffering intrinsic large volume changes, the conductive network of the Sn/PFM anode exhibited no noticeable electrically-isolated regions, which were easily observed in the case of Sn/PVDF and Sn/CMC anodes. As a result, the Sn/PFM anode achieved an initial specific discharge capacity of 610 $mAh.g^{-1}$ and showed no significant capacity decay after 10 cycles at 0.1 C rate. This finding suggests that CP-based binders may be a valuable pathway to alleviating some of the problems facing the development of commercial Na-ion battery technology.

3) Solid-state batteries

With the great scrutiny that new technologies are facing, Li-ion battery fires and explosions are widely reported and discussed in the news. Solid electrolytes become a promising replacement for flammable liquid electrolytes, leading to the development of all-solid-state batteries[35,61]. Moreover, recent developments in all-solid electrolytes have shown competitive or even superior ionic conductivity with a near-unity transfer coefficient, making them promising candidates for high-power applications and there is hope that solid electrolytes may become more stable against Lithium dendrite formation, making the use of lithium metal as ultimate high-energy anode possible[59,244]. The combination of intercalation materials with these solid electrolytes in composite electrodes remains a significant challenge, given that the rigid electrolyte structure is unable to accommodate active material volume changes[245]. This leads to mechanical electrode

disintegration and fast capacity fading when composite electrodes are applied. Good cycling performance is only observed in thin-film all-solid-state cells[61,245]. In all solid-state batteries, liquid electrolytes are replaced by solid electrolytes, which requires the battery matrix to conduct both electrons and lithium ions efficiently within the electrode structure.

Several studies recently suggest that replacing PVDF/C with a mixed-conducting CP-based matrix might allow ionic and electronic connection of all particles in the electrode while accommodating electrode volume changes. For example, Hammond *et al.* introduced a mixture of PEDOT:PSS and poly(ethylene oxide) (PEO) as a promising dual conductor[187]. Surprisingly, composites of these electron and ion-conducting polymers show increased electronic and ionic conduction than their pure forms. The mechanism of this charge transport enhancement in the composite is yet unexplained. Even though PEDOT:PSS:PEO has not been tested in a full-cell solid electrolyte Li-ion battery, the superior electronic and ionic conductivities of PEDOT:PSS:PEO compared to PVDF/C promise good adaptability of this electrode matrix for use in electrodes of all-solid-state batteries[187]. Another study from Zeng *et al.* suggested the synthesis of a dual conductive matrix for a Si anode[182], in which electronically conductive PEDOT:PSS was assembled with ionically conductive PEO and polyethylenimine (PEI). The dual conductive matrix not only provided better ionic and electronic connection within the Si anode compared to the commonly used CMC/C electrode matrix, but it also offered good mechanical strength through crosslinking and electrostatic interaction between PEDOT:PSS, PEO, and PEI. These features suggest that PEDOT:PSS:PEO:PEI might be helpful to address the issues of all solid-state batteries mentioned above.

IV. Compatibility of conducting polymer-based binders with battery environments – A knowledge gap

1) Electrochemical and chemical stability

CPs have been well-studied and used in many applications due to their combination of intrinsic conductivity with the processing, elasticity, and stability of polymers[175,246]. However, the implementation of CPs in rechargeable battery technologies is still limited. Even though the studies mentioned above suggest that CP-derived compounds are great alternative battery binders, only a few studies presented stability tests of these binders. Given that electrochemical, chemical, and thermal stability is one of the hallmarks of currently used

fluorinated polymers, the decoration of CPs and composites with typically much more reactive unsaturated bonds and polar bonding raises the question of whether these binders are suitable for battery applications.

Since battery binders are in contact with liquid electrolytes and active materials, the affinity of binders to electrolytes influences swelling and wetting, and in consequence electrode adhesion, porosity, tortuosity, and ionic conductivity of the electrode, which in turn influences battery performance[247]. Sufficient wetting of the complete composite electrode structure is needed, while excessive swelling affects structure and electrolyte availability. Several studies discussed the swelling behaviors of CP-based binders in different electrolytes. Vlad *et al.* reported that PEDOT:PSS showed no signs of solubility, and limited swelling in carbonate-based, and ether-based electrolytes[248]. Ding *et al*. claimed that PEDOT:PSS demonstrated a low affinity to carbonate-based electrolyte solvent[104]. As the low electrolyte uptake of these CPs is a concern for Li-ion and Li-S batteries, some studies combined CPs with compounds that exhibit high electrolyte affinity, such as CMC and PAA to enable good ionic transport within the electrode structure[104,199]. Some studies, on the other hand, reported high electrolyte uptake CP-based binders such as PF-COONa[202], and Poly(2,7-9,9-dioctylfluorene-co-2,7-9,9-(di(oxy-2,5,8-trioxadecane))fluorene-co-2,7-fluorenone-co-2,5-1-methylbenzoate ester) (PEFM)[140], which showed an improved lithium transport within the cell and good cycling performance. Connected to wettability is binder chemical stability in prolonged contact with electrolytes and active materials. This issue has so far found little attention in the literature. Generally, CP-based binders should have an appropriate affinity to electrolytes to run in both anode and cathode of Li-ion batteries. In addition, they should support the formation of robust, stable solid electrolyte interfaces (SEI) to work efficiently in the anode[136,249].

With respect to electrochemical stability, binders should be either redox-inactive or exhibit high reversibility in their redox-activity. Das *et al.*[32,250], corroborated by Sandu *et al.* [248], claimed that PEDOT:PSS was redox inactive in Li^+ aprotic electrolyte within the operating potential window of Li-ion battery cathode (2.5 V - 4.2 V vs Li/Li^+) after performing cyclic voltammetry (CV) at a low scan rate of 1 $mV.s^{-1}$. However, CV measurements of PEDOT:PSS at low (~10 $mV.s^{-1}$) and high scanning rate (~250 $mV.s^{-1}$)[251] suggest that PEDOT:PSS redox activity is merely slow within the voltage window of Li-ion battery cathodes, resulting in low

current signals at low scan rate. At the Li-ion battery anode, Nicolosi *et al*. reported on a PEDOT:PSS-only electrode exhibiting a reversible capacity of ~ 20 $mAh.g^{-1}$ at 0.14 C [119]. Other CP-based binders are reported to participate in reversible redox reactions, adding additional storage capacity to composite electrodes. For example, PANI was combined with carbon nanotubes (CNT) to fabricate PANI/CNT cathode[252], which cycled between 2.0 and 3.9 V vs Li/Li^+. The PANI/CNT cathode could yield a good specific capacity of 86 $mAh.g^{-1}$ and a coulombic efficiency of ~90% after 100 cycles. Another study utilized PPy nanopipes as cathode materials for lithium-ion batteries, which could deliver a capacity of up to 125 $mAh.g^{-1}$ [253]. Within the potential window from 1.5 V to 4.5 V vs Li/Li^+ a reversible pattern of redox peaks was observed that confirms electrochemical reversibility. A more complete discussion of CPs as charge-storing components in batteries can be found in review papers on organic battery electrodes[254]. These studies demonstrate the importance of considering CP contribution to charge storage, also in situations where the CP component is considered only within the electrode matrix.

2) Electrical conductivity

Most studies on CP-based binders rely on carbon additives in their electrode formulations to achieve sufficient conductivity. Carbon-additive-free electrodes take advantage of CP composites as self-conductive battery binders/matrices[119,120,178,197,199,201]. The development of carbon-free electrodes is driven by the aim to reduce the amount of inactive material in the electrode. In this context, the comparative percolation threshold between conducting polymers and traditional conductive additives plays a crucial role in defining the ability of conducting polymers to outperform carbon-containing electrodes. The electrical percolation threshold depends on the electrode porosity[255,256], composite microstructure[257] and intrinsic electrical conductivity of fillers[258]. Whereas electrode porosity is defined by the required ionic conductivity in the electrode and the intrinsic conductivity of conductive additives is typically lower in CPs than carbon additives, the long-range molecular structure of CPs affects strongly the macroscopic electronic conductivity. To quantify the extent to which CPs are “unfolded” in their microscopic structure, the fractal dimension can be determined[259], which can vary over a large range for CPs, whereas it is less variable for carbon black additives. This gives rise to differing macroscopic conductivities, dependent on the matrix within which CPs are dispersed. For example, by dispersion of PEDOT:PSS in polyethylene glycol, the electrical conductivity of the composite

material was measured to increase, compared to the pristine PEDOT:PSS material[187]. Some mixtures of CPs and carbonaceous conductive additives exhibit synergistic effects, by reducing percolation thresholds of both the conducting polymer and carbonaceous conductive filler[260]. Consequently, CP binders may reduce inactive materials also in electrode composites that contain carbon additives.

Unlike carbon additives, whose electrical conductivity is independent of the redox potentials of the electrode, the electrical conductivity of CPs changes from highly conductive to insulating when CPs are in the oxidized or reduced state, respectively[261,262]. Most CPs exhibit the highest conductivity in the oxidized state, at which the CP backbone carries positive charges and electrolyte anions serve as counter-ions[263,264]. The cathode normally operates between 2.8 to 4.2 V vs Li/Li^+, in which most CPs such as PEDOT:PSS[262] and PANI[265,266] are in a conductive form. Some of these CP composites have been shown not to exhibit any electrochemical reaction within the cathode potential window[120,250]. The resulting conductivity of those CP composites has allowed successful fabrication of carbon-free cathodes with CP-based binders. Given the low electrode potential of the anode, the same binders should thermodynamically not exist in their oxidized state. Yet, some studies confirmed that CP-based binders show negligible faradaic redox processes in the anode potential window (0-1 V vs Li/Li^+) and remain conductive without further carbon additives. For example, Nicolosi *et al.* successfully demonstrated the fabrication of a carbon-additives-free electrode with PEDOT:PSS as a conductive battery binder for Si anodes[119]. Other studies also employed PPy-based[178] and PANI-based[199,201,205] battery binders for achieving carbon-free anodes. While these studies have not discussed the conductivity of CPs at these reducing potentials, studies have previously shown that CPs may be reduced beyond their neutral state in non-aqueous electrolytes and exhibit conductivity in n-doping state[267]. Another possible explanation is that since the kinetics of redox processes of CPs, PEDOT:PSS as an example, is sluggish in non-aqueous electrolytes[32,250,251,267], CP reduction may be limited to a surface layer, leaving a sufficient magnitude of electrically conductive oxidized CP to work as a conductive network in anode electrodes. Clarification of redox activity and conductivity of CPs in battery electrolytes across the accessible potential ranges would enable a more targeted design of CPs as binders and conducting additives in battery electrodes.

3) Other concerns

Traditional PVDF/C electrode matrices have been highly successful because they are cost-effective. It is unclear whether the cost of CP-based binders can compete with traditional compositions or be offset by performance gains. While commercial PEDOT:PSS preparations are significantly more expensive than traditional PVDF and carbon additives, lower-cost alternatives, such as polypyrrole- and polyaniline-based binders may be produced at a competitive cost. Many studies aim to develop CP-based binders that are compatible with the current slurry casting process, allowing them to be used as a drop-in technology and minimizing new capital investments. While most of the current CP binder research is of academic nature and explores the opportunities that CP binders can yield, cost should be considered when new CP binders are proposed.

Many of the conducting polymers presented here can be processed in aqueous solutions[119,180,199], providing a significant advantage over PVDF that is commonly processed in the toxic and expensive solvent NMP. This reduces environmental impact and solvent costs of electrode processing[268]. Yet, there is concern that aqueous binders, such as SBR, CMC, and PAA, might trigger proton-lithium exchange in lithiated active materials[269–272], such as LCO, NCM, and NCA, as well as induce the corrosion of aluminum foil due to the rise of the pH of the cathode slurry[273–276]. The current method to alleviate the latter of these issues is the acidification of the cathode slurry[271,272] and utilizing carbon-coated aluminum foil as a current collector[275,276]. Given the fact that most CP-based binders are processed in water, future studies should consider the effect of an aqueous slurry on the current collector and active materials. The synthesis of CP-based battery binders typically involves monomers, oxidants, templates and/or cross-linkers, in which the cost and potential hazards need to be assessed. The application of CPs in medical devices as demonstrated the biocompatibility and biodegradability of many of these composites[277,278] which reduces significantly the amount of environmental contamination with perfluorinated compounds.

V. Conclusions

The complex structure of lithium-ion batteries requires the innovative design of all electrode components, including active materials, binders, conductive additives, electrolytes, and separators. This review has shown how mechanical degradation could be mitigated by the

replacement of the traditional PVDF/C electrode matrix with CP-based binders as flexible and adhesive conductors. This is one of the ways that research into passive materials and composites opens up the active material space by transferring requirements for active materials, such as low volume change, to passive materials that can accommodate those requirements, such as flexible, adhesive conductors.

Multifunctional CP-based binders have shown promising features such as compatibility with aqueous processing, sufficient electronic conductivity, strong adhesion to active materials and possible capacity contribution. Research has overcome the intrinsically poor processability of pristine CPs by forming composites with hydrophilic polymers, modifying CP side chains with hydrophilic groups and fabricating a hydrogel-derived 3D electrode framework of conducting polymer-active material via *in situ* polymerization. The two former approaches are attractive for their facile synthesis and scalability at a reasonable cost. The latter approach inherits the advantages of hydrogel materials such as tunable nanostructure and hierarchical 3D electrode frameworks with interconnected pathways for ionic and electronic conductions. More importantly, the design concept for CP-based binders mentioned above, especially hydrogel-based CP materials, may find application also in supercapacitors and flexible/wearable devices[279].

Open questions remain. Electrochemical and chemical stabilities remain an underexplored issue. While evidence has been presented that CP-based binders perform well over many cycles, a systematic study of the chemistry of these binders after long-term cycling and abuse conditions will allow a more substantial discussion of potential side-reactions and their long-term impact on battery performance. Moreover, we know little about the complex interplay of CP-based binder swelling, electrode microstructure, and effects on ionic and electronic conductivity within complex composite electrodes. Finally, it is important that reporting standards in battery research are upheld also in the exploration of CP-based binders, so that energy densities and specific energies can be easily compared to traditional battery electrode compositions. As research into CP-based binders is accelerating, we are confident that these issues can be overcome. The literature has already shown significant performance improvements in Li-ion technology, based on the application of CP-based binders. Studies into applications of CP-based binders in non-traditional rechargeable batteries may point to applications, where CP-based binders can have a more significant impact in

enabling new technologies to break through and become commercially competitive to the high-performance standards set by current Li-ion technology.

As the material scope of rechargeable batteries is widening, this review has shown that CP-based binders can have an important role to play in the development of new battery chemistries. Aqueous processing, strong adhesiveness, combined with good electronic conductivity and mechanical flexibility make CP-based binders strong candidates to support the implementation of exotic high-performance materials in rechargeable batteries. As research is progressing, the commercial success of these binders can be found when confidence in their ability to sustain long-term cycling has been established.

Chapter 3. Conducting Polymer Composites as Water-Dispersible Electrode Matrices for Li-Ion Batteries: Synthesis and Characterization

Abstract

This chapter describes the first effort in developing CP-based electrode matrices based on the unique combination of CPs and carboxylate-containing aqueous binders. Specifically, polypyrrole:carboxymethyl cellulose (PPy:CMC) composites were synthesized by in situ chemical oxidative polymerization. Several characterization techniques had been used to understand the morphology, structure, and physical/chemical properties of PPy:CMC composites. Following that, carbon-additive-free $LiCoO_2$/PPy:CMC cathodes were fabricated by using PPy:CMC composites with water as a processing solvent. Carbon-additive-free $LiCoO_2$/PPy:CMC cathodes were then cycled to study the performance of PPy:CMC electrode matrices.

I. Introduction

The more charges are stored in a smaller space, the greater is the need for structural relaxation at the atomic level in response. As such, in the search for battery materials with ever-increasing energy densities, larger volume changes during cycling become more likely. Those volume changes need to be mitigated by the electrode matrix, which provides an adhesive and conductive framework for active materials. Failing to maintain electrode integrity upon repeated charging and discharging results in capacity fading[157]. Some of the high-energy-density materials for which this has become evident are silicon-based anodes[37,135,208] and Ni-rich $LiNi_xMn_yCo_{1-x-y}O_2$ (NMC) cathode[7,269,280] materials. Nonetheless, less research has been devoted to developing electrode matrices in comparison to research on active materials. Consequently, the limitations of current battery electrode matrices are holding up the development of some promising high-energy-density materials.

The electrode matrix is usually comprised of carbonaceous conductive additives and non-conducting polymeric binders. Over the last two decades, the most commonly used electrode matrix is polyvinylidene fluoride/carbon black (PVDF/C) due to its excellent electrochemical/chemical stability and ease of processing[281]. In the development of new high-energy-density battery materials, some intrinsic drawbacks of PVDF/C are becoming more prominent[117,154,157]. Firstly, processing of battery electrodes with PVDF/C requires toxic N-Methyl-2-pyrrolidone (NMP) and electrode drying and solvent recovery are energy intensive[268].

Secondly, fluoropolymers, such as PVDF, exhibit famously weak intermolecular interactions with other substances, which makes them well suited as lubricants[282]. Simultaneously, they are very weak adhesives in electrodes, which significantly contributes to battery performance degradation due to electrode disintegration upon cycling[140,154,157]. Strong interaction between the electrode matrix and active materials is vital to suppress electrode cracking, maintain electrode architecture as well as enhance electrode stability[166]. Thirdly, carbonaceous additives exhibit little polarity at their surface. Given highly polar oxide intercalation materials and electrolytes, this lack of polar interactions within the matrix increases the occurrence of contact loss and carbon agglomeration[120,154]. The development of conductive electrode matrices with polar surfaces improves ease, cost, and environmental impact of electrode processing, and addresses longevity of electrodes with large volume changes by increasing adhesion of the conductor to the active materials[154,157,158].

Several strategies have been reported to prepare alternative electrode matrices to enhance battery performance. Most studies have focused on using aqueous battery binders and other carbonaceous additives[158,273,283]. Moving to aqueous binders, such as carboxymethyl cellulose (CMC)[90,273], alginate[166,167], and polyacrylic acid (PAA)[208,226,284], electrode processing becomes cheaper and more environmentally friendly[90,158,268]. At the same time, it exploits intermolecular interactions and chemical bonding with active materials[166,193,285], resulting in stronger adhesion. As a result, the electrode integrity and good performance in high-energy-density electrodes, such as silicon, can be maintained over more cycles. An alternative approach exploits the combination of electrical conductivity, mechanical flexibility, and extended microstructure of conducting polymers to boost the electrical conductivity of battery electrodes with promising results[12,32,177,199,286,287]. By adding a small amount of conducting polymer into a mixture of active materials, conventional binders, and carbon additives, the conducting polymers can bridge connections between conductive particles that would otherwise be lost, leading to the maintenance of a continuous conductive network. Other electrode matrix designs are based on functional group-modified conducting polymers[137,197,288] and three-dimensional conducting polymer gels[46,48,205,207,279], in which carbon additives and/or additional binders (PVDF, CMC) are involved during electrode fabrication. Chapter 2 describes these efforts in developing conducting polymer-based binders in more detail[4]. Some studies have reported the fabrication of carbon-additive-free electrodes with only active materials and poly(3,4-

ethylenedioxythiophene):polystyrene sulfonate (PEDOT:PSS)[119,120]. No additional conductive additives and binders are required to fabricate electrodes, which suggest the possibility of using conducting polymers as single-component multifunctional electrode matrices. Despite their promising results, however, the high cost of PEDOT:PSS hinders the wide-scale application as a battery electrode matrix.

The success of PEDOT:PSS is based on the combination of the conducting polymer PEDOT with a water-dispersible polymer PSS. As PEDOT carries positive charges (electronic holes) along its backbone in its conductive state and PSS contains negatively charged sulfonate groups, both polymers are permanently intertwined, forming a molecular composite[289]. In this composite, PEDOT provides electronic conductivity, whereas PSS increases adhesion, gives the composite film-forming properties and makes it dispersible in water. Inspired by the PEDOT:PSS structure, other combinations of conducting polymers and polyelectrolytes can be developed, as demonstrated herein. Our composites are synthesized through the facile and scalable *in situ* polymerization of conducting polymer monomers such as pyrrole or aniline in the presence of carboxylate-containing polymers such as carboxymethyl cellulose (CMC), alginate or polyacrylic acid (PAA).

In this chapter, polypyrrole:carboxymethyl cellulose (PPy:CMC) composites were synthesized and characterized to demonstrate the design concept of alternative conducting polymer-based electrode matrices. Despite being used previously as supercapacitor electrode materials[213,290], the structure and properties of in situ polymerized PPy:CMC composites is not well-understood, in particular for their consideration as Li-ion battery electrode matrix. Other PPy:CMC composite hydrogels have been also reported as promising bioelectrodes[291] and bioactive materials[292]. Herein, the preliminary examination of PPy:CMC composites as electrode matrices was performed on a $LiCoO_2$ cathode. This study forms the basis of investigations on similar alternative conducting polymer-derived electrode matrices that can offset the drawbacks of PVDF/C and make many high-energy-density battery materials commercially feasible.

II. Experiment

1) Chemicals

For the synthesis of polypyrrole:carboxymethyl cellulose (PPy:CMC) composites, pyrrole (Sigma-Aldrich, 98%), $FeCl_3$ (Fisher, 98%), sodium carboxymethyl cellulose (Na-CMC) (Sigma-Aldrich, MW= 250000 g/mol, degree of substitution 0.9), and ethanol (Fisher, 98%) were used as purchased without further purification. For electrode fabrication, $LiCoO_2$ (Sigma-Aldrich, 99.8%), PVDF (Sigma-Aldrich, 99%, MW= 534 000 g/mol), C-black (Cabot, black pearls 2000), and N-Methyl-2-pyrrolidone solvent (NMP) (Sigma-Aldrich, 99%) were used. Reverse osmosis (RO) water was used throughout the experiment.

2) Synthesis of PPy:CMC composites

PPy:CMC composites were synthesized via *in situ* polymerization. Firstly, Na-CMC was completely dissolved in water. After that, 400 µl (~5.8 mmol) pyrrole was added to the viscous Na-CMC solution. The mixed precursor solution was then placed in an ice bath. The mass ratio between pyrrole and CMC was varied as follow: 1:0 (0 wt% CMC), 1:0.25 (~25 wt% CMC), 1:0.5 (~33.33 wt% CMC), 1:0.75 (~42.85 wt% CMC), 1:1 (~50 wt% CMC), and 1:1.25 (~55.5 wt% CMC), which were denoted as PPy, PPy:CMC 1:0.25, PPy:CMC 1:0.5, PPy:CMC 1:0.75, PPy:CMC 1:1 and PPy:CMC 1:1.25, respectively. $FeCl_3$ was dissolved in water and added dropwise into the above precursor solution. The molar ratio between pyrrole and $FeCl_3$ was initially fixed at 1:2.5 (denoted as R2.5) and then increased to 1:2.75 and 1:3.0, which were denoted as R2.75 and R3.0, respectively. The concentration of pyrrole was 0.6 mol L^{-1}. The polymerization reaction was carried out for 4 hours in an ice bath. The product suspensions were immersed in ethanol overnight with the suspension/ethanol volume ratio of 1:4 to induce the precipitation of PPy:CMC composites. The precipitates were filtered by vacuum filtration and washed with ethanol until a colorless filtrate was observed. The products were then dried at 80 °C under vacuum for two days.

3) Material characterization

To characterize the structure of conducting polymer composites, transmission electron microscopy coupled with energy-dispersive X-ray spectroscopy (TEM/EDX), scanning electron microscopy (SEM), X-ray photoelectron spectroscopy (XPS) and scanning transmission X-ray microscopy (STXM) were used. PPy:CMC samples were dispersed in isopropanol and drop coated

on carbon-film-coated copper grids for TEM and EDX measurements on the FEI Talos F200X microscope at an accelerating voltage of 80 keV. SEM imaging was performed on an FEI Nova NanoSEM 450 microscope. SEM imaging for electrodes was performed by imaging 2x2 mm electrode pieces coated on Al substrate. XPS measurements were performed on a Kratos Axis Ultra spectrometer at a pass energy of 160 eV for survey scans and 20 eV for N 1s, C 1s, O 1s narrow scans. Charge neutralization of 2.5 eV was applied for each measurement. STXM imaging on PPy:CMC 1:1 composite was performed at the 10ID-1 SM beamline of the Canadian Light Source (CLS). Further details on sample preparation, instrument setup, and data analysis are provided in the supporting information.

To measure the electrical conductivity of PPy:CMC composites, samples were compressed into PPy:CMC pellets and measured employing the four-point probe method on a Miller Design FPP-5000 instrument. The 0.6 mm-thick pellets were prepared by grinding 100 mg of PPy:CMC sample and compressing it at 200 MPa in a hydraulic press. In order to evaluate electrode cohesion and adhesion, scratch testing was performed on 15 mm diameter electrode pieces, which contained 20-25 µm-thick electrode coatings on a 25 µm-thick Al substrate. Scratch tests were performed with assistance from Anton-Paar on an Anton Paar MST^3 Micro Scratch Tester with feed-back loop. A Rockwell diamond tip with a tip radius of 20 µm was scanned across an immobilized electrode piece at a constant speed of 3 mm min^{-1} and a loading rate of about 45 N min^{-1}. Two failure events were recorded. An initial detachment was marked at the smallest force at which a first penetration to the Al sublayer is observed, and full delamination was marked by the continuous delamination of the electrode film from the Al substrate.

4) Battery fabrication and testing

$LiCoO_2$/PPy:CMC electrode slurries were prepared by ball-milling $LiCoO_2$ and PPy:CMC composites in water with a solid content of ~30 wt%. The mass ratio between $LiCoO_2$ and PPy:CMC composites was fixed at 90:10 (wt%:wt%). The electrode slurries were cast on 25 µm thick aluminum (Al) foil (MTI, USA) using a doctor blade. The electrode thickness and mass loading were approximately 25 µm and 3 mg cm^{-2} respectively. After drying in a vacuum oven for two days at 80^{o}C, electrode sheets were cut into 15 mm disks. Standard $LiCoO_2$/PVDF/C electrodes were prepared by a similar procedure in NMP with 5 wt% PVDF and 5 wt% carbon black unless otherwise specified. In order to evaluate electrode performance, half cells of R2032-

format (MTI, USA) were assembled in an argon-filled glove box with oxygen and moisture level below 0.1 ppm. $LiCoO_2$/PPy:CMC or $LiCoO_2$/PVDF/C electrodes were used as cathodes. $LiPF_6$ in DMC/EC (50:50 v/v, Sigma-Aldrich) was used as the electrolyte. 15 mm lithium anode disks were cut from a lithium ribbon (Alfar Aesar, 99.9%, 0.75 mm thick). Whatman™ glass fiber (Fisher) was used as the separator. Coin cells were galvanostatically cycled with cut-off voltages of 2.8 V and 4.2 V *vs*. Li/Li^+ on Neware Battery Cyclers. A current density of 274 mA g^{-1} and 27.4 mA g^{-1} was applied to cycle coin cells as denoted as 1 C and 0.1 C-rate, respectively.

III. Results and Discussion

1) Structure of PPy:CMC composites

To confirm the successful synthesis of PPy:CMC composites, the chemical structure and nanoscopic morphology of the prepared composites were investigated. PPy:CMC composites were synthesized in their oxidized state by chemical oxidative polymerization of pyrrole in aqueous CMC solution. In the oxidized state, an anionic dopant is necessary to charge-balance positive charges on PPy. In the synthesis solution, those negative charges are mainly carried by carboxylate groups on CMC, which encourages the formation of a molecular composite between PPy and CMC, as presented in Figure 3.1. In such composite, the large-size CMC-based anionic dopant is immobilized, leading to a homogenous distribution of properties of both components. Since ferric chloride was used as an oxidant during the polymerization process, trace amounts of iron and chloride ions are expected to be found in the final composition. Together with protons and hydroxide ions, they serve as additional charge balancers in the structure of PPy:CMC composites. The electrical conductivity of the composites is anticipated to depend on the oxidation state and doping level of PPy[293,294], as well as the structural arrangement of PPy:CMC composites[212]. The presence of CMC in the composite structure is not only responsible for the water-dispersibility of PPy:CMC composites, but it is also expected to influence electrode adhesion and cohesion. Moreover, since CMC is a non-conductive polymer, the CMC content might affect the electrical conductivity of PPy:CMC composites.

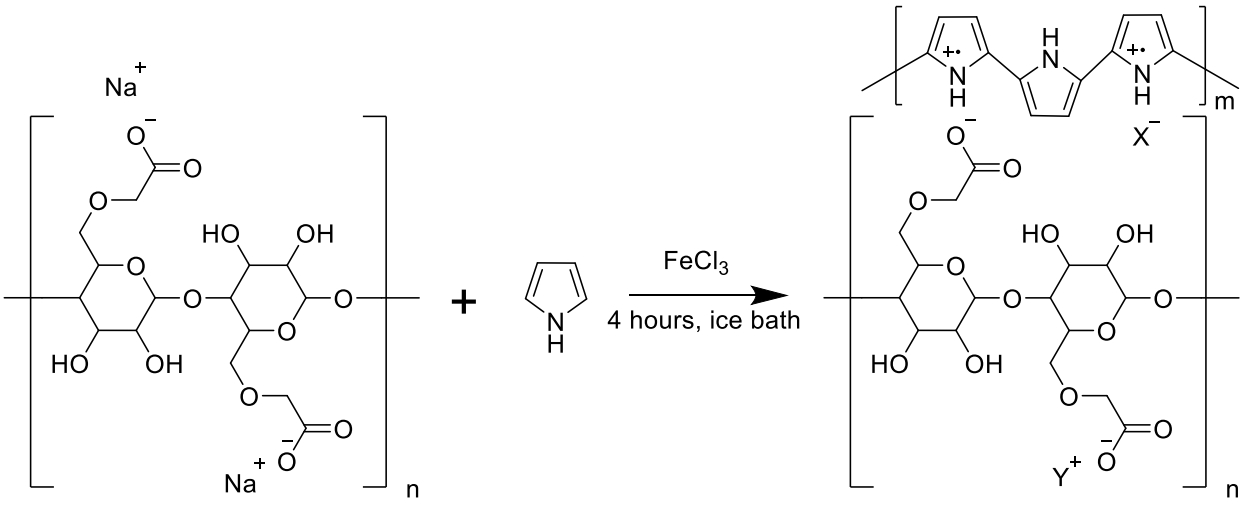

Figure 3.1. Simplified reaction scheme of the in situ polymerization of PPy:CMC composites. The targeted molecular structure of PPy:CMC composites (right) shows ionic bonding between PPy and CMC, in which carboxylate groups serve as main immobilized dopants for PPy. Generally, positively charged PPy could be doped by X^- (carboxylate, chloride and hydroxide anions). Negatively charged carboxylate groups could be balanced by Y^+ (PPy, iron, and hydrogen/hydronium cations).

A comparison between *in situ* polymerized and mechanically mixed PPy:CMC 1:1 R.2.5 composites morphology was carried out. In contrast to the *in situ* polymerized sample, PPy in the mechanically mixed composite is already oxidized and doped when it is mixed with CMC. Consequently, such a composite would exhibit a different microstructure and potentially separate phases. Figure 3.2 (a) shows the SEM image of *in situ polymerized* PPy:CMC 1:1 R.2.5 composite (denoted only as PPy:CMC 1:1 R.2.5), confirming a single homogenous morphology, consisting of fused nanospheres of approximately 50 nm in diameter. In contrast, the morphology of the mechanically mixed PPy:CMC 1:1 R.2.5 composite (Figure 3.2 (b)) shows connecting material between nanospheres.

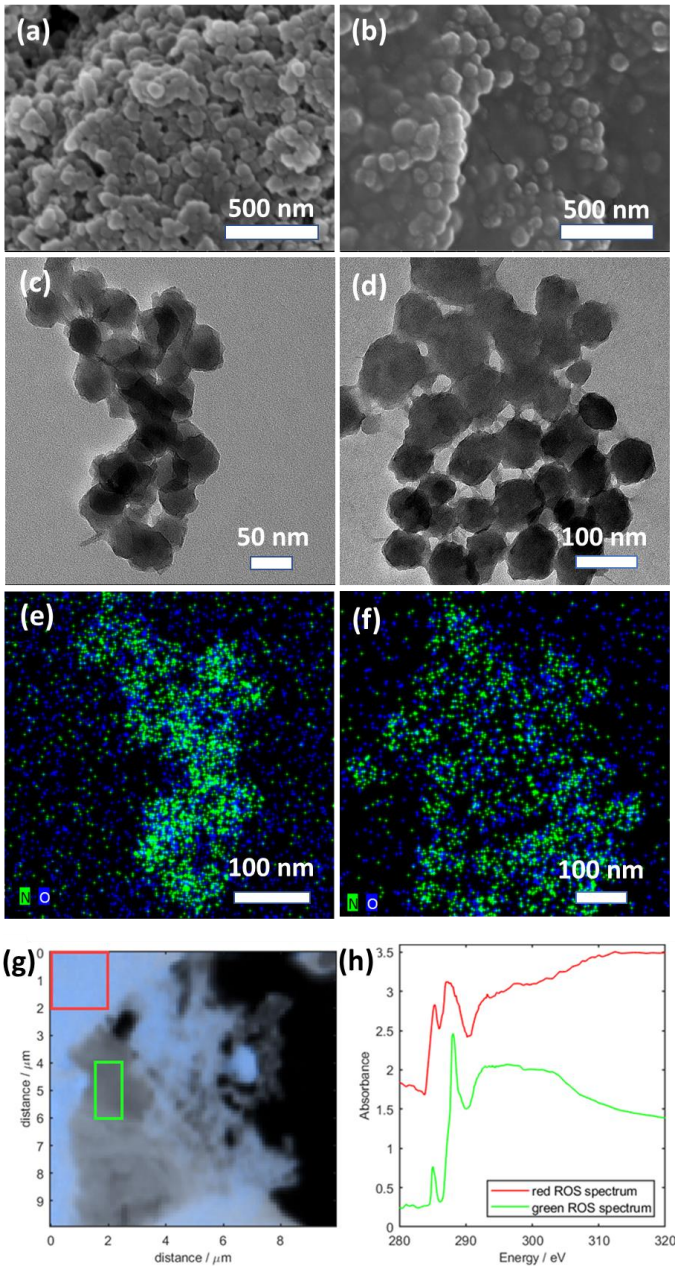

Figure 3.2. SEM and TEM images of in situ polymerized PPy:CMC 1:1 R.2.5 composite (a,c,e) and mechanically mixed PPy:CMC 1:1 R.2.5 composite (b,d,f). PPy:CMC 1:1 R.2.5 composite scanning transmission x-ray microscopy. Image overlay (g): optical density in the carbon K-edge region increases with brightness and contribution of the peak at 285 eV to overall optical density increases with color saturation. Average spectra in two regions of interest (h) within a region of high color saturation (red framed) and low color saturation (green framed) showing differences in the C1s → π transition intensity.*

TEM reveals a nano-morphology of 50.3 ± 2.1 nm spheres in the PPy:CMC 1:1 R.2.5. Figure 3.2 (e) depicts the homogeneous distribution of nitrogen and oxygen in the elemental map of PPy:CMC 1:1 composite. Using nitrogen and oxygen signals as indicators for PPy and CMC, respectively, the elemental mapping shows a homogenous distribution of both components within the resolution limit. In comparison, the mechanically mixed PPy:CMC 1:1 R.2.5 composite exhibits more discrete spherical PPy particles with a larger particle size of 72.6 ± 11.8 nm (Figure 3.2 (f)). No significant difference in elemental distribution is observed.

To verify the chemical structure of PPy:CMC 1:1 composites, X-ray absorption and photoelectron measurements were taken. The spatially-resolved STXM image reveals a complex structural arrangement of components in PPy:CMC 1:1 R.2.5 composite (Figure 3.2 (g)). The C K-edge spectrum shows two main peaks, of which the first peak at 285 eV is characteristic of the C 1s $\rightarrow \pi^*$ transition of carbon-carbon double bonds[295]. As such, this peak is indicative of the presence of PPy and it would not be expected in pure CMC[296]. While the intensity of this peak varies with location (Figure 3.2 (h)), it contributes to significant absorption intensity throughout the sample. Transitions at 288 eV and above correspond to C 1s $\rightarrow \pi^*$ transitions of carbon-oxygen double bonds, as observed in CMC, and less specific C 1s $\rightarrow \sigma^*$ transitions[295,296]. These spectra are consistent with the co-location of PPy and CMC in the sample with some variation in relative composition[297].

Similar structural complexity is observed in XPS measurements (Figure 3.3). Given the high surface sensitivity of XPS spectra, a strong spatial dependence of the nitrogen and oxygen signals is observed that suggests surfaces that are largely CMC dominated. The survey scan exposed also a ferric chloride contamination with an Fe elemental contribution well below 1%. High-resolution spectra were recorded for C 1s, N 1s and O 1s. Figure 3.3 (b) demonstrates an N 1s spectrum that is dominated by the characteristic absorption of amine/imine groups at 400.1 eV. The high binding energy shoulder corresponds to two positively charged groups $C=N^+$ and $C\text{-}N^+$, whereas, the low binding energy shoulder corresponds to the C=N group[298]. Peak fitting allows the extraction of PPy oxidation of approximately one charge per three pyrrole units. The C 1s XPS spectra show characteristic peaks at ~284.3, 285.0, 286.3, 287.5, and 289.1 eV, which corresponds to PPy Cα, PPy Cβ, C-OH/C=N/$C\text{-}N^+$, $C=O/C=N^+$ and COO^-, showing absorptions that are characteristic to PPy[299] and CMC[299]. Indications of the CMC presence are also observed in

the O 1s XPS spectra with characteristic peaks for the carboxylate (COO^-) anion. A summation of all charged groups from XPS fitting does not balance all negative charges, suggesting a role of polypyrrole protonation as positive charge carriers in the composite. While the *in situ* synthesis of PPy in the presence of CMC provides an improved environment to achieve doping of PPy with carboxylate groups from CMC, it is likely that competition with Cl^- anions lead to mixed doping.

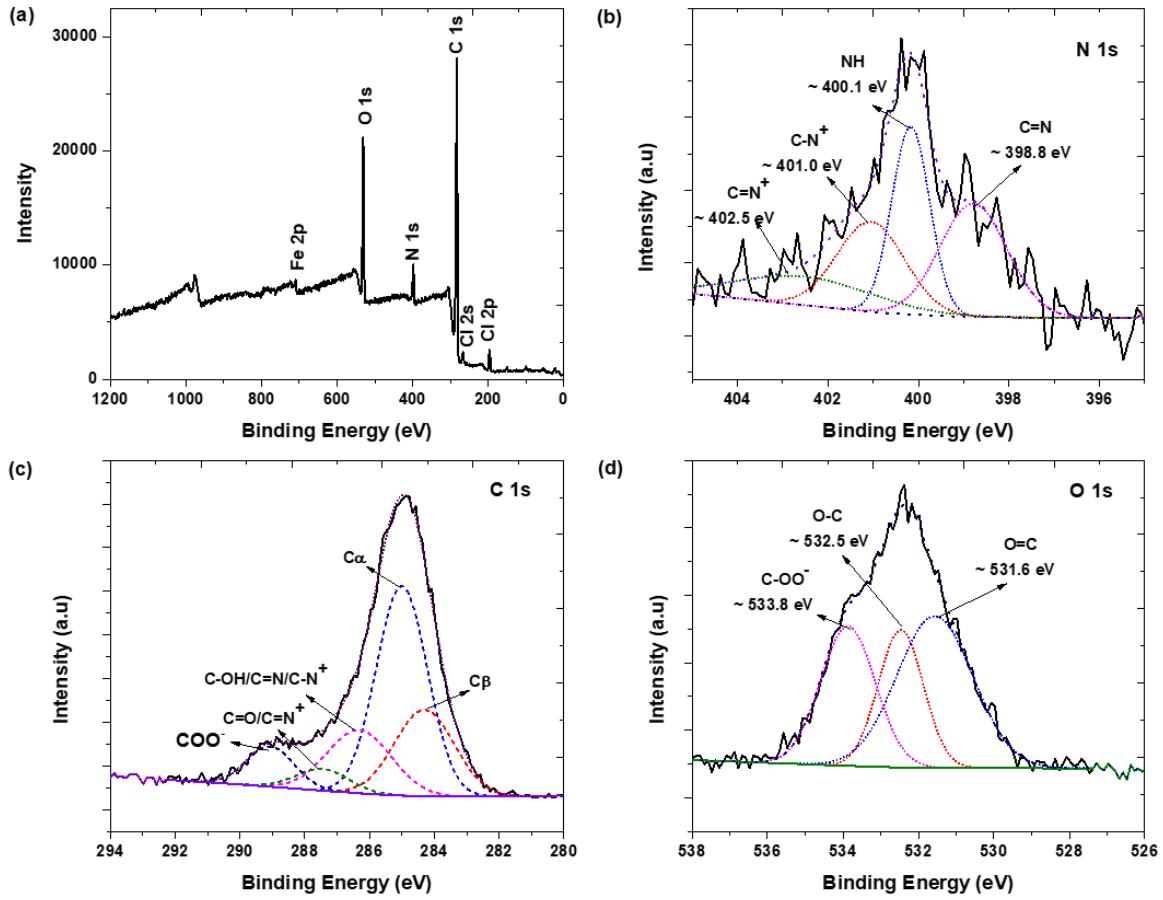

Figure 3.3. Survey XPS spectra (a) showing the complexity of the PPy:CMC 1:1 R.2.5 composite structure. High-resolution XPS scans for N 1s (b), C 1s (c), and O 1s (d).

Together, chemical and microstructural analysis of the composites demonstrate that PPy and CMC are co-located and well distributed at the nanoscale. The obtained degree of oxidation of PPy is sufficient for significant electron conduction[300]. While these methods are not able to determine whether CMC acts as a dopant in PPy, the observations confirm the successful synthesis of a composite of PPy and CMC with homogenous distribution at the nanoscale.

2) *Physical properties of PPy:CMC composites*

a) *Electrical conductivity and water-dispersibility*

To act as the sole electrode matrix, PPy:CMC composites must have sufficient electrical conductivity to support electron conduction during charging and discharging. In order to achieve a balanced electrode charging throughout the thickness of the electrode, ionic and electronic conductivity should be similar. Assuming a typical electrode with approximately 50% porosity, for standard carbonate electrolytes, at an electrode matrix weight fraction of 10% and ideal application of the Bruggeman relation, a minimum composite matrix conductivity of approximately 20 mS cm^{-1} is required. A significantly larger conductivity than this benchmark can be achieved by PPy alone (Figure 3.4 (a)). However, conductivity decreases exponentially as the CMC to PPy ratio increases. As an anionic dopant in PPy, CMC increases the distance between PPy polymer strands and is expected to increase the resistance to interchain electron transport. Moreover, surplus CMC could act as a non-conductive filler between conductive particles in the composite, resulting in the typical conductivity behavior observed for composites of conductive and non-conductive particles.

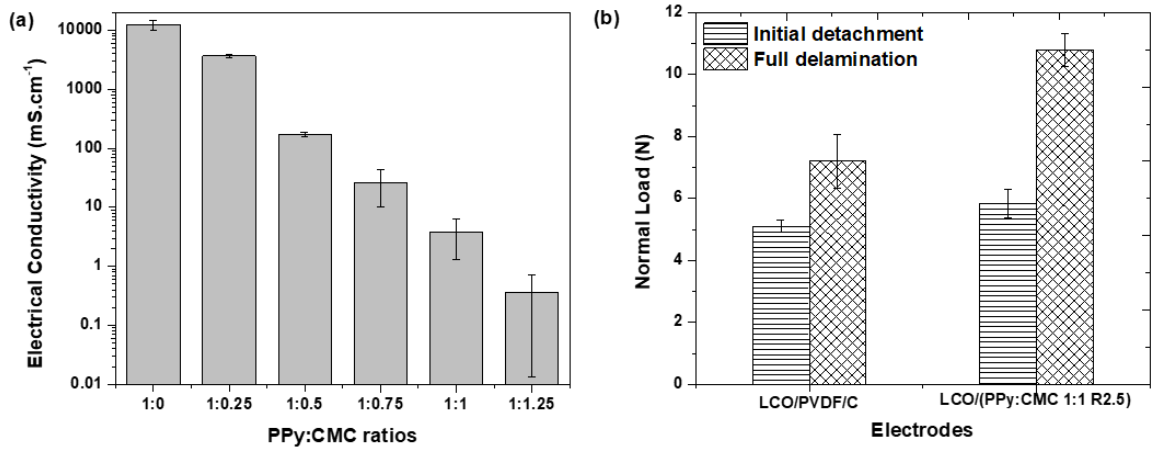

Figure 3.4. (a) Trend in electrical conductivity of PPy:CMC composites. (b) Normal Load needed to cause initial detachment and full delamination of $LiCoO_2$/PVDF/C and $LiCoO_2$/(PPy:CMC 1:1 R.2.5) electrodes from Al current collector.

According to the effective medium approximation (EMA) theory, the electrical conductivity of composites, composed of spherical insulating particles embedded in a conductive

matrix, would follow the Bruggeman relationship. Similar behaviors have been found for randomly distributed spherical conductive and non-conductive particles[256,301,302]. A simplified Bruggeman equation is described as:

$$\sigma_{eff} = \sigma_o \varepsilon^{\alpha}$$

In which, σ_{eff}, σ_o, ε, and α are effective conductivity, intrinsic conductivity, conductive volume fraction, and Bruggeman exponent, respectively. The expected Bruggeman exponent for a random mixture of near-spherical PPy and CMC particles is close to 1.5. Yet, a fit of the data reveals an exponent of 13.08 (Figure SI.3.1). This significant deviation from typical Bruggeman behavior is consistent with increased energy barriers to electron conduction with CMC content. While this effect reduces the conductivity of the composite significantly, the benchmark conductivity can be obtained with PPy:CMC composites that contain CMC at a weight ratio of CMC:PPy of 0.75 or less.

b) Electrode adhesion and cohesion

The matrix should not only be conductive but be easily processed, ideally through tape casting. Aqueous processing requires a stable dispersion of the matrix in water. While a PPy suspension settles quickly, PPy:CMC dispersions are stable for an hour (Figure SI.3.2). Figure SI.3.3 shows the appearance of a $LiCoO_2$/(PPy:CMC 1:1 R2.5) electrode fabricated with water as the solvent. The $LiCoO_2$/(PPy:CMC 1:1 R2.5) (90:10 wt%) composite film can adhere to the Al substrate without cracking or delamination. Reducing the CMC content in the composite structure could decrease dispersion stability and current collector adhesion of the composite electrode.

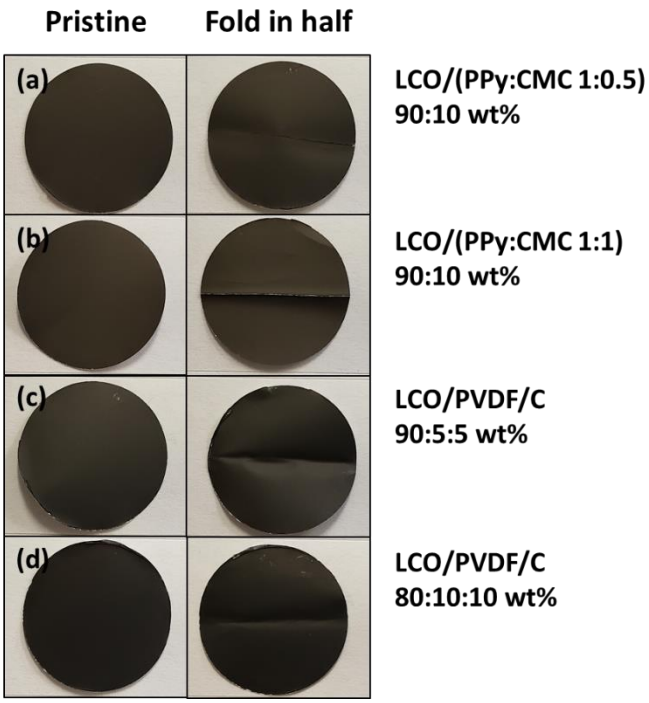

Figure 3.5. The appearances of $LiCoO_2$-based electrodes with different PPy:CMC R2.5 composites (a,b) and PVDF/C ratio (c,d). These electrodes were subjected to pristine condition (left), and half-folding (right).

Figure 3.5 depicts images of $LiCoO_2$/PPy:CMC and $LiCoO_2$/PVDF/C electrodes that adhere to Al foil without noticeable detachment. Upon folding electrodes, minor cracks are observed at the fold in the case of $LiCoO_2$/PPy:CMC electrodes, originating from the intrinsic brittleness of PPy[303,304]. Nonetheless, all electrodes remain in good contact without any detachment from the current collector. Scratch testing was performed to quantitatively evaluate the adhesion strength of different electrodes to an Al current collector (Figure 3.4 (b)). Micrographs of the formed scratch show adhesion failure points where first detachment from the Al substrate is observed, and where this detachment becomes persistent (Figure 3.6). The $LiCoO_2$/(PPy:CMC 1:1 R2.5) electrode requires a consistently higher normal load to achieve both failures, suggesting a stronger adhesion to Al foil than the $LiCoO_2$/PVDF/C electrode. The load required to cause full electrode delamination for the $LiCoO_2$/(PPy:CMC 1:1 R2.5) electrode is approximately 60% higher than that for the $LiCoO_2$/PVDF/C electrode.

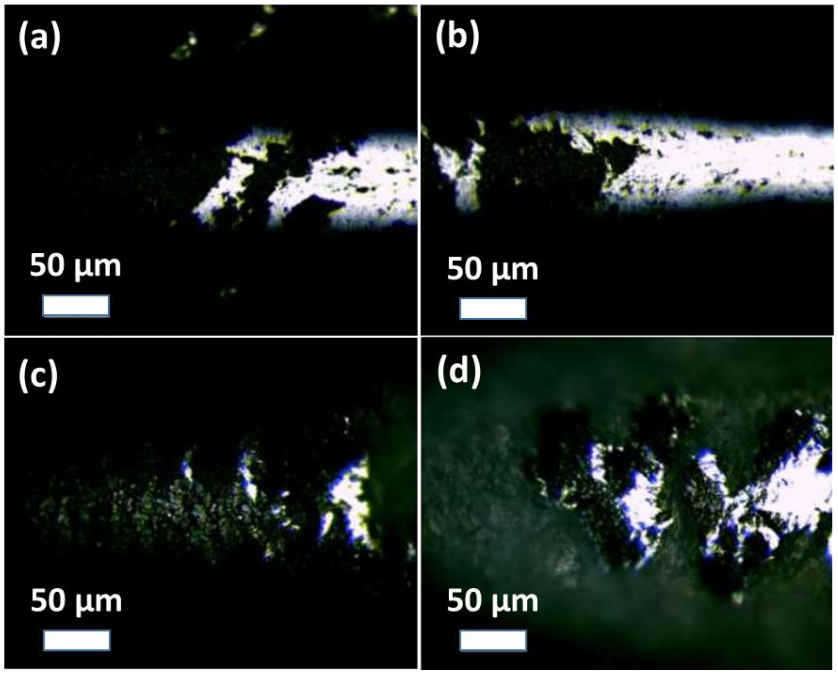

Figure 3.6. Normal Load needed to cause initial detachment and full delamination of $LiCoO_2$/PVDF/C (a,b) and $LiCoO_2$/(PPy:CMC 1:1 R2.5) (c,d) electrodes from Al current collector.

Figure 3.7 shows SEM images of electrodes with different electrode matrices. Figure SI.3.6 (c,d) shows a random distribution of PVDF/C around $LiCoO_2$ particles, including bare $LiCoO_2$ particle surfaces, and agglomerations of the PVDF/C matrix, which is typical for the weak interactions of the non-polar PVDF/C surface with the polar $LiCoO_2$ particle surfaces. The PPy:CMC matrix, on the other hand, is coating the $LiCoO_2$ surface completely, confirming the greater affinity of PPy:CMC composites toward $LiCoO_2$ (Figure SI.3.6 (a,b)). Together, the mechanical properties and observed electrode microstructure with PPy:CMC composites are promising good binding performance of PPy:CMC composites.

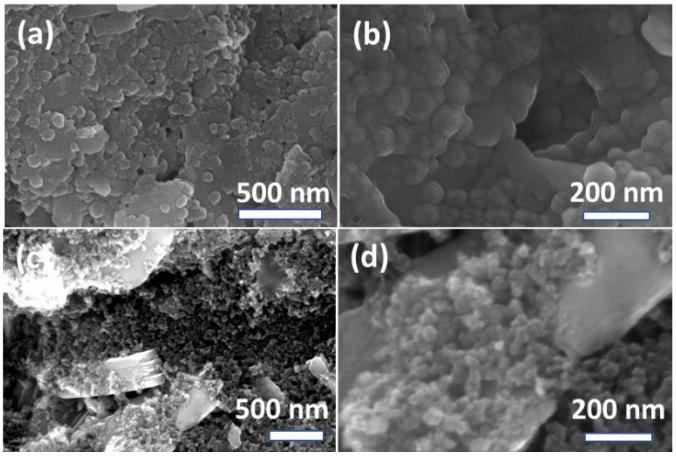

Figure 3.7. SEM images of $LiCoO_2$/(PPy:CMC 1:1 R2.50) (90:10 wt%) electrode (a,b) and $LiCoO_2$/PVDF/C (90:5:5 wt%) electrode (c,d).

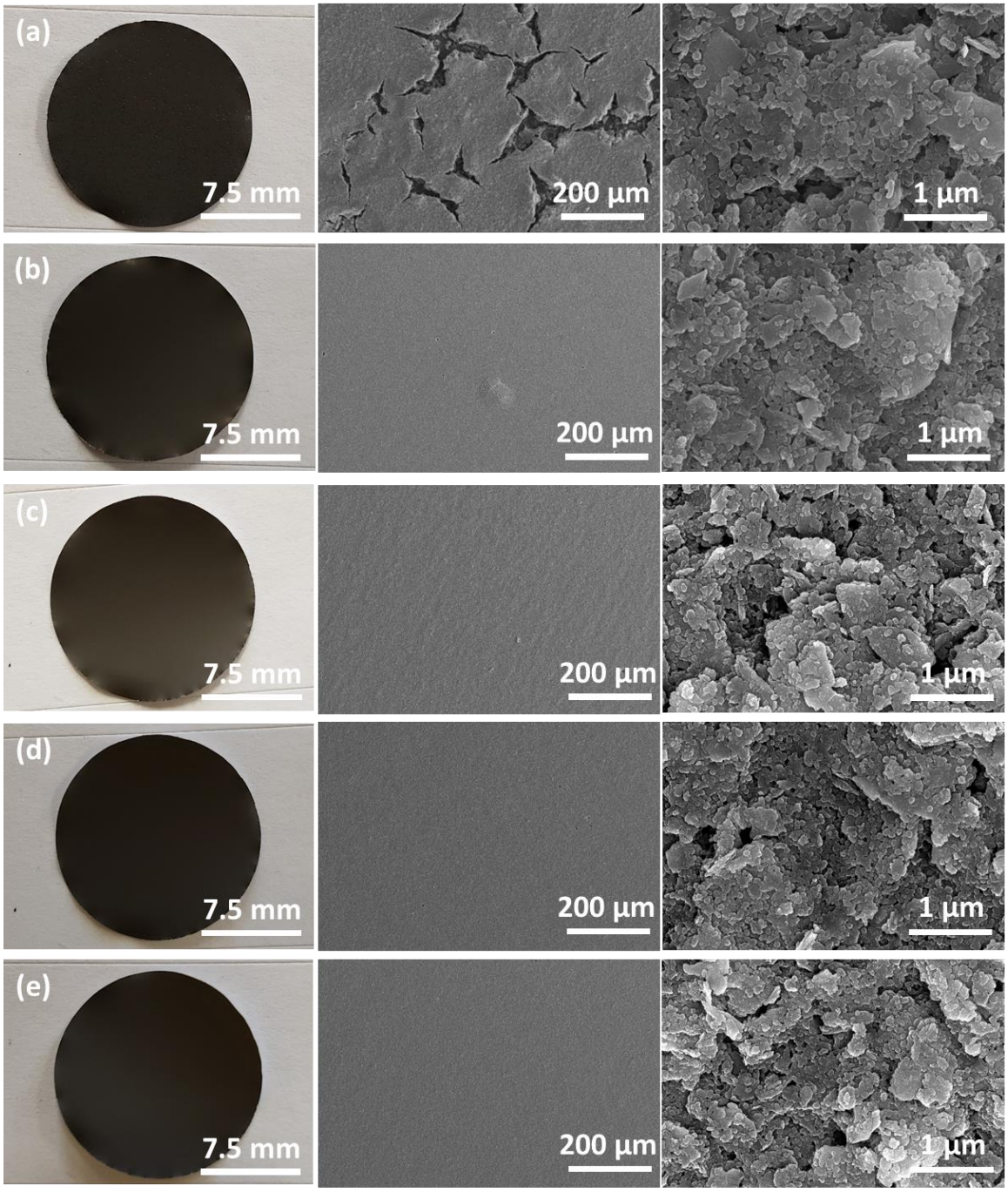

Figure 3.8. Digital and SEM images of $LiCoO_2$/(PPy:CMC 1:0.25 R2.50) electrode (set a), $LiCoO_2$/(PPy:CMC 1:0.5 R2.50) electrode (set b), $LiCoO_2$/(PPy:CMC 1:0.75 R2.50) electrode (set c), $LiCoO_2$/(PPy:CMC 1:1 R2.50) electrode (set d) and $LiCoO_2$/(PPy:CMC 1:1.25 R2.50) electrode (set e).

Figure 3.8 depicts the digital and SEM images of electrodes with different PPy:CMC composites. Some cracking was observed for the $LiCoO_2$(PPy:CMC 1:0.25 R2.5) electrode. While other electrodes showed relatively smooth surfaces. SEM imaging further confirmed the poor electrode cohesion of $LiCoO_2$(PPy:CMC 1:0.25 R2.5) electrode, where $LiCoO_2$ particles were not sufficiently covered by PPy:CMC composite. Meanwhile, no significant difference in electrode morphology was observed for other electrodes. The result suggests that low CMC content is associated with a lack of adhesive properties within electrode matrices.

3) Electrochemical performance

To evaluate the performance of PPy:CMC composites as electrode matrices, electrodes with different PPy:CMC or PVDF/C matrices were subjected to galvanostatic cycling. $LiCoO_2$/(PPy:CMC 1:1 R2.75) electrodes can be cycled at 27.4 mA g^{-1} (0.1 C) and 274 mA g^{-1} (1 C) with similar initial capacity as the benchmark $LiCoO_2$/PVDF/C electrodes (Figure 3.9). Different from standard electrode matrices, PPy:CMC composites can be oxidized and reduced, which can contribute to the overall electrode capacity. With regular small-ion dopants, the anionic dopant is released from PPy upon reduction. However, when using polyanions as dopants, the reduction of PPy leads to the intercalation of small cations into the polymer[305]. As such, the PPy:CMC matrix can act as additional charge-storage material with a behavior that is analog to traditional Li^+ intercalation materials.

It should be noted that lower electrode performance is observed with the typically suggested Py:Fe ratio of 2.5 (denoted as R2.5) during the polymerization[106,213,293], but an increased equivalent of $FeCl_3$ was required of 2.75 (denoted as R2.75). This is likely due to a small amount of ferric chloride being captured by CMC[306], as observed in the XPS results. As a result, PPy:CMC 1:1 R2.75 composite exhibited higher electrical conductivity than PPy:CMC 1:1 R2.5 composite (Figure SI.3.4). Moreover, the amount of CMC in PPy:CMC composites significantly affected electrode performance (Figure SI.3.5). Too low CMC contents in PPy:CMC composite composition results in poor electrode cohesion/adhesion. Based the morphological observations, this is likely a result of poor adhesion (Figure 3.8). Consequently, $LiCoO_2$/(PPy:CMC 1:0.25 R2.5) electrodes exhibited too large internal resistance to cycle at 0.1 C. Raising CMC content improves accessible capacity and cycling performance up to the composition PPy:CMC 1:1 R2.5. Raising the CMC content further leads again to a drop in performance, likely due to reduced electrical

conductivity at such compositions (Figure 3.4 (a)). Interestingly, mechanically mixed PPy:CMC composites showed a significantly lower electrical conductivity than *in situ* polymerized counterparts (Figure SI.3.6). Consequently, an electrode with mechanically mixed PPy:CMC 1:1 matrix cannot be cycled at 0.1 C, highlighting the importance of *in situ* polymerization of PPy in the presence of CMC to achieve sufficiently conductive nano-composite electrode matrices. This confirms that the observed distinct microscopic structures between mechanically mixed and *in situ* polymerized samples has significant performance implications.

While the initial cycling performance of PPy:CMC electrodes is similar to standard PVDF/C electrodes, capacity fading is observed almost immediately with the PPy:CMC matrices (Figure SI.3.11). This fade is correlated with a swift increase in internal resistance (Figure SI.3.7). There are several possible reasons for this performance decay. While plenty of publications show long performance stability of conducting polymer-containing electrodes[4], there is little targeted research on the compatibility and stability of conducting polymers in Li-ion batteries[307]. It is possible that conducting polymer performance decay is underestimated in many studies, where carbon additives and conducting polymers are used together, due to the reduced impact that conducting polymer conductivity has on electrode performance. In targeting the full replacement of carbon additives to avoid agglomeration, long-term conducting polymer performance becomes critical and is now the subject of ongoing work in our group. $LiCoO_2$/(PPy:CMC) cells also exhibited an initial spike in cell voltage followed by a descent in the first charging step. A number of processes could lead to this behavior including slow electrolyte infiltration or doping of PPy by the electrolyte. While the study of this phenomenon lies outside the scope of the present paper, it points to interesting targets of future work.

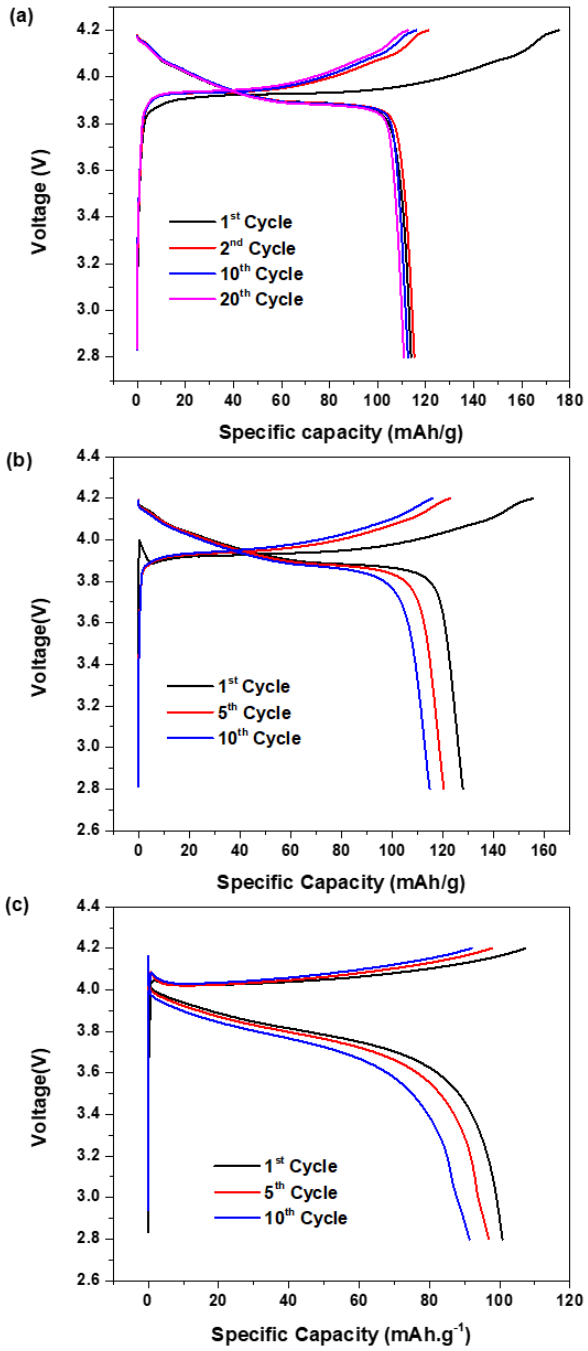

Figure 3.9. Voltage Profiles of $LiCoO_2$/PVDF/C cathode at 0.1 C (a), $LiCoO_2$/(PPy:CMC 1:1 R2.75) cathode at 0.1 C (b) and at 1 C (c).

IV. Conclusions

This chapter demonstrates the design concept of water-dispersible, self-conductive electrode matrices from conducting polymer composites synthesized *via* a simple and scalable *in*

situ polymerization. Multifunctional PPy:CMC composites, that exhibit adhesion, electronic conductivity, and contribute to charge storage are a promising replacement for PVDF and carbon additives in electrodes to reduce carbon agglomeration and achieve a conductive electrode network that actively adheres to intercalation materials during cycling. We demonstrated that a $LiCoO_2$/PPy:CMC electrode can be cycled at a high current density of 274 $mA.g^{-1}$ without carbon additives, which is a unique achievement within carbon-free Lithium intercalation cathodes. At the same time, the conductive network within the electrode appears to deteriorate during cycling, which is the subject of ongoing work.

Notwithstanding the stability limitations, this study highlights the performance potential of battery electrodes containing conducting polymer composite matrices. Those matrices are produced from low-cost, high-volume raw materials, are easily synthesized and processed in low-cost, low-impact aqueous solutions. As new electrode materials are developed with ever-increasing energy densities, the potential for larger volume change increases as well. This will require a solution to the intrinsic lack of adhesion between carbonaceous conductors and active materials, of which conducting polymer composites are shown here to be a promising candidate.

Chapter 4. Carbon-additive-free $LiNi_{1/3}Mn_{1/3}Co_{1/3}O_2$ Cathode Enabled by Conducting Polymer-based Electrode Matrix

Abstract

Chapter 3 demonstrates the proof of concept for using PPy:CMC composites as adhesive, conductive, and water-processable electrode matrices for $LiCoO_2$-based cathodes. The question remains whether PPy:CMC composites can be used as versatile electrode matrices for different types of electrode materials such as $LiNi_{1/3}Mn_{1/3}Co_{1/3}O_2$ (NMC111), which is industry-relevant cathode material. In this work, NMC111 was synthesized in-house and characterized before mixing with PPy:CMC composites in water to fabricate carbon-additive-free NMC111/PPy:CMC cathode. Regardless of eliminating carbon conductive additives from electrode composition, NMC111/PPy:CMC cathode could be able to operate at high C-rate, confirming the capability of PPy:CMC composites for providing enough electrical conductivity for battery electrodes.

I. Introduction

The demand for high-mileage electric vehicles is encouraging battery communities to explore and employ high-energy-density battery materials. For the cathode, most Li-ion battery manufacturers have shifted away from using $LiCoO_2$ due to their rising cost and limited energy density[7]. Layered lithium transition metal oxides such as $LiNi_xMn_yCo_{1-x-y}O_2$ (NMC), $LiNi_xCo_yAl_{1-x-y}O_2$ (NCA) and their Ni-rich (NMC, NCA: $x \geq 0.6$), Li-rich ($Li_2MnO_3.LiMO_2$, M=Co, Ni, Al) derivatives are considered the state-of-the-art cathode materials[308], which have been used by major Li-ion battery manufacturers[1]. The structural instabilities and corresponding mitigation strategies for these cathode materials have been reviewed in several references[7,15,308,309]. In contrast to anode materials, the volume change between charged and discharged states of cathode materials is much smaller. However, particle cracking remains a critical issue as reported in the literature[310,311]. Electrode delamination has also been reported for NMC-based cathodes prepared with the conventional PVDF/C electrode matrix[71,310], which is likely insufficient in maintaining electrode mechanical integrity. Cracked particles become electrically isolated, thus could not participate in charge/discharge processes if these cracked particles are not connected by conductive additives. These mechanical-related problems would be addressed by using a high-performance, conductive electrode matrix that offers strong interactions with cathode active materials as mentioned in Chapter 2.

Following the trend of using aqueous electrode processing for anode fabrication, some studies have reported the use of aqueous binders for fabricating NMC-based cathodes such as CMC[275,312], styrene-butadiene rubber (SBR)[313], polyurethane[273], xanthan gum[314], guar gum[315], and fluorine acrylic hybrid latex[313]. Many electrode matrices containing aqueous binders and carbon additives have shown better performance than PVDF/C. For example, by owning an abundant amount of hydroxyl and carboxylate groups on their structures, xanthan gum (XG), and guar gum (GG) binders were reported to tightly wrap Li-rich NMC particles[314,315]. Such strong surface adhesion supported bulk electrode integrity and suppressed electrode corrosion by electrolytes. As a result, these electrodes exhibited better performance than their PVDF/C-based counterparts. Similarly, thanks to the presence of hydroxyl and carboxylate functional groups, CMC binder was reported to adhere well to NMC particles[275,312]. Moreover, using CMC/C mixture as an electrode matrix reduced the charge transfer resistance during the (de)lithiation of NMC materials due to the high ionic conductivity of CMC. Therefore, NMC/CMC/C cathode exhibited higher rate-capability than NMC/PVDF/C and NMC/Alginate/C cathodes[312]. The problems, however, arise from the interfacial instabilities of NMC cathode materials upon exposure to water during the aqueous electrode slurry preparation[269,271,272,275,316]. Interfacial structure reconstruction and lithium leaching could result in particle fracture and impedance increase, which subsequently degrade cathode capacity. Adjusting the pH of electrode slurry is a common approach to shift the equilibrium of lithium dissolution against NMC deterioration[317]. Having CMC in their structure, PPy:CMC composites, which were used as electrode matrices for $LiCoO_2$ as described in Chapter 3, are expected to form strong interactions with NMC materials and improve electrode performance. More importantly, the self-conductive feature of PPy:CMC composites could eliminate the use of carbon additives, thus giving free spaces for adding more active materials to deliver higher volumetric and gravimetric capacities.

To facilitate the adoption of CP-based electrode matrices in Li-ion batteries, their compatibilities with NMC cathode materials should be investigated. Herein, $LiNi_{0.33}Mn_{0.33}Co_{0.33}O_2$ (NMC111) was synthesized by the sol-gel method. Following that, for the first time, carbon-additive-free NMC cathodes were made available by using PPy:CMC electrode matrices. This study further confirms the versatility of CP-based electrode matrices and urges future applications.

II. Experiment

1) Synthesis of PPy:CMC composite

The detailed synthesis procedure for PPy:CMC composite can be found in Chapter 3. In brief, pyrrole (Sigma-Aldrich, 98%), was chemically polymerized by $FeCl_3$ oxidant (Fisher, 98%) in the aqueous solution of Na-CMC (Sigma-Aldrich, MW= ~250.000 g/mol, degree of substitution 0.9). In this chapter, pyrrole:Na-CMC mass ratio and pyrrole:$FeCl_3$ molar ratio were fixed at 1:1 and 1:2.75, respectively. To simplify the notation, the PPy:CMC11-R275 composite that was synthesized in Chapter 3 will be denoted simply as PPy:CMC composite in this chapter. After synthesis, PPy:CMC composite was purified and dried as described in Chapter 3.

2) Synthesis of $LiNi_{0.33}Mn_{0.33}Co_{0.33}O_2$ (NMC111)

NMC111 was synthesized by a sol-gel method that followed the synthesis procedure reported by previous work[318]. $CH_3COOLi.2H_2O$ (Sigma-Alrich, 98%), $(CH_3COO)_2Ni.4H_2O$ (Sigma-Alrich, 98%), $(CH_3COO)_2Mn.4H_2O$ (Sigma-Alrich, 98%), $(CH_3COO)_2Co.4H_2O$ (Sigma-Aldrich, 98%) and citric acid (Sigma-Aldrich, 98%) were used as received without any purification. Firstly, acetate salts were dissolved together in DI water with the Li:Ni:Mn:Co ratio of 1.1:0.33:0.33:0.33. Citric acid (Sigma-Aldrich, 98%) was dissolved completely in DI water, mixed with ethylene glycol (Sigma-Aldrich, 99.8%), and then slowly added to the NMC precursor solution. The molar ratio between citric acid and total metal ions was 1:1. The solution was heated to 70 ^oC overnight to yield a pink gel that was then kept at 70 ^oC for 2 days. The dried gel was ground and transferred to a ceramic crucible before putting in a furnace. The sample was pre-calcinated at 450 ^oC for 2 hours to burn out organic components. The powder was ground and compressed into pellets at 25 MPa. The calcination was performed at 900 ^oC for 12 hours in air. A heating rate of 2 $^oC.min^{-1}$ was used throughout the experiment. The final product was ground by mortar and pestle into fine powders and dried in a vacuum oven before use.

3) Electrode preparation and coin cell fabrication

NMC111/PPy:CMC cathode was prepared by mixing NMC111 powder with PPy:CMC composite (PPy:CMC 1:1 R2.75) at a mass ratio of 90:10 wt%. The solid mixture was dispersed in water with a solid content of 30 wt% and then stirred vigorously on a magnetic stirrer for 6 hours. A homogenous electrode slurry was cast on aluminum to yield ~ 25 μm-thick electrode sheets on 25 μm-thick Al foil (MTI, USA) by using a doctor blade. For comparison,

NMC111/PVDF/C (90:5:5 wt%) reference cathode was prepared in N-Methyl-2-Pyrrolidone (NMP) solvent by a similar procedure. Electrode mass loading was controlled at approximately 3 $mg.cm^{-2}$. Electrode sheets were carefully dried in a vacuum oven at 80 ^{o}C for two days and cut into 15-mm in diameter electrode disks before use.

CR2032-type coin cells *(MTI, USA)* were used to fabricate half-cell Li-ion batteries for testing cathode performance. Coin cell fabrication was performed in an argon-filled glove box (Unilab Mbraun) with oxygen and moisture level below 0.1 ppm. Each coin cell contains 15 mm disc cathode, 20 mm disc glass fiber separator (Whatman^{TM}), 15 mm lithium disc (Alfar Aesar, 99.9%, 0.75 mm thick, $LiPF_6$ in DMC/EC (50:50 v/v) electrolyte (Sigma-Aldrich).

4) Material characterization

The crystal structure of NMC111 cathode materials was confirmed by powder X-ray diffraction (XRD) measurement on the D4 Endeavor instrument with Cu Kα source at a working voltage of 40 kV. Data treatment was performed on QuaIX software with Crystallography Open Database[121]. The morphologies of NMC111 were studied by SEM (FEI Nova NanoSEM 450) and TEM/EDX (FEI Talos F200X S/TEM).

5) Electrochemical and post-mortem analyses

Coin cells were galvanostatically charged and discharged within the fixed potential window of 3.0 V – 4.3 V Li/Li^+ on Neware battery testers. The applied current density of 275 $mA.g^{-1}$, 27.5 $mA.g^{-1}$, and 13.75 $mA.g^{-1}$ were denoted as 1 C, 0.1 C, and 0.05 C-rate, respectively.

After cycling for 100 cycles at 1 C, a coin cell was opened in an argon-filled glovebox. Cathode material was disassembled and then washed in propylene carbonate (PC) solvent. The washed cathode was dried in a vacuum oven at 85 ^{o}C for 2 days. The sample was then stored in the argon-filled glovebox prior to mount on the sample holder for SEM measurement.

III. Results and discussion

The structure of lab-synthesized $LiNi_{0.33}Mn_{0.33}Co_{0.33}O_2$ (NMC111) cathode materials was confirmed by powder X-ray diffraction. Figure 4.1 (a) shows that major X-ray diffraction peaks were identical to the NMC111 standard structure[319]. NMC111 particles exhibited a narrow size distribution in the range of 200-300 nm as confirmed by SEM and TEM (Figure 4.1 (b,c)). EDX analysis suggested that the molar ratio between transition metal ions was close to the desired value.

The HRTEM shows crystallinity reaches the particle surface (Figure 4.2 (a)). Homogeneous distribution of Mn, Ni, and Co elements was confirmed by elemental mapping (Figure 4.2 (b,c,d,e)).

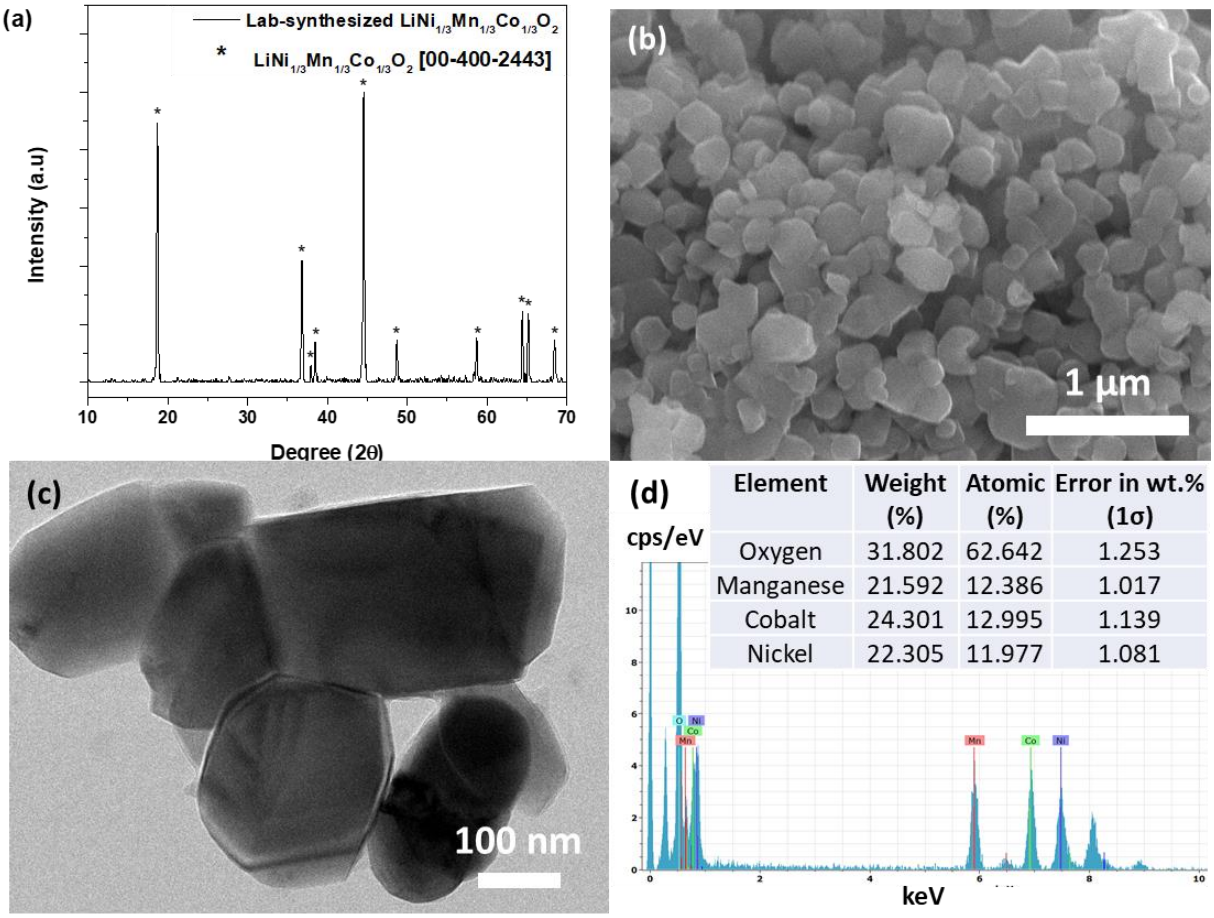

Element	Weight (%)	Atomic (%)	Error in wt.% (1σ)
Oxygen	31.802	62.642	1.253
Manganese	21.592	12.386	1.017
Cobalt	24.301	12.995	1.139
Nickel	22.305	11.977	1.081

Figure 4.1. (a) XRD diffractogram; (b) SEM image; (c) TEM image; (d)EDX analysis result of lab-synthesized $LiNi_{1/3}Mn_{1/3}Co_{1/3}O_2$ (NMC111).

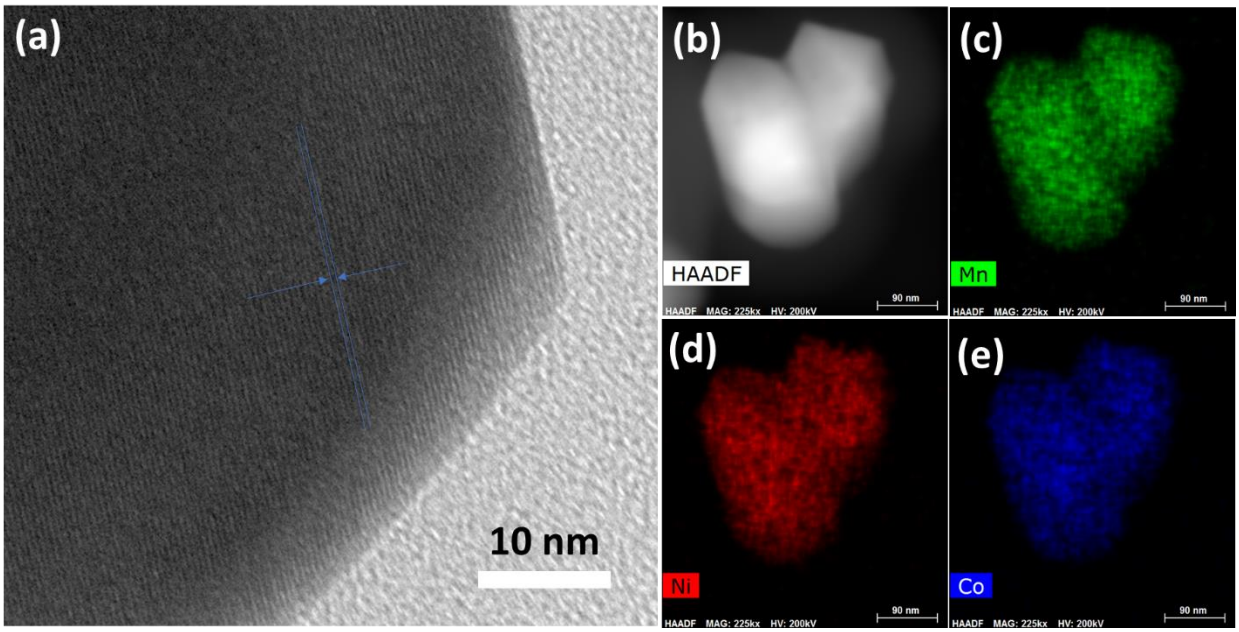

Figure 4.2. (a) HRTEM image of NMC111; (b,c,d,e) elemental mapping images of NMC111.

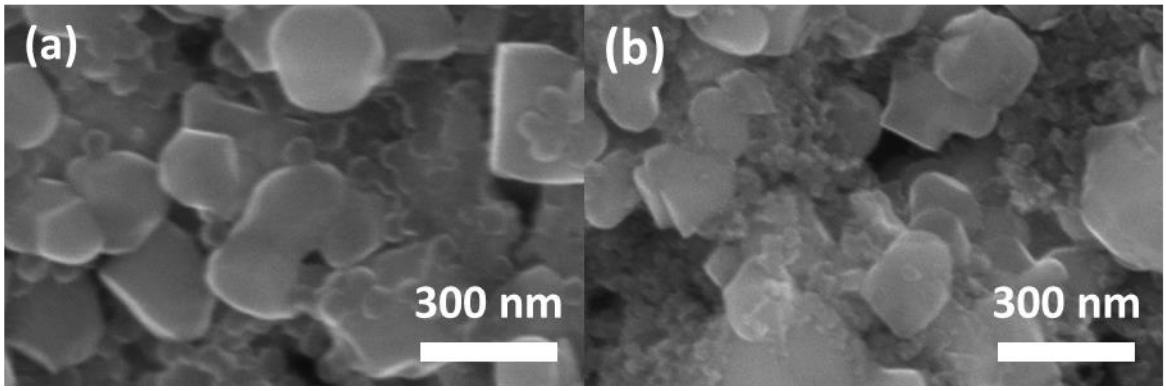

Figure 4.3. SEM images of NMC111/PPy:CMC cathode (a);
and NMC111/PVDF/C cathode (b).

A comparison between the morphologies of NMC111-based electrodes with PVDF/C and PPy:CMC electrode matrices was demonstrated in Figure 4.3. The PPy:CMC composite showed greater adhesion towards the surface of NMC111 particles compared to that of PVDF/C, which loosely surrounded NMC111 nanoparticles. The good surface affinity of the PPy:CMC composite was consistent with the result from a previous study on $LiCoO_2$/PPy:CMC cathodes[3] as reported in Chapter 3. In contrast with a non-polar PVDF/C mixture, the PPy:CMC composite was composed of charged molecules, allowing them to form stronger intermolecular interactions with

NMC particles. In addition, their strong surface adhesion to NMC particles could be attributed to the abundance of hydroxyl and carboxyl groups on the structure of CMC. This explanation was in agreement with other studies, where they claimed the strong surface adhesion between Li-rich NMC particles and xanthan gum[314], guar gum[315] resulted from a large number of hydroxyl and carboxyl functional groups on the structure of polysaccharide gums.

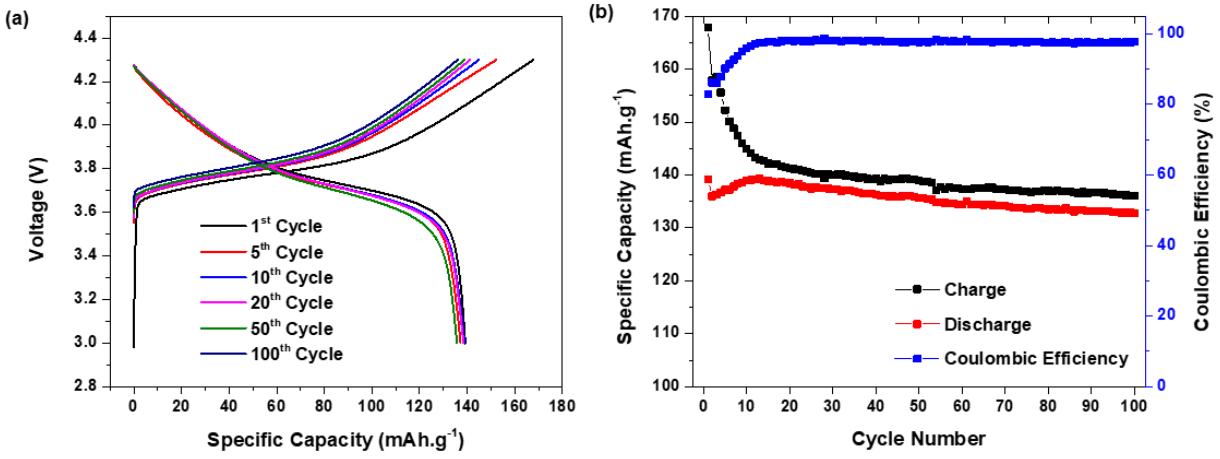

Figure 4.4. (a) Voltage profiles, and (b) plot of charge/discharge capacity and coulombic efficiency versus cycle numbers of NMC111/PVDF/C reference cathode at 0.1 C (27.5 mA.g^{-1}).

The NMC111/PVDF/C reference cathode showed great capacity retention, maintaining a specific discharge capacity of approximately 135 mAh.g^{-1} after 100 cycles at 0.1 C (27.5 mA.g^{-1}). In comparison to the NMC111/PVDF/C reference cathode, NMC111/PPy:CMC cathode demonstrated a higher initial discharge capacity of 150 mAh.g^{-1} (Figure 4.5). As for the presented battery cell, however, there was a noticeable decrease in electrode performance from the 23rd cycle due to unknown reasons. Other battery coin cells with similar NMC111/PPy:CMC cathode composition also suffered from unexpected capacity fading or shorting after running for 30-50 cycles. The underlying reasons for this poor life cycle are unknown, but they might result from parasitic reactions between NMC111, PPy:CMC composite and electrolytes

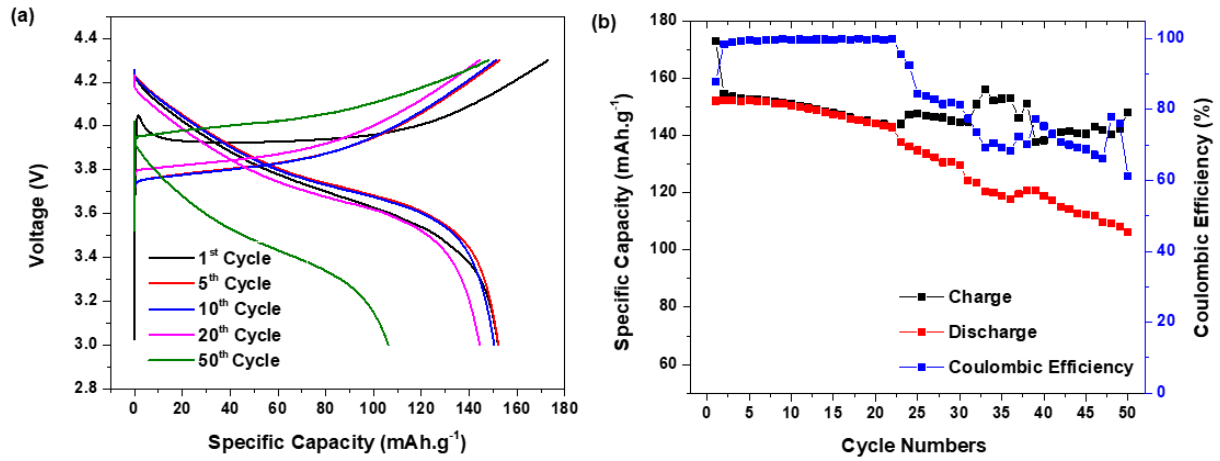

Figure 4.5. (a) Voltage profiles, and (b) plot of charge/discharge capacity and coulombic efficiency versus cycle numbers of NMC111/PPy:CMC cathode at 0.1 C (27.5 mA.g^{-1}).

Nonetheless, carbon-additive-free NMC111/PPy:CMC cathode was able to operate at 1 C with great capacity retention. After cycling for 100 cycles at 1 C, they still delivered ~ 90 mAh.g^{-1}. The result confirmed that the PPy:CMC composite provided sufficient electrical conductivity for NMC111 active materials to run without using carbon additives. Despite having lower intrinsic electrical conductivity than carbon black, the high affinity toward NMC111 of the PPy:CMC composite allowed them to offer a great electrical connection between individual NMC111 particles.

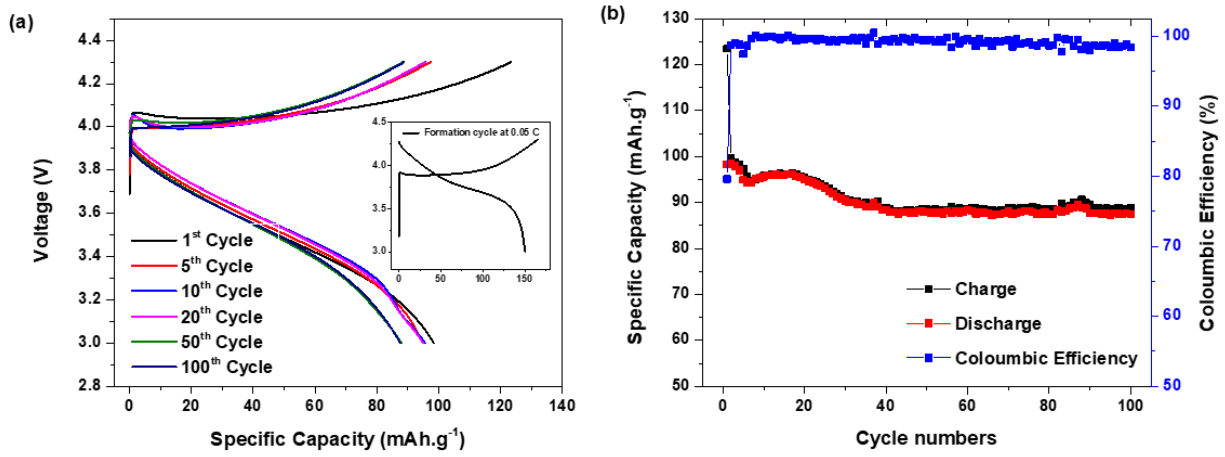

Figure 4.6. (a) Voltage profiles, and (b) plot of charge/discharge capacity and coulombic efficiency versus cycle numbers of NMC111/PPy:CMC cathode at 1 C (275 mA.g^{-1}).

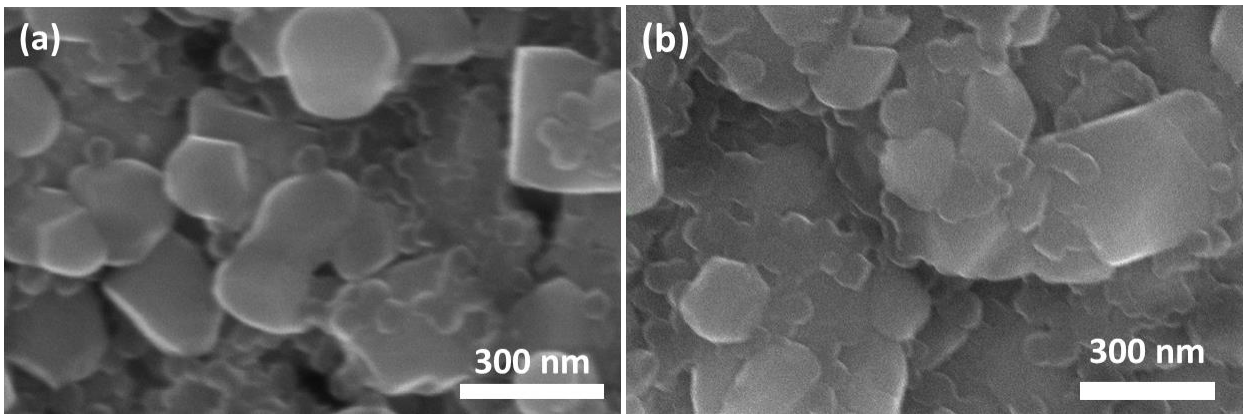

Figure 4.7. Morphologies of NMC111/PPy:CMC cathode after galvanostatic charge/discharge cycling for 100 cycles at 1 C (275 mA.g^{-1}).

To investigate changes in the morphology of NMC/PPy:CMC cathode upon repeated charge/discharge cycling at 1 C for 100 cycles, the NMC/PPy:CMC coin cell was disassembled. The cycled NMC/PPy:CMC cathode was characterized by SEM. Figure 4.7 shows that no distinct changes in the morphology of NMC/PPy:CMC cathode were observed. PPy:CMC composite still covered NMC111 particles sufficiently.

The sudden capacity fading of NMC111/PPy:CMC cathode after operating for more than 20 cycles at 0.1 C could have resulted from unknown side reactions. However, the cell that cycled

at 1 C demonstrated relatively stable performance. It is worth noting that cycling at 1 C is theoretically 10 times faster than cycling at 0.1 C. For that reason, the sudden cell failure after cycling for 20 cycles at 0.1 C might not be observed after cycling for 100 cycles at 1 C. Unlike the cycle life, which is closely related to the performance degradation due to electrochemical reactions during the repeated charge/discharge cycles, the calendar life depends on the operating time of battery cells rather than the cycle number. The discrepancy in the performance of NMC111/PPy:CMC cathode cycled at 1 C and 0.1 C rate could be attributed to their limited calendar life, indicating some unwanted chemical reactions occurred between battery components.

IV. Conclusions

The study has shown that PPy:CMC composites are versatile for usage as electrode matrices for different types of intercalation materials ranging from traditional $LiCoO_2$ to NMC111. PPy:CMC composite plays dual roles as electrode binder and conductor. Despite having very low intrinsic electrical conductivity as mentioned in Chapter 3, PPy:CMC composite was capable of providing a sufficient conductive matrix for NMC111 particles thanks to their strong adhesion with NMC111 particles. As a result, carbon-additive-free NMC111/PPy:CMC cathode could cycle at a high C-rate. The result suggests that the electrical conductivity of battery electrodes depends not only on the intrinsic electrical conductivity of conductive agents but also on how conductive agents interact with active materials.

Chapter 5. Revisiting the Degradation of Li-ion Battery Electrode Containing Conducting Polymer-based Electrode Matrix

Abstract

Polypyrrole:carboxymethyl cellulose (PPy:CMC) composites, examples of conducting polymer-based (CP-based) electrode matrices, have been employed for fabricating carbon-additive-free $LiCoO_2$-based cathodes as metioned in Chapter 3. $LiCoO_2$/PPy:CMC cathodes, however, suffered from capacity fading. It is important to investigate the degradation mechanisms to understand the compatibility of PPy:CMC composites in Li-ion batteries, which could also proliferate the use of other CP-based battery electrode matrices. In this chapter, the causes of capacity fading were investigated by means of electrochemical and post-mortem chemical analyses. The result suggests that PPy:CMC composites were electrochemically stable within the cathode operating voltage window. As the cycle number increased, electrolyte anions became dopants for PPy units in PPy:CMC composites. The sharp spike in cell voltage of $LiCoO_2$/PPy:CMC cathodes in the first charging cycle suggested that undoped/neutral PPy units in PPy:CMC composite were oxidized and doped to become fully conductive. This unique phenomena suggested an activation procedure for using other CP-based electrode matrices in Li-ion batteries such as polyaniline:carboxymethyl cellulose (PANI:CMC) composites.

I. Introduction

Conducting polymers have long been used as complementary conductive additives in Li-ion batteries as described in Chapter 2. Their usage is always accompanied with other conventional binder and carbon additives. Chapter 3 and 4 reported the fabrication of carbon-additive-free electrodes with PPy:CMC composites as electrode matrices[3]. In these electrodes, PPy:CMC composites play a dual role as binder and conductive agents. Without adding carbon additives, PPy:CMC composites provide sufficient electrical conductivity for $LiCoO_2$/PPy:CMC cathodes to function at high C-rates. Having CMC in their structure, PPy:CMC composites allow aqueous electrode casting with good electrode adhesion on aluminum current collectors. In order to facilitate the use of CP-based electrode matrices in Li-ion batteries, It is worth investigating their properties and compatibility in Li-ion battery operating conditions.

Unfortunately, the stability of CPs in Li-ion battery conditions is not well-studied in the literature[4]. Several CPs such as poly(3,4-ethylenedioxythiophene) polystyrene sulfonate (PEDOT:PSS)[32,185,250,262], polyaniline (PANI)[320], polypyrrole (PPy)[253] showed good electrochemical stability or reversibility within the typical voltage window of Li-ion batteries (~ 2.5-4.2 V vs Li/Li^+)[32,250,251,253,260]. However, these studies were mainly dedicated to organic electrode development, where CPs were the only active materials that participated in redox events.

Some studies integrated CPs into battery electrodes at a very small quantity to boost electrode conductivity. However, carbon additives and other binders were still mainly responsible for providing electrode electrical and mechanical connections[48,181,286,321]. At such a low quantity, CP degradation over long-term operation may have been underestimated. Any changes in the performance of CPs did not significantly impact the overall performance of battery cells. No interaction with inorganic electrode materials such as $LiCoO_2$ or $LiNi_xMn_yCo_{1-x-y}O_2$ was studied. Owning unsaturated bonds and polar structure, CPs might react with active materials and electrolytes, thus potentially cause capacity fading.

This study, however, worked on carbon-additive-free cathodes. For that reason, the performance of CP composites would have a profound impact on battery performance. Therefore, this chapter is dedicated to investigating the structural/chemical changes and degradation mechanisms of $LiCoO_2$/PPy:CMC cathode to seek further improvements.

II. Experiment

1) Material synthesis

PPy:CMC composites were synthesized by chemically *in-situ* polymerizing pyrrole in aqueous sodium carboxymethyl cellulose solution with $FeCl_3$ as oxidant as reported in Chapter 3. According to Chapter 3, the PPy:CMC composite that was synthesized with Py:Na-CMC 1:1 mass ratio and Py:$FeCl_3$ 1:2.75 molar ratio yielded the best electrode performance. Therefore, PPy:CMC11 R2.75 composite was chosen to study in this chapter. The PPy:CMC 1:1 R2.75 composite reported in Chapter 3 was now denoted as PPy:CMC composite for simplicity.

2) Electrode preparation and coin cell fabrication

Carbon-additive-free $LiCoO_2$/PPy:CMC cathodes (90:10 wt%) were prepared by ball-milling a mixture of $LiCoO_2$ and PPy:CMC composite in water. The electrode slurry was then cast on a hard temper Al current collector[3]. Reference $LiCoO_2$/PVDF/C (90:5:5 wt%) cathodes were prepared by a similar procedure in NMP solvent. PPy:CMC-only cathodes were made by compressing 25 mg of PPy:CMC composite into ~0.1 mm-thick, 13mm diameter pellets. R2032 coin cell fabrication was carried out in an argon-filled glovebox. $LiCoO_2$/PPy:CMC, $LiCoO_2$/PVDF/C, or PPy:CMC-pellet were used as cathodes. Lithium metal (Alfar Aesar, 99.9%, 0.75 mm thick) and glass-fiber (Whatman^{TM}) were used as anode, and separator, respectively. All coin cells used $LiPF_6$ in DMC/EC (50:50 v/v) (Sigma-Aldrich) as liquid electrolyte unless otherwise specified.

3) Electrochemical and post-mortem analyses

$LiCoO_2$/PPy:CMC coin cells underwent galvanostatic charge/discharge at 0.1 C (27.4 $mA.g^{-1}$) for 1 cycle, 10 cycles, and 100 cycles within a voltage range of 2.8 V – 4.2 V vs Li/Li^+ on Neware battery testers. After undergoing certain cycling numbers, coin cells were disassembled in an argon-filled glovebox. Cathode materials, that were attached to Al foil, were immersed in propylene carbonate 3 times (5 mins/each) and then dried in a vacuum oven at 85 ^oC for 2 days. Samples were stored in the argon-filled glovebox prior to mount on the sample holder for SEM (FEI Nova NanoSEM 450) and XPS (Kratos Axis Nova spectrometer, Al X-ray source) measurements.

Galvanostatic electrochemical impedance spectroscopy (EIS) measurement was carried out on coin cells assembled with $LiCoO_2$/PVDF/C reference cathode or $LiCoO_2$/PPy:CMC cathode. Frequencies were scanned from 100 kHz to 10 mHz by Interface 1010E (Gamry Instrument). EIS equivalent circuit fitting was performed on Gamry Echem Analyst by the simplex method. Cyclic voltammetry (CV) was carried out within two potential ranges of 2.8-4.2 V vs Li/Li^+ and 0-5 V vs Li/Li^+ on CR2032 coin cells assembled with ~0.1 mm thick PPy:CMC pellets as cathode materials.

III. Results and discussion

1) Electrochemical analyses of PPy:CMC composite and $LiCoO_2$/PPy:CMC cathode

Figure 5.1 shows a similar magnitude of capacity fading within the first 50 cycles of $LiCoO_2$/PVDF/C reference cathode and $LiCoO_2$/PPy:CMC cathode. The question was whether the

two cathodes shared a similar degradation mechanism. The performance of carbon-additive-free $LiCoO_2$/PPy:CMC cathode would depend on the electrochemical, chemical properties of PPy:CMC composite and their interactions with other battery components such as $LiCoO_2$ and electrolytes. Understanding the stability of PPy:CMC composite in Li-ion battery working conditions would be beneficial for the adoption of other CP-based electrode matrices.

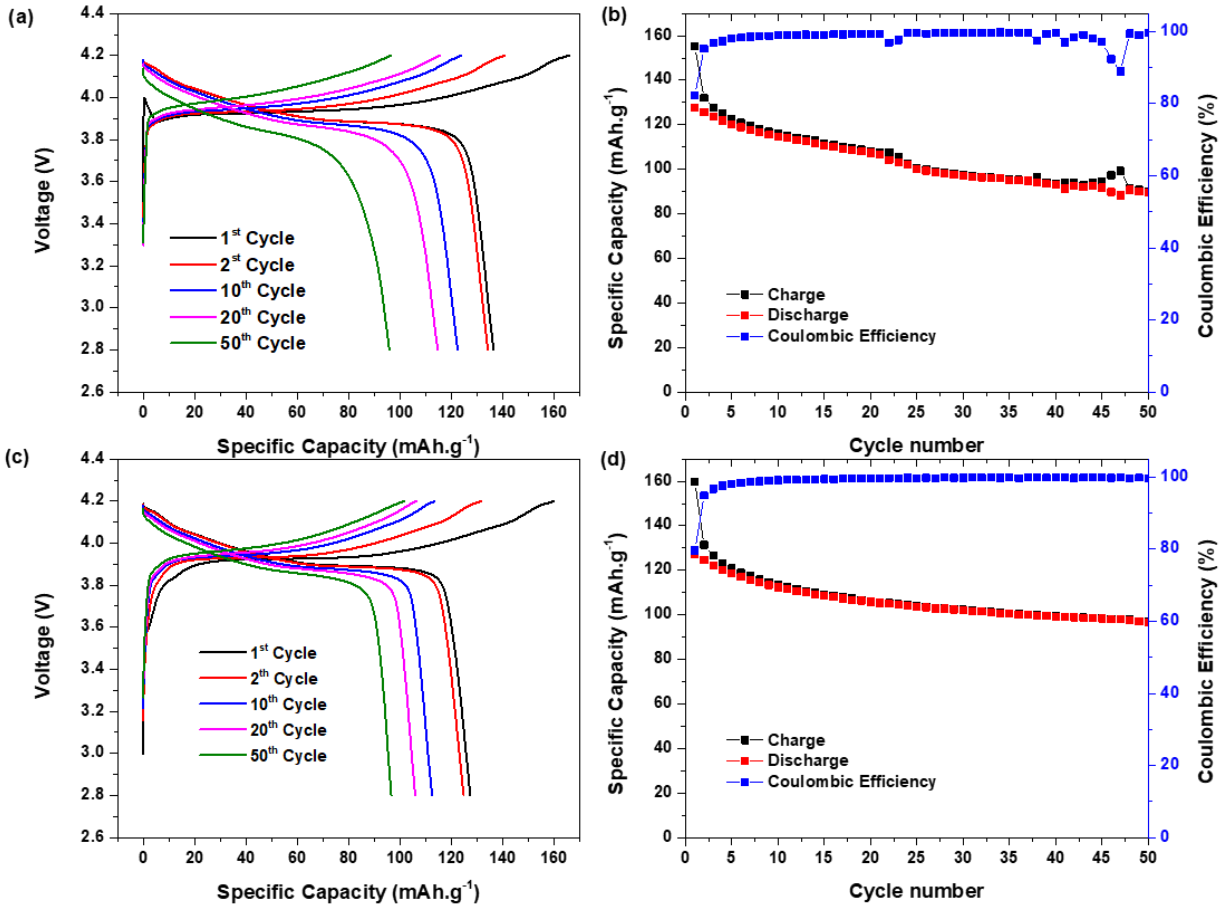

Figure 5.1. Voltage profiles and coulombic efficiency versus cycle number plots of $LiCoO_2$/PPy:CMC cathode (a,b) and $LiCoO_2$/PVDF/C reference cathode (c,d) cycled at 0.1 C.

Figure 5.2 shows the XRD diffractogram of $LiCoO_2$/PPy:CMC powder prepared by ball-milling $LiCoO_2$ with PPy:CMC composite for 6 hours in water. There was no noticeable change in the structure of $LiCoO_2$, suggesting no noticeable chemical reaction between PPy:CMC composite and $LiCoO_2$ during electrode slurry preparation.

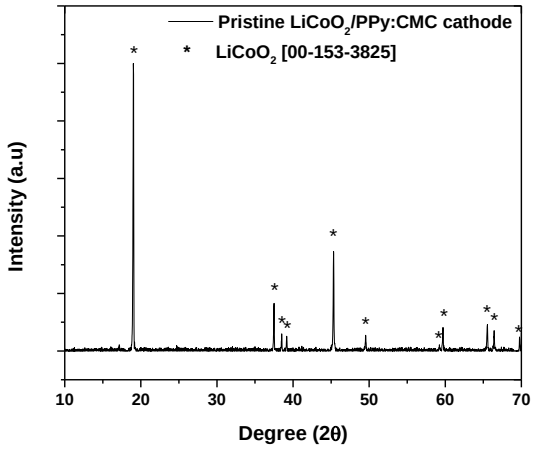

Figure 5.2. The XRD diffractogram of pristine $LiCoO_2$/PPy:CMC powder.

According to the voltage profiles of $LiCoO_2$/PVDF/C reference cathode in Figure 5.1 (c), during the charging process, the cell voltage normally increases fast to ~3.6 V vs Li/Li^+ and then slowly go up to 4.2 V vs Li/Li^+ during the de-lithiation of $LiCoO_2$ following the reaction: $LiCoO_2 \rightarrow Li_{1-x}CoO_2 + xLi^+ + xe^-$. However, as shown in Figure 5.1 (a), the voltage profile of $LiCoO_2$/PPy:CMC cathode in the first charging cycle was unique. There was a sharp voltage increase to approximately 4.0 V vs Li/Li^+ followed by a rapid voltage decline. This unique voltage profile has been seen for many $LiCoO_2$/PPy:CMC cathodes with different PPy:CMC composites as mentioned in Chapter 3. This voltage behavior could be attributed to the oxidation of neutral/undoped PPy in the as-prepared PPy:CMC composite. Undoped PPy molecules were expected to be oxidized and doped by anionic dopants. More importantly, the oxidation of neutral PPy in PPy:CMC composite occurred only in the first charging step (Figure 5.1 (a)), suggesting that PPy remained fully-doped within the potential window of cathode regardless of further charge/discharge processes.

The electrochemical behavior of PPy:CMC composite at the cathode working potentials was tested by performing cyclic voltammetry measurement on PPy:CMC-pellet coin cells. Within the cathode operating potential window, there was no redox reaction observed as shown in Figure 5.4 (a). Cycling beyond that voltage range provided some characteristic redox information of PPy:CMC composite (Figure 5.4 (b)). In the first cycle, a low-intensity oxidation peak between

2.5 V to 4.0 V vs Li/Li^+ indicated the oxidation of undoped PPy molecules, yielding fully-charged PPy molecules in PPy:CMC composite. In the subsequent CV cycle, there was a reduction peak at around 1.5 V vs Li/Li^+ (Figure 5.4 (b)). Over multiple cycles, these redox processes remained reversible with oxidation and reduction onset near 3V *vs.* Li/Li^+. Oxidation is kinetically slow, peaking beyond the 5V potential window, which limits the amount of charge passed within the typical cathode battery cycling window. However, there was no additional redox peak within the voltage window of the cathode. The results suggested that PPy:CMC composite was electrochemically stable at the cathode side.

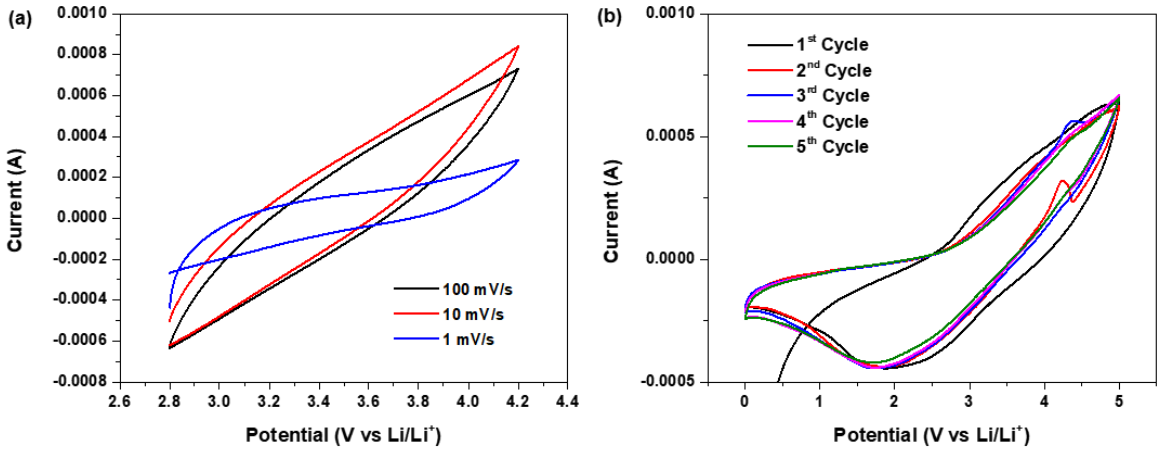

Figure 5.3. Cyclic voltammograms of pelletized PPy:CMC composite (a) between 2.8-4.2 V vs Li/Li^+ at different scanning rates; (b) between 0-5 V vs Li/Li^+ at 1 $mV.s^{-1}$ for 5 cycles.

Figure 5.4 (a,c) compares the differential capacity (dQ/dV) diagrams of $LiCoO_2$/PPy:CMC and $LiCoO_2$/PVDF/C cathodes. In comparison to $LiCoO_2$/PVDF/C reference cathode, $LiCoO_2$/PPy:CMC cathode showed faster $Co^{3+/}Co^{4+}$ redox peak shift during the phase transition of $LiCoO_2 \leftrightarrow Li_{1-x}CoO_2$, which correlated to the higher electrode polarization as the cycle number increased. The results indicated that the overall electrical conductivity of $LiCoO_2$/PPy:CMC cathode decreased relatively faster than that of $LiCoO_2$/PVDF/C reference cathode. The reduction of peak intensity at two reversible reduction/oxidation events at 4.03 V/4.07 V and 4.15 V/4.19 V that are corresponded to the transition between ordered and disordered lithium ions in CoO_2 structure during (de)lithiation process (Figure 5.5 (b,d))[6,322], suggesting the depletion of electrochemically accessible $LiCoO_2$ upon cycling for both cathodes.

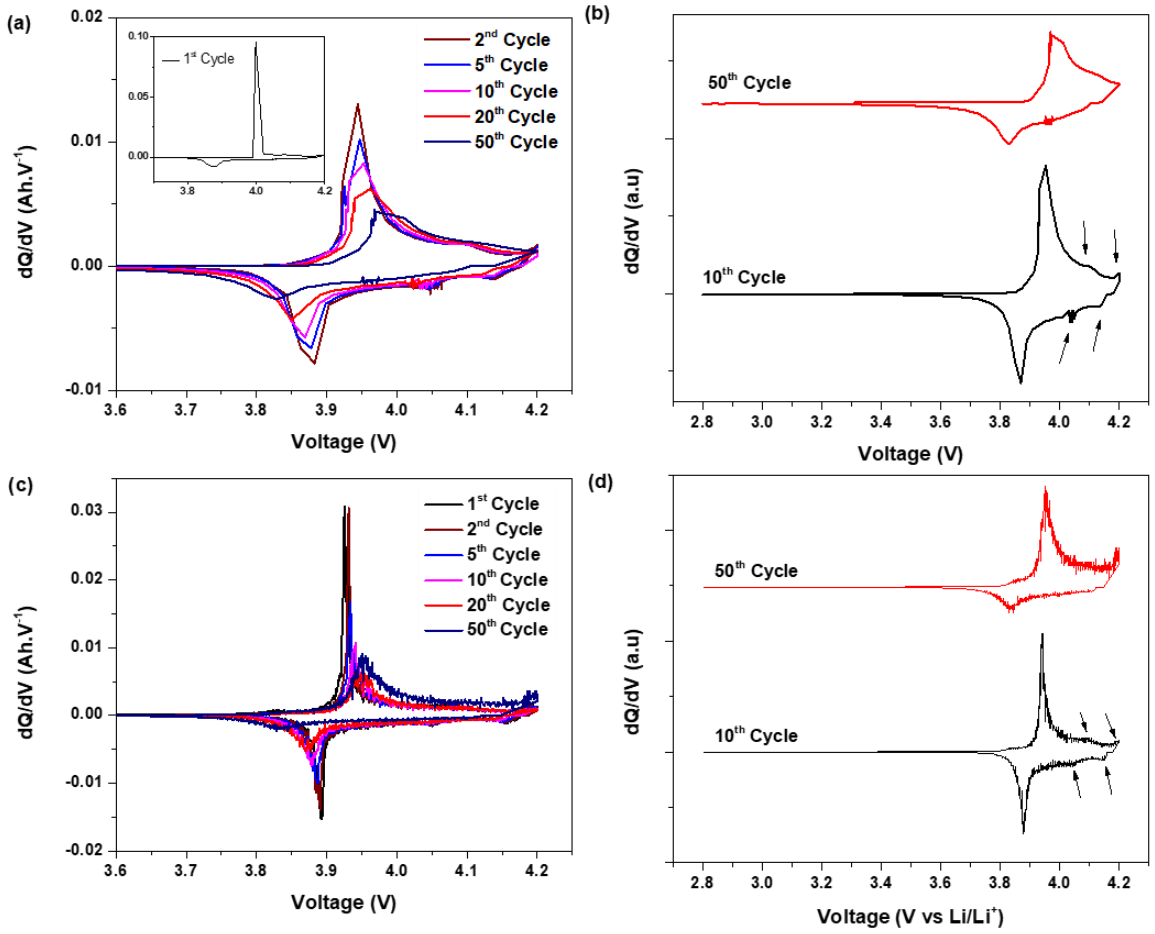

Figure 5.4. Differential capacity (dQ/dV) analysis of $LiCoO_2$/PPy:CMC cathode (a,b); $LiCoO_2$/PVDF/C reference cathode (c,d).

The evolution of electrode impedance after each charge/discharge process would provide information about electrochemical processes that occurred in battery cells. In contrast to the coin cell assembled with $LiCoO_2$/PVDF/C cathode, interestingly, the as-prepared coin cell assembled with $LiCoO_2$/PPy:CMC cathode did not yield any charge and discharge capacities during the first charge/discharge coupled with EIS measurement. As shown in Figure 5.5, there were high impedances in both charge and discharge conditions. A possible explanation is that undoped PPy molecule in the pristine PPy:CMC composite needed to be oxidized and then doped by electrolyte anions to become electrically conductive. After the first failed charge/discharge cycle, the coin cell assembled with $LiCoO_2$/PPy:CMC cathode started to deliver expected charge/discharge capacities

with much lower impedances in the first workable charge and discharge steps as shown in Figure 5.6 (a,b).

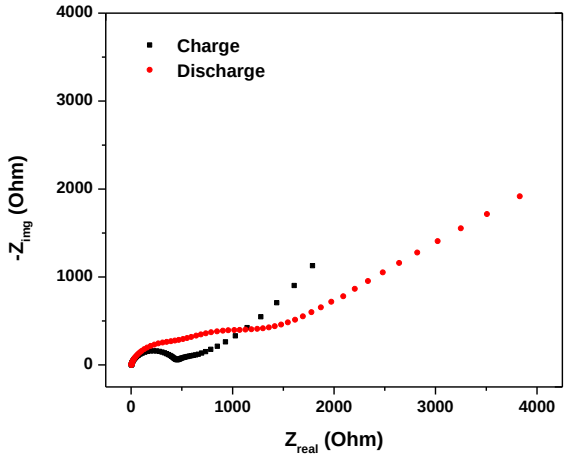

Figure 5.5. Nyquist plot of the as-prepared coin cell assembled with $LiCoO_2$/PPy:CMC cathode during the first failed charge/discharge and EIS measurement.

Figure 5.7 describes the proposed equivalent circuit at fully charged (a) and fully discharged (b) states of coin cells assembled with $LiCoO_2$/PPy:CMC cathode (Figure 5.6 (a,b)), and $LiCoO_2$/PVDF/C reference cathode (Figure 5.6 (c,d)). At the fully charged state (Figure 5.7 (a)), electrolyte resistance (R_e), recorded at the high frequency, was as small as 2-3 Ohm for the coin cells studied, Therefore, it is usually ignored. There were two Randles circuits at high and medium frequencies, representing impedance at anode and cathode, respectively. The Randles circuit typically consists of charge transfer resistance in series with Walburg element, which was then connected in parallel with the constant phase element (CPE). At the fully discharged state, $LiCoO_2$ was in its original composition. The equivalent circuit consisted of one Randle circuit representing cathode impedance (Figure 5.7 (b)). The perfect Warburg diffusion element was a constant phase element (CPE) with a phase of 45°, yielding a 45° straight line at low frequencies. To yield the best fit for the $LiCoO_2$/PPy:CMC coin cell, the Warburg element was replaced by a CPE_w, whose phase was different from 45°.

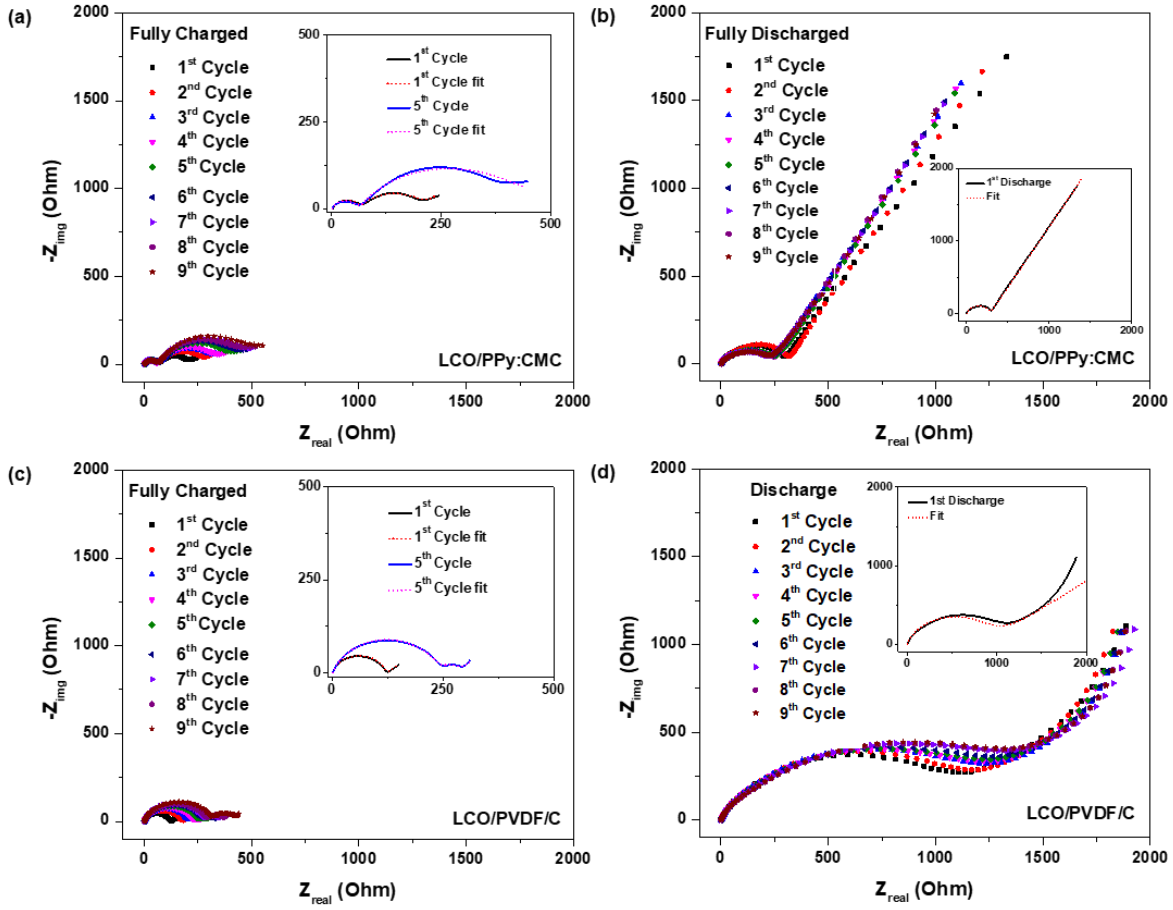

Figure 5.6. Nyquist plots of coin cells assembled with $LiCoO_2$/PPy:CMC cathode (a,b); and $LiCoO_2$/PVDF/C reference cathode (c,d).

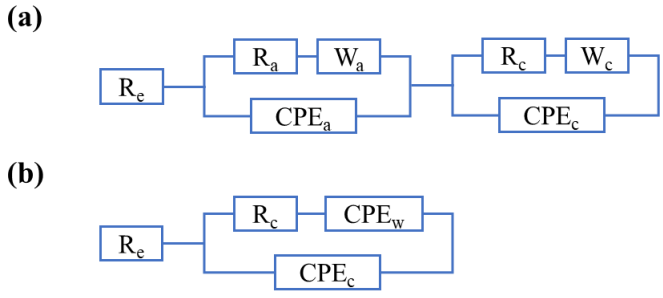

Figure 5.7. EIS equivalent circuit for half-cell Li-ion batteries at fully charged state (a), and fully discharged state (b).

At the fully charged state, there were two clear depressed semi-circles at high and medium frequencies corresponded to two Randles circuits at anode and cathode, respectively. The impedance evolution routes for the two coin cells were different. As the cycle number increased, the anode charge transfer resistance (R_{ct}) of the reference $LiCoO_2$/PVDF/C coin cell increased relatively fast (Figure 5.6 (c)) while the cathode R_{ct} slowly increased, indicating stable electrical conductivity of the $LiCoO_2$/PVDF/C cathode. In contrast, the anode R_{ct} of $LiCoO_2$/PPy:CMC coin cell did not change after 5 cycles. But there was a rapid increase in cathode R_{ct}, which was relevant to the differential capacity analysis result (Figure 5.4(a)). This observation may support the hypothesis that high surface coverage of PPy:CMC composite on $LiCoO_2$ particles prevents lithium ions from re-entering Li_xCoO_2 structure in the fully charged state.

In the fully discharged state, It was clear that $LiCoO_2$/PVDF/C reference cathode showed higher cathode impedance than $LiCoO_2$/PPy:CMC cathode. As discussed in Chapter 3, the intrinsic electrical conductivity of as-prepared PPy:CMC composite was 10 000 times lower than that of carbon black additives. However, PPy:CMC composite seemed to offer better electrical conductivity for $LiCoO_2$ electrode than PVDF/C electrode matrix. There are several possible explanations. Firstly, undoped PPy molecules in PPy:CMC composite were likely to be oxidized and doped by polyanions and anions from battery electrolyte during the first charging process of battery cells. As the result, the actual electrical conductivity of PPy:CMC composite in Li-ion battery cells was higher than that of their pristine state. Secondly, PPy:CMC composite adhered strongly on the surface of $LiCoO_2$ particles, thus providing good electrical conduction from particle to particle. In contrast, most carbon additives do not adhere to $LiCoO_2$ particles and are trapped inside the non-conductive PVDF binder, which reduces the effective electrical conductivity of the PVDF/C electrode matrix.

2) Post-Mortem Analysis

After cycling for several charge/discharge cycles, coin cells were disassembled to characterize morphological and structural changes of $LiCoO_2$/PPy:CMC cathode upon cycling. XPS survey spectra (Figure 5.8) showed that chloride ions were not completely washed from the PPy:CMC composite, which was consistent with XPS data reported in the previous study on PPy:CMC composite in Chapter 3. Several studies even added LiCl into battery electrolyte solution to suppress electrolyte degradation[323] or protect Li metal anode[324]. Chlorine gas

evolution has not been reported when chloride-contaminated electrolytes underwent charge/discharge cycling[323,324].

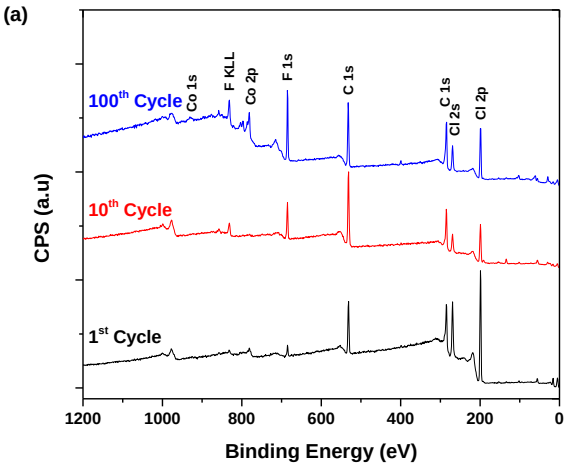

Figure 5.8. XPS survey spectra of $LiCoO_2$/PPy:CMC cathode after galvanostatic charge/discharge cycling for 1 cycle, 10 cycles, and 100 cycles at 0.1 C.

As the cycle number increased, the peak intensity of Cl 2p decreased while the peak intensity of F 1s increased simultaneously. According to the previous study on PPy:CMC composite, positively charged PPy was doped by carboxyl groups (from CMC structure) and residual chloride ions (from residual $FeCl_3$ oxidant)[3]. Initially, chloride ions were key dopants for PPy, which explained the high peak intensity of Cl 2p in the XPS spectrum of the electrode that cycled for 1 cycle. During the continuous charge/discharge process, PF_6^- ions were likely to substitute Cl^- ions as anionic dopants for PPy due to the excess use of $LiPF_6$ electrolyte. Free chloride ions were easily washed out during the electrode washing prior to XPS measurement. In contrast, doping Cl^- and PF_6^- ions were trapped within PPy:CMC electrode matrix. As a result, the XPS spectra for the cathode that cycled 100 times exhibited strong peak intensity for F 1s (Figure 5.8).

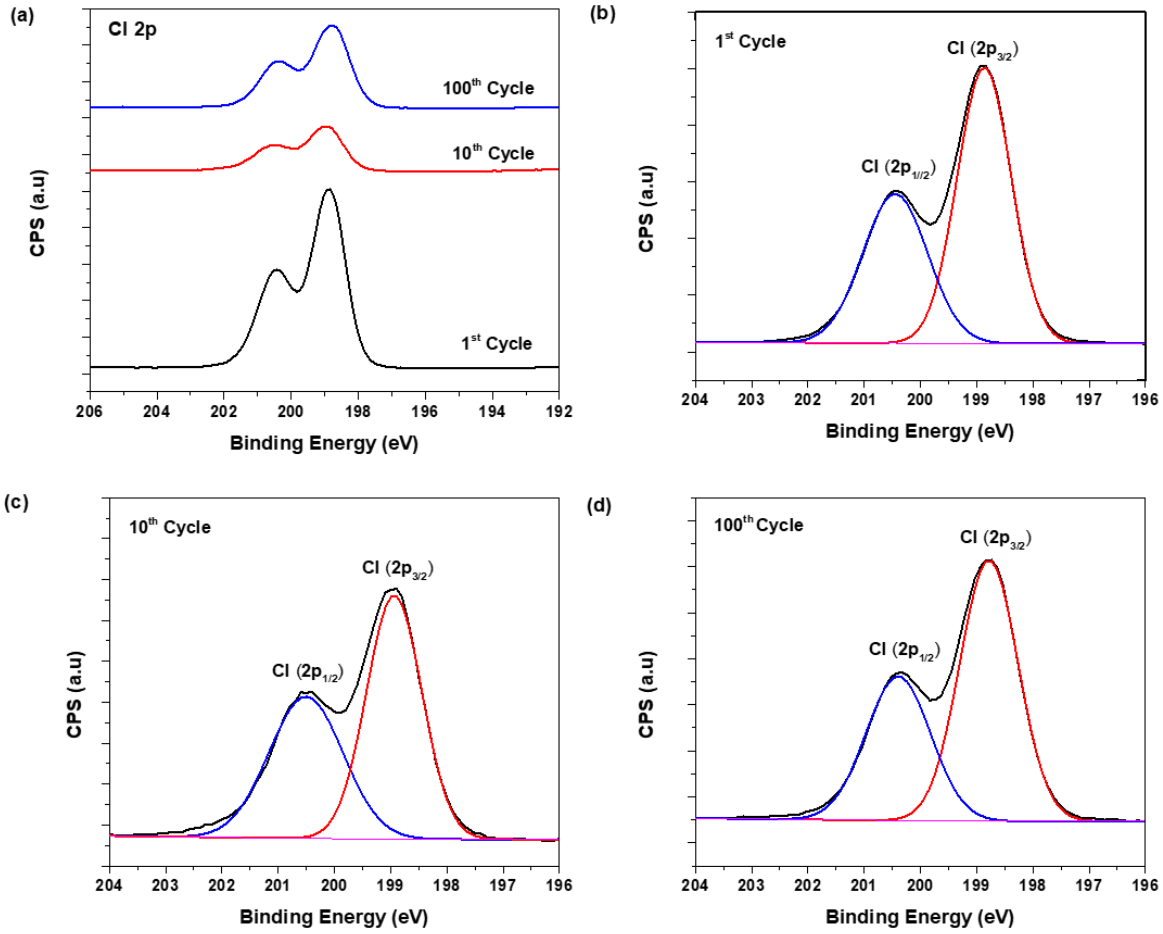

Figure 5.9. Evolution of Cl 2p XPS spectrum after cycling $LiCoO_2$/PPy:CMC cathode.

Figure 5.9 (b,c,d) shows the consistency of Cl 2p peak doublet regardless of the cycle number, indicating that residual chloride ions did not involve in redox events within the working potential range of cathode.

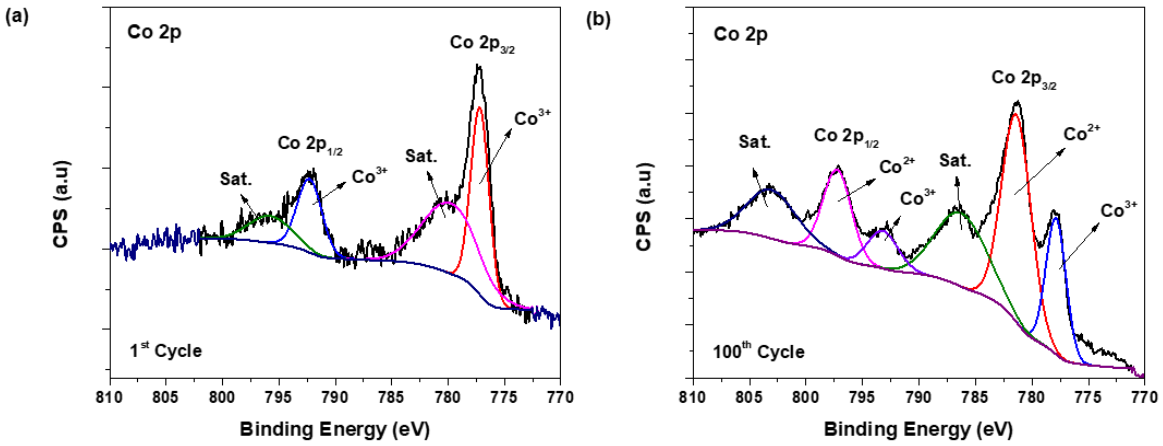

Figure 5.10. Co 2p XPS spectra of $LiCoO_2$/PPy:CMC cathode after cycling for (a) 1 cycle, and (b) 100 cycles.

After cycling for 1 cycle, the Co 2p XPS spectrum of $LiCoO_2$/PPy:CMC cathode was identical to pristine $LiCoO_2$ as reported in the previous studies[325]. However, there was a significant change in the Co 2p XPS spectrum of $LiCoO_2$/PPy:CMC cathode following the 100^{th} cycle. Such changes in the specification of Co 2p peaks indicate changes in the surface structure of $LiCoO_2$. The question remained whether PPy:CMC composite contribute to the degradation of $LiCoO_2$ because the magnitude of capacity fading of $LiCoO_2$/PPy:CMC cathode and $LiCoO_2$/PVDF/C reference cathode were similar.

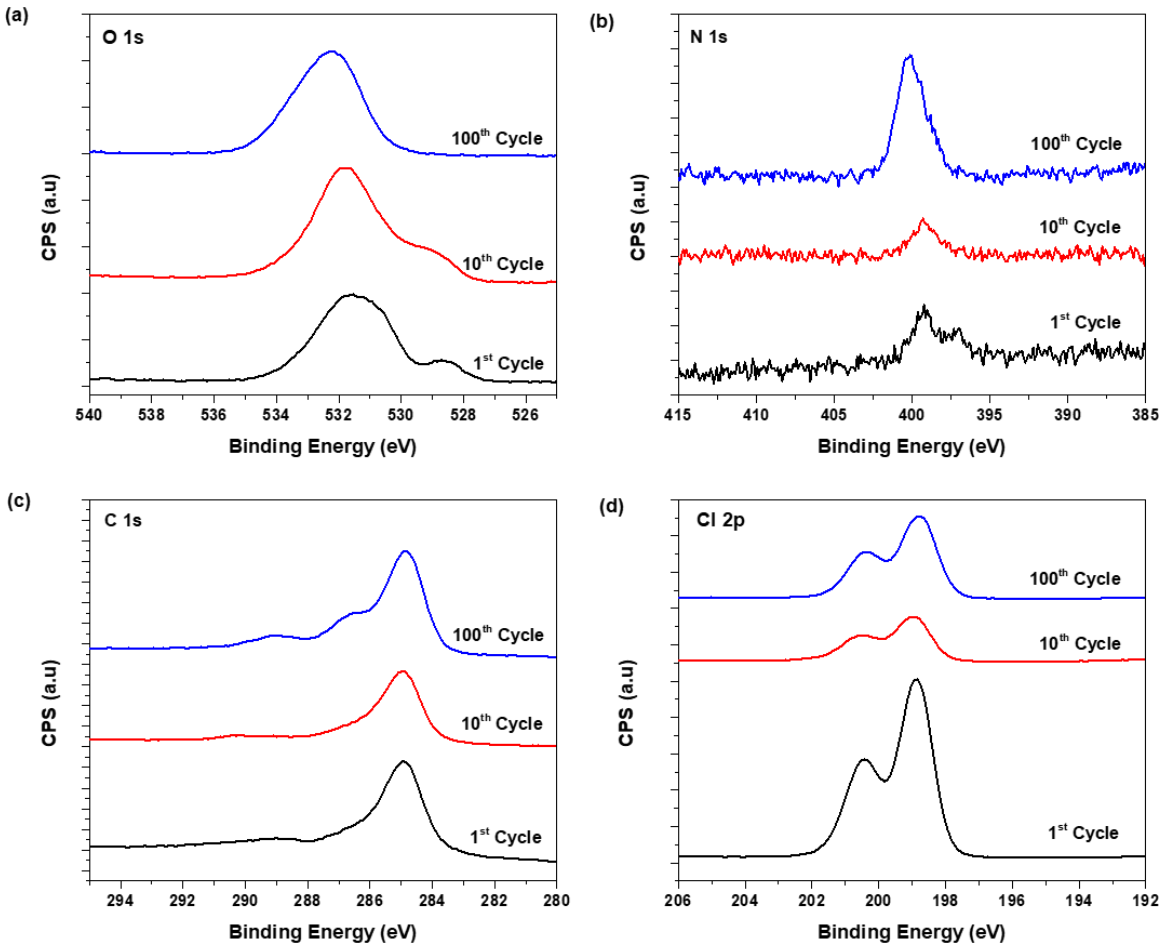

Figure 5.11. Evolution of elemental XPS spectra after cycling $LiCoO_2$/PPy:CMC cathode for 1 cycles, 10 cycles and 100 cycles. (a) O 1s; (b) N 1s; (c) C 1s; (d) Cl 2p.

At the 100th cycle, two C 1s peaks appeared at approximately 287 eV and 289 eV that could be attributed to ester and ether groups of CMC (Figure 5.11 (c)), suggesting a slow increase in the average oxidation state of carbon as the cycle number increased. The N 1s XPS spectra were shifted to higher binding energy, suggesting increased oxidation state and doping level of PPy.

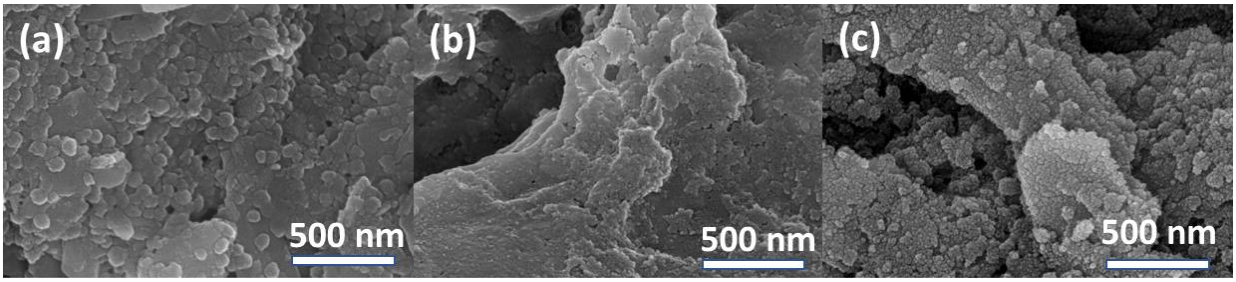

Figure 5.12. SEM images of $LiCoO_2$/PPy:CMC electrodes
(a) Pristine; (b) after 10 charge/discharge cycles; (c) after 100 charge/discharge cycles.

The morphologies of $LiCoO_2$/PPy:CMC cathode became rougher as the cycle number raised (Figure 5.12). Good contact between electrode composite components sustained repeated cycling. The amorphous coverage layer of $LiCoO_2$ was probably a mixture of PPy:CMC composites and cathode electrolyte interface (CEI) product.

3) Comparative experiments for determining root causes of capacity fading

The performance degradation of Li-ion battery cells could be attributed to many factors ranging from the intrinsic properties of electrode materials, to impurities in the electrolyte and other electrode components. It is worth noting that the magnitude of capacity fading was the same for both $LiCoO_2$/PVDF/C reference cathode and $LiCoO_2$/PPy:CMC cathode. The capacity fading mechanism might originate from the intrinsic degradation of $LiCoO_2$ in the investigated system. For example, some electrolyte additives were reported to suppress the degradation of $LiCoO_2$ in carbonate electrolytes. This study, however, used commercial 1 M $LiPF_6$ DMC:EC (50:50 v:v) electrolyte without electrolyte additives, which might contribute to the degradation observed. One possible cause for the degradation of $LiCoO_2$/PPy:CMC cathode could be impurities in liquid electrolytes used. However, as shown in Chapter 4, the NMC111/PVDF/C cathode exhibited excellent capacity retention regardless of using the same bottle of $LiFP_6$-based liquid electrolyte. Therefore, electrolyte impurities would not be the reason for the capacity fading of these $LiCoO_2$ cathodes.

Residual chloride ions were reported in the composition of PPy:CMC composites that were previously purified by vacuum filtration. However, the chloride contamination would not affect electrochemical stability of PPy:CMC composites as explained in the cyclic voltammograms. The impact of residual chloride ions on the performance of $LiCoO_2$/PPy:CMC cathodes was not well-

understood. In order to get rid of residual chloride ions in PPy:CMC composites, centrifugation was used to purify PPy:CMC composites. Figure 5.13 (c) depicts the performance of $LiCoO_2$/PPy:CMC-centrifuged cathode, which was as same as that of normal $LiCoO_2$/PPy:CMC cathode, whose PPy:CMC composite was purified by vacuum filtration. Interestingly, the $LiCoO_2$/PPy:CMC-centrifuged cathode was not able to undergo charge/discharge processes when the normal battery cycling program was applied. It is confirmed that residual chloride ions acted as additional dopants for PPy in the structure of PPy:CMC composites. Upon removing residual chloride ions, the electrical conductivity of PPy:CMC composites was expected to decrease. As a result, the $LiCoO_2$/PPy:CMC-centrifuged cathode could not able to run when applying a fixed potential of 2.8 V to 4.2 V vs Li/Li^+. However, by setting the charge potential limit to 4.5 V vs Li/Li^+ in the first few minutes of the charging process, PPy:CMC composite was activated and the $LiCoO_2$/PPy:CMC-centrifuged cathode started to run as usual. As shown in Figure 5.13 (c), the cell voltage of the $LiCoO_2$/PPy:CMC-centrifuged cathode went up to approximately 4.4 V vs Li/Li^+ in seconds followed by decaying to around 4.0 V vs Li/Li^+. This behavior further confirmed the hypothesis that PPy:CMC composite would undergo an activation process, where undoped PPy was doped by electrolyte anions.

As for $LiPF_6$ electrolyte, it is well-known that traces of moisture in electrode could react with $LiPF_6$, forming corrosive HF gas that attacks $LiCoO_2$ and degrades overall cell performance. Therefore, one could argue that the hygroscopic nature of the CMC component in PPy:CMC composite might lead to moisture absorption during the handling of $LiCoO_2$/PPy:CMC electrodes. To reject this hypothesis, several coin cells with $LiCoO_2$/PPy:CMC cathodes were made with 1M $LiClO_4$ in polypropylene carbonate electrolyte, which is insusceptible to moisture contamination. However, the electrode still suffered from capacity fading as shown in Figure 5.13 (d).

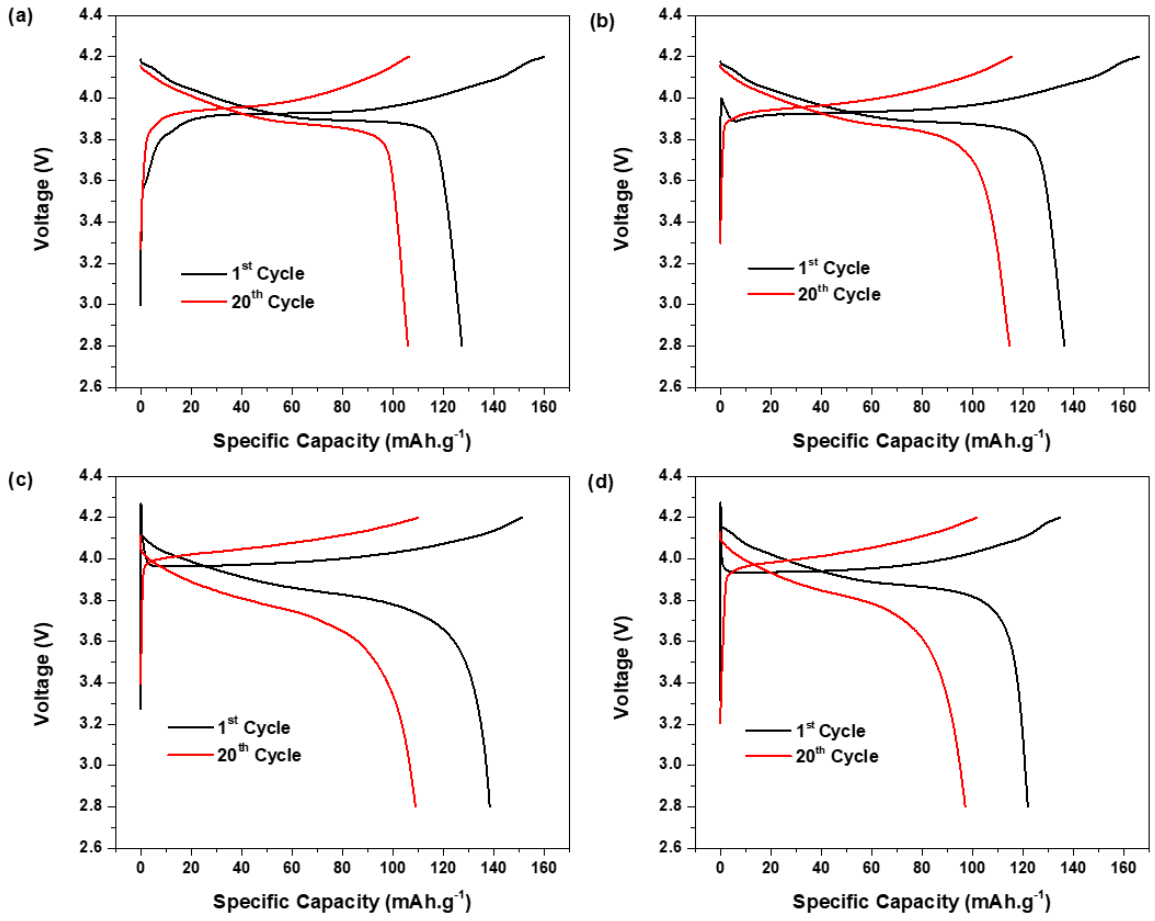

Figure 5.13. Voltage profiles of (a) $LiCoO_2$/PVDF/C reference cathode, (b) $LiCoO_2$/PPy:CMC cathode,(c) $LiCoO_2$/PPy:CMC-centrifuged cathode with 1M $LiPF_6$ in DMC:EC (50:50 v:v) electrolyte. (d) Voltage profiles of $LiCoO_2$/PPy:CMC-centrifuged cathode with 1 M $LiClO_4$ in polyethylene carbonate (PC) electrolyte

To sum up, the degradation of the $LiCoO_2$/PPy:CMC cathode was likely due to the intrinsic problem of $LiCoO_2$ active materials. Nevertheless, more studies should have been done to fully understand the properties of CP-based electrode matrices such as PPy:CMC composites in the working environment of Li-ion batteries.

4) Activating CP-based composites in the first charging process

It is imperative to emphasize the importance of activating CPs in Li-ion batteries by setting a high charging potential limit in the first charging stage. This unique protocol of activating CPs in Li-ion batteries has not been reported elsewhere. Without activation, the electrical conductivity of CPs would be too low to conduct electrons in carbon-additive-free electrodes. As a result, most of the studies still added carbon additives to CP-containing electrodes. This intriguing activation phenomenon suggests a good strategy to activate CPs in Li-ion batteries. For example, PANI:CMC composite was able to function carbon-additive-free $LiCoO_2$/PANI:CMC cathode as depicted in Figure 5.14. More information on the activation mechanism of CPs in Li-ion batteries would facilitate the adoption of CP-based electrode matrices for many types of rechargeable batteries.

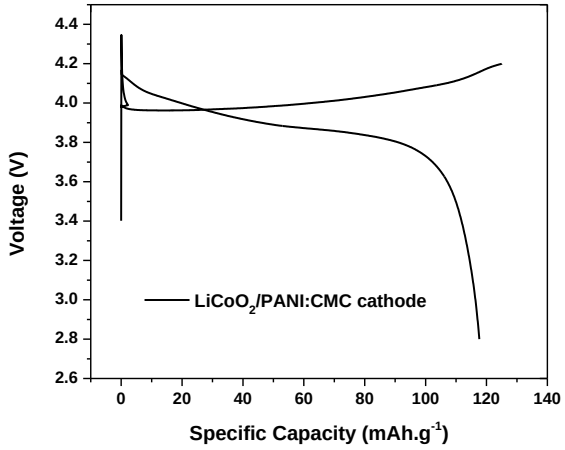

Figure 5.14. Voltage Profile of $LiCoO_2$/PANI:CMC cathode cycled at 0.1 C.

IV. Conclusions

The study proved that PPy:CMC composite demonstrated good electrochemical stability within the potential range of cathode. Having a high number of carboxyl and hydroxyl groups, CMC offered a great affinity towards the surface of $LiCoO_2$, forming a good coverage on $LiCoO_2$ particles. During the first charging step, undoped PPy in PPy:CMC composite was oxidized to become fully-charged, which explained the abnormally sharp increase in the voltage profile within few seconds of the charging process. When the amount of residual chloride ions in PPy:CMC composites decreases by more careful purification, the activation potential was observed to increase accordingly. Once the activation potential goes beyond the upper working potential range

of cathode (4.2 V vs Li/Li^+ for $LiCoO_2$), setting a high potential limit (4.5 V vs Li/Li^+ for $LiCoO_2$) in the first charging step is necessary to allow neutral PPy unit to be oxidized and doped, thus activating PPy:CMC composites. The same activation protocol has been applied successfully to activate PANI:CMC composites as electrode matrices. Further studies should be carried out to understand this unique activation mechanism, which would pave the way for using more CPs in Li-ion batteries. Based on the XPS measurement, as the cycle number increased, PF_6^- ions continued to substitute carboxyl groups and residual chloride ions to become one of the main dopants for positively charged PPy molecules. The degradation of $LiCoO_2$/PPy:CMC cathodes was likely to originate from the degradation of $LiCoO_2$, whose changes in cobalt speciation need to be investigated further.

Chapter 6. Conclusions and Suggestions for future works

I. Research Summary

Getting prepared for the next generation of Li-ion batteries requires multidisciplinary research ranging from material exploration, battery cell design, performance testing to manufacturing innovation, and battery system management. From the material science point of view, each battery component has room for improvement. The electrode matrix is commonly considered an inactive component in Li-ion batteries. However, their performance as a conductive and adhesive framework for active materials significantly impacts battery performance as a whole. The conventional electrode matrix consisting of polyvinylidene fluoride (PVDF) and carbon-black (C) has been proven to be ineffective for the next generation of Li-ion batteries, where high-energy-density active materials are used[117,140,247,326].

This thesis aimed to design a new class of electrode matrices for Li-ion batteries. New electrode matrices are composites of conducting polymers and water-dispersible carboxyl-containing polymers, combining in such a way that yields water-dispersible, electrically conductive, and strongly adhesive electrode matrices for electrode active materials. In particular, polypyrrole:carboxymethyl cellulose (PPy:CMC) composites were synthesized and investigated as representative examples for the class of CP-based electrode matrices. The study has yielded several research outcomes:

1) A proof of concept for designing CP-based composites

New electrode matrices derived from composites of CPs and aqueous carboxyl-containing polymers were synthesized by *in situ* polymerization, which is relevant to the industrial process of producing CPs[327]. CP monomers were slowly polymerized and oxidized by oxidants and then simultaneously doped by the carboxyl groups of carboxyl-containing polymers. Solvent immersion allows CP composites to precipitate without washing out carboxyl-containing polymers at the end. The vacuum filtration process allows cost-effective purification. Starting from low-cost precursors, CP composites were synthesized by a facile, scalable process to yield inexpensive battery electrode matrices. The unique arrangement of composite components via charge balancing mechanism, allowing the homogeneous molecular structure to form. Even though this work has mainly focused on PPy:CMC composites, the general electrode matrix design concept may extend to other combinations where CPs are polypyrrole (PPy), polyaniline (PANI), polythiophene (Pth),

and so on. Likewise, water-dispersible carboxyl-containing polymers can be chosen from or combined with several carboxyl-containing polymers such as carboxymethyl cellulose (CMC), alginate (SA), polyacrylic acid (PAA) (Figure 6.1).

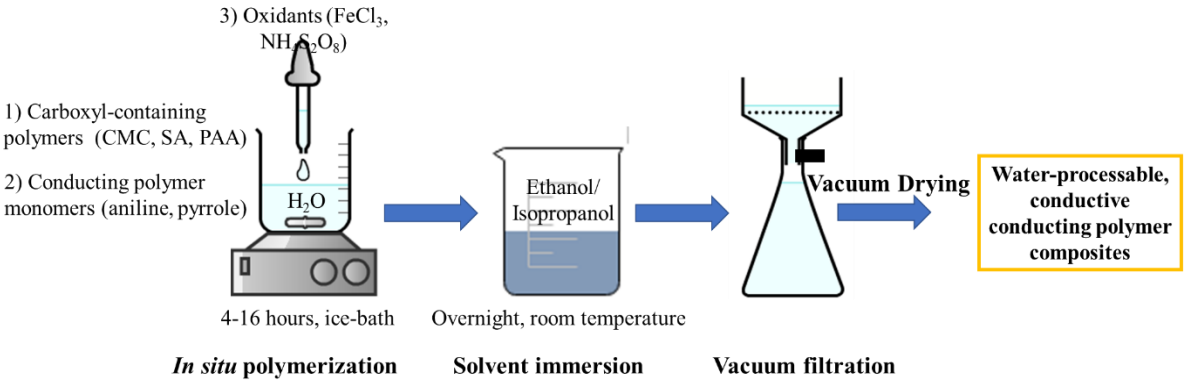

Figure 6.1. A general synthesis route for CP-based composites.

2) Understanding the structural formation of PPy:CMC molecular composites

Multiple characterization tools such as TEM/EDX, STXM, XPS were applied to characterize the structure, physical/chemical properties of PPy:CMC composites in the light of seeking multifunctional electrode matrices. The structure of PPy:CMC composite can be considered as a molecular composite. Positively charged PPy molecules were doped by carboxyl (R-COO-) groups (from CMC), and chloride ions (residual from $FeCl_3$ oxidant)[3]. Such doping mechanism is responsible for the electrical conductivity of PPy:CMC composites. The electrical conductivity of PPy:CMC composite, however, did not follow the Bruggeman relationship for common conductor-insulator composites. The surface coverage of PPy particles by CMC layers may result in quantum tunneling electrical conduction.

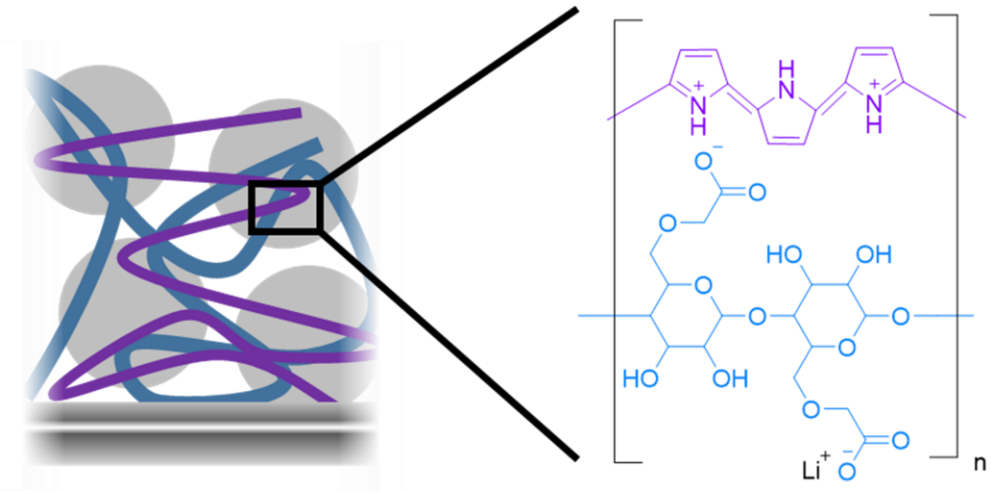

Figure 6.2. A schematic representation of carbon-additive-free $LiCoO_2$/PPy:CMC cathode. Grey spheres represent $LiCoO_2$ particles surrounded by PPy:CMC composites.

3) Fabricating carbon-additive-free cathodes

As shown in Figure 6.2, PPy:CMC composites were applied as electrode matrices for common cathode active materials such as $LiCoO_2$ and NMC111. By forming ionic interactions, PPy:CMC composites were self-doped, leading to such an electrical conductivity that was sufficient to make fully functional cathodes without adding carbon additives. High C-rate battery cycling was achieved for carbon-additive-free cathodes by using self-conductive PPy:CMC composites, which has been rarely reported in the literature. Only one report from Kim et al. demonstrated the fabrication of a carbon-additive-free cathode by coating commercial PEDOT:PSS on the surface of $LiCoO_2$[120]. $LiCoO_2$@PEDOT:PSS cathode delivered a discharge capacity of ~140 $mAh.g^{-1}$ at 1 C, but also suffered from capacity fading as similar as $LiCoO_2$/PPy:CMC cathodes reported in Chapter 3.

The two studies on carbon-additive-free cathodes suggested the possibility of using CP composites as conductive electrode matrices[119,120]. This study further confirms that conducting polymers are capable of providing good electrode conductivity. Moreover, the presence of CMC, a well-known aqueous binder, in the PPy:CMC composite structure allowed PPy:CMC composites to disperse well in water for electrode slurry preparation. PPy:CMC composites showed strong adhesion to $LiCoO_2$, $LiNi_{1/3}Mn_{1/3}Co_{1/3}O_2$ surfaces as revealed by SEM imaging. Good electrode adhesion to the aluminum current collector was also achieved as confirmed by the scratch test. The

dual functionality of PPy:CMC composites enables them to be used as mono-component electrode matrices to substitute conventional PVDF/C mixtures.

4) Studying the compatibilities of CP-based electrode matrices in Li-ion batteries.

Unexpected capacity fading was a challenge for using water-based binders and electrode matrices at the cathode side[117,120,272,275]. For example, Kim et al. reported the fast capacity fading of $LiCoO_2$ cathode with aqueous PEDOT:PSS electrode matrix[120], but without detailed investigation on the degradation mechanism. Some studies suggested that the degradation resulted from the interfacial instabilities of cathode active materials processed with aqueous binders[317]. The pH of aqueous electrode slurry increases as a result of lithium leaching would also lead to structural changes and Al current collector corrosion. Adjusting the pH of electrode slurry could address these problems[274,317].

With PPy:CMC composites as water-based electrode matrices, the capacity fading was still observed. Electrochemical analyses confirmed that PPy:CMC composites showed good electrochemical stability within the operating potential range of the cathode. No structural change was observed for active materials after mixing with PPy:CMC composites in water. Post-mortem analyses were applied to study the degradation causes of $LiCoO_2$/PPy:CMC cathodes. After performing comparative analyses, the capacity fading observed for $LiCoO_2$/PPy:CMC cathodes was likely to originate from the intrinsic performance of $LiCoO_2$. Nonetheless, more studies should be done to understand better the compatibilities of PPy:CMC composites and other CP-based electrode matrices with other components in Li-ion batteries.

In conclusion, the research project has placed the first step in developing a new class of electrode matrices for Li-ion batteries by simply combining CPs and carboxyl-containing aqueous binders. One of the examples for multifunctional CP-based electrode matrices is PPy:CMC composite. As a conductor, PPy:CMC composite provides electrical conduction pathways between electrode active materials, allowing batteries to function at high C-rates without carbon additives added. As an adhesive binder, PPy:CMC composite was found to have strong interactions with $LiCoO_2$ and NMC111 cathode materials. Strong interactions are also expected between PPy:CMC composites and other electrode materials such as silicon/tin-based materials (Li-ion battery anodes), and sulfur (Li-S battery cathodes), to name a few. Such unique features could be beneficial for the development of other rechargeable batteries such as Li-S batteries, multivalent

metal-ions batteries. Aqueous electrode processing was also achieved by using this class of electrode matrices, thus contributing to the development of a greener battery fabrication process. This class of electrode matrices, however, is still in its infancy. Future studies are needed for understanding the behaviors of CP-based electrode matrices in Li-ion batteries for future applications.

II. Research Suggestions

This study has shown a proof of concept for designing and applying CP-based electrode matrices in Li-ion batteries. Two representatives, including PPy:CMC and PANI:CMC composites, have shown promising performances as conductive, adhesive, and water-processable battery electrode matrices. However, the development of CP-based electrode matrices is still in its infancy with many open questions on their chemical/electrochemical stability and compatibility. To commercialize this class of CP-based electrode matrices, future studies should focus on:

1) Exploring other CP-based composites

Other composite combinations such as PPy:PAA, PANI:PAA composites have unexplored characteristics. Different CPs have their unique electrochemical and chemical properties, which could be more compatible with Li-ion batteries. Because polyanions are dopants for CPs in CP-based composites, changing polyanions in terms of size, functionality, polarity could tune the mobility, structural stability of CP-based composites. It should be noted that too strong interactions between PPy:CMC and $LiCoO_2$ might be responsible for capacity fading. Therefore, exploring other composites could lead to fruitful results.

2) Studying stability of CP-based composites in Li-ion batteries

A limitation of this study is that the reactions and interactions between CP-based electrode matrices and other electrode components such as active materials and electrolytes have not been fully investigated. Therefore, a strong conclusion about the stability of CP-based electrode matrices in Li-ion battery cells is not available. A natural progression of this work is to test the performance of CP-based electrode matrices in battery cells containing different types of cathode, and anode materials. Some electrolyte additives should be used to extend the cycle life of battery cells.

It is worth mentioning that the cycling data is collected by running several half-cell CR2032 coin cells, which used reference lithium metal anode. To study the actual battery

performance, It is recommended to fabricate and test full-cell coin cells, which use graphite or silicon-based anodes. More coin cells for each sample should be fabricated and tested to have good statistical data. Using a high-precision battery tester is also a good way to predict battery lifetime by measuring coulombic efficiency more accurately[328].

3) Studying the architecture of electrodes that used CP-based electrode matrices

The ways that CP-based electrode matrices interact and support active materials are different from that of conventional PVDF/C electrode matrices. Investigating mechanical properties could reveal root causes for capacity fading. By performing *ex-situ* or *in-situ* X-ray imaging of battery electrodes after certain charge/discharge cycles, morphological changes could be analyzed to study electrode mechanical integrity[220,329,330], which was claimed as one of the main advantages of using CP-based electrode matrices[3].

The synchrotron-based X-ray microscope could be applied to collect a series of radiographs of electrodes rotated 180 ^{o} on a sample holder. By using tomography data analysis software, 3D images of electrode structure could be constructed after performing appropriate segmentation and image construction. Following that, quantitative analyses could be performed to estimate volume fraction, porosity, tortuosity of the electrodes[220,331,332], which yield important information about changes in electrode architecture upon galvanostatic cycling [247,287].

4) Implementing CP-based electrode matrices in different types of rechargeable batteries

It is well-known that the performance of CMC binder outweighs that of PVDF binder for high-energy-density anodes where silicon[159,193,247,287,333], and tin[117,137] anode active materials were used. Strong intermolecular interactions between CMC and those anode materials maintain good electrode mechanical integrity during repeated cycling, thus retains high capacity over many cycles. Due to time constraints, this research project mainly focuses on the cathode side of Li-ion batteries. Future research should be undertaken to explore how CP-based electrode matrices work at the anode side of Li-ion batteries.

As the closest analog to Li-ion batteries, Na-ion batteries own the same problem that is found in Li-ion batteries[72]. For example, catastrophic volume changes during the (de)solidation of silicon-based, tin-based anodes could result in fast capacity fading[74,218,242]. The selection of electrode matrix for Na-ion batteries could differentiate between failed and workable electrodes.

Further application of CP-based electrode matrices on Na-ion batteries, therefore, is required to confirm their versatility for rechargeable batteries.

The importance of electrode matrix design becomes even more critical in lithium-sulfur (Li-S) batteries[98]. The working principle of Li-S batteries relies on the electrochemical reaction between lithium (anode) with sulfur (cathode). Technical challenges mostly arise from the sulfur-based cathode. For example, sulfur experiences remarkable volume changes between charged and discharged, which induces large structural stresses[98]. Replicative volume expansion and shrinking result in particle pulverization and electrode delamination, which are similar to the degradation mechanism of silicon and tin anodes in Li-ion batteries. Strongly adhesive electrode matrices are vital for ensuring the mechanical integrity of sulfur cathode[91,98,154]. Strong interactions between electrode matrices and sulfur compounds could suppress the devastating shuttle effect by capturing polysulfides[98,99,239]. Besides, conductive electrode matrices are of paramount importance to address the low electrical conductivity of sulfur cathode. Because carbon additives are loosely connected to sulfur particles, a large quantity of carbon additives is needed to provide sufficient electrode conductivity[91,93,239], which lowers the volumetric and gravimetric capacity advantages of Li-S batteries. Theoretically, CP-based electrode matrices seem to address the above-mentioned issues simultaneously. Containing charged molecules, PPy:CMC could form strong intermolecular interactions with sulfur to minimize the shuttle effect of polysulfides while ensuring mechanical integrity during operation. The intrinsic electrical conductivity of CP-based electrode matrices would reduce or even eliminate carbon additives used, thus improving the overall volumetric and gravimetric capacity of Li-S batteries.

By designing alternative electrode matrices, this work lays the groundwork for future study to address the limitations of conventional PVDF/C electrode matrices to prepare for the next generation of rechargeable batteries, whose electrodes exhibit large volume change, unstable mechanical structure, and poor electrical conductivity. Considerably more work will need to be done to fully understand the behaviors of CP-based electrode matrices in Li-ion battery cells from mechanical to chemical aspects. Future research, investigating a wide range of composite combinations, could introduce promising electrode matrices for wide-scale applications in Li-ion batteries. Last but not least, expanding the implication of CP-based electrode matrices to the next

generation of rechargeable batteries such as Na-ion, multivalent metal-ion, Li-S batteries is the next step to exploit the unique properties of CP-based electrode matrices.

Appendix

Supporting Information for Chapter 4: Conducting Polymer Composites as Water-Dispersible Electrode Matrices for Li-Ion Batteries: Synthesis and Characterization

Particle size analysis

TEM images were imported into ImageJ, where individual particles were manually assigned. The diameter for each particle was then measured. The sample size for *in situ polymerized* PPy:CMC 1:1 composite and mechanically mixed PPy:CMC 1:1 composite were 22 and 31 particles, respectively. The particle size distribution is estimated by applying the student's t-distribution with a confidence interval of 95%.

STXM measurement and data treatment

The PPy:CMC 1:1 sample was sonicated in water to form a homogenous suspension before depositing onto a Si_3N_4 window, which was immobilized on an STXM sample plate by carbon tape. After drying the specimen, the sample plate was transferred into the STXM chamber, which was vacuumed and then back-filled with helium gas (~1/6 atm) prior to analysis.

STXM imaging was performed at the 10ID-1 SM beamline of the Canadian Light Source (CLS), Canada with the detailed instrument information and data treatment reported in a previous study[334]. The incident photon energy ranged from 280 eV to 425 eV to cover C 1s and N 1s was used to acquire STXM-XANES image stacks. The energy step was varied in steps of 0.1 eV near the absorption edge and 1 eV for the pre-edge and continuum regions. The scan area covered sample regions as well as a blank region for I_o measurement.

By measuring the intensity of incident X-rays (I_o) and transmitted X-rays (I), the XANES spectra were recorded in transmission mode according to the Beer-Lambert law and converted into optical density scales by the following equation:

$$T = \frac{Io}{I}$$

$$OD = A = -lnT = \ln\left(\frac{Io}{I}\right) = \mu\rho l$$

where *OD* is optical density (also called absorbance (*A*)) and *T* denotes transmittance. The energy-dependent mass absorption coefficient (cm^2/g), density (g/cm^3), and thickness (mm) of the sample were denoted as μ, ρ, and l, respectively.

Data treatment was performed with the aXis2000 and Matlab R2018a software packages. All images in the stack were aligned automatically by using the Jacobsen Stack Analyze and Zimba techniques. After that, the aligned image stack in transmission mode was converted to optical density mode by normalizing the transmitted light intensity (*I*) by incident light intensity (I_o), which was measured in the blank region. The image was created by dividing the integrated *OD* in the region between 284 eV to 286 eV by the total integrated *OD* of the C 1s spectrum and assigning the result to the color saturation scale. The brightness scale was set by the integrated *OD* of the full C 1s spectrum.

XPS data analysis

The XPS spectra were analyzed by the CasaXPS software. The calibration of binding energies is based on the C 1s peak at 284.8 eV. Peak fittings of C 1s, N 1s, O 1s spectra, used a Shirley background and a simplex algorithm to fit components with pure Gaussian line shape.

Electrical conductivity measurement

Error bars on electrical conductivity graphs (Figure 3.4 (a), Figure SI.3.8 and Figure SI.3.10) represent a confidence interval of 95% by t-distribution with sample sizes ranging from 8 to 15).

Supporting Figures

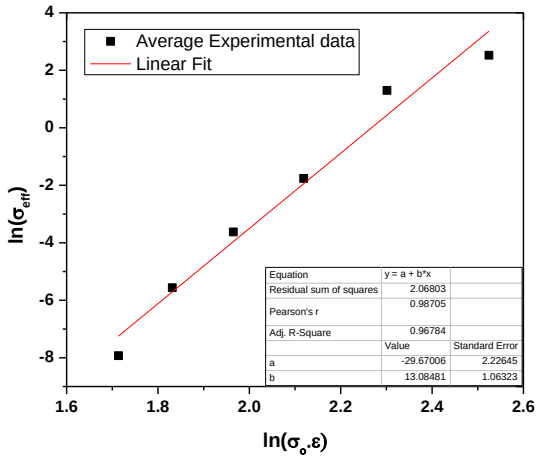

Figure SI.3.1. Bruggeman model for the electrical conductivity of PPy:CMC R2.5 composites.

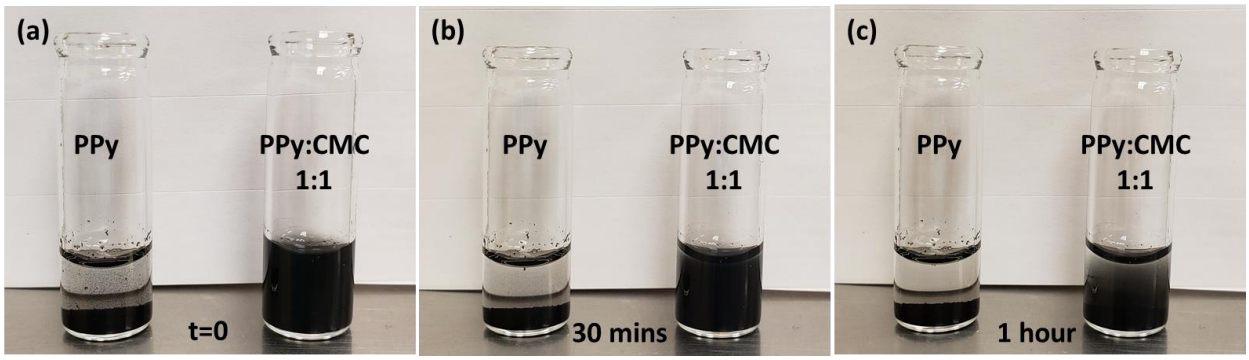

Figure SI.3.2. Dispersion stability of PPy and PPy:CMC 1:1 R2.5 composite in water with a concentration of 4 mg/ml.

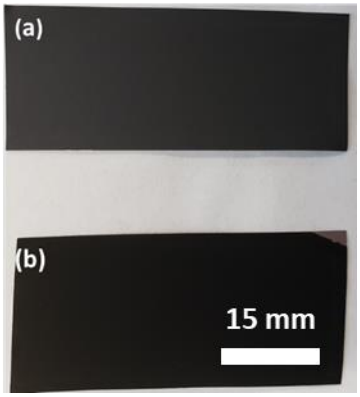

Figure SI.3.3. Digital images of $LiCoO_2$/(PPy:CMC 1:1 R2.5) electrode with H_2O as solvent (a) and $LiCoO_2$/PVDF/C electrode with NMP as solvent (b).

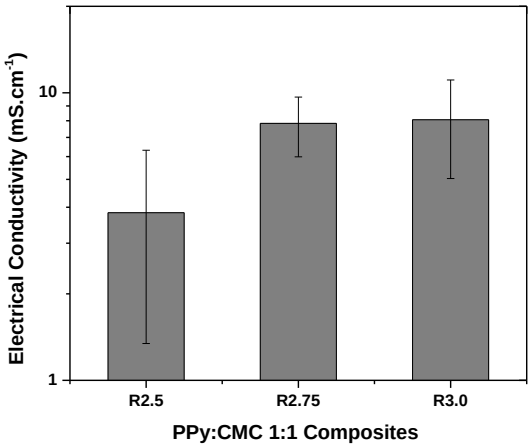

Figure SI.3.4. Electrical conductivity of PPy:CMC 1:1 composites synthesized at different Py:$FeCl_3$ ratio of 1:2.5 (R2.5), 1:2.75 (R2.75) and 1:3.0 (R3.0).

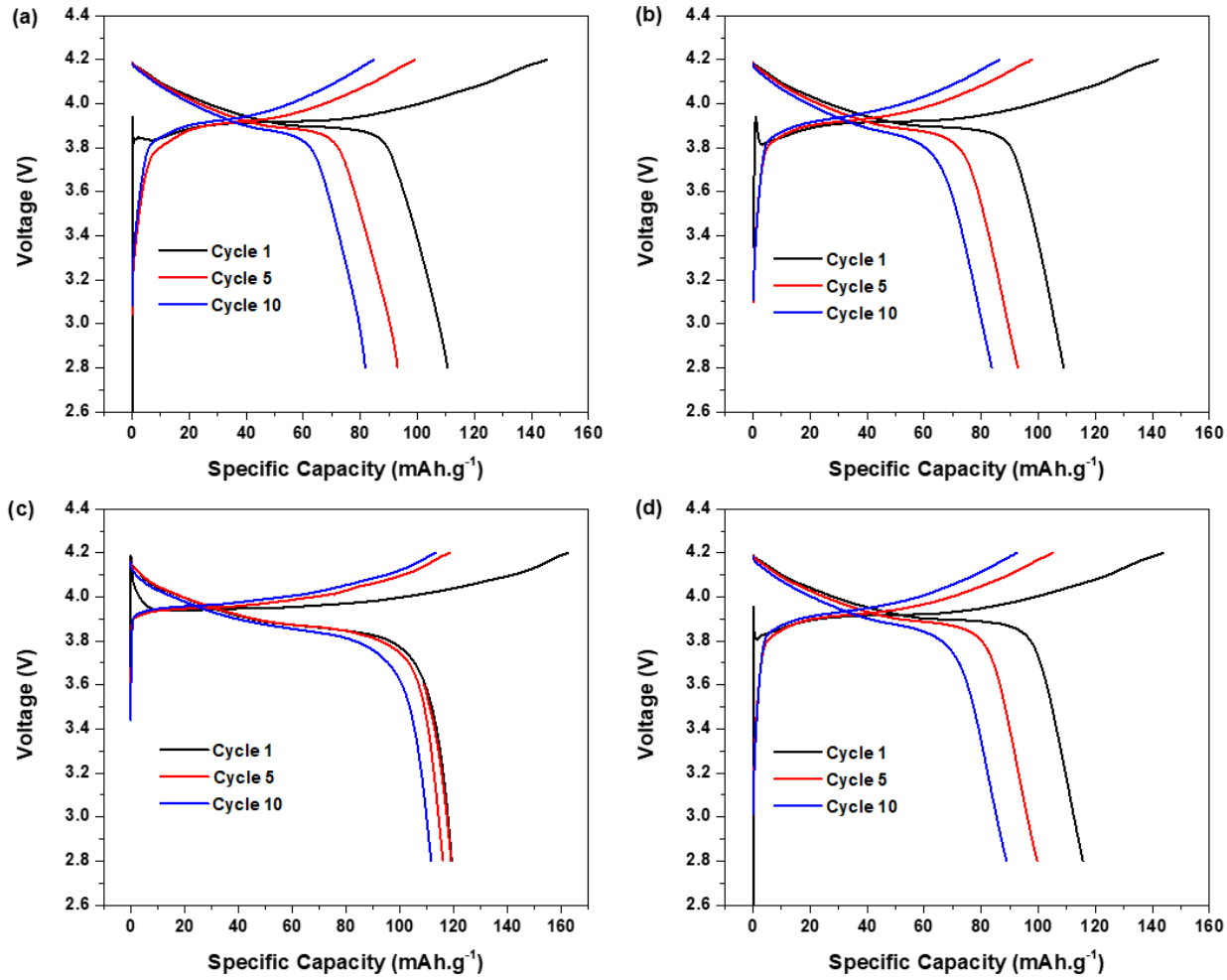

Figure SI.3.5. Galvanostatic charge and discharge voltage profiles at 0.1 C of $LiCoO_2$/(PPy:CMC 1:0.5 R2.50) electrode (a), $LiCoO_2$/(PPy:CMC 1:0.75 R2.50) electrode (b), $LiCoO_2$/(PPy:CMC 1:1 R2.50) electrode (c), $LiCoO_2$/(PPy:CMC 1:1.25 R2.50) electrode (d).

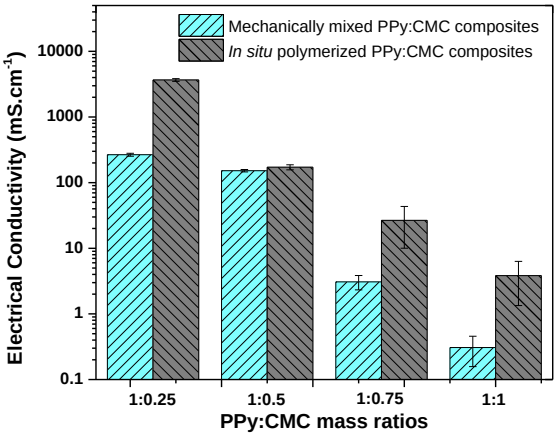

Figure SI.3.6. Comparison between the electrical conductivity of mechanically mixed and in situ polymerized PPy:CMC composites.

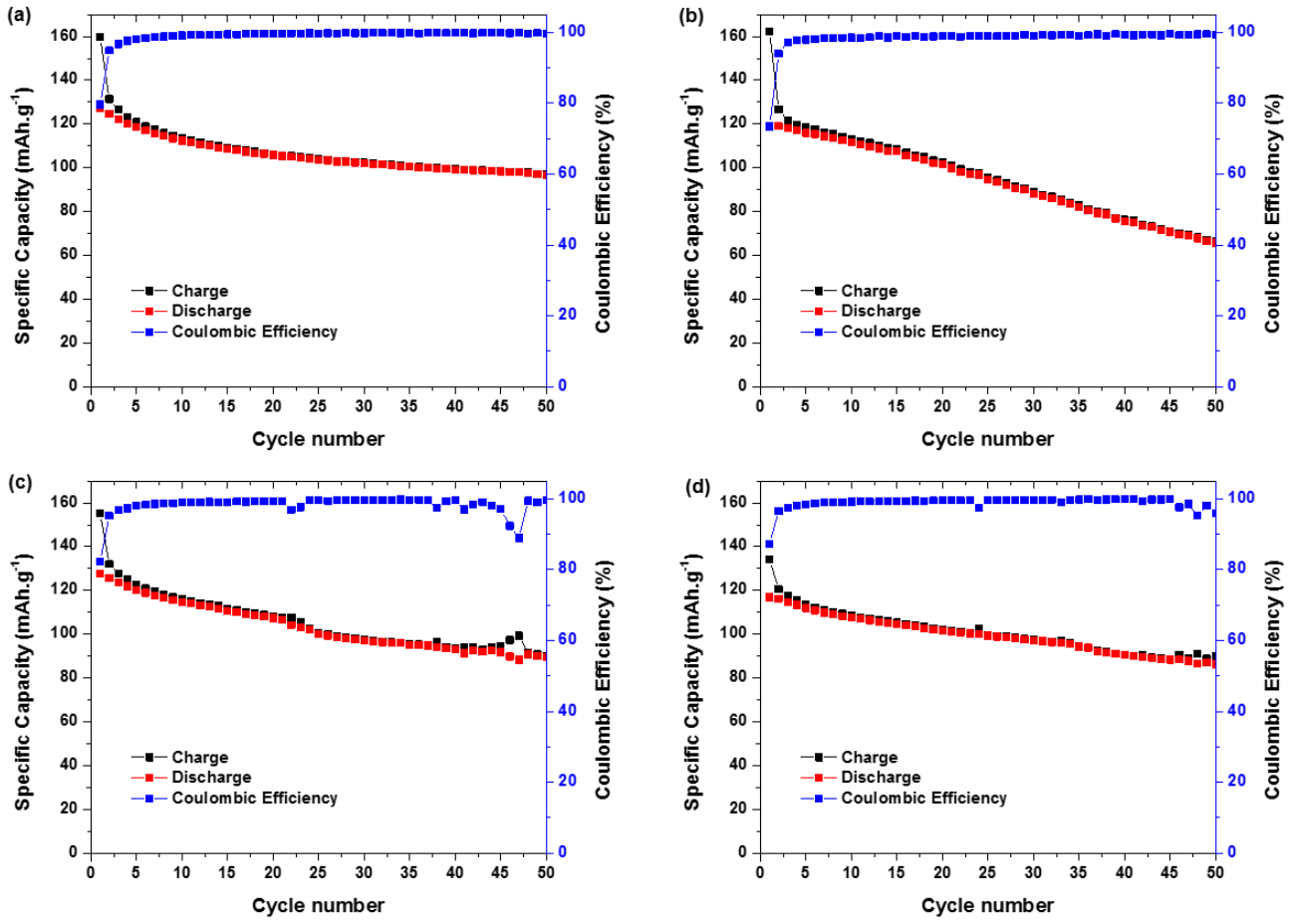

Figure SI.3.7. Plots of charge/discharge capacity and coulombic efficiency at 0.1 C vs. cycle number of $LiCoO_2$/PVDF/C electrode (a), $LiCoO_2$/(PPy:CMC 1:1 R.2.50) electrode (b), $LiCoO_2$/(PPy:CMC 1:1 R2.75) electrode (c), and $LiCoO_2$/(PPy:CMC 1:1 R3.0) electrode (d).

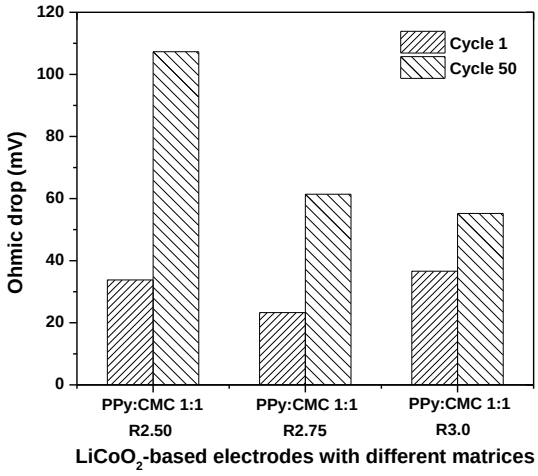

Figure SI.3.8. The comparison of IR drops between $LiCoO_2$-based electrodes with PPy:CMC 1:1 composites synthesized at Py:$FeCl_3$ ratio of 1:2.5 (R2.50), 1:2.75 (R2.75) and 1:3.0 (R3.0).

Supporting Information for Chapter 5:
Revisiting the Degradation of Li-ion Battery Electrode Containing Conducting Polymer-based Electrode Matrix

Synthesis of polyaniline:carboxymethyl cellulose (PANI:CMC) composite

PANI:CMC composite was synthesized by chemically *in situ* polymerization. First of all, sodium carboxymethyl cellulose (MW= 250000 g/mol, DS= 0.9, Sigma-Aldrich) was dissolved in deionized water to form a viscous solution. Following that, aniline (≥99.5%, Sigma-Aldrich) was mixed with the above Na-CMC solution. An ice bath was used to cool down the precursor solution before adding ammonium persulfate (≥98%, Sigma-Aldrich) solution. The aniline:CMC mass ratio and aniline:$(NH_4)_2S_2O_8$ molar ratio were fixed as 1:1 and 1:1.25, respectively. The concentration of aniline in the reaction mixture was approximately 0.6 mol.L^{-1}. The chemical polymerization reaction was carried out for 6 hours in an ice bath and then 18 hours at room temperature. After immersing product suspension in ethanol overnight with the suspension:ethanol volume ratio of 1:4, vacuum filtration was used to purify precipitates with ethanol until the filtrate solution became colorless. The purified product was dried in a vacuum oven at 80 ^oC before use.

Activation procedure for CP-based electrode matrices.

After fabrication, coin cells were kept at their open circuit potential for 12 hours. In the first charging step, the potential was set at 4.5 V vs Li/Li^+ for a maximum of 10 mins. After 10 mins, the charge/discharge cycling program was set at a normal potential range of 2.8-4.2 V vs Li/Li^+.

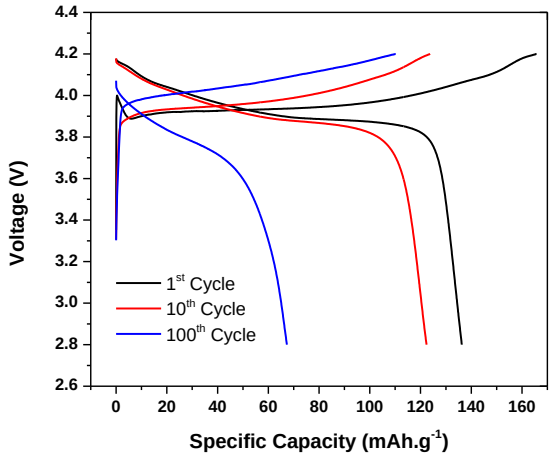

Figure SI.5.1. Voltage profile of $LiCoO_2$/PPy:CMC cathode cycled at 0.1 C.

Bibliography

[1] G. Zubi, R. Dufo-López, M. Carvalho, G. Pasaoglu, The lithium-ion battery: State of the art and future perspectives, Renew. Sustain. Energy Rev. 89 (2018) 292–308. https://doi.org/10.1016/j.rser.2018.03.002.

[2] U.S. Department of Energy, Batteries, Department of Energy, Vehicle Technologies Officies. (2019).

[3] V.A. Nguyen, J. Wang, C. Kuss, Conducting polymer composites as water-dispersible electrode matrices for Li-Ion batteries: Synthesis and characterization, J. Power Sources Adv. 6 (2020) 100033. https://doi.org/10.1016/j.powera.2020.100033.

[4] V.A. Nguyen, C. Kuss, Review—Conducting Polymer-Based Binders for Lithium-Ion Batteries and Beyond, J. Electrochem. Soc. 167 (2020) 065501. https://doi.org/10.1149/1945-7111/ab856b.

[5] Q. Lin, Q. Li, K.E. Gray, J.F. Mitchell, Vapor Growth and Chemical Delithiation of Stoichiometric LiCoO2 Crystals, Cryst. Growth Des. 12 (2012) 1232–1238. https://doi.org/10.1021/cg201238n.

[6] J.N. Reimers, J.R. Dahn, Electrochemical and In Situ X-Ray Diffraction Studies of Lithium Intercalation in LixCoO2, J. Electrochem. Soc. 139 (1992) 2091–2097. https://doi.org/10.1149/1.2221184.

[7] P. Rozier, J.M. Tarascon, Review-Li-rich layered oxide cathodes for next-generation Li-ion batteries: Chances and challenges, J. Electrochem. Soc. 162 (2015) A2490–A2499. https://doi.org/10.1149/2.0111514jes.

[8] J.N. Reimers, J.R. Dahn, U. von Sacken, Effects of Impurities on the Electrochemical Properties of LiCoO2, J. Electrochem. Soc. 140 (1993) 2752–2754. https://doi.org/10.1149/1.2220905.

[9] J.F. Peters, M. Weil, A critical assessment of the resource depletion potential of current and future lithium-ion batteries, Resources. 5 (2016) 1–15. https://doi.org/10.3390/resources5040046.

[10] T. Kim, L.K. Ono, Y. Qi, Elucidating the Mechanism Involved in the Performance Improvement of Lithium-Ion Transition Metal Oxide Battery by Conducting Polymer, Adv. Mater. Interfaces. 6 (2019) 1801785. https://doi.org/10.1002/admi.201801785.

[11] J. Zheng, M. Gu, J. Xiao, P. Zuo, C. Wang, J.G. Zhang, Corrosion/fragmentation of layered composite cathode and related capacity/voltage fading during cycling process, Nano Lett. 13 (2013) 3824–3830. https://doi.org/10.1021/nl401849t.

[12] F. Wu, J. Liu, L. Li, X. Zhang, R. Luo, Y. Ye, R. Chen, Surface modification of Li-rich cathode materials for lithium-ion batteries with a PEDOT:PSS conducting polymer, ACS Appl. Mater. Interfaces. 8 (2016) 23095–23104. https://doi.org/10.1021/acsami.6b07431.

[13] S. Chen, T. He, Y. Su, Y. Lu, L. Bao, L. Chen, Q. Zhang, J. Wang, R. Chen, F. Wu, Ni-Rich LiNi0.8Co0.1Mn0.1O2 Oxide Coated by Dual-Conductive Layers as High Performance Cathode Material for Lithium-Ion Batteries, ACS Appl. Mater. Interfaces. 9 (2017) 29732–29743. https://doi.org/10.1021/acsami.7b08006.

[14] P. Hou, H. Zhang, Z. Zi, L. Zhang, X. Xu, Core-shell and concentration-gradient cathodes prepared via co-precipitation reaction for advanced lithium-ion batteries, J. Mater. Chem. A. 5 (2017) 4254–4279. https://doi.org/10.1039/c6ta10297b.

[15] T. Li, X.-Z. Yuan, L. Zhang, D. Song, K. Shi, C. Bock, Degradation Mechanisms and Mitigation Strategies of Nickel-Rich NMC-Based Lithium-Ion Batteries, Electrochem. Energy Rev. 3 (2020) 43–80. https://doi.org/10.1007/s41918-019-00053-3.

[16] S. Maeng, Y. Chung, S. Min, Y. Shin, Enhanced mechanical strength and electrochemical performance of core–shell structured high–nickel cathode material, J. Power Sources. 448 (2020) 227395. https://doi.org/10.1016/j.jpowsour.2019.227395.

[17] X. Dong, J. Yao, W. Zhu, X. Huang, X. Kuai, J. Tang, X. Li, S. Dai, L. Shen, R. Yang, L. Gao, J. Zhao, Enhanced high-voltage cycling stability of Ni-rich cathode materials: Via the self-assembly of Mn-rich shells, J. Mater. Chem. A. 7 (2019) 20262–20273. https://doi.org/10.1039/c9ta07147d.

[18] H. Shi, X. Wang, P. Hou, E. Zhou, J. Guo, J. Zhang, D. Wang, F. Guo, D. Song, X. Shi, L. Zhang, Core-shell structured Li[(Ni0.8Co0.1Mn0.1)0.7(Ni0.45Co0.1Mn0.45)0.3]O2

cathode material for high-energy lithium ion batteries, J. Alloys Compd. 587 (2014) 710–716. https://doi.org/10.1016/j.jallcom.2013.10.226.

[19] H. Li, J. Li, X. Ma, J.R. Dahn, Synthesis of Single Crystal LiNi0.6Mn0.2Co0.2O2 with Enhanced Electrochemical Performance for Lithium Ion Batteries, J. Electrochem. Soc. 165 (2018) A1038–A1045. https://doi.org/10.1149/2.0951805jes.

[20] J. Li, H. Li, W. Stone, R. Weber, S. Hy, J.R. Dahn, Synthesis of Single Crystal LiNi0.5Mn0.3Co0.2O2 for Lithium Ion Batteries, J. Electrochem. Soc. 164 (2017) A3529–A3537. https://doi.org/10.1149/2.0401714jes.

[21] Y. Liu, J. Harlow, J. Dahn, Microstructural Observations of "Single Crystal" Positive Electrode Materials Before and After Long Term Cycling by Cross-section Scanning Electron Microscopy, J. Electrochem. Soc. 167 (2020) 020512. https://doi.org/10.1149/1945-7111/ab6288.

[22] H. Li, J. Li, N. Zaker, N. Zhang, G.A. Botton, J.R. Dahn, Synthesis of Single Crystal LiNi0.88Co0.09Al0.03O2 with a Two-Step Lithiation Method, J. Electrochem. Soc. 166 (2019) A1956–A1963. https://doi.org/10.1149/2.0681910jes.

[23] Z.D. Huang, X.M. Liu, S.W. Oh, B. Zhang, P.C. Ma, J.K. Kim, Microscopically porous, interconnected single crystal LiNi1/3Co1/3Mn1/3O2 cathode material for Lithium ion batteries, J. Mater. Chem. 21 (2011) 10777–10784. https://doi.org/10.1039/c1jm00059d.

[24] G. Qian, Y. Zhang, L. Li, R. Zhang, J. Xu, Z. Cheng, S. Xie, H. Wang, Q. Rao, Y. He, Y. Shen, L. Chen, M. Tang, Z.F. Ma, Single-crystal nickel-rich layered-oxide battery cathode materials: synthesis, electrochemistry, and intra-granular fracture, Energy Storage Mater. 27 (2020) 140–149. https://doi.org/10.1016/j.ensm.2020.01.027.

[25] D.Y. Wang, J. Xia, L. Ma, K.J. Nelson, J.E. Harlow, D. Xiong, L.E. Downie, R. Petibon, J.C. Burns, A. Xiao, W.M. Lamanna, J.R. Dahn, A Systematic Study of Electrolyte Additives in Li[Ni1/3Mn1/3Co1/3]O2 (NMC)/Graphite Pouch Cells, J. Electrochem. Soc. 161 (2014) A1818–A1827. https://doi.org/10.1149/2.0511412jes.

[26] A. Tornheim, S. Sharifi-Asl, J.C. Garcia, J. Bareño, H. Iddir, R. Shahbazian-Yassar, Z. Zhang, Effect of electrolyte composition on rock salt surface degradation in NMC cathodes

during high-voltage potentiostatic holds, Nano Energy. 55 (2019) 216–225. https://doi.org/10.1016/j.nanoen.2018.10.065.

[27] S.K. Heiskanen, N. Laszczynski, B.L. Lucht, Perspective—Surface Reactions of Electrolyte with LiNixCoyMnzO2 Cathodes for Lithium Ion Batteries, J. Electrochem. Soc. 167 (2020) 100519. https://doi.org/10.1149/1945-7111/ab981c.

[28] S. Yang, Y. Song, P.Y. Zavalij, M. Stanley Whittingham, Reactivity, stability and electrochemical behavior of lithium iron phosphates, Electrochem. Commun. 4 (2002) 239–244. https://doi.org/10.1016/S1388-2481(01)00298-3.

[29] D. Jugović, D. Uskoković, A review of recent developments in the synthesis procedures of lithium iron phosphate powders, J. Power Sources. 190 (2009) 538–544. https://doi.org/10.1016/j.jpowsour.2009.01.074.

[30] L.X. Yuan, Z.H. Wang, W.X. Zhang, X.L. Hu, J.T. Chen, Y.H. Huang, J.B. Goodenough, Development and challenges of LiFePO4 cathode material for lithium-ion batteries, Energy Environ. Sci. 4 (2011) 269–284. https://doi.org/10.1039/c0ee00029a.

[31] J. Wang, X. Sun, Understanding and recent development of carbon coating on LiFePO4 cathode materials for lithium-ion batteries, Energy Environ. Sci. 5 (2012) 5163–5185. https://doi.org/10.1039/c1ee01263k.

[32] P.R. Das, L. Komsiyska, O. Osters, G. Wittstock, PEDOT:PSS as a Functional Binder for Cathodes in Lithium Ion Batteries, J. Electrochem. Soc. 162 (2015) A674–A678. https://doi.org/10.1149/2.0581504jes.

[33] J. Liu, J. Wang, X. Yan, X. Zhang, G. Yang, A.F. Jalbout, R. Wang, Long-term cyclability of LiFePO4/carbon composite cathode material for lithium-ion battery applications, Electrochim. Acta. 54 (2009) 5656–5659. https://doi.org/10.1016/j.electacta.2009.05.003.

[34] C. Liu, Z.G. Neale, G. Cao, Understanding electrochemical potentials of cathode materials in rechargeable batteries, Mater. Today. 19 (2016) 109–123. https://doi.org/10.1016/j.mattod.2015.10.009.

[35] A. Manthiram, X. Yu, S. Wang, Lithium battery chemistries enabled by solid-state electrolytes, Nat. Rev. Mater. 2 (2017) 16103.

https://doi.org/10.1038/natrevmats.2016.103.

[36] R. Yazami, P. Touzain, A reversible graphite-lithium negative electrode for electrochemical generators, J. Power Sources. 9 (1983) 365–371. https://doi.org/10.1016/0378-7753(83)87040-2.

[37] X. Zuo, J. Zhu, P. Müller-Buschbaum, Y.-J. Cheng, Silicon based lithium-ion battery anodes: A chronicle perspective review, Nano Energy. 31 (2017) 113–143. https://doi.org/10.1016/j.nanoen.2016.11.013.

[38] H. Zhao, N. Yuca, Z. Zheng, Y. Fu, V.S. Battaglia, K. Zaghib, G. Liu, High Capacity and High Density Functional Conductive Polymer and SiO Anode for High-Energy Lithium-Ion Batteries, ACS Appl. Mater. Interfaces. 7 (2015) 862–866. https://doi.org/10.1021/am507376f.

[39] H. Zhao, Z. Wang, P. Lu, M. Jiang, F. Shi, X. Song, Z. Zheng, X. Zhou, Y. Fu, G. Abdelbast, X. Xiao, Z. Liu, V.S. Battaglia, K. Zaghib, G. Liu, Toward Practical Application of Functional Conductive Polymer Binder for a High-Energy Lithium-Ion Battery Design, Nano Lett. 14 (2014) 6704–6710. https://doi.org/10.1021/nl503490h.

[40] M. Wachtler, J.O. Besenhard, M. Winter, Tin and tin-based intermetallics as new anode materials for lithium-ion cells, J. Power Sources. 94 (2001) 189–193. https://doi.org/10.1016/S0378-7753(00)00585-1.

[41] C.J. Wen, R.A. Huggins, Thermodynamic Study of the Lithium-Tin System, J. Electrochem. Soc. 128 (1981) 1181–1187. https://doi.org/10.1149/1.2127590.

[42] V. Vanpeene, J. Villanova, A. King, B. Lestriez, E. Maire, L. Roué, Dynamics of the Morphological Degradation of Si-Based Anodes for Li-Ion Batteries Characterized by In Situ Synchrotron X-Ray Tomography, Adv. Energy Mater. 9 (2019) 1–13. https://doi.org/10.1002/aenm.201803947.

[43] X. Su, Q. Wu, J. Li, X. Xiao, A. Lott, W. Lu, B.W. Sheldon, J. Wu, Silicon-Based nanomaterials for lithium-ion batteries: A review, Adv. Energy Mater. 4 (2014) 1–23. https://doi.org/10.1002/aenm.201300882.

[44] C.K. Chan, H. Peng, G. Liu, K. McIlwrath, X.F. Zhang, R.A. Huggins, Y. Cui, High-

performance lithium battery anodes using silicon nanowires, Nat. Nanotechnol. 3 (2008) 31–35. https://doi.org/10.1038/nnano.2007.411.

[45] M.H. Park, M.G. Kim, J. Joo, K. Kim, J. Kim, S. Ahn, Y. Cui, J. Cho, Silicon nanotube battery anodes, Nano Lett. 9 (2009) 3844–3847. https://doi.org/10.1021/nl902058c.

[46] F. Zhao, J. Bae, X. Zhou, Y. Guo, G. Yu, Nanostructured Functional Hydrogels as an Emerging Platform for Advanced Energy Technologies, Adv. Mater. 30 (2018) 1–16. https://doi.org/10.1002/adma.201801796.

[47] Y. Shi, J. Zhang, L. Pan, Y. Shi, G. Yu, Energy gels: A bio-inspired material platform for advanced energy applications, Nano Today. 11 (2016) 738–762. https://doi.org/10.1016/j.nantod.2016.10.002.

[48] B. Liu, P. Soares, C. Checkles, Y. Zhao, G. Yu, Three-dimensional hierarchical ternary nanostructures for high-performance Li-ion battery anodes, Nano Lett. 13 (2013) 3414–3419. https://doi.org/10.1021/nl401880v.

[49] C. Chen, S.H. Lee, M. Cho, J. Kim, Y. Lee, Cross-Linked Chitosan as an Efficient Binder for Si Anode of Li-ion Batteries, ACS Appl. Mater. Interfaces. 8 (2016) 2658–2665. https://doi.org/10.1021/acsami.5b10673.

[50] D. Aurbach, Y. Talyosef, B. Markovsky, E. Markevich, E. Zinigrad, L. Asraf, J.S. Gnanaraj, H.J. Kim, Design of electrolyte solutions for Li and Li-ion batteries: A review, Electrochim. Acta. 50 (2004) 247–254. https://doi.org/10.1016/j.electacta.2004.01.090.

[51] G.E. Blomgren, Electrolytes for advanced batteries, J. Power Sources. 81–82 (1999) 112–118. https://doi.org/10.1016/S0378-7753(99)00188-3.

[52] S.S. Zhang, A review on the separators of liquid electrolyte Li-ion batteries, J. Power Sources. 164 (2007) 351–364. https://doi.org/10.1016/j.jpowsour.2006.10.065.

[53] S.S. Zhang, A review on electrolyte additives for lithium-ion batteries, J. Power Sources. 162 (2006) 1379–1394. https://doi.org/10.1016/j.jpowsour.2006.07.074.

[54] Q. Wang, B. Mao, S.I. Stoliarov, J. Sun, A review of lithium ion battery failure mechanisms and fire prevention strategies, Prog. Energy Combust. Sci. 73 (2019) 95–131.

https://doi.org/10.1016/j.pecs.2019.03.002.

[55] H. Srour, L. Chancelier, E. Bolimowska, T. Gutel, S. Mailley, H. Rouault, C.C. Santini, Ionic liquid-based electrolytes for lithium-ion batteries: review of performances of various electrode systems, J. Appl. Electrochem. 46 (2016) 149–155. https://doi.org/10.1007/s10800-015-0905-1.

[56] Y. Wang, L. Fu, L. Shi, Z. Wang, J. Zhu, Y. Zhao, S. Yuan, Gel Polymer Electrolyte with High Li + Transference Number Enhancing the Cycling Stability of Lithium Anodes, ACS Appl. Mater. Interfaces. 11 (2019) 5168–5175. https://doi.org/10.1021/acsami.8b21352.

[57] A.M. Stephan, Review on gel polymer electrolytes for lithium batteries, Eur. Polym. J. 42 (2006) 21–42. https://doi.org/10.1016/j.eurpolymj.2005.09.017.

[58] Q. Li, J. Chen, L. Fan, X. Kong, Y. Lu, Progress in electrolytes for rechargeable Li-based batteries and beyond, Green Energy Environ. 1 (2016) 18–42. https://doi.org/10.1016/j.gee.2016.04.006.

[59] J. Kasemchainan, P.G. Bruce, All-solid-state batteries and their remaining challenges, Johnson Matthey Technol. Rev. 62 (2018) 177–180. https://doi.org/10.1595/205651318X696747.

[60] J.B. Dunn, L. Gaines, M. Barnes, M. Wang, J. Sullivan, Material and energy flows in the materials production, assembly, and end-of-life stages of the automotive lithium-ion battery life cycle, Argonne, IL (United States), 2012. https://doi.org/10.2172/1044525.

[61] F. Zheng, M. Kotobuki, S. Song, M.O. Lai, L. Lu, Review on solid electrolytes for all-solid-state lithium-ion batteries, J. Power Sources. 389 (2018) 198–213. https://doi.org/10.1016/j.jpowsour.2018.04.022.

[62] X. Bai, Y. Duan, W. Zhuang, R. Yang, J. Wang, Research progress in Li-argyrodite-based solid-state electrolytes, J. Mater. Chem. A. 8 (2020) 25663–25686. https://doi.org/10.1039/d0ta08472g.

[63] S. Ohno, B. Helm, T. Fuchs, G. Dewald, M.A. Kraft, S.P. Culver, A. Senyshyn, W.G. Zeier, Further Evidence for Energy Landscape Flattening in the Superionic Argyrodites Li6+ xP1-xMxS5I (M = Si, Ge, Sn), Chem. Mater. 31 (2019) 4936–4944.

https://doi.org/10.1021/acs.chemmater.9b01857.

[64] L. Zhou, K.H. Park, X. Sun, F. Lalère, T. Adermann, P. Hartmann, L.F. Nazar, Solvent-Engineered Design of Argyrodite Li6PS5X (X = Cl, Br, I) Solid Electrolytes with High Ionic Conductivity, ACS Energy Lett. 4 (2019) 265–270. https://doi.org/10.1021/acsenergylett.8b01997.

[65] A.J. Samson, K. Hofstetter, S. Bag, V. Thangadurai, A bird's-eye view of Li-stuffed garnet-type Li7La3Zr2O12 ceramic electrolytes for advanced all-solid-state Li batteries, Energy Environ. Sci. 12 (2019) 2957–2975. https://doi.org/10.1039/c9ee01548e.

[66] C. Wang, K. Fu, S.P. Kammampata, D.W. McOwen, A.J. Samson, L. Zhang, G.T. Hitz, A.M. Nolan, E.D. Wachsman, Y. Mo, V. Thangadurai, L. Hu, Garnet-Type Solid-State Electrolytes: Materials, Interfaces, and Batteries, Chem. Rev. 120 (2020) 4257–4300. https://doi.org/10.1021/acs.chemrev.9b00427.

[67] A. Mauger, C.M. Julien, A. Paolella, M. Armand, K. Zaghib, Building better batteries in the solid state: A review, Materials. 12 (2019) 1–86. https://doi.org/10.3390/ma122333892.

[68] Y. Gambe, Y. Sun, I. Honma, Development of Bipolar All-solid-state Lithium Battery Based on Quasi-solid-state Electrolyte Containing Tetraglyme-LiTFSA Equimolar Complex, Sci. Rep. 5 (2015) 10–13. https://doi.org/10.1038/srep08869.

[69] S.T. Myung, Y. Sasaki, S. Sakurada, Y.K. Sun, H. Yashiro, Electrochemical behavior of current collectors for lithium batteries in non-aqueous alkyl carbonate solution and surface analysis by ToF-SIMS, Electrochim. Acta. 55 (2009) 288–297. https://doi.org/10.1016/j.electacta.2009.08.051.

[70] S.T. Myung, Y. Hitoshi, Y.K. Sun, Electrochemical behavior and passivation of current collectors in lithium-ion batteries, J. Mater. Chem. 21 (2011) 9891–9911. https://doi.org/10.1039/c0jm04353b.

[71] J. Chen, J. Liu, Y. Qi, T. Sun, X. Li, Unveiling the Roles of Binder in the Mechanical Integrity of Electrodes for Lithium-Ion Batteries, J. Electrochem. Soc. 160 (2013) A1502–A1509. https://doi.org/10.1149/2.088309jes.

[72] C. Bommier, X. Ji, Electrolytes, SEI Formation, and Binders: A Review of Nonelectrode

Factors for Sodium-Ion Battery Anodes, Small. 14 (2018) 1–20. https://doi.org/10.1002/smll.201703576.

[73] K. Chayambuka, G. Mulder, D.L. Danilov, P.H.L. Notten, Sodium-Ion Battery Materials and Electrochemical Properties Reviewed, Adv. Energy Mater. 8 (2018) 1800079. https://doi.org/10.1002/aenm.201800079.

[74] M. Sawicki, L.L. Shaw, Advances and challenges of sodium ion batteries as post lithium ion batteries, RSC Adv. 5 (2015) 53129–53154. https://doi.org/10.1039/c5ra08321d.

[75] X. Xiang, K. Zhang, J. Chen, Recent advances and prospects of cathode materials for sodium-ion batteries, Adv. Mater. 27 (2015) 5343–5364. https://doi.org/10.1002/adma.201501527.

[76] H. Kang, Y. Liu, K. Cao, Y. Zhao, L. Jiao, Y. Wang, H. Yuan, Update on anode materials for Na-ion batteries, J. Mater. Chem. A. 3 (2015) 17899–17913. https://doi.org/10.1039/c5ta03181h.

[77] N. Yabuuchi, K. Kubota, M. Dahbi, S. Komaba, Research development on sodium-ion batteries, Chem. Rev. 114 (2014) 11636–11682. https://doi.org/10.1021/cr500192f.

[78] A. Anani, R.A. Huggins, Multinary alloy electrodes for solid state batteries I. A phase diagram approach for the selection and storage properties determination of candidate electrode materials, J. Power Sources. 38 (1992) 351–362. https://doi.org/10.1016/0378-7753(92)80125-U.

[79] F. Klein, B. Jache, A. Bhide, P. Adelhelm, Conversion reactions for sodium-ion batteries, Phys. Chem. Chem. Phys. 15 (2013) 15876. https://doi.org/10.1039/c3cp52125g.

[80] J. Asenbauer, T. Eisenmann, M. Kuenzel, A. Kazzazi, Z. Chen, D. Bresser, The success story of graphite as a lithium-ion anode material-fundamentals, remaining challenges, and recent developments including silicon (oxide) composites, Sustain. Energy Fuels. 4 (2020) 5387–5416. https://doi.org/10.1039/d0se00175a.

[81] Y. Liu, B. V. Merinov, W.A. Goddard, Origin of low sodium capacity in graphite and generally weak substrate binding of Na and Mg among alkali and alkaline earth metals, Proc. Natl. Acad. Sci. U. S. A. 113 (2016) 3735–3739.

https://doi.org/10.1073/pnas.1602473113.

[82] D.A. Stevens, J.R. Dahn, The Mechanisms of Lithium and Sodium Insertion in Carbon Materials, J. Electrochem. Soc. 148 (2001) A803. https://doi.org/10.1149/1.1379565.

[83] J.S. Chen, D. Luan, C.M. Li, F.Y.C. Boey, S. Qiao, X.W. Lou, TiO2 and SnO2@TiO2 hollow spheres assembled from anatase TiO2 nanosheets with enhanced lithium storage properties, Chem. Commun. 46 (2010) 8252–8254. https://doi.org/10.1039/c0cc02973d.

[84] L.D. Ellis, B.N. Wilkes, T.D. Hatchard, M.N. Obrovac, In Situ XRD Study of Silicon, Lead and Bismuth Negative Electrodes in Nonaqueous Sodium Cells, J. Electrochem. Soc. 161 (2014) A416–A421. https://doi.org/10.1149/2.080403jes.

[85] M.H. Han, E. Gonzalo, G. Singh, T. Rojo, A comprehensive review of sodium layered oxides: powerful cathodes for Na-ion batteries, Energy Environ. Sci. 8 (2015) 81–102. https://doi.org/10.1039/C4EE03192J.

[86] S.C. Han, H. Lim, J. Jeong, D. Ahn, W.B. Park, K.S. Sohn, M. Pyo, Ca-doped NaxCoO2 for improved cyclability in sodium ion batteries, J. Power Sources. 277 (2015) 9–16. https://doi.org/10.1016/j.jpowsour.2014.11.150.

[87] J. Billaud, G. Singh, A.R. Armstrong, E. Gonzalo, V. Roddatis, M. Armand, T. Rojo, P.G. Bruce, Na0.67Mn1-xMgxO2 ($0 \leq x \leq 0.2$): A high capacity cathode for sodium-ion batteries, Energy Environ. Sci. 7 (2014) 1387–1391. https://doi.org/10.1039/c4ee00465e.

[88] M.H. Cao, Y. Wang, Z. Shadike, J.L. Yue, E. Hu, S.M. Bak, Y.N. Zhou, X.Q. Yang, Z.W. Fu, Suppressing the chromium disproportionation reaction in O3-type layered cathode materials for high capacity sodium-ion batteries, J. Mater. Chem. A. 5 (2017) 5442–5448. https://doi.org/10.1039/c6ta10818k.

[89] W. Zhang, M. Dahbi, S. Komaba, Polymer binder: a key component in negative electrodes for high-energy Na-ion batteries, Curr. Opin. Chem. Eng. 13 (2016) 36–44. https://doi.org/10.1016/j.coche.2016.08.001.

[90] J. Zhao, X. Yang, Y. Yao, Y. Gao, Y. Sui, B. Zou, H. Ehrenberg, G. Chen, F. Du, Moving to Aqueous Binder: A Valid Approach to Achieving High-Rate Capability and Long-Term Durability for Sodium-Ion Battery, Adv. Sci. 5 (2018) 1700768.

https://doi.org/10.1002/advs.201700768.

[91] W. Kang, N. Deng, J. Ju, Q. Li, D. Wu, X. Ma, L. Li, M. Naebe, B. Cheng, A review of recent developments in rechargeable lithium-sulfur batteries, Nanoscale. 8 (2016) 16541–16588. https://doi.org/10.1039/c6nr04923k.

[92] P. Han, S.-H. Chung, A. Manthiram, Designing a high-loading sulfur cathode with a mixed ionic-electronic conducting polymer for electrochemically stable lithium-sulfur batteries, Energy Storage Mater. 17 (2019) 317–324. https://doi.org/10.1016/j.ensm.2018.11.002.

[93] H. Gao, Q. Lu, Y. Yao, X. Wang, F. Wang, Significantly Raising the Cell Performance of Lithium Sulfur Battery via the Multifunctional Polyaniline Binder, Electrochim. Acta. 232 (2017) 414–421. https://doi.org/10.1016/j.electacta.2017.02.160.

[94] A.B. Puthirath, A. Baburaj, K. Kato, D. Salpekar, N. Chakingal, Y. Cao, G. Babu, P.M. Ajayan, High sulfur content multifunctional conducting polymer composite electrodes for stable Li-S battery, Electrochim. Acta. 306 (2019) 489–497. https://doi.org/10.1016/j.electacta.2019.03.136.

[95] P. Zhu, J. Zhu, C. Yan, M. Dirican, J. Zang, H. Jia, Y. Li, Y. Kiyak, H. Tan, X. Zhang, In Situ Polymerization of Nanostructured Conductive Polymer on 3D Sulfur / Carbon Nanofiber Composite Network as Cathode for High-Performance Lithium – Sulfur Batteries, Adv. Mater. Interfaces. 5 (2018) 1701598–1701608. https://doi.org/10.1002/admi.201701598.

[96] W. Li, Q. Zhang, G. Zheng, Z.W. Seh, H. Yao, Y. Cui, Understanding the role of different conductive polymers in improving the nanostructured sulfur cathode performance, Nano Lett. 13 (2013) 5534–5540. https://doi.org/10.1021/nl403130h.

[97] Z. Wang, Y. Chen, V. Battaglia, G. Liu, Improving the performance of lithium-sulfur batteries using conductive polymer and micrometric sulfur powder, J. Mater. Res. 29 (2014) 1027–1033. https://doi.org/10.1557/jmr.2014.85.

[98] H. Yuan, J.Q. Huang, H.J. Peng, M.M. Titirici, R. Xiang, R. Chen, Q. Liu, Q. Zhang, A Review of Functional Binders in Lithium–Sulfur Batteries, Adv. Energy Mater. 8 (2018) 1–20. https://doi.org/10.1002/aenm.201802107.

[99] H. Yi, T. Lan, Y. Yang, H. Zeng, T. Zhang, T. Tang, C. Wang, Y. Deng, A robust aqueous-processable polymer binder for long-life, high-performance lithium sulfur battery, Energy Storage Mater. 21 (2019) 61–68. https://doi.org/10.1016/j.ensm.2018.12.009.

[100] C. Milroy, A. Manthiram, An Elastic, Conductive, Electroactive Nanocomposite Binder for Flexible Sulfur Cathodes in Lithium–Sulfur Batteries, Adv. Mater. 28 (2016) 9744–9751. https://doi.org/10.1002/adma.201601665.

[101] L. Wang, Z. Yi, X. Wang, Y. Zhang, M. Jin, G. Zhou, A Novel Binder-Free Sulfur / Polypyrrole Cathode for Lithium / Sulfur Batteries, Int. J. Electrochem. Sci. 12 (2017) 5521–5528. https://doi.org/10.20964/2017.06.82.

[102] J. Zhang, H. Huang, J. Bae, S.-H. Chung, W. Zhang, A. Manthiram, G. Yu, Nanostructured Host Materials for Trapping Sulfur in Rechargeable Li-S Batteries: Structure Design and Interfacial Chemistry, Small Methods. 2 (2018) 1700279. https://doi.org/10.1002/smtd.201700279.

[103] J. Sun, Y. Huang, W. Wang, Z. Yu, A. Wang, K. Yuan, Application of gelatin as a binder for the sulfur cathode in lithium-sulfur batteries, Electrochim. Acta. 53 (2008) 7084–7088. https://doi.org/10.1016/j.electacta.2008.05.022.

[104] J. Pan, G. Xu, B. Ding, Z. Chang, A. Wang, H. Dou, X. Zhang, PAA/PEDOT:PSS as a multifunctional, water-soluble binder to improve the capacity and stability of lithium-sulfur batteries, RSC Adv. 6 (2016) 40650–40655. https://doi.org/10.1039/c6ra04230a.

[105] T.-H. Le, Y. Kim, H. Yoon, Electrical and Electrochemical Properties of Conducting Polymers, Polymers. 9 (2017) 150. https://doi.org/10.3390/polym9040150.

[106] N. V. Blinova, J. Stejskal, M. Trchová, J. Prokeš, M. Omastová, Polyaniline and polypyrrole: A comparative study of the preparation, Eur. Polym. J. 43 (2007) 2331–2341. https://doi.org/10.1016/j.eurpolymj.2007.03.045.

[107] L. Vinet, A. Zhedanov, A “missing” family of classical orthogonal polynomials, Mater. Today Proc. 4 (2010) 5721–5726. https://doi.org/10.1088/1751-8113/44/8/085201.

[108] J.L. Bredas, G.B. Street, Polarons, bipolarons, and solitons in conducting polymers, Acc. Chem. Res. 18 (1985) 309–315. https://doi.org/10.1021/ar00118a005.

[109] D.M. de Leeuw, M.M.J. Simenon, A.R. Brown, R.E.F. Einerhand, Stability of n-type doped conducting polymers and consequences for polymeric microelectronic devices, Synth. Met. 87 (1997) 53–59. https://doi.org/10.1016/S0379-6779(97)80097-5.

[110] A. Manthiram, An Outlook on Lithium Ion Battery Technology, ACS Cent. Sci. 3 (2017) 1063–1069. https://doi.org/10.1021/acscentsci.7b00288.

[111] P. Roy, S.K. Srivastava, Nanostructured anode materials for lithium ion batteries, J. Mater. Chem. A. 3 (2015) 2454–2484. https://doi.org/10.1039/c4ta04980b.

[112] E. Markevich, G. Salitra, D. Aurbach, Influence of the PVDF binder on the stability of LiCoO2 electrodes, Electrochem. Commun. 7 (2005) 1298–1304. https://doi.org/10.1016/j.elecom.2005.09.010.

[113] S. Zhang, Chemomechanical modeling of lithiation-induced failure in high-volume-change electrode materials for lithium ion batteries, Npj Comput. Mater. 3 (2017) 7. https://doi.org/10.1038/s41524-017-0009-z.

[114] J. Vetter, P. Novák, M.R. Wagner, C. Veit, K.-C. Möller, J.O. Besenhard, M. Winter, M. Wohlfahrt-Mehrens, C. Vogler, A. Hammouche, Ageing mechanisms in lithium-ion batteries, J. Power Sources. 147 (2005) 269–281. https://doi.org/10.1016/j.jpowsour.2005.01.006.

[115] R. Scipioni, P.S. Jørgensen, D.-T. Ngo, S.B. Simonsen, Z. Liu, K.J. Yakal-Kremski, H. Wang, J. Hjelm, P. Norby, S.A. Barnett, S.H. Jensen, Electron microscopy investigations of changes in morphology and conductivity of LiFePO4/C electrodes, J. Power Sources. 307 (2016) 259–269. https://doi.org/10.1016/j.jpowsour.2015.12.119.

[116] C. Yuan, Y. Deng, T. Li, F. Yang, Manufacturing energy analysis of lithium ion battery pack for electric vehicles, CIRP Ann. - Manuf. Technol. 66 (2017) 53–56. https://doi.org/10.1016/j.cirp.2017.04.109.

[117] J. Zhao, X. Yang, Y. Yao, Y. Gao, Y. Sui, B. Zou, H. Ehrenberg, G. Chen, F. Du, Moving to Aqueous Binder: A Valid Approach to Achieving High-Rate Capability and Long-Term Durability for Sodium-Ion Battery, Adv. Sci. 5 (2018) 1700768. https://doi.org/10.1002/advs.201700768.

[118] S. El Khakani, N. Verdier, D. Lepage, A. Prébé, D. Aymé-Perrot, D. Rochefort, M. Dollé, Melt-processed electrode for lithium ion battery, J. Power Sources. 454 (2020) 227884. https://doi.org/10.1016/j.jpowsour.2020.227884.

[119] T.M. Higgins, S.H. Park, P.J. King, C. Zhang, N. McEvoy, N.C. Berner, D. Daly, A. Shmeliov, U. Khan, G. Duesberg, V. Nicolosi, J.N. Coleman, A Commercial Conducting Polymer as Both Binder and Conductive Additive for Silicon Nanoparticle-Based Lithium-Ion Battery Negative Electrodes, ACS Nano. 10 (2016) 3702–3713. https://doi.org/10.1021/acsnano.6b00218.

[120] J.M. Kim, H.S. Park, J.H. Park, T.H. Kim, H.K. Song, S.Y. Lee, Conducting polymer-skinned electroactive materials of lithium-ion batteries: Ready for monocomponent electrodes without additional binders and conductive agents, ACS Appl. Mater. Interfaces. 6 (2014) 12789–12797. https://doi.org/10.1021/am502736m.

[121] A. Altomare, N. Corriero, C. Cuocci, A. Falcicchio, A. Moliterni, R. Rizzi, QUALX2.0 : a qualitative phase analysis software using the freely available database POW_COD, J. Appl. Crystallogr. 48 (2015) 598–603. https://doi.org/10.1107/S1600576715002319.

[122] H. Iwai, J.S. Hammond, S. Tanuma, Recent Status of Thin Film Analyses by XPS, J. Surf. Anal. 15 (2009) 264–270. https://doi.org/10.1384/jsa.15.264.

[123] G. Deroubaix, P. Marcus, X-ray photoelectron spectroscopy analysis of copper and zinc oxides and sulphides, Surf. Interface Anal. 18 (1992) 39–46. https://doi.org/10.1002/sia.740180107.

[124] N. Pauly, S. Tougaard, F. Yubero, LMM Auger primary excitation spectra of copper, Surf. Sci. 630 (2014) 294–299. https://doi.org/10.1016/j.susc.2014.08.029.

[125] F.M. Smits, Measurement of sheet resistivities with the four-point probe, Bell Syst. Tech. J. 37 (1958) 711–718. https://doi.org/10.1002/j.1538-7305.1958.tb03883.x.

[126] A. Yoshino, The birth of the lithium-ion battery, Angew. Chemie - Int. Ed. 51 (2012) 5798–5800. https://doi.org/10.1002/anie.201105006.

[127] H. S, Overview of cell balancing methods for Li-ion battery technology, Energy Storage. (2020) 1–12. https://doi.org/10.1002/est2.203.

[128] M.D. Murbach, D.T. Schwartz, Analysis of Li-Ion Battery Electrochemical Impedance Spectroscopy Data: An Easy-to-Implement Approach for Physics-Based Parameter Estimation Using an Open-Source Tool, J. Electrochem. Soc. 165 (2018) A297–A304. https://doi.org/10.1149/2.1021802jes.

[129] G. Patry, A. Romagny, S. Martinet, D. Froelich, Cost modeling of lithium-ion battery cells for automotive applications, Energy Sci. Eng. 3 (2015) 71–82. https://doi.org/10.1002/ese3.47.

[130] K. Mizushima, P.C. Jones, P.J. Wiseman, J.B. Goodenough, LixCoO2 (0<x<1): A new cathode material for batteries of high energy density, Mater. Res. Bull. 15 (1980) 783–789. https://doi.org/10.1016/0025-5408(80)90012-4.

[131] M.S. Whittingham, Electrical Energy Storage and Intercalation Chemistry, Science. 192 (1976) 1126–1127. https://doi.org/10.1126/science.192.4244.1126.

[132] J.W. Choi, D. Aurbach, Promise and reality of post-lithium-ion batteries with high energy densities, Nat. Rev. Mater. 1 (2016) 1–16. https://doi.org/10.1038/natrevmats.2016.13.

[133] Z.P. Guo, J.Z. Wang, H.K. Liu, S.X. Dou, Study of silicon/polypyrrole composite as anode materials for Li-ion batteries, J. Power Sources. 146 (2005) 448–451. https://doi.org/10.1016/j.jpowsour.2005.03.112.

[134] H. Zhao, Y. Wei, R. Qiao, C. Zhu, Z. Zheng, M. Ling, Z. Jia, Y. Bai, Y. Fu, J. Lei, X. Song, V.S. Battaglia, W. Yang, P.B. Messersmith, G. Liu, Conductive polymer binder for high-tap-density nanosilicon material for lithium-ion battery negative electrode application, Nano Lett. 15 (2015) 7927–7932. https://doi.org/10.1021/acs.nanolett.5b03003.

[135] L. Luo, P. Zhao, H. Yang, B. Liu, J.-G. Zhang, Y. Cui, G. Yu, S. Zhang, C.-M. Wang, Surface Coating Constraint Induced Self-Discharging of Silicon Nanoparticles as Anodes for Lithium Ion Batteries, Nano Lett. 15 (2015) 7016–7022. https://doi.org/10.1021/acs.nanolett.5b03047.

[136] Y. Zhao, L. Yang, D. Liu, J. Hu, L. Han, Z. Wang, F. Pan, A Conductive Binder for High-Performance Sn Electrodes in Lithium-Ion Batteries, ACS Appl. Mater. Interfaces. 10 (2018) 1672–1677. https://doi.org/10.1021/acsami.7b13692.

[137] K. Dai, H. Zhao, Z. Wang, X. Song, V. Battaglia, G. Liu, Toward high specific capacity and high cycling stability of pure tin nanoparticles with conductive polymer binder for sodium ion batteries, J. Power Sources. 263 (2014) 276–279. https://doi.org/10.1016/j.jpowsour.2014.04.012.

[138] L.J. Fu, H. Liu, C. Li, Y.P. Wu, E. Rahm, R. Holze, H.Q. Wu, Electrode materials for lithium secondary batteries prepared by sol-gel methods, Prog. Mater. Sci. 50 (2005) 881–928. https://doi.org/10.1016/j.pmatsci.2005.04.002.

[139] M.N. Obrovac, L.J. Krause, Reversible cycling of crystalline silicon powder, J. Electrochem. Soc. 154 (2007) 103–108. https://doi.org/10.1149/1.2402112.

[140] M. Wu, X. Xiao, N. Vukmirovic, S. Xun, P.K. Das, X. Song, P. Olalde-Velasco, D. Wang, A.Z. Weber, L.W. Wang, V.S. Battaglia, W. Yang, G. Liu, Toward an ideal polymer binder design for high-capacity battery anodes, J. Am. Chem. Soc. 135 (2013) 12048–12056. https://doi.org/10.1021/ja4054465.

[141] Z.P. Cai, Y. Liang, W.S. Li, L.D. Xing, Y.H. Liao, Preparation and performances of LiFePO4 cathode in aqueous solvent with polyacrylic acid as a binder, J. Power Sources. 189 (2009) 547–551. https://doi.org/10.1016/j.jpowsour.2008.10.040.

[142] P.K. Nayak, J. Grinblat, M. Levi, O. Haik, E. Levi, S. Kim, J.W. Choi, D. Aurbach, Multiphase LiNi0.33Mn0.54Co0.13O2 Cathode Material with High Capacity Retention for Li-Ion Batteries, ChemElectroChem. 2 (2015) 1957–1965. https://doi.org/10.1002/celc.201500339.

[143] A.M. Hashem, R.S. El-Tawil, M. Abutabl, A.E. Eid, Pristine and coated LiNi1/3Mn1/3Co1/3O2 as positive electrode materials for li-ion batteries, Res. Eng. Struct. Mater. 1 (2015) 81–87. https://doi.org/10.17515/resm2015.07en0315.

[144] A. Purwanto, C.S. Yudha, U. Ubaidillah, H. Widiyandari, T. Ogi, H. Haerudin, NCA cathode material: synthesis methods and performance enhancement efforts, Mater. Res. Express. 5 (2018) 122001. https://doi.org/10.1088/2053-1591/aae167.

[145] A.S. Andersson, J.O. Thomas, B. Kalska, L. Häggström, Thermal Stability of LiFePO 4 - Based Cathodes, Electrochem. Solid-State Lett. 3 (2000) 66–68.

[146] G. Arnold, J. Garche, R. Hemmer, S. Ströbele, C. Vogler, M. Wohlfahrt-Mehrens, Fine-particle lithium iron phosphate LiFePO4 synthesized by a new low-cost aqueous precipitation technique, J. Power Sources. 119–121 (2003) 247–251. https://doi.org/10.1016/S0378-7753(03)00241-6.

[147] G.X. Wang, S.L. Bewlay, K. Konstantinov, H.K. Liu, S.X. Dou, J.H. Ahn, Physical and electrochemical properties of doped lithium iron phosphate electrodes, Electrochim. Acta. 50 (2004) 443–447. https://doi.org/10.1016/j.electacta.2004.04.047.

[148] A. Yamada, S.C. Chung, K. Hinokuma, Optimized LiFePO4 for Lithium Battery Cathodes, J. Electrochem. Soc. 148 (2001) A224. https://doi.org/10.1149/1.1348257.

[149] Y.Y. Zhang, S.J. Zhang, J.T. Li, K. Wang, Y.C. Zhang, Q. Liu, R.S. Xie, Y.R. Pei, L. Huang, S.G. Sun, Improvement of electrochemical properties of P2-type Na2/3Mn2/3Ni1/3O2 sodium ion battery cathode material by water-soluble binders, Electrochim. Acta. 298 (2019) 496–504. https://doi.org/10.1016/j.electacta.2018.12.089.

[150] X.-Q. Yang, J. McBreen, W.-S. Yoon, C.P. Grey, Crystal structure changes of LiMn0.5Ni0.5O2 cathode materials during charge and discharge studied by synchrotron based in situ XRD, Electrochem. Commun. 4 (2002) 649–654. https://doi.org/10.1016/S1388-2481(02)00406-X.

[151] A.O. Kondrakov, A. Schmidt, J. Xu, H. Geßwein, R. Mönig, P. Hartmann, H. Sommer, T. Brezesinski, J. Janek, Anisotropic Lattice Strain and Mechanical Degradation of High- and Low-Nickel NCM Cathode Materials for Li-Ion Batteries, J. Phys. Chem. C. 121 (2017) 3286–3294. https://doi.org/10.1021/acs.jpcc.6b12885.

[152] I. Bloom, S.A. Jones, V.S. Battaglia, G.L. Henriksen, J.P. Christophersen, R.B. Wright, C.D. Ho, J.R. Belt, C.G. Motloch, Effect of cathode composition on capacity fade, impedance rise and power fade in high-power, lithium-ion cells, J. Power Sources. 124 (2003) 538–550. https://doi.org/10.1016/S0378-7753(03)00806-1.

[153] H.Q. Pham, G. Kim, H.M. Jung, S.W. Song, Fluorinated Polyimide as a Novel High-Voltage Binder for High-Capacity Cathode of Lithium-Ion Batteries, Adv. Funct. Mater. 28 (2018) 1–9. https://doi.org/10.1002/adfm.201704690.

[154] H. Chen, M. Ling, L. Hencz, H.Y. Ling, G. Li, Z. Lin, G. Liu, S. Zhang, Exploring Chemical, Mechanical, and Electrical Functionalities of Binders for Advanced Energy-Storage Devices, Chem. Rev. 118 (2018) 8936–8982. https://doi.org/10.1021/acs.chemrev.8b00241.

[155] S. Lee, Molecular Dynamics Study of the Separation Behavior at the Interface between PVDF Binder and Copper Current Collector, J. Nanomater. 2016 (2016) 1–12. https://doi.org/10.1155/2016/4253986.

[156] N.H. Kwon, The effect of carbon morphology on the LiCoO2 cathode of lithium ion batteries, Solid State Sci. 21 (2013) 59–65. https://doi.org/10.1016/j.solidstatesciences.2013.04.010.

[157] Y. Shi, X. Zhou, G. Yu, Material and Structural Design of Novel Binder Systems for High-Energy, High-Power Lithium-Ion Batteries, Acc. Chem. Res. 50 (2017) 2642–2652. https://doi.org/10.1021/acs.accounts.7b00402.

[158] D. Bresser, D. Buchholz, A. Moretti, A. Varzi, S. Passerini, Alternative binders for sustainable electrochemical energy storage – the transition to aqueous electrode processing and bio-derived polymers, Energy Environ. Sci. 11 (2018) 3096–3127. https://doi.org/10.1039/C8EE00640G.

[159] H. Buqa, M. Holzapfel, F. Krumeich, C. Veit, P. Novák, Study of styrene butadiene rubber and sodium methyl cellulose as binder for negative electrodes in lithium-ion batteries, J. Power Sources. 161 (2006) 617–622. https://doi.org/10.1016/j.jpowsour.2006.03.073.

[160] J. Guo, C. Wang, A polymer scaffold binder structure for high capacity silicon anode of lithium-ion battery, Chem. Commun. 46 (2010) 1428–1430. https://doi.org/10.1039/b918727h.

[161] F.M. Courtel, S. Niketic, D. Duguay, Y. Abu-Lebdeh, I.J. Davidson, Water-soluble binders for MCMB carbon anodes for lithium-ion batteries, J. Power Sources. 196 (2011) 2128–2134. https://doi.org/10.1016/j.jpowsour.2010.10.025.

[162] Z. Wang, N. Dupré, A.-C. Gaillot, B. Lestriez, J.-F. Martin, L. Daniel, S. Patoux, D. Guyomard, CMC as a binder in LiNi0.4Mn1.6O4 5V cathodes and their electrochemical

performance for Li-ion batteries, Electrochim. Acta. 62 (2012) 77–83. https://doi.org/10.1016/j.electacta.2011.11.094.

[163] H. Zhong, J. He, L. Zhang, Better cycle stability and rate capability of high-voltage LiNi0.5Mn1.5O4 cathode using water soluble binder, Mater. Res. Bull. 93 (2017) 194–200. https://doi.org/10.1016/j.materresbull.2017.04.036.

[164] P.F. Cao, M. Naguib, Z. Du, E. Stacy, B. Li, T. Hong, K. Xing, D.N. Voylov, J. Li, D.L. Wood, A.P. Sokolov, J. Nanda, T. Saito, Effect of Binder Architecture on the Performance of Silicon/Graphite Composite Anodes for Lithium Ion Batteries, ACS Appl. Mater. Interfaces. 10 (2018) 3470–3478. https://doi.org/10.1021/acsami.7b13205.

[165] M. Sun, H. Zhong, S. Jiao, H. Shao, L. Zhang, Investigation on Carboxymethyl Chitosan as New Water Soluble Binder for LiFePO4 Cathode in Li-Ion Batteries, Electrochim. Acta. 127 (2014) 239–244. https://doi.org/10.1016/j.electacta.2014.02.027.

[166] J. Hu, Y. Wang, D. Li, Y.T. Cheng, Effects of adhesion and cohesion on the electrochemical performance and durability of silicon composite electrodes, J. Power Sources. 397 (2018) 223–230. https://doi.org/10.1016/j.jpowsour.2018.06.103.

[167] F. Bigoni, F. De Giorgio, F. Soavi, C. Arbizzani, Sodium Alginate: A Water-Processable Binder in High-Voltage Cathode Formulations, J. Electrochem. Soc. 164 (2017) A6171–A6177. https://doi.org/10.1149/2.0281701jes.

[168] S. Zhang, S. Ren, D. Han, M. Xiao, S. Wang, Y. Meng, Aqueous sodium alginate as binder: Dramatically improving the performance of dilithium terephthalate-based organic lithium ion batteries, J. Power Sources. 438 (2019) 227007. https://doi.org/10.1016/j.jpowsour.2019.227007.

[169] M.H. Ryou, S. Hong, M. Winter, H. Lee, J.W. Choi, Improved cycle lives of LiMn2O4 cathodes in lithium ion batteries by an alginate biopolymer from seaweed, J. Mater. Chem. A. 1 (2013) 15224–15229. https://doi.org/10.1039/c3ta13514d.

[170] R. Wang, L. Feng, W. Yang, Y. Zhang, Y. Zhang, W. Bai, B. Liu, W. Zhang, Y. Chuan, Z. Zheng, H. Guan, Effect of Different Binders on the Electrochemical Performance of Metal Oxide Anode for Lithium-Ion Batteries, Nanoscale Res. Lett. 12 (2017) 575.

https://doi.org/10.1186/s11671-017-2348-6.

[171] J. Xu, Q. Zhang, Y.T. Cheng, High capacity silicon electrodes with nafion as binders for lithium-ion batteries, J. Electrochem. Soc. 163 (2016) A401–A405. https://doi.org/10.1149/2.0261603jes.

[172] Z. Chen, L. Christensen, J.R. Dahn, Mechanical and electrical properties of poly(vinylidene fluoride-tetrafluoroethylene-propylene)/super-S carbon black swelled in liquid solvent as an electrode binder for lithium-ion batteries, J. Appl. Polym. Sci. 91 (2004) 2958–2965. https://doi.org/10.1002/app.13505.

[173] C.-C. Li, Y.-S. Lin, Interactions between organic additives and active powders in water-based lithium iron phosphate electrode slurries, J. Power Sources. 220 (2012) 413–421. https://doi.org/10.1016/j.jpowsour.2012.07.125.

[174] J. Jang, Conducting Polymer Nanomaterials and Their Applications, in: Adv. Polym. Sci., Springer, 2006: pp. 189–260. https://doi.org/10.1007/12_075.

[175] C. Li, H. Bai, G. Shi, Conducting polymer nanomaterials: electrosynthesis and applications, Chem. Soc. Rev. 38 (2009) 2397. https://doi.org/10.1039/b816681c.

[176] M. Gerard, B.D. Malhotra, Application of conducting polymers to biosensors, Biosens. Bioelectron. 17 (2002) 345–359. https://doi.org/10.1016/S0956-5663(01)00312-8.

[177] Y. Shi, L. Peng, G. Yu, Nanostructured conducting polymer hydrogels for energy storage applications, Nanoscale. 7 (2015) 12796–12806. https://doi.org/10.1039/c5nr03403e.

[178] Y. Shi, X. Zhou, J. Zhang, A.M. Bruck, A.C. Bond, A.C. Marschilok, K.J. Takeuchi, E.S. Takeuchi, G. Yu, Nanostructured Conductive Polymer Gels as a General Framework Material To Improve Electrochemical Performance of Cathode Materials in Li-Ion Batteries, Nano Lett. 17 (2017) 1906–1914. https://doi.org/10.1021/acs.nanolett.6b05227.

[179] J. Ouyang, "secondary doping" methods to significantly enhance the conductivity of PEDOT:PSS for its application as transparent electrode of optoelectronic devices, Displays. 34 (2013) 423–436. https://doi.org/10.1016/j.displa.2013.08.007.

[180] H. Zhong, A. He, J. Lu, M. Sun, J. He, L. Zhang, Carboxymethyl chitosan/conducting

polymer as water-soluble composite binder for LiFePO4 cathode in lithium ion batteries, J. Power Sources. 336 (2016) 107–114. https://doi.org/10.1016/j.jpowsour.2016.10.041.

[181] D. Shao, H. Zhong, L. Zhang, Water-Soluble Conductive Composite Binder Containing PEDOT:PSS as Conduction Promoting Agent for Si Anode of Lithium-Ion Batteries, ChemElectroChem. 1 (2014) 1679–1687. https://doi.org/10.1002/celc.201402210.

[182] W. Zeng, L. Wang, X. Peng, T. Liu, Y. Jiang, F. Qin, L. Hu, P.K. Chu, K. Huo, Y. Zhou, Enhanced Ion Conductivity in Conducting Polymer Binder for High-Performance Silicon Anodes in Advanced Lithium-Ion Batteries, Adv. Energy Mater. 8 (2018) 1702314. https://doi.org/10.1002/aenm.201702314.

[183] S.N. Eliseeva, E. V. Shkreba, M.A. Kamenskii, E.G. Tolstopjatova, R. Holze, V. V. Kondratiev, Effects of conductive binder on the electrochemical performance of lithium titanate anodes, Solid State Ionics. 333 (2019) 18–29. https://doi.org/10.1016/j.ssi.2019.01.011.

[184] Y. Yao, N. Liu, M.T. McDowell, M. Pasta, Y. Cui, Improving the cycling stability of silicon nanowire anodes with conducting polymer coatings, Energy Environ. Sci. 5 (2012) 7927–7930. https://doi.org/10.1039/c2ee21437g.

[185] J. Kim, H.S. Park, T.H. Kim, S. Yeol Kim, H.K. Song, An inter-tangled network of redox-active and conducting polymers as a cathode for ultrafast rechargeable batteries, Phys. Chem. Chem. Phys. 16 (2014) 5295–5300. https://doi.org/10.1039/c3cp54624a.

[186] T.Y. Chi, H. Li, G.C. Wang, Hierarchically porous carbon/DMcT/PEDOT-PSS ternary composite as a cathode material for lithium-ion battery, Acta Physico-Chimica Sin. 29 (2013) 1981–1988. https://doi.org/10.3866/PKU.WHXB201306272.

[187] M.B. McDonald, P.T. Hammond, Efficient Transport Networks in a Dual Electron/Lithium-Conducting Polymeric Composite for Electrochemical Applications, ACS Appl. Mater. Interfaces. 10 (2018) 15681–15690. https://doi.org/10.1021/acsami.8b01519.

[188] H. Li, A High Capacity Nano-Si Composite Anode Material for Lithium Rechargeable Batteries, Electrochem. Solid-State Lett. 2 (1999) 547. https://doi.org/10.1149/1.1390899.

[189] L.Y. Beaulieu, K.W. Eberman, R.L. Turner, L.J. Krause, J.R. Dahn, Colossal Reversible

Volume Changes in Lithium Alloys, Electrochem. Solid-State Lett. 4 (2001) A137. https://doi.org/10.1149/1.1388178.

[190] M. Dahbi, T. Nakano, N. Yabuuchi, T. Ishikawa, K. Kubota, M. Fukunishi, S. Shibahara, J.-Y. Son, Y.-T. Cui, H. Oji, S. Komaba, Sodium carboxymethyl cellulose as a potential binder for hard-carbon negative electrodes in sodium-ion batteries, Electrochem. Commun. 44 (2014) 66–69. https://doi.org/10.1016/j.elecom.2014.04.014.

[191] S.L. Chou, X.W. Gao, J.Z. Wang, D. Wexler, Z.X. Wang, L.Q. Chen, H.K. Liu, Tin/polypyrrole composite anode using sodium carboxymethyl cellulose binder for lithium-ion batteries, Dalt. Trans. 40 (2011) 12801–12807. https://doi.org/10.1039/c1dt10396b.

[192] G.T. Kim, S.S. Jeong, M. Joost, E. Rocca, M. Winter, S. Passerini, A. Balducci, Use of natural binders and ionic liquid electrolytes for greener and safer lithium-ion batteries, J. Power Sources. 196 (2011) 2187–2194. https://doi.org/10.1016/j.jpowsour.2010.09.080.

[193] U.S. Vogl, P.K. Das, A.Z. Weber, M. Winter, R. Kostecki, S.F. Lux, Mechanism of interactions between CMC binder and si single crystal facets, Langmuir. 30 (2014) 10299–10307. https://doi.org/10.1021/la501791q.

[194] G.N. Zhu, Y.G. Wang, Y.Y. Xia, Ti-based compounds as anode materials for Li-ion batteries, Energy Environ. Sci. 5 (2012) 6652–6667. https://doi.org/10.1039/c2ee03410g.

[195] T.F. Yi, L.J. Jiang, J. Shu, C.B. Yue, R.S. Zhu, H. Bin Qiao, Recent development and application of Li4Ti5O12 as anode material of lithium ion battery, J. Phys. Chem. Solids. 71 (2010) 1236–1242. https://doi.org/10.1016/j.jpcs.2010.05.001.

[196] J.E. McCarthy, C.A. Hanley, L.J. Brennan, V.G. Lambertini, Y.K. Gun'Ko, Fabrication of highly transparent and conducting PEDOT:PSS films using a formic acid treatment, J. Mater. Chem. C. 2 (2014) 764–770. https://doi.org/10.1039/c3tc31951b.

[197] M. Ling, J. Qiu, S. Li, C. Yan, M.J. Kiefel, G. Liu, S. Zhang, Multifunctional SA-PProDOT Binder for Lithium Ion Batteries, Nano Lett. 15 (2015) 4440–4447. https://doi.org/10.1021/acs.nanolett.5b00795.

[198] H. Guo, L. Liu, Q. Wei, H. Shu, X. Yang, Z. Yang, M. Zhou, J. Tan, Z. Yan, X. Wang, Electrochemical characterization of polyaniline-LiV3O8 nanocomposite cathode material

for lithium ion batteries, Electrochim. Acta. 94 (2013) 113–123. https://doi.org/10.1016/j.electacta.2013.01.127.

[199] K. Lee, S. Lim, A. Tron, J. Mun, Y. Kim, T. Yim, T.-H. Kim, Polymeric binder based on PAA and conductive PANI for high performance silicon-based anodes, RSC Adv. 6 (2016) 101622–101625. https://doi.org/10.1039/C6RA23805J.

[200] K. Lee, S. Lim, T.H. Kim, Dopamine-conjugated Poly(acrylic acid) Blended with an Electrically Conductive Polyaniline Binder for Silicon Anode, Bull. Korean Chem. Soc. 39 (2018) 873–878. https://doi.org/10.1002/bkcs.11492.

[201] X. Wang, Y. Zhang, Y. Shi, X. Zeng, R. Tang, L. Wei, Conducting polyaniline/poly (acrylic acid)/phytic acid multifunctional binders for Si anodes in lithium ion batteries, Ionics. 25 (2019) 5323–5331. https://doi.org/10.1007/s11581-019-03122-1.

[202] D. Liu, Y. Zhao, R. Tan, L.L. Tian, Y. Liu, H. Chen, F. Pan, Novel conductive binder for high-performance silicon anodes in lithium ion batteries, Nano Energy. 36 (2017) 206–212. https://doi.org/10.1016/j.nanoen.2017.04.043.

[203] H. Zhao, Y. Fu, M. Ling, Z. Jia, X. Song, Z. Chen, J. Lu, K. Amine, G. Liu, Conductive Polymer Binder-Enabled SiO-SnxCoyCz Anode for High-Energy Lithium-Ion Batteries, ACS Appl. Mater. Interfaces. 8 (2016) 13373–13377. https://doi.org/10.1021/acsami.6b00312.

[204] L. Yue, S. Wang, X. Zhao, L. Zhang, Nano-silicon composites using poly(3,4-ethylenedioxythiophene):poly(styrenesulfonate) as elastic polymer matrix and carbon source for lithium-ion battery anode, J. Mater. Chem. 22 (2012) 1094–1099. https://doi.org/10.1039/c1jm14568a.

[205] H. Wu, G. Yu, L. Pan, N. Liu, M.T. McDowell, Z. Bao, Y. Cui, Stable Li-ion battery anodes by in-situ polymerization of conducting hydrogel to conformally coat silicon nanoparticles, Nat. Commun. 4 (2013) 1943–1946. https://doi.org/10.1038/ncomms2941.

[206] Y. Shi, J. Zhang, A.M. Bruck, Y. Zhang, J. Li, E.A. Stach, K.J. Takeuchi, A.C. Marschilok, E.S. Takeuchi, G. Yu, A Tunable 3D Nanostructured Conductive Gel Framework Electrode for High-Performance Lithium Ion Batteries, Adv. Mater. 29 (2017) 1603922.

https://doi.org/10.1002/adma.201603922.

[207] J. Zheng, X. Yu, C. Wang, Z. Cao, H. Yang, D. Ma, X. Xu, Facile synthesis of three-dimensional reinforced Sn@polyaniline/sodium alginate nanofiber hydrogel network for high performance lithium-ion battery, J. Mater. Sci. Mater. Electron. 27 (2016) 4457–4464. https://doi.org/10.1007/s10854-016-4317-8.

[208] A. Magasinski, B. Zdyrko, I. Kovalenko, B. Hertzberg, R. Burtovyy, C.F. Huebner, T.F. Fuller, I. Luzinov, G. Yushin, Toward efficient binders for Li-ion battery Si-based anodes: Polyacrylic acid, ACS Appl. Mater. Interfaces. 2 (2010) 3004–3010. https://doi.org/10.1021/am100871y.

[209] B. Hertzberg, A. Alexeev, G. Yushin, Deformations in Si-Li anodes upon electrochemical alloying in nano-confined space, J. Am. Chem. Soc. 132 (2010) 8548–8549. https://doi.org/10.1021/ja1031997.

[210] I. Kovalenko, B. Zdyrko, A. Magasinski, B. Hertzberg, Z. Milicev, R. Burtovyy, I. Luzinov, G. Yushin, A Major Constituent of Brown Algae for Use in High-Capacity Li-Ion Batteries, Science. 334 (2011) 75–79. https://doi.org/10.1126/science.1209150.

[211] J.S. Bridel, T. Azaïs, M. Morcrette, J.M. Tarascon, D. Larcher, Key parameters governing the reversibility of Si/carbon/CMC electrodes for Li-ion batteries, Chem. Mater. 22 (2010) 1229–1241. https://doi.org/10.1021/cm902688w.

[212] C. Sasso, E. Zeno, M. Petit-Conil, D. Chaussy, M.N. Belgacem, S. Tapin-Lingua, D. Beneventi, Highly conducting polypyrrole/cellulose nanocomposite films with enhanced mechanical properties, Macromol. Mater. Eng. 295 (2010) 934–941. https://doi.org/10.1002/mame.201000148.

[213] Y. Xu, Y. Zhang, Synthesis of polypyrrole/sodium carboxymethyl cellulose nanospheres with enhanced supercapacitor performance, Mater. Lett. 139 (2015) 145–148. https://doi.org/10.1016/j.matlet.2014.10.074.

[214] Y. Li, X. Zhao, Q. Xu, Q. Zhang, D. Chen, Facile preparation and enhanced capacitance of the polyaniline/sodium alginate nanofiber network for supercapacitors, Langmuir. 27 (2011) 6458–6463. https://doi.org/10.1021/la2003063.

[215] J. Fu, Z. Pang, J. Yang, F. Huang, Y. Cai, Q. Wei, Fabrication of polyaniline/carboxymethyl cellulose/cellulose nanofibrous mats and their biosensing application, Appl. Surf. Sci. 349 (2015) 35–42. https://doi.org/10.1016/j.apsusc.2015.04.215.

[216] N. Su, Improving Electrical Conductivity, Thermal Stability, and Solubility of Polyaniline-Polypyrrole Nanocomposite by Doping with Anionic Spherical Polyelectrolyte Brushes, Nanoscale Res. Lett. 10 (2015) 301. https://doi.org/10.1186/s11671-015-0997-x.

[217] S.N. Eliseeva, O. V Levin, E.G. Tolstopyatova, E. V Alekseeva, V. V Kondratiev, Effect of addition of a conducting polymer on the properties of the LiFePO4-based cathode material for lithium-ion batteries, Russ. J. Appl. Chem. 88 (2015) 1146–1149. https://doi.org/10.1134/s1070427215070071.

[218] H. Zhu, Z. Jia, Y. Chen, N. Weadock, J. Wan, O. Vaaland, X. Han, T. Li, L. Hu, Tin anode for sodium-ion batteries using natural wood fiber as a mechanical buffer and electrolyte reservoir, Nano Lett. 13 (2013) 3093–3100. https://doi.org/10.1021/nl400998t.

[219] S.-J. Park, H. Zhao, G. Ai, C. Wang, X. Song, N. Yuca, V.S. Battaglia, W. Yang, G. Liu, Side-Chain Conducting and Phase-Separated Polymeric Binders for High-Performance Silicon Anodes in Lithium-Ion Batteries, J. Am. Chem. Soc. 137 (2015) 2565–2571. https://doi.org/10.1021/ja511181p.

[220] O.O. Taiwo, D.P. Finegan, D.S. Eastwood, J.L. Fife, L.D. Brown, J.A. Darr, P.D. Lee, D.J.L. Brett, P.R. Shearing, Comparison of three-dimensional analysis and stereological techniques for quantifying lithium-ion battery electrode microstructures, J. Microsc. 263 (2016) 280–292. https://doi.org/10.1111/jmi.12389.

[221] A.G. Kashkooli, S. Farhad, D.U. Lee, K. Feng, S. Litster, S.K. Babu, L. Zhu, Z. Chen, Multiscale modeling of lithium-ion battery electrodes based on nano-scale X-ray computed tomography, J. Power Sources. 307 (2016) 496–509. https://doi.org/10.1016/j.jpowsour.2015.12.134.

[222] M. Ebner, F. Geldmacher, F. Marone, M. Stampanoni, V. Wood, X-Ray Tomography of Porous, Transition Metal Oxide Based Lithium Ion Battery Electrodes, Adv. Energy Mater. 3 (2013) 845–850. https://doi.org/10.1002/aenm.201200932.

[223] Y.H. Kwon, K. Minnici, J.J. Park, S.R. Lee, G. Zhang, E.S. Takeuchi, K.J. Takeuchi, A.C. Marschilok, E. Reichmanis, SWNT Anchored with Carboxylated Polythiophene “links” on High-Capacity Li-Ion Battery Anode Materials, J. Am. Chem. Soc. 140 (2018) 5666–5669. https://doi.org/10.1021/jacs.8b00693.

[224] Z. Chen, J.W.F. To, C. Wang, Z. Lu, N. Liu, A. Chortos, L. Pan, F. Wei, Y. Cui, Z. Bao, A Three-Dimensionally Interconnected Carbon Nanotube-Conducting Polymer Hydrogel Network for High-Performance Flexible Battery Electrodes, Adv. Energy Mater. 4 (2014) 1400207. https://doi.org/10.1002/aenm.201400207.

[225] H. Li, S. Yang, Y. Zhao, T. Tan, X. Wang, Z. Bakenov, Synthesis of ZnO/Polypyrrole Nanoring Composite as High-Performance Anode Materials for Lithium Ion Batteries, J. Nanomater. 2019 (2019) 1–8. https://doi.org/10.1155/2019/4702849.

[226] J. Li, G. Zhang, Y. Yang, D. Yao, Z. Lei, S. Li, Y. Deng, C. Wang, Glycinamide modified polyacrylic acid as high-performance binder for silicon anodes in lithium-ion batteries, J. Power Sources. 406 (2018) 102–109. https://doi.org/10.1016/j.jpowsour.2018.10.057.

[227] Y. Shi, L. Pan, B. Liu, Y. Wang, Y. Cui, Z. Bao, G. Yu, Nanostructured conductive polypyrrole hydrogels as high-performance, flexible supercapacitor electrodes, J. Mater. Chem. A. 2 (2014) 6086–6091. https://doi.org/10.1039/c4ta00484a.

[228] Y. Zhao, B. Liu, L. Pan, G. Yu, 3D nanostructured conductive polymer hydrogels for high-performance electrochemical devices, Energy Environ. Sci. 6 (2013) 2856–2870. https://doi.org/10.1039/c3ee40997j.

[229] P. Sengodu, A.D. Deshmukh, Conducting polymers and their inorganic composites for advanced Li-ion batteries: A review, RSC Adv. 5 (2015) 42109–42130. https://doi.org/10.1039/c4ra17254j.

[230] D.A. Semenenko, D.M. Itkis, T.L. Kulova, T.S. Yashuk, A.M. Skundin, E.A. Goodilin, Y.D. Tretyakov, Fabrication of microporous cathode materials containing polyaniline-vanadia self-scrolled nanoribbons, Electrochim. Acta. 63 (2012) 329–334. https://doi.org/10.1016/j.electacta.2011.12.116.

[231] J. Li, L. Fang, W.R. Tait, L. Sun, L. Zhao, L. Qian, Preparation of conductive composite

hydrogels from carboxymethyl cellulose and polyaniline with a nontoxic crosslinking agent, RSC Adv. 7 (2017) 54823–54828. https://doi.org/10.1039/c7ra10788a.

[232] Z. Du, D.L. Wood, C. Daniel, S. Kalnaus, J. Li, Understanding limiting factors in thick electrode performance as applied to high energy density Li-ion batteries, J. Appl. Electrochem. 47 (2017) 405–415. https://doi.org/10.1007/s10800-017-1047-4.

[233] M. Singh, J. Kaiser, H. Hahn, Thick electrodes for high energy lithium ion batteries, J. Electrochem. Soc. 162 (2015) A1196–A1201. https://doi.org/10.1149/2.0401507jes.

[234] K.G. Gallagher, S.E. Trask, C. Bauer, T. Woehrle, S.F. Lux, M. Tschech, P. Lamp, B.J. Polzin, S. Ha, B. Long, Q. Wu, W. Lu, D.W. Dees, A.N. Jansen, Optimizing areal capacities through understanding the limitations of lithium-ion electrodes, J. Electrochem. Soc. 163 (2016) A138–A149. https://doi.org/10.1149/2.0321602jes.

[235] X. Judez, G.G. Eshetu, C. Li, L.M. Rodriguez-Martinez, H. Zhang, M. Armand, Opportunities for Rechargeable Solid-State Batteries Based on Li-Intercalation Cathodes, Joule. 2 (2018) 2208–2224. https://doi.org/10.1016/j.joule.2018.09.008.

[236] K. Lee, S. Kim, J. Park, S.H. Park, A. Coskun, D.S. Jung, W. Cho, J.W. Choi, Selection of binder and solvent for solution-processed all-solid-state battery, J. Electrochem. Soc. 164 (2017) A2075–A2081. https://doi.org/10.1149/2.1341709jes.

[237] G. Zheng, Y. Yang, J.J. Cha, S.S. Hong, Y. Cui, Hollow carbon nanofiber-encapsulated sulfur cathodes for high specific capacity rechargeable lithium batteries, Nano Lett. 11 (2011) 4462–4467. https://doi.org/10.1021/nl2027684.

[238] B. Ding, C. Yuan, L. Shen, G. Xu, P. Nie, Q. Lai, X. Zhang, Chemically tailoring the nanostructure of graphene nanosheets to confine sulfur for high-performance lithium-sulfur batteries, J. Mater. Chem. A. 1 (2013) 1096–1101. https://doi.org/10.1039/c2ta00396a.

[239] L. Yan, X. Gao, J.P. Thomas, J. Ngai, H. Altounian, K.T. Leung, Y. Meng, Y. Li, Ionically cross-linked PEDOT:PSS as a multi-functional conductive binder for high-performance lithium-sulfur batteries, Sustain. Energy Fuels. 2 (2018) 1574–1581. https://doi.org/10.1039/c8se00167g.

[240] M. Rana, S.A. Ahad, M. Li, B. Luo, L. Wang, I. Gentle, R. Knibbe, Review on areal

capacities and long-term cycling performances of lithium sulfur battery at high sulfur loading, Energy Storage Mater. 18 (2019) 289–310. https://doi.org/10.1016/j.ensm.2018.12.024.

[241] Y. Luo, R. Guo, T. Li, F. Li, Z. Liu, M. Zheng, B. Wang, Z. Yang, H. Luo, Y. Wan, Application of Polyaniline for Li-Ion Batteries, Lithium–Sulfur Batteries, and Supercapacitors, ChemSusChem. 12 (2019) 1591–1611. https://doi.org/10.1002/cssc.201802186.

[242] M.K. Datta, R. Epur, P. Saha, K. Kadakia, S.K. Park, P.N. Kumta, Tin and graphite based nanocomposites: Potential anode for sodium ion batteries, J. Power Sources. 225 (2013) 316–322. https://doi.org/10.1016/j.jpowsour.2012.10.014.

[243] X. Xu, S. Ji, R. Gao, J. Liu, Facile synthesis of P2-type Na0.4Mn0.54Co0.46O2 as a high capacity cathode material for sodium-ion batteries, RSC Adv. 5 (2015) 51454–51460. https://doi.org/10.1039/c5ra06275f.

[244] Z. Gao, H. Sun, L. Fu, F. Ye, Y. Zhang, W. Luo, Y. Huang, Promises, Challenges, and Recent Progress of Inorganic Solid-State Electrolytes for All-Solid-State Lithium Batteries, Adv. Mater. 30 (2018) 1705702. https://doi.org/10.1002/adma.201705702.

[245] J. Janek, W.G. Zeier, A solid future for battery development, Nat. Energy. 1 (2016) 16141. https://doi.org/10.1038/nenergy.2016.141.

[246] S. Nambiar, J.T.W. Yeow, Conductive polymer-based sensors for biomedical applications, Biosens. Bioelectron. 26 (2011) 1825–1832. https://doi.org/10.1016/j.bios.2010.09.046.

[247] T.C. Nirmale, B.B. Kale, A.J. Varma, A review on cellulose and lignin based binders and electrodes: Small steps towards a sustainable lithium ion battery, Int. J. Biol. Macromol. 103 (2017) 1032–1043. https://doi.org/10.1016/j.ijbiomac.2017.05.155.

[248] G. Sandu, B. Ernould, J. Rolland, N. Cheminet, J. Brassinne, P.R. Das, Y. Filinchuk, L. Cheng, L. Komsiyska, P. Dubois, S. Melinte, J.F. Gohy, R. Lazzaroni, A. Vlad, Mechanochemical Synthesis of PEDOT:PSS Hydrogels for Aqueous Formulation of Li-Ion Battery Electrodes, ACS Appl. Mater. Interfaces. 9 (2017) 34865–34874. https://doi.org/10.1021/acsami.7b08937.

[249] M.B. Pinson, M.Z. Bazant, Theory of SEI Formation in Rechargeable Batteries: Capacity Fade, Accelerated Aging and Lifetime Prediction, J. Electrochem. Soc. 160 (2013) A243–A250. https://doi.org/10.1149/2.044302jes.

[250] P.K.R. Das, L. Komsiyska, O. Osters, G. Wittstock, Electrochemical stability of PEDOT:PSS as cathodic binder for Li-ion batteries, ECS Trans. 68 (2015) 45–58. https://doi.org/10.1149/06802.0045ecst.

[251] A.R. Hillman, S.J. Daisley, S. Bruckenstein, Kinetics and mechanism of the electrochemical p-doping of PEDOT, Electrochem. Commun. 9 (2007) 1316–1322. https://doi.org/10.1016/j.elecom.2007.01.009.

[252] S.R. Sivakkumar, D.W. Kim, Polyaniline/carbon nanotube composite cathode for rechargeable lithium polymer batteries assembled with gel polymer electrolyte, J. Electrochem. Soc. 154 (2007) 134–139. https://doi.org/10.1149/1.2404901.

[253] D. Dubal, A. Jagadale, N.R. Chodankar, D.H. Kim, P. Gomez-Romero, R. Holze, Polypyrrole Nanopipes as a Promising Cathode Material for Li-ion Batteries and Li-ion Capacitors: Two-in-One Approach, Energy Technol. 7 (2019) 193–200. https://doi.org/10.1002/ente.201800551.

[254] A. Mauger, C. Julien, A. Paolella, M. Armand, K. Zaghib, Recent Progress on Organic Electrodes Materials for Rechargeable Batteries and Supercapacitors, Materials. 12 (2019) 1770. https://doi.org/10.3390/ma12111770.

[255] H. Meng, Q. Shi, T. Liu, F.X. Liu, P. Chen, The percolation properties of electrical conductivity and permeability for fractal porous media, Energies. 12 (2019) 1–15. https://doi.org/10.3390/en12061085.

[256] I. V. Thorat, D.E. Stephenson, N.A. Zacharias, K. Zaghib, J.N. Harb, D.R. Wheeler, Quantifying tortuosity in porous Li-ion battery materials, J. Power Sources. 188 (2009) 592–600. https://doi.org/10.1016/j.jpowsour.2008.12.032.

[257] M. Zhuo, D. Grazioli, A. Simone, Active material utilization and capacity of fiber-based battery electrodes, Electrochim. Acta. 333 (2020) 134929. https://doi.org/10.1016/j.electacta.2019.134929.

[258] R. Tian, N. Alcala, S.J. O'Neill, D. Horvath, J. Coelho, A. Griffin, Y. Zhang, V. Nicolosi, C. O'Dwyer, J.N. Coleman, Quantifying the effect of electronic conductivity on the rate-performance of nanocomposite battery electrodes, ACS Appl. Energy Mater. (2020) 1–24. https://doi.org/10.1021/acsaem.0c00034.

[259] J. Fournier, G. Boiteux, G. Seytre, G. Marichy, Percolation network of polypyrrole in conducting polymer composites, Synth. Met. 84 (1997) 839–840. https://doi.org/10.1016/S0379-6779(96)04173-2.

[260] A.B. Da Silva, J. Marini, G. Gelves, U. Sundararaj, R. Gregório, R.E.S. Bretas, Synergic effect in electrical conductivity using a combination of two fillers in PVDF hybrids composites, Eur. Polym. J. 49 (2013) 3318–3327. https://doi.org/10.1016/j.eurpolymj.2013.06.039.

[261] J.G. Martinez, B. Berrueco, T.F. Otero, Deep Reduced PEDOT Films Support Electrochemical Applications: Biomimetic Color Front, Front. Bioeng. Biotechnol. 3 (2015) 1–6. https://doi.org/10.3389/fbioe.2015.00015.

[262] H.S. Park, S.J. Ko, J.S. Park, J.Y. Kim, H.K. Song, Redox-active charge carriers of conducting polymers as a tuner of conductivity and its potential window, Sci. Rep. 3 (2013) 1–6. https://doi.org/10.1038/srep02454.

[263] J.K. Kim, J. Manuel, M.H. Lee, J. Scheers, D.H. Lim, P. Johansson, J.H. Ahn, A. Matic, P. Jacobsson, Towards flexible secondary lithium batteries: Polypyrrole-LiFePO4 thin electrodes with polymer electrolytes, J. Mater. Chem. 22 (2012) 15045–15049. https://doi.org/10.1039/c2jm30965c.

[264] Y. Huang, J.B. Goodenough, High-Rate LiFePO 4 Lithium Rechargeable Battery Promoted by Electrochemically Active Polymers, Chem. Mater. 20 (2008) 7237–7241.

[265] H. Chen, K. Aoki, F. Kawaguchi, J. Chen, T. Nishiumi, Voltammetric potentials of polyaniline varying with electric percolation, Electrochim. Acta. 55 (2010) 6959–6963. https://doi.org/10.1016/j.electacta.2010.06.048.

[266] R. Mažeikienappproaches the limit, A. Malinauskas, Electrochemical stability of polyaniline, Eur. Polym. J. 38 (2002) 1947–1952. https://doi.org/10.1016/S0014-

3057(02)00103-9.

[267] H.J. Ahonen, J. Lukkari, J. Kankare, n- and p-doped poly(3,4-ethylenedioxythiophene): Two electronically conducting states of the polymer, Macromolecules. 33 (2000) 6787–6793. https://doi.org/10.1021/ma0004312.

[268] D.L. Wood, J.D. Quass, J. Li, S. Ahmed, D. Ventola, C. Daniel, Technical and economic analysis of solvent-based lithium-ion electrode drying with water and NMP, Dry. Technol. 36 (2018) 234–244. https://doi.org/10.1080/07373937.2017.1319855.

[269] M. Wood, J. Li, R.E. Ruther, Z. Du, E.C. Self, H.M. Meyer, C. Daniel, I. Belharouak, D.L. Wood, Chemical stability and long-term cell performance of low-cobalt, Ni-Rich cathodes prepared by aqueous processing for high-energy Li-Ion batteries, Energy Storage Mater. 24 (2020) 188–197. https://doi.org/10.1016/j.ensm.2019.08.020.

[270] M. Bichon, D. Sotta, N. Dupré, E. De Vito, A. Boulineau, W. Porcher, B. Lestriez, Study of Immersion of LiNi0.5Mn0.3Co0.2O2 Material in Water for Aqueous Processing of Positive Electrode for Li-Ion Batteries, ACS Appl. Mater. Interfaces. 11 (2019) 18331–18341. https://doi.org/10.1021/acsami.9b00999.

[271] W. Bauer, F.A. Çetinel, M. Müller, U. Kaufmann, Effects of pH control by acid addition at the aqueous processing of cathodes for lithium ion batteries, Electrochim. Acta. 317 (2019) 112–119. https://doi.org/10.1016/j.electacta.2019.05.141.

[272] A. Kazzazi, D. Bresser, A. Birrozzi, J. Von Zamory, M. Hekmatfar, S. Passerini, Comparative Analysis of Aqueous Binders for High-Energy Li-Rich NMC as a Lithium-Ion Cathode and the Impact of Adding Phosphoric Acid, ACS Appl. Mater. Interfaces. 10 (2018) 17214–17222. https://doi.org/10.1021/acsami.8b03657.

[273] N. Loeffler, T. Kopel, G.T. Kim, S. Passerini, Polyurethane binder for aqueous processing of Li-ion battery electrodes, J. Electrochem. Soc. 162 (2015) A2692–A2698. https://doi.org/10.1149/2.0641514jes.

[274] S.Y. Li, B.C. Church, Effect of aqueous-based cathode slurry pH and immersion time on corrosion of aluminum current collector in lithium-ion batteries, Mater. Corros. 67 (2016) 978–987. https://doi.org/10.1002/maco.201608843.

[275] I. Doberdò, N. Löffler, N. Laszczynski, D. Cericola, N. Penazzi, S. Bodoardo, G.T. Kim, S. Passerini, Enabling aqueous binders for lithium battery cathodes - Carbon coating of aluminum current collector, J. Power Sources. 248 (2014) 1000–1006. https://doi.org/10.1016/j.jpowsour.2013.10.039.

[276] N. Loeffler, J. Von Zamory, N. Laszczynski, I. Doberdo, G.T. Kim, S. Passerini, Performance of LiNi1/3Mn1/3Co1/3O 2/graphite batteries based on aqueous binder, J. Power Sources. 248 (2014) 915–922. https://doi.org/10.1016/j.jpowsour.2013.10.018.

[277] R.K. Pal, A.A. Farghaly, C. Wang, M.M. Collinson, S.C. Kundu, V.K. Yadavalli, Conducting polymer-silk biocomposites for flexible and biodegradable electrochemical sensors, Biosens. Bioelectron. 81 (2016) 294–302. https://doi.org/10.1016/j.bios.2016.03.010.

[278] J.G. Hardy, J.Y. Lee, C.E. Schmidt, Biomimetic conducting polymer-based tissue scaffolds, Curr. Opin. Biotechnol. 24 (2013) 847–854. https://doi.org/10.1016/j.copbio.2013.03.011.

[279] Y. Guo, J. Bae, F. Zhao, G. Yu, Functional Hydrogels for Next-Generation Batteries and Supercapacitors, Trends Chem. 1 (2019) 335–348. https://doi.org/10.1016/j.trechm.2019.03.005.

[280] P. Teichert, G.G. Eshetu, H. Jahnke, E. Figgemeier, Degradation and Aging Routes of Ni-Rich Cathode Based Li-Ion Batteries, Batteries. 6 (2020) 8. https://doi.org/10.3390/batteries6010008.

[281] R.J. Brodd, W. Huang, J.R. Akridge, Polymer battery R&D in the U.S., Macromol. Symp. 159 (2000) 229–246. https://doi.org/10.1002/1521-3900(200010)159:1<229::AID-MASY229>3.0.CO;2-O.

[282] M. Dong, M. Hafezi, Z. Tong, L. Qin, Preparation and oil lubrication of polyvinylidene fluoride (PVDF) nanospheres, Mater. Res. Express. 6 (2019) 085093. https://doi.org/10.1088/2053-1591/ab220e.

[283] C.R. Hernandez, A. Etiemble, T. Douillard, D. Mazouzi, Z. Karkar, E. Maire, D. Guyomard, B. Lestriez, L. Roué, A Facile and Very Effective Method to Enhance the Mechanical Strength and the Cyclability of Si-Based Electrodes for Li-Ion Batteries, Adv. Energy

Mater. 8 (2018) 1–13. https://doi.org/10.1002/aenm.201701787.

[284] Z. Zhang, T. Zeng, C. Qu, H. Lu, M. Jia, Y. Lai, J. Li, Cycle performance improvement of LiFePO4 cathode with polyacrylic acid as binder, Electrochim. Acta. 80 (2012) 440–444. https://doi.org/10.1016/j.electacta.2012.07.054.

[285] D. Mazouzi, R. Grissa, M. Paris, Z. Karkar, L. Huet, D. Guyomard, L. Roué, T. Devic, B. Lestriez, CMC-citric acid Cu(II) cross-linked binder approach to improve the electrochemical performance of Si-based electrodes, Electrochim. Acta. 304 (2019) 495–504. https://doi.org/10.1016/j.electacta.2019.03.026.

[286] K. Sun, S. Zhang, P. Li, Y. Xia, X. Zhang, D. Du, F.H. Isikgor, J. Ouyang, Review on application of PEDOTs and PEDOT:PSS in energy conversion and storage devices, J. Mater. Sci. Mater. Electron. 26 (2015) 4438–4462. https://doi.org/10.1007/s10854-015-2895-5.

[287] M. Zheng, C. Wang, Y. Xu, K. Li, D. Liu, A water-soluble binary conductive binder for Si anode lithium ion battery, Electrochim. Acta. 305 (2019) 555–562. https://doi.org/10.1016/j.electacta.2019.02.080.

[288] X. Li, H. An, J. Strzalka, J. Lutkenhaus, R. Verduzco, Self-doped conjugated polymeric binders improve the capacity and mechanical properties of V2O5 cathodes, Polymers. 11 (2019) 589. https://doi.org/10.3390/polym11040589.

[289] X. Crispin, F.L.E. Jakobsson, A. Crispin, P.C.M. Grim, P. Andersson, A. Volodin, C. Van Haesendonck, M. Van Der Auweraer, W.R. Salaneck, M. Berggren, The origin of the high conductivity of poly(3,4-ethylenedioxythiophene)-poly(styrenesulfonate) (PEDOT-PSS) plastic electrodes, Chem. Mater. 18 (2006) 4354–4360. https://doi.org/10.1021/cm061032+.

[290] Y. Cheng, X. Ren, L. Duan, G. Gao, A transparent and adhesive carboxymethyl cellulose/polypyrrole hydrogel electrode for flexible supercapacitors, J. Mater. Chem. C. 8 (2020) 8234–8242. https://doi.org/10.1039/D0TC01039A.

[291] Y. Wang, Q. Wen, Y. Chen, W. Li, Conductive polypyrrole-carboxymethyl cellulose-titanium nitride/carbon brush hydrogels as bioanodes for enhanced energy output in

microbial fuel cells, Energy. 204 (2020) 117942. https://doi.org/10.1016/j.energy.2020.117942.

[292] Y. Bu, H.X. Xu, X. Li, W.J. Xu, Y.X. Yin, H.L. Dai, X. Bin Wang, Z.J. Huang, P.H. Xu, A conductive sodium alginate and carboxymethyl chitosan hydrogel doped with polypyrrole for peripheral nerve regeneration, RSC Adv. 8 (2018) 10806–10817. https://doi.org/10.1039/c8ra01059e.

[293] L. Qie, L.X. Yuan, W.X. Zhang, W.M. Chen, Y.H. Huang, Revisit of polypyrrole as cathode material for lithium-ion battery, J. Electrochem. Soc. 159 (2012) 1624–1629. https://doi.org/10.1149/2.042210jes.

[294] A.A. Pavlychev, K.H. Hallmeier, C. Hennig, L. Hennig, R. Szargan, Nitrogen K-shell excitations in complex molecules and polypyrrole, Chem. Phys. 201 (1995) 547–555. https://doi.org/10.1016/0301-0104(95)00287-1.

[295] W.E.S. Unger, A. Lippitz, C. Wöll, W. Heckmann, X-ray absorption spectroscopy (NEXAFS) of polymer surfaces, Fresenius. J. Anal. Chem. 358 (1997) 89–92. https://doi.org/10.1007/s002160050352.

[296] C. Karunakaran, C.R. Christensen, C. Gaillard, R. Lahlali, L.M. Blair, V. Perumal, S.S. Miller, A.P. Hitchcock, Introduction of soft x-ray spectromicroscopy as an advanced technique for plant biopolymers research, PLoS One. 10 (2015) 1–18. https://doi.org/10.1371/journal.pone.0122959.

[297] G.D. Cody, J. Brandes, C. Jacobsen, S. Wirick, Soft X-ray induced chemical modification of polysaccharides in vascular plant cell walls, J. Electron Spectros. Relat. Phenomena. 170 (2009) 57–64. https://doi.org/10.1016/j.elspec.2008.09.007.

[298] A. Azioune, F. Siroti, J. Tanguy, M. Jouini, M.M. Chehimi, B. Miksa, S. Slomkowski, Interactions and conformational changes of human serum albumin at the surface of electrochemically synthesized thin polypyrrole films, Electrochim. Acta. 50 (2005) 1661–1667. https://doi.org/10.1016/j.electacta.2004.10.014.

[299] F. Zhang, J. Dou, H. Zhang, Mixed Membranes Comprising Carboxymethyl Cellulose (as Capping Agent and Gas Barrier Matrix) and Nanoporous ZIF-L Nanosheets for Gas

Separation Applications, Polymers. 10 (2018) 1340. https://doi.org/10.3390/polym10121340.

[300] F.T.A. Vork, B.C.A.M. Schuermans, E. Barendrecht, Influence of inserted anions on the properties of polypyrrole, Electrochim. Acta. 35 (1990) 567–575. https://doi.org/10.1016/0013-4686(90)87045-4.

[301] S.J. Davies, T.G. Ryan, C.J. Wilde, G. Beyer, Processable forms of conductive polyaniline, Synth. Met. 69 (1995) 209–210. https://doi.org/10.1016/0379-6779(94)02418-X.

[302] R.E.D. La Rue, C.W. Tobias, On the Conductivity of Dispersions, J. Electrochem. Soc. 106 (1959) 827. https://doi.org/10.1149/1.2427505.

[303] A.S. Hutchison, T.W. Lewis, S.E. Moulton, G.M. Spinks, G.G. Wallace, Development of polypyrrole-based electromechanical actuators, Synth. Met. 113 (2000) 121–127. https://doi.org/10.1016/S0379-6779(00)00190-9.

[304] P. Murray, G.M. Spinks, G.G. Wallace, R.P. Burford, Electrochemical induced ductile-brittle transition in tosylate-doped (pTS) polypyrrole, Synth. Met. 97 (1998) 117–121. https://doi.org/10.1016/s0379-6779(98)00119-2.

[305] G. Bidan, B. Ehui, M. Lapkowski, Conductive polymers with immobilised dopants: Ionomer composites and auto-doped polymers-a review and recent advances, J. Phys. D. Appl. Phys. 21 (1988) 1043–1054. https://doi.org/10.1088/0022-3727/21/7/001.

[306] C. Sasso, D. Beneventi, E. Zeno, D. Chaussy, M. Petit-Conil, P. Nortier, N. Belgacem, Polypyrrole synthesis via carboxymethylcellulose-iron complexes, BioResources. 5 (2010) 2348–2361. https://doi.org/10.15376/biores.5.4.2348-2361.

[307] J. Yang, Y. Liu, S. Liu, L. Li, C. Zhang, T. Liu, Conducting polymer composites: Material synthesis and applications in electrochemical capacitive energy storage, Mater. Chem. Front. 1 (2017) 251–268. https://doi.org/10.1039/c6qm00150e.

[308] A. Manthiram, J.C. Knight, S.T. Myung, S.M. Oh, Y.K. Sun, Nickel-Rich and Lithium-Rich Layered Oxide Cathodes: Progress and Perspectives, Adv. Energy Mater. 6 (2016). https://doi.org/10.1002/aenm.201501010.

[309] S. Sharifi-Asl, J. Lu, K. Amine, R. Shahbazian-Yassar, Oxygen Release Degradation in Li-Ion Battery Cathode Materials: Mechanisms and Mitigating Approaches, Adv. Energy Mater. 9 (2019) 1–19. https://doi.org/10.1002/aenm.201900551.

[310] T.M.M. Heenan, A. Wade, C. Tan, J.E. Parker, D. Matras, A.S. Leach, J.B. Robinson, A. Llewellyn, A. Dimitrijevic, R. Jervis, P.D. Quinn, D.J.L. Brett, P.R. Shearing, Identifying the Origins of Microstructural Defects Such as Cracking within Ni-Rich NMC811 Cathode Particles for Lithium-Ion Batteries, Adv. Energy Mater. 10 (2020) 2002655. https://doi.org/10.1002/aenm.202002655.

[311] R. Xu, H. Sun, L.S. de Vasconcelos, K. Zhao, Mechanical and Structural Degradation of LiNixMnyCozO2 Cathode in Li-Ion Batteries: An Experimental Study, J. Electrochem. Soc. 164 (2017) A3333–A3341. https://doi.org/10.1149/2.1751713jes.

[312] J. Xu, S.-L. Chou, Q. Gu, H.-K. Liu, S.-X. Dou, The effect of different binders on electrochemical properties of LiNi1/3Mn1/3Co1/3O2 cathode material in lithium ion batteries, J. Power Sources. 225 (2013) 172–178. https://doi.org/10.1016/j.jpowsour.2012.10.033.

[313] Q. Wu, S. Ha, J. Prakash, D.W. Dees, W. Lu, Investigations on high energy lithium-ion batteries with aqueous binder, Electrochim. Acta. 114 (2013) 1–6. https://doi.org/10.1016/j.electacta.2013.09.068.

[314] G. Zhang, B. Qiu, Y. Xia, X. Wang, Q. Gu, Y. Jiang, Z. He, Z. Liu, Double-helix-superstructure aqueous binder to boost excellent electrochemical performance in Li-rich layered oxide cathode, J. Power Sources. 420 (2019) 29–37. https://doi.org/10.1016/j.jpowsour.2019.02.086.

[315] T. Zhang, J. Li, J. Liu, Y. Deng, Z. Wu, Z. Yin, D. Guo, L. Huang, S. Sun, Suppressing the voltage-fading of layered lithium-rich cathode materials via an aqueous binder for Li-ion batteries, Chem. Commun. 52 (2016) 4683–4686. https://doi.org/10.1039/C5CC10534J.

[316] L. Azhari, X. Zhou, B. Sousa, Z. Yang, G. Gao, Y. Wang, Effects of Extended Aqueous Processing on Structure, Chemistry, and Performance of Polycrystalline LiNixMnyCozO2 Cathode Powders, ACS Appl. Mater. Interfaces. 12 (2020) 57963–57974.

https://doi.org/10.1021/acsami.0c20105.

[317] W.B. Hawley, A. Parejiya, Y. Bai, H.M. Meyer, D.L. Wood, J. Li, Lithium and transition metal dissolution due to aqueous processing in lithium-ion battery cathode active materials, J. Power Sources. 466 (2020) 228315. https://doi.org/10.1016/j.jpowsour.2020.228315.

[318] X. Jiang, Y. Sha, R. Cai, Z. Shao, The solid-state chelation synthesis of LiNi1/3Co1/3Mn1/3O2 as a cathode material for lithium-ion batteries, J. Mater. Chem. A. 3 (2015) 10536–10544. https://doi.org/10.1039/C5TA01236H.

[319] S.-C. Yin, Y.-H. Rho, I. Swainson, L.F. Nazar, X-ray/Neutron Diffraction and Electrochemical Studies of Lithium De/Re-Intercalation in Li1-xCo1/3Ni1/3Mn1/3O2 (x = 0 → 1), Chem. Mater. 18 (2006) 1901–1910. https://doi.org/10.1021/cm0511769.

[320] B. Kavitha, K.S. Kumar, N. Narsimlu, Synthesis and characterization of polyaniline nano-fibers, Indian J. Pure Appl. Phys. 51 (2013) 207–209.

[321] W.M. Chen, L. Qie, L.X. Yuan, S.A. Xia, X.L. Hu, W.X. Zhang, Y.H. Huang, Insight into the improvement of rate capability and cyclability in LiFePO4/polyaniline composite cathode, Electrochim. Acta. 56 (2011) 2689–2695. https://doi.org/10.1016/j.electacta.2010.12.041.

[322] T. Ohzuku, A. Ueda, Solid-State Redox Reactions of LiCoO2 (R3m) for 4 Volt Secondary Lithium Cells, J. Electrochem. Soc. 141 (1994) 2972–2977. https://doi.org/10.1149/1.2059267.

[323] T. Kawamura, T. Sonoda, S. Okada, J. Yamaki, Improvement of the Stability of LiPF6 Electrolytes toward Water by the Addition of LiCl, Electrochemistry. 71 (2003) 1139–1141. https://doi.org/10.5796/electrochemistry.71.1139.

[324] L. Lin, F. Liang, K. Zhang, H. Mao, J. Yang, Y. Qian, Lithium phosphide/lithium chloride coating on lithium for advanced lithium metal anode, J. Mater. Chem. A. 6 (2018) 15859–15867. https://doi.org/10.1039/c8ta05102j.

[325] L. Dahéron, H. Martinez, R. Dedryvère, I. Baraille, M. Ménétrier, C. Denage, C. Delmas, D. Gonbeau, Surface Properties of LiCoO2 Investigated by XPS Analyses and Theoretical Calculations, J. Phys. Chem. C. 113 (2009) 5843–5852. https://doi.org/10.1021/jp803266w.

[326] S.F. Lux, F. Schappacher, A. Balducci, S. Passerini, M. Winter, Low Cost, Environmentally Benign Binders for Lithium-Ion Batteries, J. Electrochem. Soc. 157 (2010) A320. https://doi.org/10.1149/1.3291976.

[327] X. Guo, A. Facchetti, The journey of conducting polymers from discovery to application., Nat. Mater. 19 (2020) 922–928. https://doi.org/10.1038/s41563-020-0778-5.

[328] A.J. Smith, J.C. Burns, D. Xiong, J.R. Dahn, Interpreting High Precision Coulometry Results on Li-ion Cells, J. Electrochem. Soc. 158 (2011) A1136. https://doi.org/10.1149/1.3625232.

[329] M. Ebner, F. Marone, M. Stampanoni, V. Wood, Visualization and quantification of Electrochemical and Mechanical, Science. 342 (2013) 716–721.

[330] M. Wolf, B.M. May, J. Cabana, Visualization of Electrochemical Reactions in Battery Materials with X-ray Microscopy and Mapping, Chem. Mater. 29 (2017) 3347–3362. https://doi.org/10.1021/acs.chemmater.6b05114.

[331] R.I. Al-raoush, I.T. Madhoun, TORT3D : A MATLAB code to compute geometric tortuosity from 3D images of unconsolidated porous media, Powder Technol. 320 (2017) 99–107. https://doi.org/10.1016/j.powtec.2017.06.066.

[332] S.J. Cooper, A. Bertei, P.R. Shearing, J.A. Kilner, N.P. Brandon, TauFactor: An open-source application for calculating tortuosity factors from tomographic data, SoftwareX. 5 (2016) 203–210. https://doi.org/10.1016/j.softx.2016.09.002.

[333] Z. Karkar, D. Guyomard, L. Roué, B. Lestriez, A comparative study of polyacrylic acid (PAA) and carboxymethyl cellulose (CMC) binders for Si-based electrodes, Electrochim. Acta. 258 (2017) 453–466. https://doi.org/10.1016/j.electacta.2017.11.082.

[334] J. Zhou, J. Wang, H. Fang, C. Wu, J.N. Cutler, T.K. Sham, Nanoscale chemical imaging and spectroscopy of individual RuO2 coated carbon nanotubes, Chem. Commun. 46 (2010) 2778–2780. https://doi.org/10.1039/b921590e.